Fall 12-22-2010

Novel Amino Acid and Ethanolamine Derivatives as Potential Tumor Imaging Agents for Positron Emission Tomography

Limin Wang
limin.liminw@gmail.com

Novel Amino Acid and Ethanolamine Derivatives as Potential Tumor Imaging Agents for Positron Emission Tomography

Abstract
Malignant tumors can be detected with high sensitivity and specificity by imaging their increased metabolic rate for glucose, amino acids and fatty acids. Positron emission tomography (PET) with glucose analog [18F]FDG, which utilizes increased glucose metabolism, has become a routine clinical test for diagnosis, staging and restaging a variety of cancers. Despite the tremendous success of PET-FDG, there are some well-known limitations of [18F]FDG such as high cerebral uptake, uptake in inflammatory tissues, high excretion through urinary tract and low or negligent uptake in certain type of tumors. Decades of nuclear medicine research have lead to development of other PET imaging agents to overcome such limitations.

We examined two series of tracers targeting two different altered metabolic processes in the tumor cells in order to improve on imaging properties of existing clinically utilized PET ligands. One series is 18F labeled tyrosine and phenylalanine derivatives, which targets altered amino acid metabolism – increased amino acids uptake and protein synthesis rate in cancer cells. We synthesized three new 18F labeled fluoroalkyl tyrosine derivatives, in vitro studies in human glioblastoma cells of these tyrosine derivatives indicated they were not very promising tumor-imaging agents since in comparison to clinically utilized imaging agent O-(2-[18F]fluoroethyl)-L-tyrosine (FET), their uptake was much lower. We also synthesized and evaluated L- and D-isomers of new phenylalanine derivatives, p-(2-[18F]fluoroethyl)-phenylalanine (FEP) and p-(3-[18F]fluoropropyl)-phenylalanine (FPP) in comparison to clinically utilized FET and its D-isomer. In vitro studies in 9L glioma cells as well as biodistribution and small animal PET imaging studies demonstrated that L- isomer of FEP is comparable to FET and it is a potential useful tracer for tumor imaging with PET. Comparison of L- and D-isomers of phenylalanine derivatives showed that D-isomers did not have improved imaging properties than their corresponding L-isomers. Of all new aromatic amino acid derivatives, L- isomer of FEP had the best outcome and is comparable to clinically established FET in imaging rats bearing 9L tumor model.

The other series of tracers is 11C labeled ethanolamine amine derivatives, which targets the altered lipid metabolism associated with increased cellular proliferation in tumors. Here, we developed 11C labeled ethanolamine and two ethanolamine derivatives — N-methyl ethanolamine and N,N-dimethyl ethanolamine. In vitro studies demonstrated that they could be more sensitive PET tracers than clinically utilized [11C]choline for the imaging of phospholipids biosynthesis in tumors.

Degree Type
Dissertation

Degree Name
Doctor of Philosophy (PhD)

Graduate Group
Chemistry

NOVEL AMINO ACID AND ETHANOLAMINE DERIVATIVES AS POTENTIAL TUMOR IMAGING AGENTS FOR POSITRON EMISSION TOMOGRAPHY

Limin Wang

A DISSERTATION
in
Chemistry

Presented to the Faculties of the University of Pennsylvania in Partial Fulfillment of the Requirements for the Degree of Doctor of Philosophy

2010

_____
Hank F. Kung, Ph.D.
Professor of Radiology and Pharmacology
Supervisor of Dissertation

_____
Datta E. Ponde, Ph.D.
Assistant Professor of Radiology
Co-Supervisor of Dissertation

_____
Garry Molander, Ph.D.
Professor of Chemistry
Graduate Group Chair

Dissertation Committee Members:
Ivan J. Dmochowski, Ph.D., Associate Professor of Chemistry, Thesis Committee Chair
Donna Huryn, Ph.D., Adjunct Professor of Chemistry
Chaitanya R. Divgi, M.D., Professor of Radiology

Dedicated to my parents
and
in loving memory of my grandparents

ACKNOWLEDGMENTS

There are many people I would like to thank for their support, advice and help during my graduate studies in University of Pennsylvania. First, I would like to express my great gratitude to my research advisor Dr. Hank Kung for providing me the opportunity to join his group. I am honored to have studied under his guidance and learned from him and the great people in his lab. He has always been supportive and provided all resources to accomplish this research project. I truly admire Dr. Kung for his many contributions to the development of tumor imaging agents for PET and SPECT. I am also very thankful to my co-advisor Dr. Datta Ponde for opening my eyes to the field of nuclear medicine. From him I learned the essential knowledge in radiochemistry as well as labeling techniques.

I am extremely grateful for having the chance to work with many wonderful people in the Kung group. I would especially acknowledge Dr. Wenchao Qu, who guided me and always provide most insightful information regarding the chemical synthesis, which made the synthesis of new tracers possible. I want to give special thanks to Brian Lieberman who performed the in vivo evaluations for new amino acid derivatives. He also trained and assisted me on biological studies. I am also indebted to Dr. Karl Ploessl who carried out HRMS analysis for all compounds and always provides timely help in labeling problems. I cannot forget all the past and present members of the Kung lab for their camaraderie through the years. It have been a great pleasure to work with all these talented and kind people, from them I see an excellent collaborative work environment.

I would like to thank Dr. Rajesh Gowswami and Rajesh Kamble for their advice and help with chemistry in ethanolamine project, Dr. Qiao Hui who helped me in cell culture work, Dr. Richard Freifield for providing cyclotron facilities for radiolabeling of ethanolamine derivatives, Rahul Poria and Boby Mathew from whom I learned ^{11}C radiolabeling techniques.

The comments, suggestions and encouragement of my thesis committee members, Dr. Ivan Dmochowski, Dr. Chaitanya Divgi and Dr. Donna Huryn, have been very important in maintaining the progress in my graduate research.

Thanks to Dr. Kung, Dr. Ponde and small animal image facilities for the financial support. The Department of Defense and new investigator award (to Dr. Ponde) under prostate cancer research program provided funding for ethanolamine project. The GAPSA and the society of nuclear medicine provided additional travel support for me to attend conference and present the research work.

I cannot thank enough my parents – Mom and Dad, thank you for your unconditional love and support for me to pursue my academic career in such a long distance from you. I am also very grateful to all the friends, who brought a lot of laughers and good advice in the graduate study. Finally, I would like to thank my husband Rony, with his warm personality and great breadth of knowledge, not only gave me lots of love, comfort and support, but also taught me a lot of thing in life as well as in science. I feel extremely lucky to share my life in graduate school and unknown future with him.

ABSTRACT

NOVEL AMINO ACID AND ETHANOLAMINE DERIVATIVES AS POTENTIAL TUMOR IMAGING AGENTS FOR POSITRON EMISSION TOMOGRAPHY

Limin Wang

Hank F. Kung, Ph.D.
Datta E. Ponde, Ph.D.

Malignant tumors can be detected with high sensitivity and specificity by imaging their increased metabolic rate for glucose, amino acids and fatty acids. Positron emission tomography (PET) with glucose analog [^{18}F]FDG, which utilizes increased glucose metabolism, has become a routine clinical test for diagnosis, staging and restaging a variety of cancers. Despite the tremendous success of PET-FDG, there are some well-known limitations of [^{18}F]FDG such as high cerebral uptake, uptake in inflammatory tissues, high excretion through urinary tract and low or negligent uptake in certain type of tumors. Decades of nuclear medicine research have lead to development of other PET imaging agents to overcome such limitations.

We examined two series of tracers targeting two different altered metabolic processes in the tumor cells in order to improve on imaging properties of existing clinically utilized PET ligands. One series is ^{18}F labeled tyrosine and phenylalanine derivatives, which targets altered amino acid metabolism – increased amino acids uptake and protein synthesis rate in cancer cells. We synthesized three new ^{18}F labeled fluoroalkyl tyrosine derivatives, in vitro studies in human glioblastoma cells of these

tyrosine derivatives indicated they were not very promising tumor-imaging agents since in comparison to clinically utilized imaging agent *O*-(2-[^{18}F]fluoroethyl)-L-tyrosine (FET), their uptake was much lower. We also synthesized and evaluated L- and D-isomers of new phenylalanine derivatives, *p*-(2-[^{18}F]fluoroethyl)-phenylalanine (FEP) and *p*-(3-[^{18}F]fluoropropyl)-phenylalanine (FPP) in comparison to clinically utilized FET and its D-isomer. In vitro studies in 9L glioma cells as well as biodistribution and small animal PET imaging studies demonstrated that L- isomer of FEP is comparable to FET and it is a potential useful tracer for tumor imaging with PET. Comparison of L- and D-isomers of phenylalanine derivatives showed that D-isomers did not have improved imaging properties than their corresponding L-isomers. Of all new aromatic amino acid derivatives, L- isomer of FEP had the best outcome and is comparable to clinically established FET in imaging rats bearing 9L tumor model.

The other series of tracers is ^{11}C labeled ethanolamine amine derivatives, which targets the altered lipid metabolism associated with increased cellular proliferation in tumors. Here, we developed ^{11}C labeled ethanolamine and two ethanolamine derivatives — *N*-methyl ethanolamine and *N,N*-dimethyl ethanolamine. In vitro studies demonstrated that they could be more sensitive PET tracers than clinically utilized [^{11}C]choline for the imaging of phospholipids biosynthesis in tumors.

Table of Contents

List of Figures

Chapter 1

Chapter 2

Chapter 3

Chapter 4

Chapter 5

List of Tables

Chapter 1

Chapter 2

Chapter 3

Chapter 4

Chapter 5

List of Schemes

Chapter 2

Chapter 3

Chapter 4

Chapter 5

List of Abbreviations

Abbreviation	Full Name	Chemical Structure
AA	amino acid	NA
Ala	alanine	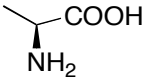
A-PET	small animal positron emission tomography	NA
ASC	alanine-serine-cysteine	NA
BBN (9-BBN)	9-borabicyclo[3.3.1]nonane	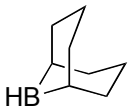
BCH	2-aminobicyclo-(2,2,1)-heptane-2-carboxylic acid	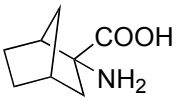
Boc	*t*-butoxycarbobnyl	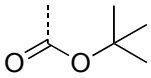
Bq	Becquerel	NA
BSA	bovine serum albumin	NA
$CDCl_3$	deuterated chloroform	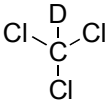
CH	choline	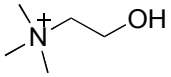
Ci	curie	NA
d	day	NA
DIAD	diisopropyl azodicarboxylate	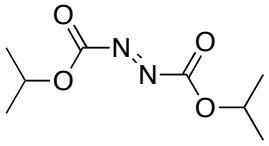
DIPEA	diisopropylethylamine	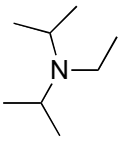
DMEA	*N,N*-Dimethyl ethanolamine	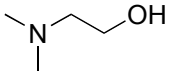

Abbreviation	Full Name	Chemical Structure
DMF	dimethylfomamide	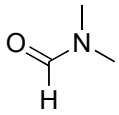
dppf	1,1'-Bis(diphenylphosphino)ferrocene	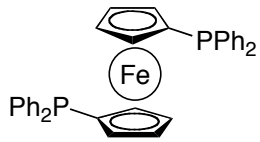
EA	ethanolamine	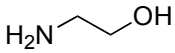
EOB	end-of-bombardment	NA
EOS	end-of-synthesis	NA
EtOAc	ethyl acetate	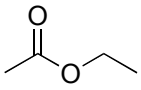
EtOH	ethanol	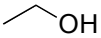
FC	flash chromatography	NA
FDG	2-fluorodeoxyglucose	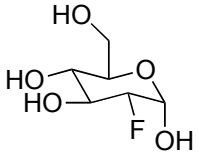
FEAT	*O*-(2-fluoroethyl)-2- azatyrosine	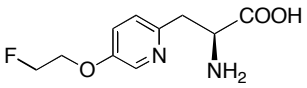
FEMT	*O*-(2-fluoroethyl)-α-methyl-tyrosine	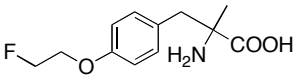
FEP	*p*-(2-fluoroethyl)-phenylalanine	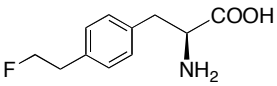
FET	*O*-(2-fluoroethyl)-tyrosine	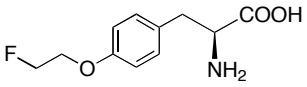
FETA	*O*-(2-fluoroethyl)-tyrosineamide	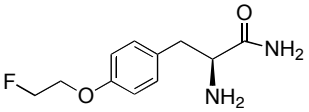
FPP	*p*-(3-fluoropropyl)-phenylalanine	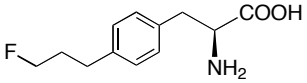
h	hours	NA
HPLC	high performance liquid chromatography	NA
HRMS	high-resolution mass spectrometry	NA

Abbreviation	Full Name	Chemical Structure
ID	initial dose	NA
IACUC	Institutional Animal Care and Use Committee	NA
K[2.2.2]	Kryptofix 2.2.2 (or 1,10-diaza-4,7,13,16,21,24-hexaoxabicyclo[8.8.8]hexacosane)	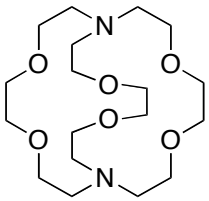
LAH	Lithium aluminum hydride	$LiAlH_4$
LATs	System L amino acid transporters	NA
LC/MSD TOF	liquid chromatography/mass selective detector with time of flight	NA
Me	Methyl	
MEA	*N*-methylethanolamine	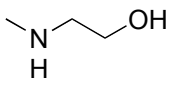
MeAIB	2-(methylamino)-isobutyrate	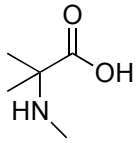
MET	methionine	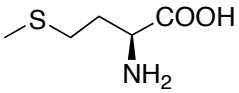
MeOH	methanol	CH_3OH
min	minute	NA
MRS	magnetic resonance spectroscopy	NA
MS	mass spectrometry	NA
NaH	sodium hydride	NaH
NEM	*N*-ethyl ethylmaleimide	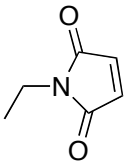
NMR	nuclear magnetic resonance	NA
PCho	phosphocholine	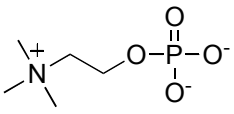

Abbreviation	Full Name	Chemical Structure
PET	positron emission tomography	NA
PEPPSI	Pyridine-Enhanced Precatalyst Preparation Stabilization and Initiation	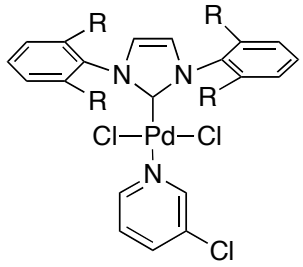
PEtn	phosphoethanolamine	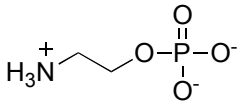
Phe	phenylalanine	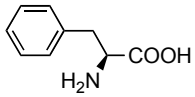
Py	pyridine	
RCP	radiochemical purity	NA
RCY	radiochemical yield	NA
ROI	region of interest	NA
rt	room temperature	NA
s	second	NA
SAIF	small animal imaging facility	NA
SD	standard deviation	NA
SPECT	single photon emission computed tomography	NA
$t_{1/2}$	half-life	NA
t_R	rentention time	NA
TAC	time activity curve	NA
TBAHCO3	tetrabutylammonium bicarbonate	Bu_4NHCO_3
TBAF	tetrabutylammonium fluoride	Bu_4NF
TBDMS	t-butyldimethylsilyl	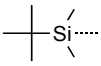

Abbreviation	Full Name	Chemical Structure
TFA	trifluoroacetic acid	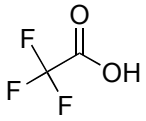
THF	tetrahydrofuran	
Tmob	trimethoxylbenzyl	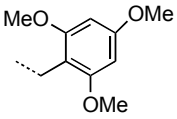
Ts	p-toluenesulfonyl	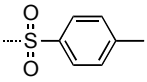
Tyr	tyrosine	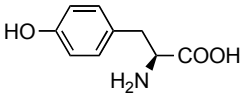

Chapter 1

Introduction

1.1 Altered metabolism of cancer cells

Cellular metabolism within tumors is significantly different from that of corresponding normal cells. Metabolism of neoplastic cells has been studied for many decades, with the aim of designing new strategies for cancer prevention, diagnosis and therapy, based upon the identification of tumor-specific enzymatic alterations. One of the major metabolic changes in tumors is the high rate of aerobic glycolysis, also known as the "Warburg effect". Since Otto Warburg first discovered that tumor cells consume glucose at higher rate than normal cells over 80 years ago [1], the "Warburg effect" has been observed in many cancers. This increased glucose uptake in tumors provided the basis for the development of glucose analog 2-[^{18}F]fluoro-2-deoxy glucose (FDG) as a positron emission tomography (PET) tracer [2], which is widely used clinically for detection, staging and restaging of various cancers. Besides glucose, cancer cells also have increased metabolism of nutrient such as amino acids and fatty acids that meet or exceed the bioenergetic demands of cell growth and proliferation [3, 4]. Figure 1.1 presents an overview of the possible drivers, advantage and potential liabilities of altered metabolism of cancer cells [5].

In recent years, there have been great advance in our understanding of the causes, benefits and vulnerability of cancer cell metabolism. This advance has led to the identification of new drug targets and facilitated the design of tumor specific metabolic substrates. Research in profiling metabolites and enzymatic activities has enabled us to develop diagnostic test and tracers for molecular imaging of cancer. In comparison to other molecular imaging probes, tracers based on altered tumor metabolism could provide

unique information about integrated function of multiple transporters and enzymes in a metabolic pathway [6].

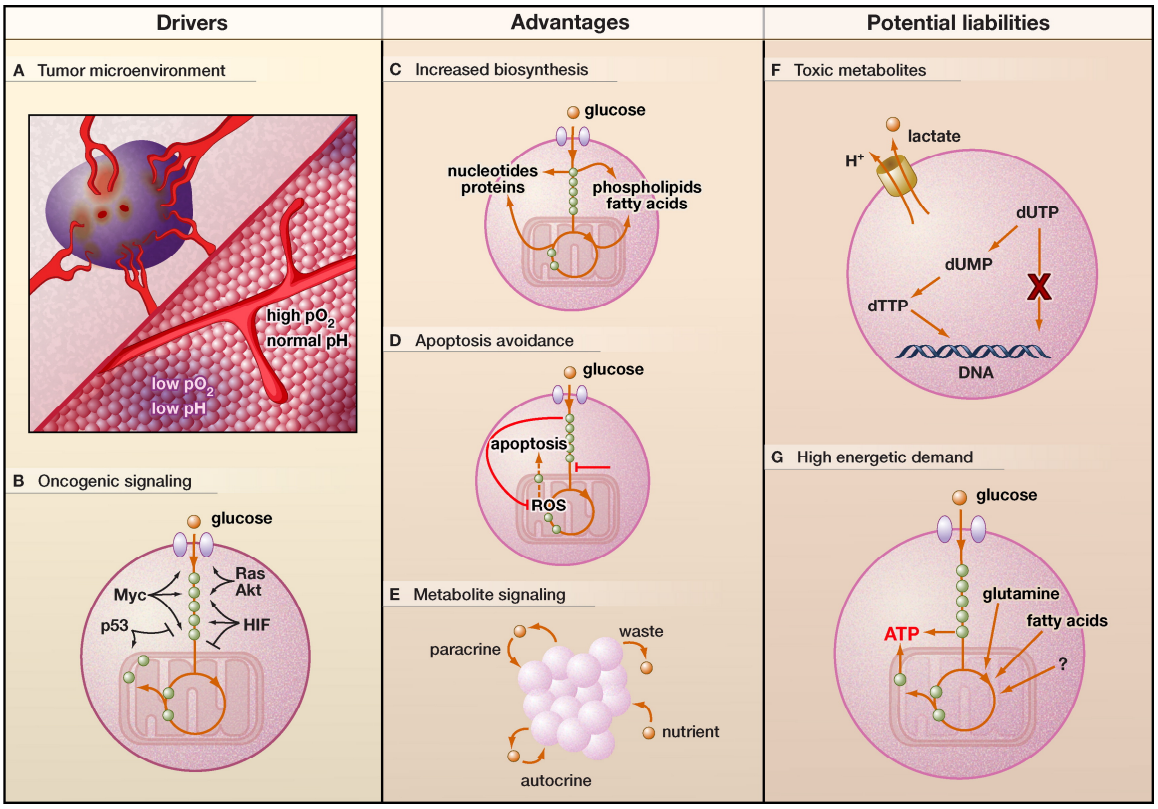

Figure 1.1. The altered metabolism of cancer cells. Drivers (A, low oxygen and low pH microenviroment and B, cancer-associated signaling pathways induce metabolic reprogramming). Advantages (C, increased biosynthesis, D, avoid apoptosis and E, engage in local metabolite-based paracrine and autocrine signaling). Potential liabilities (F, build up of toxic metabolites and G, high energetic demand). Adapted from [5].

1.2 Imaging

Molecular imaging methods can non-invasively detect specific biological processes that are aberrant in cancer. These methods can be used in detection, staging and restaging of various cancers, evaluation and prediction of treatment response, and assist in determining the prognosis of patients. Several modalities can be used for tumor cell metabolic imaging, including PET, single photon emission computed tomography

(SPECT) and Magnetic Resonance Spectroscopy Imaging (MRS). Metabolic imaging is increasingly fused with Computed Tomography (CT)/MRI for precise anatomical localization [7, 8].

The development of MRSI is result of combining imaging techniques with magnetic resonance spectroscopy (MRS). MRSI is used for detecting endogenous cellular metabolites and can provide information for cancer diagnosis and treatment planning, particularly for brain, breast and prostate cancers [9]. The application of MRSI is limited by its low sensitivity and spatial resolution. An emerging technique, hyperpolarizing ^{13}C MRS imaging, dramatically enhances the sensitivity for detection and could further extend the clinical use of MRS [10]. PET and SPECT, which are based on radiotracers, are highly sensitive and can target a specific protein. The existing imaging modalities mainly differ in five aspects: detection limit, spatial and temporal resolution, depth of penetration, energy for imaging generation and availability of molecular probes [11]. Table 1.1 lists some of the general characteristics of available imaging modalities for altered tumor metabolism.

Table 1.1. Comparison of modalities for tumor metabolic imaging [11, 12]

Imaging Modality	Isotopes	Radiation spectrum in image generation	Spatial resolution	Temporal resolution	Detection limit	Amount of molecular probe used
MRSI	^{1}H, ^{19}F, ^{31}P, ^{13}C	Radiowave	5 to 7 mm	mins to h	~10^{-3} to ~10^{-5} M	µg to mg
PET	^{11}C, ^{18}F, ^{15}N, ^{15}O, ^{64}Cu, ^{124}I, ^{68}Ga,	High energy γ rays	1-2 mm (micro); ~ 4-5 mm (clinical)	10s to mins	10^{-11} to 10^{-12} M	ng to µg
SPECT	^{99m}Tc, ^{111}In, ^{123}I	low energy γ rays	1-2mm (micro); >4mm (clinical)	mins	10^{-10} to 10^{-11} M	ng to µg

1.2.1. Radionuclide imaging

Radionuclide imaging is a specialty of medical imaging that uses radiopharmaceuticals (radionuclides incorporated into pharmaceutically-active molecules) and relies on the process of radioactive decay for image generation. The fundamental principle in nuclear imaging is the tracer principle invented in 1912 by Nobel laureate George de Hevesy, who found that radioactive elements had identical chemical properties to the nonradioactive form and therefore could be used to trace chemical behavior in solutions or in the body [13]. Radioactive tracers allow the distribution of labeled molecules to be followed, making it possible to study the biochemistry within the various organs of the living body. Radionuclide imaging can trace biochemical pathways without perturbing native biochemistry by using submicromolar quantities of tracers thus having little chance of pharmacologic toxicity and minimal radiation burden for the patients.

Of the available radioisotope imaging methods, PET has been gaining widespread use thanks to its advantages over more conventional SPECT [14, 15]. PET provides a superior combination of sensitivity and spatial resolution over single-photon imaging, and allows accurate quantification of dynamic regional tracer concentration [14]. Furthermore, PET offers a greater range of radiopharmaceuticals for cancer imaging and many PET isotopes have natural occurrence in biologically active molecules in contrast to heavy isotopes used in SPECT, resulting in higher possibility of synthesizing physiologically active tracers for PET. Now PET has become an increasingly important tool for clinical oncology, so in this thesis work we mainly focus on developing imaging agents for PET.

1.2.1.1 Positron Emission Tomography (PET)

PET detects high energy γ rays generated from positron emitting radionuclides. The unstable radioisotopes undergo β^+ decay and emit a positron (e^+) and neutrino (ν). The emitted positrons travels a short distance (~1.1 mm) before they encounter electrons (e^+) in the surrounding medium, consequently annihilate and give off two coincident γ rays with 511 Kev energy in opposite direction (Figure 1.2). These γ rays can be detected within nanoseconds from each other, which defines the line of events in space and thus the direction of flight. These events are registered and reconstructed into volumetric images of radiotracers in vivo (Figure 1.3) [13].

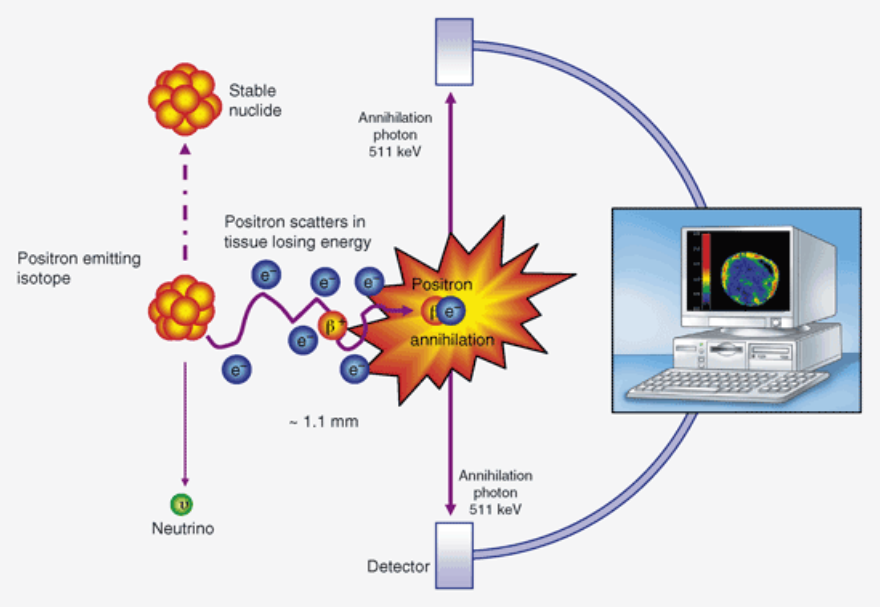

Figure 1.2. Principles of positron emission tomography image acquisition. (http://www.heartandmetabolism.org/images/HM34/HM3407gr1.gif)

A number of commonly occurring elements, such as carbon, oxygen, nitrogen, and fluorine have positron-emitting isotopes. The stable nuclides of these elements can be potentially replaced by their positron emitting counterparts in a number of compounds

and used as PET imaging agents. The short half-life of certain positron emitting nuclides ($t_{½}$ for O^{15}, N^{13} and C^{11} are 2, 10 and 20 min respectively) poses limit on the applications of the radiotracers because their production requires an on-site cyclotron. Tracers with isotopes of longer half-life such as ^{18}F ($t_{½}$ is 110 min) may overcome such limitation. Advances in radiochemistry could lead to a greater number of radiotracers for PET [16]. PET currently has remarkable impact in the field of oncology as a diagnostic, staging and restaging tool. Furthermore, PET can provide information pertaining to the drugs effectiveness, the potential of PET to influence cancer therapy is significant and its role in anti-cancer drug development and therapy is being increasingly recognized [17].

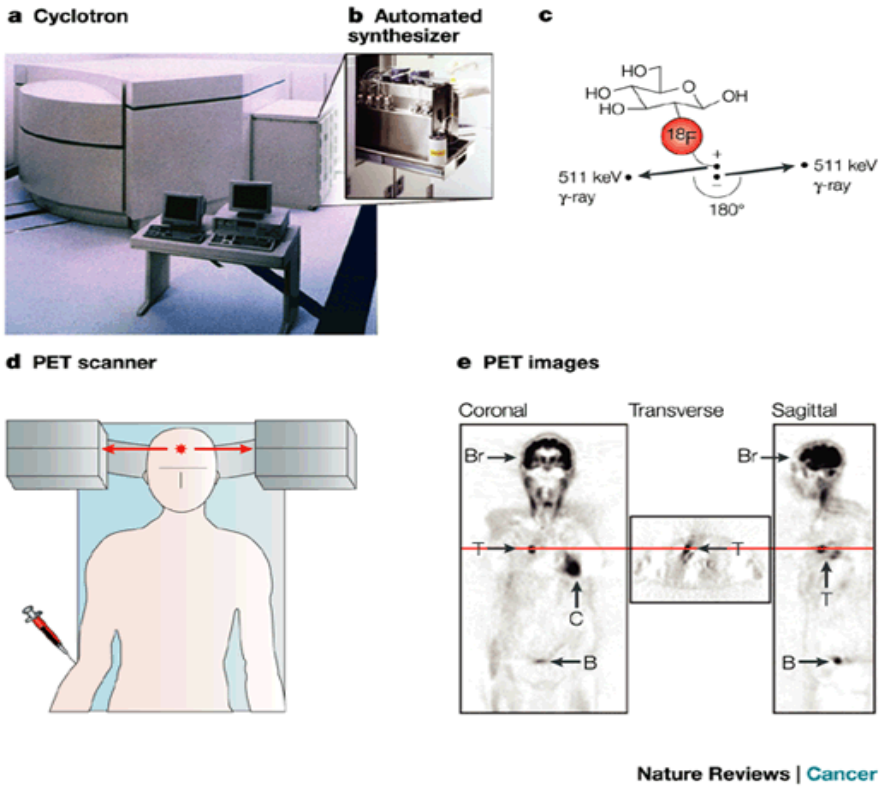

Figure 1.3. Principles of positron emission tomography. a. A cyclotron is used to produce short-lived positron-emitting isotopes. b. Well-established molecular probe can be prepared using automated synthesizers. c. The tracers (e.g. FDG) can be synthesized and intravenously injected. d. The PET scanner can detect the coincident gamma-rays, and images can be reconstructed showing the location(s) and concentration of the tracer of interest. e. Cross-sectional FDG-PET images are shown. Uptake in tumor (T), brain (Br), myocardium (C) and renal excretion into the urinary bladder (B) are visible. Adapted from [2].

1.3 Tumor metabolism imaging

Imaging altered tumor cell metabolism has been tremendously successful in recent years. Numerous studies have shown that various cancers can be detected with high sensitivity and specificity based on their increased metabolic rates for glucose, amino acids or lipids [6] (Figure 1.4). A number of analogs of glucose, choline and amino acids have been developed as PET or SPECT imaging agents and have shown promising clinical results (Table 1.2). Here we will focus on discussion of altered tumor glucose, amino acids and phospholipids metabolism and their clinical applications.

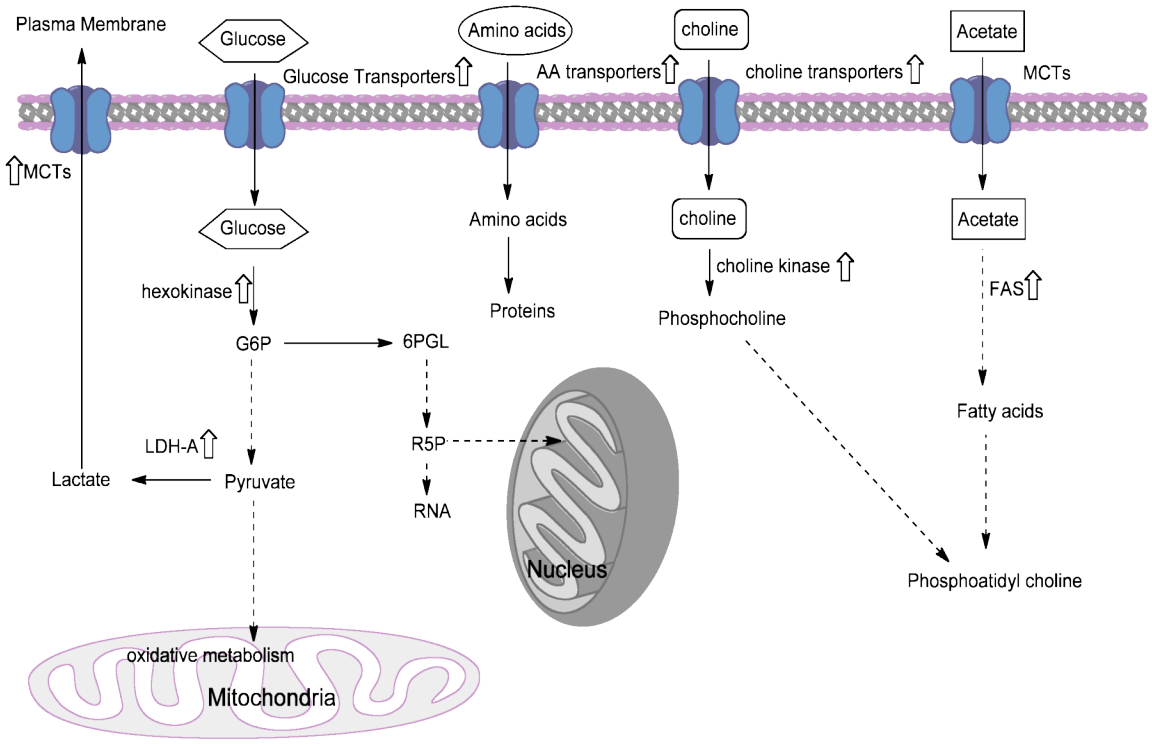

Figure 1.4 Simplified overview of metabolic processes targeted by PET. AA = amino acid; FAS = fatty acid synthase; G6P = glucose-6-phosphate; LDH = lactate dehydrogenase; MCT = monocarboxylate transporter; Ribose 5P = ribose-5-phosphate. Arrows indicates upregulation.

Table 1.2. Selected clinically used tumor metabolic imaging agents for PET
Modified from Vallabhajosula [18]

Radiotracers	Biochemical Process	Mechanism of Uptake or Localization	Reported clinical applications
[^{18}F]FDG	Glucose metabolism	Facilitated diffusion via glucose transporters. Substrate for hexo- kinase in glucose metabolism	Colorectal cancer, melanoma, Non-small cell lung cancer, lymphoma, et al. [18]
[^{11}C]Methionine (MET), [^{18}F]Fluoroethyl tyrosine (FET)	Amino acid transport and protein synthesis	Transport into the cells involves amino acid carrier protein	Brain tumors et al. [19, 20]
[^{11}C]Choline, [^{18}F]Fluorocholine (FCH)	Membrane synthesis	Substrates for choline kinase in choline metabolism	Prostate cancer, brain tumors et al.[21, 22]
[^{11}C]Acetate [^{18}F]Fluoroacetate	Lipid synthesis	Acetate is activated to acetyl-CoA in both the cytosol and mitochondria by acetyl-CoA synthetase	Prostate cancer, brain tumors et al. [23]

1.4 Tumor glucose metabolism and its clinical applications

1.4.1 Tumor glucose metabolism and the development of FDG

The most well known altered metabolism in tumor cells is increased aerobic glycolysis (the Warburg effect). In comparison to normal cells, cancerous cells mainly use glycolysis without entering kreb cycle in mitochondria even when oxygen is present [24]. It seems to be paradoxical as pointed out by Gatenby [25] since cancer cells have high demand for energy while glycolytic metabolism is very inefficient (producing only 2 mol of adenosine triphosphate (ATP) per mole of glucose vs. 36 mol of ATP per mole of glucose for the citric acid cycle) and generates an acidic, potentially toxic environment [26]. It is suggested that increased glycolysis confers survival and growth advantages for cancer cells and it is an adaptation to intermittent hypoxia in malignant lesions [27]. Furthermore, increased glycolysis is result of oncogenic action. Re-programming of gene expression may be an important mechanism for altered tumor cell metabolism. Activation

of oncogenes such as (e.g. HIF1, Akt, Myc [28-30]) or loss of tumor suppressor genes (e.g. p53 [31]) could be the underlying mechanism for increased glycolysis in cancer cells.

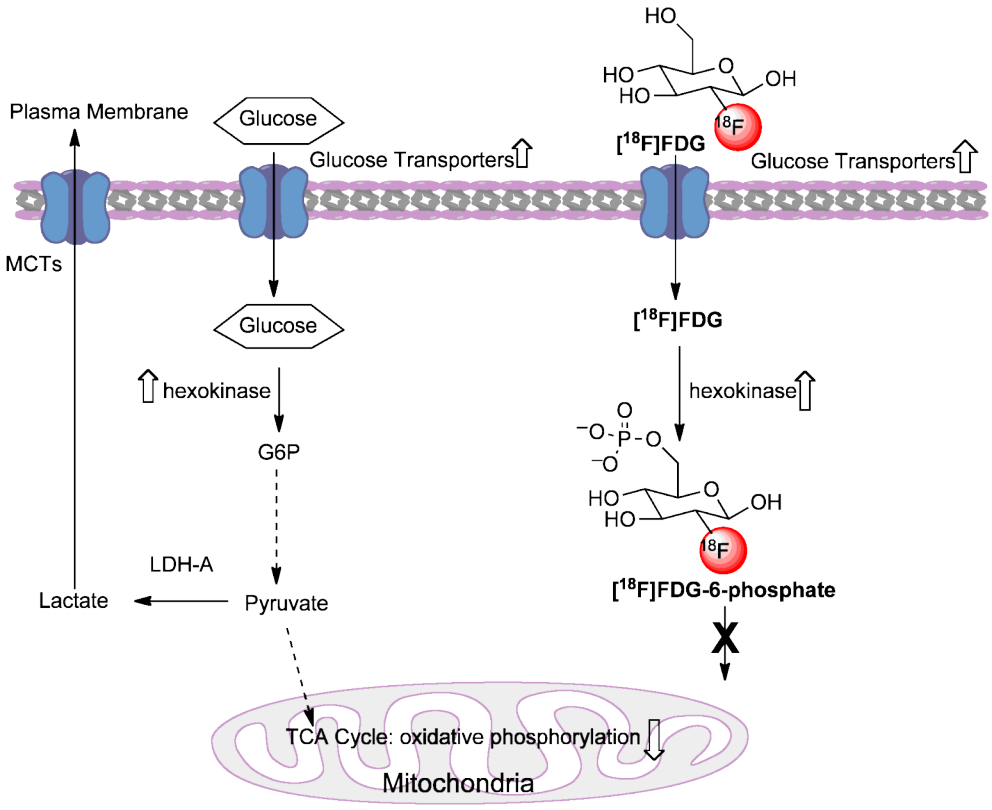

Figure 1.5. The cellular metabolism of glucose and [^{18}F]FDG. G6P = glucose-6-phosphate; LDH = lactate dehydrogenase; MCT = monocarboxylate transporter. Arrows indicates upregulation or downregulation.

1.4.2 Clinical success and limitations of FDG-PET

FDG-PET, which is based on altered tumor glucose metabolism, is the most widely used imaging method by far. It is a routine clinical test for diagnosing, staging, restaging and monitoring therapy for a variety of cancers including lung cancer, lymophoma, colorectal cancer et al [18]. Uptake and trapping of FDG results from upregulation of glucose transporters (GLUT, notably GLUT1 [32], GLUT3 [33] and

GLUT12 [34]) and hexokinase [35]. FDG is transported across the cell membrane by sodium independent, facilitative glucose transporters and is then phosporylated by hexokinase to FDG-6-phosphate (as in Figure 1.5). In contrast to glucose-6-phosphate, which can further be metabolized to fructose-1, 6-biphosphate via glycolysis pathway, FDG-6-phosphate cannot be further metabolized because of substitution of F atom at C2 position. As a result of lack of transporters for FDG-6-phosphate, it is trapped and steadily accumulates in metabolically active tumor cells.

The current clinical applications of FDG in cancer diagnosis and management are very broad [36]. Despite the tremendous success of FDG, it has several well-known drawbacks that limit its applications: 1) the normal brain depends exclusively on glucose metabolism for energy demand. As a result, normal cerebral cortex has high accumulation of FDG. In case of diagnosis of brain tumor, this leads to low contrast making differentiation of tumor from surrounding grey matter difficult; 2) inflammatory cells and macrophages have same level of uptake of FDG as tumor cells, this could cause false-positive results [37]; 3) some tumors do not have increased uptake of FDG thus could not be detected by FDG-PET. The reasons for lack of uptake include relatively low glucose metabolism, as seen in prostate cancer, high mucin content, low proliferation rates and necrosis [38]; 4) FDG has high urinary excretion, because pelvic malignancies such as prostate cancer, urinary bladder carcinoma and renal cell carcinoma, are close to the urinary route, thus can not be satisfactorily visualized via FDG-PET [39]. To overcome these limitations of FDG, various radiopharmaceuticals have been developed for PET studies. We will focus on the advance of amino acid and choline based ligands as

tumor imaging agents in the following sections. The new tracers we developed in this thesis work will be discussed in the meantime.

1.5 Developing new PET tracers for tumor metabolism imaging

Developing new PET tracers is a multidisciplinary process involving selecting desirable targets, organic synthesis, radiolabeling, and in vitro/in vivo biological evaluations before tracers could be used in preclinical or clinical settings [40]. A promising imaging agent for aberrant tumor metabolism should have but not limited to the following properties: 1) ease of synthesis of radioactive ligands and their corresponding non-radioactive precursors and standards; 2) high affinity and selectivity towards enzymes associated with altered tumor metabolism; 3) good in vivo stability; 4) desirable in vivo pharmacokinetics (e.g. fast accumulation in targets, appropriate clearance rate). To evaluate the potential of new tracers as PET imaging agents, in vitro and/or in vivo tests should be performed. In vitro tests such as uptake studies provide a way to test tracers' accumulation in target tumor cells. Protein binding and competition studies allow assessing the affinity and/or selectivity of tracers to the target enzymes. Biodistribution and small animal PET imaging studies in rat or mice tumor models enable evaluation of in vivo pharmacokinetics of the PET tracers. Further metabolites analysis to study tracers' in vivo stability and metabolic pathways could be carried out via HPLC analysis of plasma sample after certain time post-injection. Preclinical evaluations are important and provide insightful information before the new PET tracers go into clinically trials. But the data acquired in these biological evaluations need to be interpreted with caution considering the interspecies difference.

1.5.1 Tumor amino acid metabolism and novel amino acid based tracers

1.5.1.1 Tumor amino acid metabolism

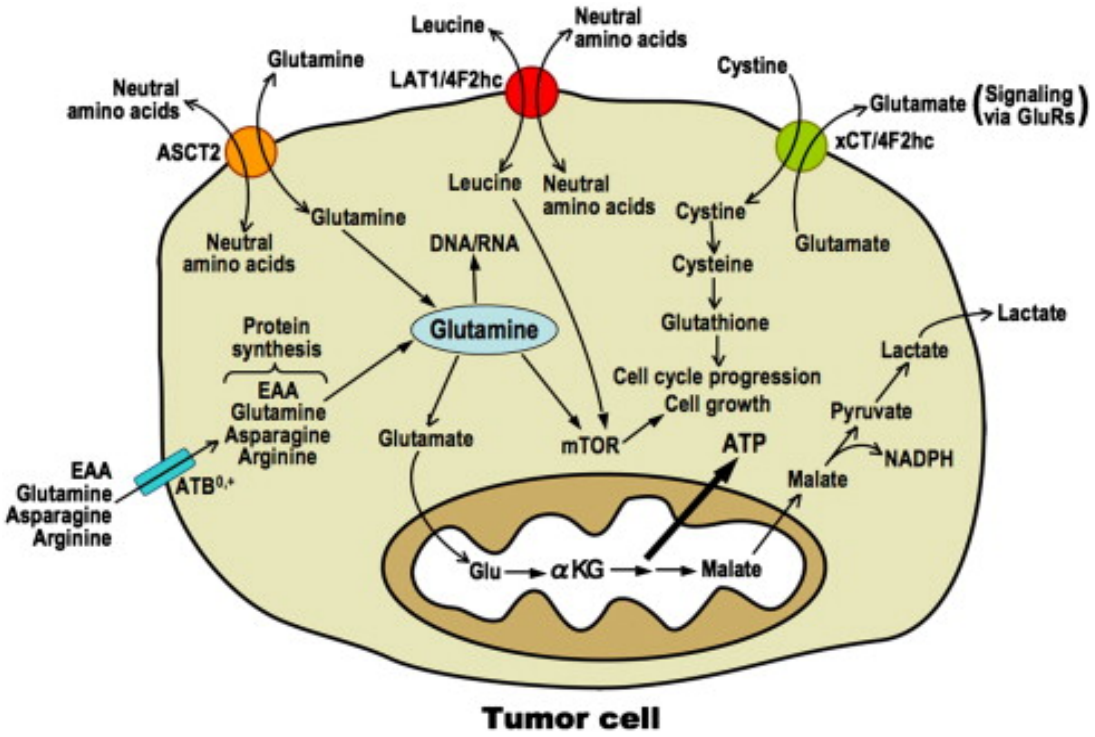

Figure 1.6. Tumor cell amino acid metabolism. There are at least four amino acid transporters that are generally upregulated in tumor cells: ASCT2, LAT1/4F2hc, xCT/4F2hc, and $ATB^{0,+}$. All four transporters participate in providing tumor cells with amino acids necessary for protein synthesis. EAA, essential amino acids; Glu, glutamate; αKG, α-ketoglutarate. Adapted from [41].

Amino acids (AAs) are not only essential for protein synthesis, but also function as an energy source and precursors for biomolecules such as nucleotides, amino sugars and serotonin. Tumor cells have increased transport of amino acids and/or protein synthesis to support their growth and survival (Figure 1.6). The essential mechanisms involved in uptake of amino acids are the carrier-mediated transport into cells and the esterification of the amino acids to form the aminoacyl-t-RNA, which forms the polypeptide chain in the ribosome (incorporation into protein). Of these two mechanisms, transport and incorporation into protein, uptake of amino acid tracers is generally

dominated by carrier-mediated transport [42-44]. So amino acid transporters have been the main focus of the development of amino acid tracers in recent years.

Amino acid transporters are classified into distinct systems based on ion dependence, substrate selectivity, sensitivity to selective inhibitors, kinetics, regulatory properties et al [45]. A number of amino acid transport systems have been shown to be upregulated in a variety of cancer cell lines and play important roles for tumor growth and survival (Table 1.3). System L (LATs), in particular its subtype LAT1, has attracted special interest. It is a promising target for imaging agents and cancer therapy for a number of reasons: 1) elevated expression correlates well with tumor growth and poor prognosis [46]; 2) low expression in normal and inflammatory tissues ensuring high tumor specificity [47]; 3) pivotal in transport of amino acids through blood-brain barrier [48]; 4) plays important role in transporting certain anti-cancer drugs such as melphalan [49]; 5) inhibition of LAT1 suppresses cancer growth [50]; 6) substrates of LATs have demonstrated promising clinical imaging results (as shown in Table 1.4).

Table 1.3. Major amino acid transport system upregulated in cancer cells

System	Protein	Na^+ dependence	Substrate specificity	Comments
A	SAT1 SAT2 SAT3	Na^+ dependent	Short, polar, straight chain AAs such as Gly and Ala,	Influx transporter, inducible by starvation, hormones, growth factors [51]
ASC	ASCT1 ASCT2	Na^+ dependent	Small polar AAs such as Ala, Ser,Cys, Gln et al	Upregulation observed in prostate cancer and colorectal carcinoma [52, 53]
$B^{0,+}$	$ATB^{0,+}$	Na^+ dependent	Neutral and cationic amino acids such as Gln, Lys et al,	Broad substrate selectivity, accepts 18 of 20 natural amino acids, induced in cervical cancer and colorectal cancer [54, 55]
L	LAT1 LAT2 LAT3 LAT4	Na^+ independent	Large branched neutral AAs such as Phe, Tyr, Met, Trp et al	Broad substrate selectivity, subytpe LAT1 can accept D-isomer, upregulation has been observed in brain, colon, lung, liver and skin cancers [56]

1.5.1.2 Clinical applications of amino acid based tracers

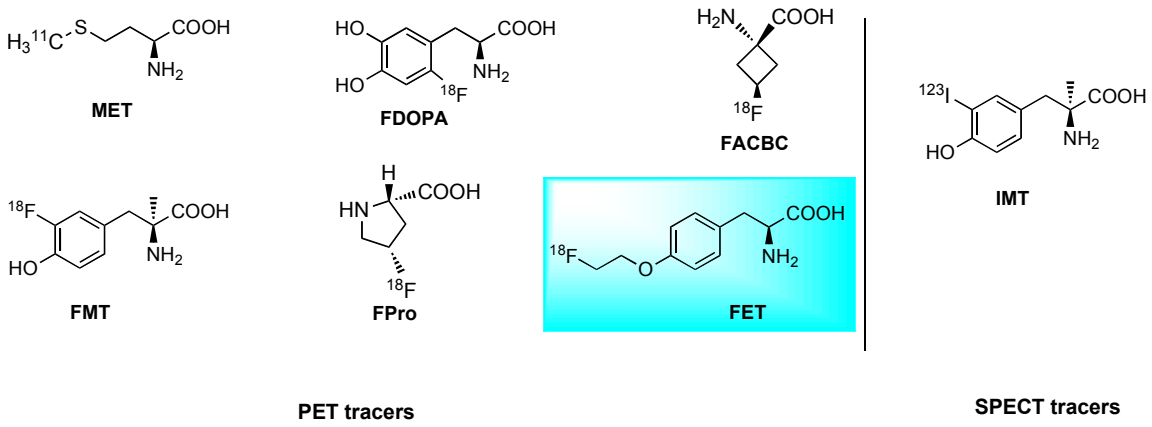

Figure 1.7. Structures of clinically utilized amino acid based tracers.

Table 1.4. Selected clinically utilized amino acid tracers and their uptake mechanism.

Tracers	Transport mechanism	Clinical applications	Comments
MET	A; LATs [57]	Brian tumors, head and neck, lung, malignant lymphomas, and breast cancer	Short half life, high excretion through bladder, complicate in vivo metabolism
IMT	LATs [58, 59]	Brian tumor, non-small cell lung cancer	May not differentiate low grade glioma from non-neoplasmatic lesions or high grade gliomas
FPro	A; PAT1 [60]	Brain tumors	Uptake is limited to areas of blood brain barrier disruption
FDOPA	LATs [61]*	Parkinson's disease	Substrate for aromatic amino acid decarboxylase, undergoes extensive in vivo metabolism with multiple metabolites
FACBC	LATs [62]	Brain tumor, prostate cancers and renal cell carcinomas	Low urinary excretion
FET	LATs; $B^{0,+}$ contribute to a lesser extent [20]	Brain tumor, head and neck cancer	Efficient labeling process, limited applications in extracranial tumors (negligible uptake in peripheral tumors such as breast cancer, lung cancer, lymphomas)

Currently, the most widely used amino acid based tracer is [^{11}C]methionine (MET), which has proven useful for imaging brain, head and neck, lung, malignant lymphomas, and breast cancer [19, 63]. However, it has high uptake in liver, pancreas,

and intestine and is excreted through the bladder, characteristics that interfere with tumor imaging in the abdominal region and in the region of the bladder or prostate. Its uptake also reflects non-protein metabolic pathways such as transamination and transmethylation, which makes imaging kinetic analysis difficult [64]. In additional, short half-life of ^{11}C necessitates onsite cyclotron, limiting its clinical applications. This led to the development of non-natural amino acid labeled with longer half-life isotopes such as ^{18}F and ^{123}I. A variety of tyrosine and phenylalanine derivatives have been developed for tumor imaging (Figure 1.7) such as 3-[^{123}I]-α-methyl-L-tyrosine (IMT) [59], 3-[^{18}F]fluoro-α-methyl-L-tyrosine (FMT) [65], 3,4-dihydroxy-6-[^{18}F]fluorophenylalanine (FDOPA) [66], and *O*-(2-[^{18}F]fluoroethyl)-L-tyrosine (FET) [20]. Other compounds such as cyclic 1-amino-3-[^{18}F]fluorocyclobutane-1-carboxylic acid (FACBC) [67] and proline derivatives *cis*-4-[^{18}F]fluoro-L-proline (FPro) [68] have also been clinically used. As we can see from Table 1.4, system L represents the major underlying uptake mechanism for these amino acid tracers.

1.5.1.3 Design of novel aromatic amino acids derivatives

As we stated in section 1.5.1, system L, in particular its subtype LAT1, is a promising target for developing amino acid based tracers. For a radiotracer to be clinically successfully and reflect specific protein activity associated with altered tumor metabolism, it should have efficient radiolabeling process, high selectivity and/or affinity towards target protein, desirable in vivo kinetics, and stability in vitro and in vivo. From studying substrate recognition for LAT1 [69], it is proposed that for a ligand to be substrate for LAT1, it should satisfy the following requirements (as shown in Figure 1.8):

1) have a free carboxyl and an amino group; 2) The carbonyl oxygen in the binding site needs an appropriate polarity and must not participate in hydrogen bonding; 3) desirable hydrophobic interaction in the side change.

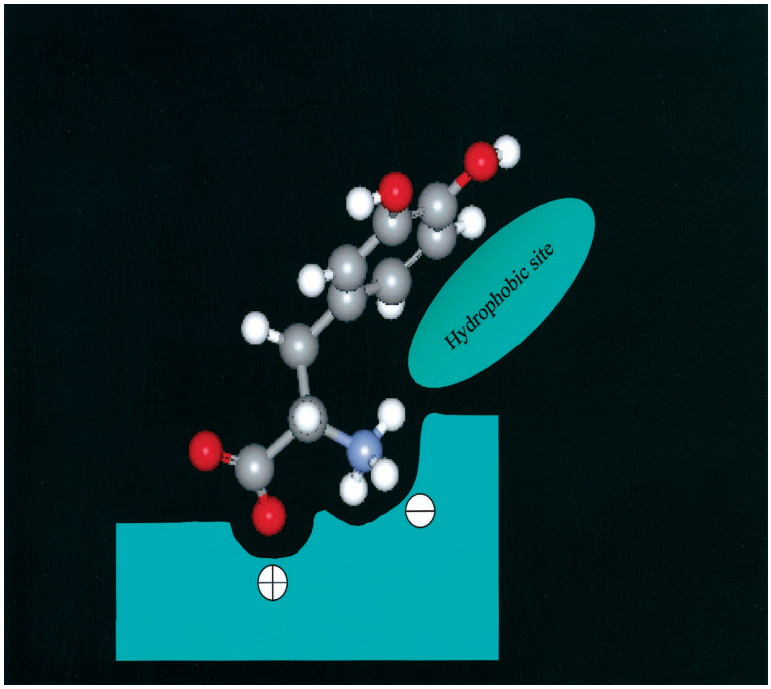

Figure 1.8. Proposed model for the substrate-binding sites of LAT1. 3,4-dihydroxy L-phenylalanine (DOPA) used as the model compound. Adapted from [68].

There are no extensive quantitative studies on structure-activity of LATs. In search of new amino acid based tracers with potential improved imaging characteristics, we chose one of clinically established LATs L-[^{18}F]FET, as our reference tracer and parent compound for further modification. L-[^{18}F]FET is one of the first ^{18}F labeled amino acid based tracers that could be produced in a large quantity for clinically use and satellite distribution similar to FDG. It has high radiochemical yield, low accumulation in normal brain and peripheral tissues, rapid tumor uptake, and good in vivo stability and has established clinically applications in imaging brain tumors and head and neck cancer [20, 70, 71]. However, it has negligible accumulations in many extracranial tumors and

high urinary excretion, which limit its applications [72]. Using the fluoroalkyl tyrosine core structure of L-[^{18}F]FET as the lead, modifications (as Figure 1.9) were made to structure to probe the affinity and selectivity for amino acid transporters.

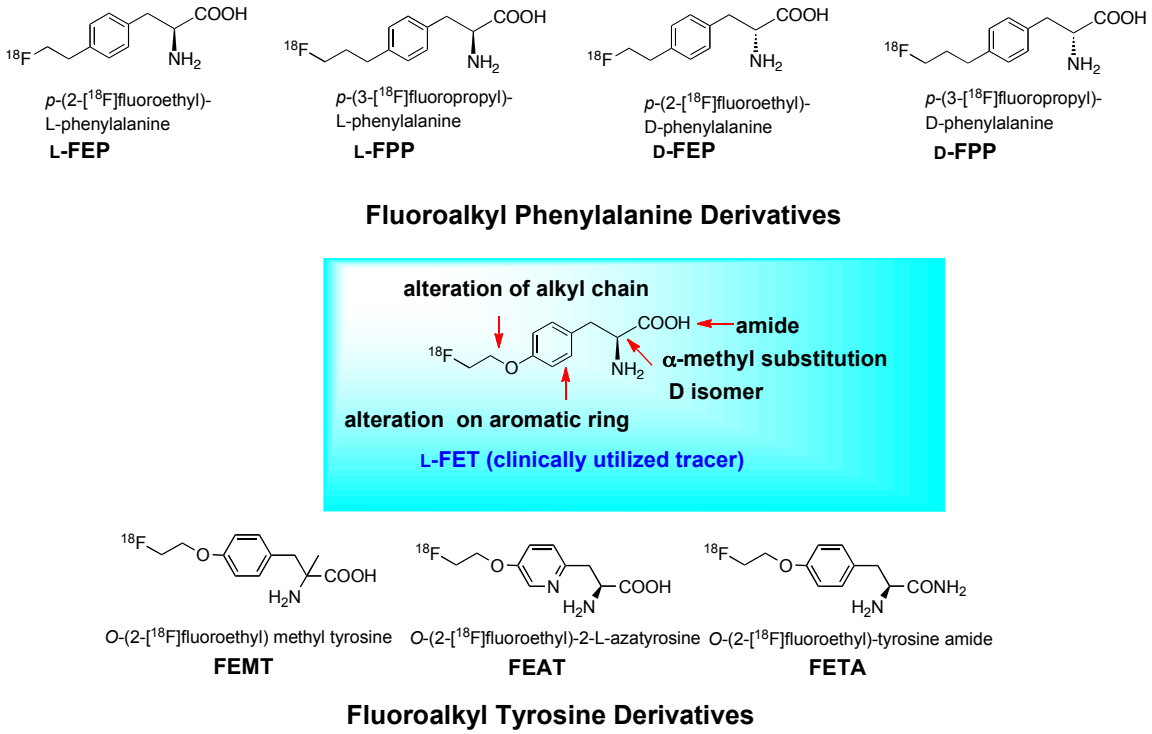

Figure 1.9 Design of novel aromatic amino acid derivatives as potential PET imaging agents

In designing this new series of amino acid tracers, we kept alkyl chain as the linker for ^{18}F. In this way, ^{18}F can be incorporated in to the target molecule through a direct nucleophilic reaction to form fluroalkyl side chain, which generally has high radiochemical yield. From α-methyl substitution (FEMT), alteration in aromatic ring (FEAT) and change of carboxyl group to amide (FETA), a series of tyrosine derivatives were prepared. Via alteration in alkyl chain (i.e. elimination of oxygen atom may enhance the hydrophobic interaction with LAT1), we developed a series of phenylalanine derivatives (FEP and FPP). Because LAT1 could transport D-isomers of phenylalaine, we also prepared the D-isomers of the phenylalanine derivatives. One of the FET analog, L-

isomer of FEP was found to be transported predominately via LATs and demonstrated preference towards subtype LAT1. The selectivity for LATs does not guarantee that a radiotracer will be potential useful imaging agents for increased amino acid transport activity in tumor cells. In vivo studies such as kinetic studies and imaging studies need to be executed to determine whether tumors could be appropriately imaged.

1.5.2 Tumor phospholipid metabolism and new ethanolamine tracers

1.5.2.1 Tumor phospholipid metabolism

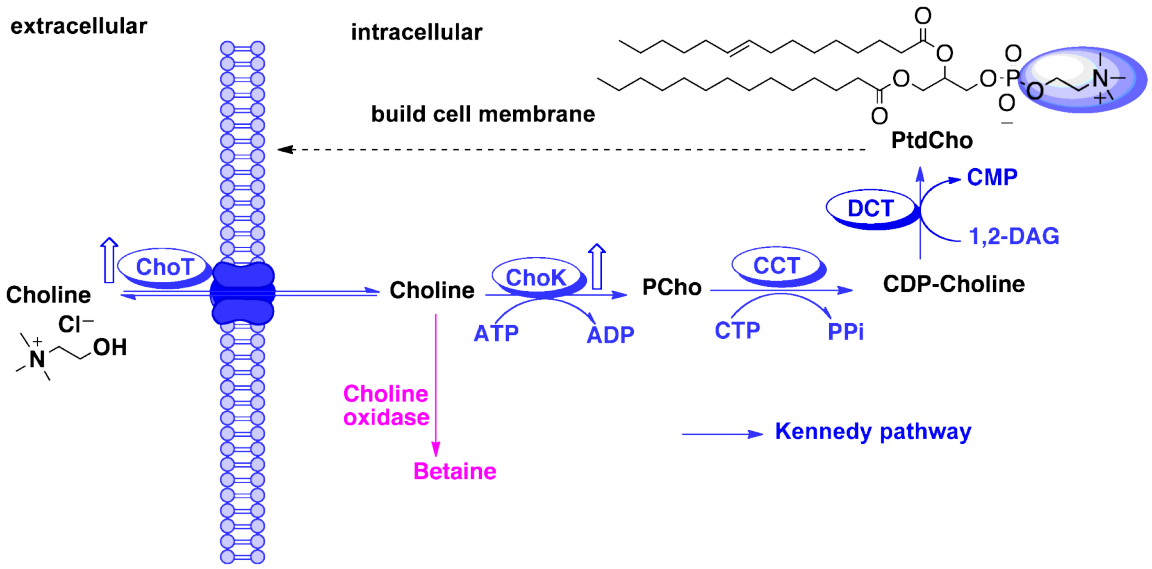

Figure 1.10 Choline phospholipid metabolism. Metabolites are given in bold letters. CCT = CTP:phosphocholine cytidylyltransferase; ChoT = choline transporters; ChoK = Choline kinase; PCho = phosphocholine; PtdCho = phosphoatidyl choline; Arrows indicates upregulation.

Phosphoglycerides are important in formation of cellular and organelle membranes in rapidly growing tumors. The elevation of phosphocholine (PCho) or phosphoethanolamine (PEtn) is one of widely established characteristics of cancer cells [73]. Numerous in vivo and in vitro ^{1}H and ^{31}P MR spectroscopic studies have detected

high levels of PCho or PEtn, or both, in a variety of cancers such as breast, prostate, and different types of brain tumors, whereas low levels of these metabolites were found in corresponding normal tissues [74, 75]. These studies demonstrate the significance of phospholipid precursors and catabolites as biochemical indicators of tumor progression and response to therapy. Most notable mechanisms underlying the increased PCho levels (as in Figure 1.10) include increased expression and activity of choline kinase [76, 77], a higher rate of choline transport [78], and increased phospholipase (PLD) [79]. Choline kinase (ChoK) phosphorylates free choline to PCho in the CDP-Choline pathway (or kennedy pathway). ChoK is considered to be an important target for cancer because it regulates oncogene activation and correlates with tumor growth and prognosis [80, 81].

1.5.2.2 Clinical applications of choline and its derivatives

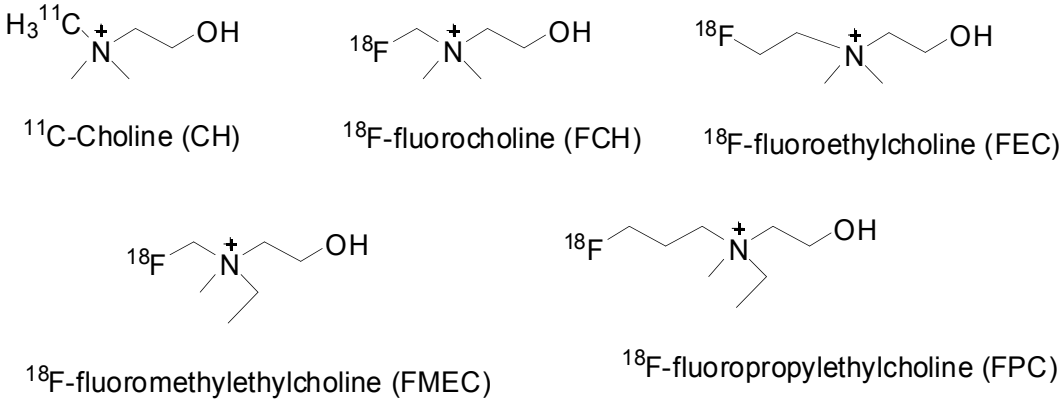

Figure 1.11. Choline and its derivatives as PET imaging agents

Choline ([^{11}C]CH) and its derivatives (Figure 1.11) have been developed as biomarkers for aberrant choline phospholipids metabolism in tumors. In particular, [^{11}C]CH and [^{18}F]FCH-PET are valuable tools for imaging prostate cancer, breast carcinoma, and brain tumors [82, 83]. But [^{11}C]CH and its derivatives have limitations

including high bladder uptake and high radiation dose to kidney, liver and spleen [84]. The most activity accumulates into the liver and kidney because choline oxidase oxidazes choline into betaine and causes activity to be trapped there.

1.5.2.3 Rational for new ^{11}C labeled ethanolamine and its derivatives

[^{11}C]ethanolamine (EA) [^{11}C]*N*-methyl ethanolamine (MEA) [^{11}C]*N, N*-Dimethyl ethanolamine (DMEA)

Figure 1.12. ^{11}C labeled ethanolamine and its derivatives

Elevated PEtn concentration is found to be even higher than PCho in a variety of tumors [85, 86]. Ethanolamine is subject to biosynthetic pathway for phosphoatidylethanolamine (major phospholipid component in cell membrane) similar to choline [87, 88]. This might be an indication that ethanolamine, the precursor of PEtn, could be a potential useful and more sensitive imaging agents than choline for tumor phospholipids metabolism.

We first conducted preliminary studies using ^{14}C labeled ethanolamine and N, N'-dimethyl ethanolamine to validate the potential of ethanolamine tracers for tumor detection. The results demonstrated that ^{14}C labeled ethanolamine tracers were taken up significantly better (2-7 fold) than [^{14}C]choline in a wide variety of tumor cells including colorectal cancer (HCT116), prostate (PC-3), melanoma (A375 and 1618), glioblastoma (SF767, A172), and lymphoma (DLCL2) [89]. Since ^{11}C labeled compound would behave the same as their natural and ^{14}C labeled counterpart, we hypothesize that ^{11}C labeled ethanolamine and its derivatives could potentially be more sensitive biomarkers for tumor phospholipid metabolism than [^{11}C]CH. We then proceeded with the synthesis

and biological evaluations of the series of ^{11}C labeled ethanolamine and its derivatives (Figure 1.12).

1.6 Scope of the thesis research

The ultimate goal of this thesis work is to develop new PET tracers with better imaging properties than current clinically utilized imaging agents for certain types of tumors such as brain tumor and prostate cancer based on altered tumor metabolism. This thesis work included early radiopharmaceuticals discovery phase up to preclinical PET imaging studies in rats. Chapter two to four describes the development of new ^{18}F labeled aromatic amino acid derivatives as potential PET imaging agents based on tumor amino acid metabolism. Chapter two covers the synthesis of a series of new fluoroethyl tyrosine derivatives and their in vitro characterization through cell uptake studies in the human glioma cell line. Chapter three describes the preparation of fluoroalkyl phenylalanine derivatives and their biological evaluations including in vitro evaluations through cell uptake studies and uptake mechanism characterization and in vivo characterization through biodistribution and small animal PET imaging studies. Chapter four describes comparative studies of D- and L-isomers of fluoroalkyl phenylalanine derivative via in vitro cell uptake and transport characterization and in vivo PET imaging studies in rats. Chapter five covers the development of new ^{11}C labeled ethanolamine derivatives as potential PET tracers based on tumor phospholipid metabolism. Preliminary studies of ^{14}C ethanolamine and its derivatives, labeling of ^{11}C ligands and in vitro studies in prostate cancer cell lines are described.

1.7 Clinical significance of this work

Metabolic imaging has a significant impact on patient management by improving tumor staging, treatment planning and monitoring response to therapy. There is growing evidence demonstrating a close link between oncogene activation and metabolic change in cancer cells. Altered tumor metabolism is increasingly considered to represent a group of promising therapeutic targets, and tumor metabolic imaging provides a way to monitor such targeted therapies [3]. Increased amino acid transporter activity and choline/ethanolamine phospholipids metabolism are observed in a wide variety of cancers. It is our hope that these novel metabolic tracers could provide better tools for imaging altered amino acid transport and phospholipid metabolism in tumors.

1.8 Reference

[1] Warburg O, Posener K, and Negelein E. The metabolism of the carcinoma cell. Zeitschrift 1924;152:319-44.

[2] Gambhir SS. Molecular imaging of cancer with positron emission tomography. Nat Rev Cancer 2002;2:683-93.

[3] Kroemer G and Pouyssegur J. Tumor Cell Metabolism: Cancer's Achilles' Heel. Cancer Cell 2008;13:472-82.

[4] DeBerardinis RJ, Lum JJ, Hatzivassiliou G, and Thompson CB. The biology of cancer: metabolic reprogramming fuels cell growth and proliferation. Cell Metab 2008;7:11-20.

[5] Hsu PP and Sabatini DM. Cancer Cell Metabolism: Warburg and Beyond. 2008;134:703-7.

[6] Plathow C and Weber WA. Tumor cell metabolism imaging. J Nucl Med 2008;49 Suppl 2:43S-63S.

[7] von Schulthess GK, Steinert HC, and Hany TF. Integrated PET/CT: current applications and future directions. Radiology 2006;238:405-22.

[8] Catana C, Wu Y, Judenhofer MS, Qi J, Pichler BJ, and Cherry SR. Simultaneous acquisition of multislice PET and MR images: initial results with a MR-compatible PET scanner. J Nucl Med 2006;47:1968-76.

[9] Glunde K, Artemov D, Penet MF, Jacobs MA, and Bhujwalla ZM. Magnetic resonance spectroscopy in metabolic and molecular imaging and diagnosis of cancer. Chemical reviews 2010;110:3043-59.

[10] Golman K, Zandt RI, Lerche M, Pehrson R, and Ardenkjaer-Larsen JH. Metabolic imaging by hyperpolarized 13C magnetic resonance imaging for in vivo tumor diagnosis. Cancer Res 2006;66:10855-60.

[11] Massoud TF and Gambhir SS. Molecular imaging in living subjects: seeing fundamental biological processes in a new light. Genes & development 2003;17:545-80.

[12] Jaffer FA and Weissleder R. Molecular imaging in the clinical arena. Jama 2005;293:855-62.

[13] Wernick MN, Aarsvold, John N. Emission Tomography: The Fundamentals of PET and SPECT, San Diego: Elsevier Academic Press,2004.

[14] Rahmim A and Zaidi H. PET versus SPECT: strengths, limitations and challenges. Nucl Med Commun 2008;29:193-207.

[15] Alavi A and Basu S. Planar and SPECT imaging in the era of PET and PET-CT: can it survive the test of time? Eur J Nucl Med Mol Imaging 2008;35:1554-9.

[16] Wadsak W and Mitterhauser M. Basics and principles of radiopharmaceuticals for PET/CT. European journal of radiology 2010;73:461-9.

[17] Laing RE, Nair-Gill E, Witte ON, and Radu CG. Visualizing cancer and immune cell function with metabolic positron emission tomography. Curr opinion gen dev;20:100-5.

[18] Czernin J. Clinical applications of FDG-PET in oncology. Acta medica Austriaca 2002;29:162-70.

[19] Singhal T, Narayanan TK, Jain V, Mukherjee J, and Mantil J. 11C-L-methionine positron emission tomography in the clinical management of cerebral gliomas. Mol Imaging Biol 2008;10:1-18.

[20] Langen KJ, Hamacher K, Weckesser M, Floeth F, Stoffels G, Bauer D, et al. O-(2-[18F]fluoroethyl)-L-tyrosine: uptake mechanisms and clinical applications. Nucl Med Biol 2006;33:287-94.

[21] Hara T, Kosaka N, Shinoura N, and Kondo T. PET imaging of brain tumor with [methyl-11C]choline. J Nucl Med 1997;38:842-7.

[22] DeGrado TR, Coleman RE, Wang S, Baldwin SW, Orr MD, Robertson CN, et al. Synthesis and evaluation of 18F-labeled choline as an oncologic tracer for positron emission tomography: initial findings in prostate cancer. Cancer research 2001;61:110-7.

[23] Oyama N, Miller TR, Dehdashti F, Siegel BA, Fischer KC, Michalski JM, et al. 11C-acetate PET imaging of prostate cancer: detection of recurrent disease at PSA relapse. J Nucl Med 2003;44:549-55.

[24] Racker E. History of Pasteur Effect and Its Pathobiology. Mol Cell Biochem 1974;5:17-23.

[25] Gatenby RA and Gillies RJ. Why do cancers have high aerobic glycolysis? Nat Rev Cancer 2004;4:891-9.

[26] Rich PR. The molecular machinery of Keilin's respiratory chain. Biochem Soc trans 2003;31:1095-105.

[27] Gatenby RA and Gillies RJ. A microenvironmental model of carcinogenesis. Nat Rev Cancer 2008;8:56-61.

[28] Denko NC. Hypoxia, HIF1 and glucose metabolism in the solid tumour. Nat Rev Cancer 2008.

[29] Elstrom RL, Bauer DE, Buzzai M, Karnauskas R, Harris MH, Plas DR, et al. Akt stimulates aerobic glycolysis in cancer cells. Cancer research 2004;64:3892-9.

[30] Shim H, Dolde C, Lewis BC, Wu CS, Dang G, Jungmann RA, et al. c-Myc transactivation of LDH-A: implications for tumor metabolism and growth. Proc Natl Acad Sci U S A 1997;94:6658-63.

[31] Smith TA, Sharma RI, Thompson AM, and Paulin FE. Tumor 18F-FDG incorporation is enhanced by attenuation of P53 function in breast cancer cells in vitro. J Nucl Med 2006;47:1525-30.

[32] Macheda ML, Rogers S, and Best JD. Molecular and cellular regulation of glucose transporter (GLUT) proteins in cancer. J cell phys 2005;202:654-62.

[33] Kawauchi K, Araki K, Tobiume K, and Tanaka N. p53 regulates glucose metabolism through an IKK-NF-kappaB pathway and inhibits cell transformation. Nat cell bio 2008;10:611-8.

[34] Chandler JD, Williams ED, Slavin JL, Best JD, and Rogers S. Expression and localization of GLUT1 and GLUT12 in prostate carcinoma. Cancer 2003;97:2035-42.

[35] Mathupala SP, Rempel A, and Pedersen PL. Aberrant glycolytic metabolism of cancer cells: a remarkable coordination of genetic, transcriptional, post-translational, and mutational events that lead to a critical role for type II hexokinase. J bioenerg biomembr 1997;29:339-43.

[36] Gambhir SS, Czernin J, Schwimmer J, Silverman DH, Coleman RE, and Phelps ME. A tabulated summary of the FDG PET literature. J Nucl Med 2001;42:1S-93S.

[37] Kubota R, Yamada S, Kubota K, Ishiwata K, Tamahashi N, and Ido T. Intratumoral distribution of fluorine-18-fluorodeoxyglucose in vivo: high accumulation in macrophages and granulation tissues studied by microautoradiography. J Nucl Med 1992;33:1972-80.

[38] Mathews D, Anderson J, and Oz O. Diagnostic dilemmas in PET/CT. Non FDG avid malignancies. J Nucl Med Meeting Abs 2007;48:215P.

[39] Schoder H and Larson SM. Positron emission tomography for prostate, bladder, and renal cancer. Semi Nucl Med 2004;34:274-92.

[40] Serdons K, Verbruggen A, and Bormans GM. Developing new molecular imaging probes for PET. Methods (San Diego, Calif) 2009;48:104-11.

[41] Ganapathy V, Thangaraju M, and Prasad PD. Nutrient transporters in cancer: relevance to Warburg hypothesis and beyond. Pharmacol Ther 2009;121:29-40.

[42] Couturier O, Luxen A, Chatal J-F, Vuillez J-P, Rigo P, and Hustinx R. Fluorinated tracers for imaging cancer with positron emission tomography. Eur J Nucl Med Mol Imaging 2004;31:1182-206.

[43] McConathy J and Goodman Mark M. Non-natural amino acids for tumor imaging using positron emission tomography and single photon emission computed tomography. Cancer metastasis rev 2008;27:555-73.

[44] Laverman P, Boerman OC, Corstens FHM, and Oyen WJG. Fluorinated amino acids for tumour imaging with positron emission tomography. Eur J Nucl Med Mol Imaging 2002;29:681-90.

[45] Palacin M, Estevez R, Bertran J, and Zorzano A. Molecular biology of mammalian plasma membrane amino acid transporters. Physiol Rev 1998;78:969-1054.

[46] Kaira K, Oriuchi N, Imai H, Shimizu K, Yanagitani N, Sunaga N, et al. l-type amino acid transporter 1 and CD98 expression in primary and metastatic sites of human neoplasms. Cancer Sci 2008;99:2380-6.

[47] Yanagida O, Kanai Y, Chairoungdua A, Kim DK, Segawa H, Nii T, et al. Human L-type amino acid transporter 1 (LAT1): characterization of function and expression in tumor cell lines. Biochim Biophys Acta 2001;1514:291-302.

[48] Christensen HN. Role of amino acid transport and countertransport in nutrition and metabolism. Physiol Rev 1990;70:43-77.

[49] del Amo EM, Urtti A, and Yliperttula M. Pharmacokinetic role of L-type amino acid transporters LAT1 and LAT2. Eur J Pharm Sci 2008;35:161-74.

[50] Shennan DB and Thomson J. Inhibition of system L (LAT1/CD98hc) reduces the growth of cultured human breast cancer cells. Oncology reports 2008;20:885-9.

[51] McGivan JD and Pastor-Anglada M. Regulatory and molecular aspects of mammalian amino acid transport. Biochem J 1994;299 (Pt 2):321-34.

[52] Witte D, Ali N, Carlson N, and Younes M. Overexpression of the neutral amino acid transporter ASCT2 in human colorectal adenocarcinoma. Anticancer research 2002;22:2555-7.

[53] Li R, Younes M, Frolov A, Wheeler TM, Scardino P, Ohori M, et al. Expression of neutral amino acid transporter ASCT2 in human prostate. Anticancer research 2003;23:3413-8.

[54] Gupta N, Miyauchi S, Martindale RG, Herdman AV, Podolsky R, Miyake K, et al. Upregulation of the amino acid transporter ATB0,+ (SLC6A14) in colorectal cancer and metastasis in humans. Biochimica et biophysica acta 2005;1741:215-23.

[55] Gupta N, Prasad PD, Ghamande S, Moore-Martin P, Herdman AV, Martindale RG, et al. Up-regulation of the amino acid transporter ATB(0,+) (SLC6A14) in carcinoma of the cervix. Gynecologic oncology 2006;100:8-13.

[56] Fuchs BC and Bode BP. Amino acid transporters ASCT2 and LAT1 in cancer: partners in crime? Semin Cancer Biol 2005;15:254-66.

[57] Okubo S, Zhen HN, Kawai N, Nishiyama Y, Haba R, and Tamiya T. Correlation of L-methyl-11C-methionine (MET) uptake with L-type amino acid transporter 1 in human gliomas. J Neurooncol;99:217-25.

[58] Jager PL, De Vries EGE, Piers DA, and Timmer-Bosscha H. Uptake mechanisms of L-3-[125I]iodo-alpha-methyl-tyrosine in a human small-cell lung cancer cell line: comparison with L-1-[14C]tyrosine. Nucl Med Commun 2001;22:87-96.

[59] Langen K-J, Pauleit D, and Coenen HH. 3-[123I]iodo-a-methyl-L-tyrosine: uptake mechanisms and clinical applications. Nucl Med Bio 2002;29:625-31.

[60] Metzner L, Neubert K, and Brandsch M. Substrate specificity of the amino acid transporter PAT1. Amino acids 2006;31:111-7.

[61] Stout DB, Huang SC, Melega WP, Raleigh MJ, Phelps ME, and Barrio JR. Effects of large neutral amino acid concentrations on 6-[F-18]Fluoro-L-DOPA kinetics. J Cereb Blood Flow Metab 1998;18:43-51.

[62] Yu W, Williams L, Camp VM, Olson JJ, and Goodman MM. Synthesis and biological evaluation of anti-1-amino-2-[18F]fluoro-cyclobutyl-1-carboxylic acid (anti-2-[18F]FACBC) in rat 9L gliosarcoma. Bioorg Med Chem Lett 2010;20:2140-3.

[63] Jager PL, Vaalburg W, Pruim J, de Vries EG, Langen KJ, and Piers DA. Radiolabeled amino acids: basic aspects and clinical applications in oncology. Journal of nuclear medicine 2001;42:432-45.

[64] Fujibayashi Y, Kawai K, Yonekura Y, Matsumoto K, Konishi J, and Yokoyama A. Problems of [S-methyl-11C]-L-methionine as a protein synthesis marker in the pancreas. Ann Nucl Med 1990;4:29-33.

[65] Kaira K, Oriuchi N, Shimizu K, Ishikita T, Higuchi T, Imai H, et al. Evaluation of thoracic tumors with (18)F-FMT and (18)F-FDG PET-CT: a clinicopathological study. Intern J cancer 2009;124:1152-60.

[66] Nurmi E, Ruottinen HM, Bergman J, Haaparanta M, Solin O, Sonninen P, et al. Rate of progression in Parkinson's disease: a 6-[18F]fluoro-L-dopa PET study. Movement Disorders 2001;16:608-15.

[67] Schuster DM, Votaw JR, Nieh PT, Yu W, Nye JA, Master V, et al. Initial experience with the radiotracer anti-1-amino-3-18F-fluorocyclobutane-1-carboxylic acid with PET/CT in prostate carcinoma. J Nucl Med 2007;48:56-63.

[68] Langen KJ, Jarosch M, Hamacher K, Muhlensiepen H, Weber F, Floeth F, et al. Imaging of gliomas with Cis-4-[18F]fluoro-L-proline. Nucl Med Biol 2004;31:67-75.

[69] Uchino H, Kanai Y, Kim DK, Wempe MF, Chairoungdua A, Morimoto E, et al. Transport of amino acid-related compounds mediated by L-type amino acid transporter 1 (LAT1): insights into the mechanisms of substrate recognition. Mol pharma 2002;61:729-37.

[70] Rau FC, Weber WA, Wester HJ, Herz M, Becker I, Kruger A, et al. O-(2-[(18)F]Fluoroethyl)- L-tyrosine (FET): a tracer for differentiation of tumour from inflammation in murine lymph nodes. Eur J Nucl Med Mol Imaging 2002;29:1039-46.

[71] Balogova S, Perie S, Kerrou K, Grahek D, Montravers F, Angelard B, et al. Prospective comparison of FDG and FET PET/CT in patients with head and neck squamous cell carcinoma. Mol Imaging Biol 2008;10:364-73.

[72] Pauleit D, Stoffels G, Schaden W, Hamacher K, Bauer D, Tellmann L, et al. PET with O-(2-18F-Fluoroethyl)-L-Tyrosine in peripheral tumors: first clinical results. J Nucl Med 2005;46:411-6.

[73] Ackerstaff E, Glunde K, and Bhujwalla ZM. Choline phospholipid metabolism: a target in cancer cells? J Cell Biochem 2003;90:525-33.

[74] Negendank W. Studies of human tumors by MRS: a review. NMR Biomed 1992;5:303-24.

[75] De Certaines JD, Larsen VA, Podo F, Carpinelli G, Briot O, and Henriksen O. In vivo 31P MRS of experimental tumours. NMR Biomed 1993;6:345-65.

[76] Ramirez de Molina A, Penalva V, Lucas L, and Lacal JC. Regulation of choline kinase activity by Ras proteins involves Ral-GDS and PI3K. Oncogene 2002;21:937-46.

[77] Ramirez de Molina A, Rodriguez-Gonzalez A, Gutierrez R, Martinez-Pineiro L, Sanchez J, Bonilla F, et al. Overexpression of choline kinase is a frequent feature in human tumor-derived cell lines and in lung, prostate, and colorectal human cancers. Biochem Biophys Res Commun 2002;296:580-3.

[78] Katz-Brull R and Degani H. Kinetics of choline transport and phosphorylation in human breast cancer cells; NMR application of the zero trans method. Anticancer research 1996;16:1375-80.

[79] Noh DY, Ahn SJ, Lee RA, Park IA, Kim JH, Suh PG, et al. Overexpression of phospholipase D1 in human breast cancer tissues. Cancer lett 2000;161:207-14.

[80] Shah T, Wildes F, Penet MF, Winnard PT, Jr., Glunde K, Artemov D, et al. Choline kinase overexpression increases invasiveness and drug resistance of human breast cancer cells. NMR Biomed;23:633-42.

[81] Janardhan S, Srivani P, and Sastry GN. Choline kinase: an important target for cancer. Curr Med Chem 2006;13:1169-86.

[82] Mertens K, Slaets D, Lambert B, Acou M, De Vos F, and Goethals I. PET with (18)F-labelled choline-based tracers for tumour imaging: a review of the literature. Eur J Nucl Med Mol Imaging.

[83] Hara T, Kondo T, Hara T, and Kosaka N. Use of 18F-choline and 11C-choline as contrast agents in positron emission tomography imaging-guided stereotactic biopsy sampling of gliomas. J Neurosurg 2003;99:474-9.

[84] DeGrado TR, Reiman RE, Price DT, Wang S, and Coleman RE. Pharmacokinetics and radiation dosimetry of 18F-fluorocholine. J Nucl Med 2002;43:92-6.

[85] Dixon RM and Tian M. Phospholipid synthesis in the lymphomatous mouse liver studied by 31P nuclear magnetic resonance spectroscopy in vitro and by administration of 14C-radiolabelled compounds in vivo. Biochimica et biophysica acta 1993;1181:111-21.

[86] Podo F. Tumour phospholipid metabolism. NMR Biomed 1999;12:413-39.

[87] Kennedy EP. The biosynthesis of phospholipids. Am J Clin Nutr 1958;6:216-20.

[88] Tijburg LB, Geelen MJ, and Van Golde LM. Biosynthesis of phosphatidylethanolamine via the CDP-ethanolamine route is an important pathway in isolated rat hepatocytes. Biochem Biophys Res Commun 1989;160:1275-80.

[89] Mintz A, Wang L, and Ponde DE. Comparison of radiolabeled choline and ethanolamine as probe for cancer detection. Cancer biol Ther 2008;7:742-7.

Chapter 2

Synthesis and in vitro evaluation of ^{18}F labeled tyrosine derivatives as potential PET imaging agents

2.1 Introduction

A number of classes of metabolically based radiotracers such as radiolabeled glucose, amino acids, fatty acids and their analogs were developed for tumor imaging and have shown tremendous success in recent years. [^{18}F]fluorodeoxyglucose (FDG), which utilizes upregulated aerobic glycolysis in tumor cells [1], is routinely used in clinics for detecting, staging and restaging of lymphomas [2] and many solid tumors [3]. However, it has certain limitations such as high uptake in the cerebral cortex and non-specific accumulation in inflammatory tissues [4]. In search of new imaging agents, a variety of radiolabeled amino acids were prepared based on increased amino acid uptake and protein metabolism in cancer cells. Numerous studies have demonstrated that amino acid based tracers show better results than FDG in detecting and delineating certain tumors, particularly in brain tumors [5].

Currently, the most commonly used labeled amino acid in PET is [^{11}C]methionine (MET) [6, 7]. Despite the success, its susceptibility to multiple metabolic pathways complicates the pharmacokinetic analysis [8, 9] and its short half-life (20.3 min) limits its clinical applicability. To overcome these disadvantages, a number of ^{18}F (half-life 109.8 min) labeled amino acid analogs such as *O*-(2-[^{18}F]fluoroethyl)-L-tyrosine (FET, [^{18}F]**1**) [10], L-3-[^{18}F]fluoro-α-methyl tyrosine (FMT) [11], 6-[^{18}F]fluoro-L-dihydroxy phenyl-alanine (FDOPA) [12], and anti-1-amino-3-[^{18}F]fluorocyclobutyl-1-carboxylic acid (FACBC) [13, 14] were developed. In particular FET ([^{18}F]**1)**, is a successful ^{18}F labeled amino acid tracer and it has been used in imaging brain tumors and head-neck carcinomas for diagnosis and therapy planning [15, 16].

Several close analogs of FET ([^{18}F]**1**), such as *O*-(^{18}F]fluoromethyl)-L-tyrosine [17], *O*-(3-[^{18}F]fluoropropyl)-L-tyrosine [18] and *O*-(3-[^{18}F]fluoropropenyl)-L-tyrosine [19] have been developed and evaluated. The uptake of these structurally similar tyrosine derivatives in tumor cells is most likely attributed to elevated amino acid transporter activity, in particular system L amino acid transporters (LATs) [5, 20, 21], a Na^+ independent transport system which mediates transport of branched and aromatic amino acids [22]. LAT, generally upregulated in many cancer cell lines, is a target for development of tumor imaging agents [23-25]. System L has broad substrate selectivity; substitutions on aromatic ring with fluorine, hydroxy or fluoroalkyl group as well as substitutions on α-hydrogen with methyl are generally tolerated, this enables developing a variety of structurally similar analogs as potential LATs substrates [26].

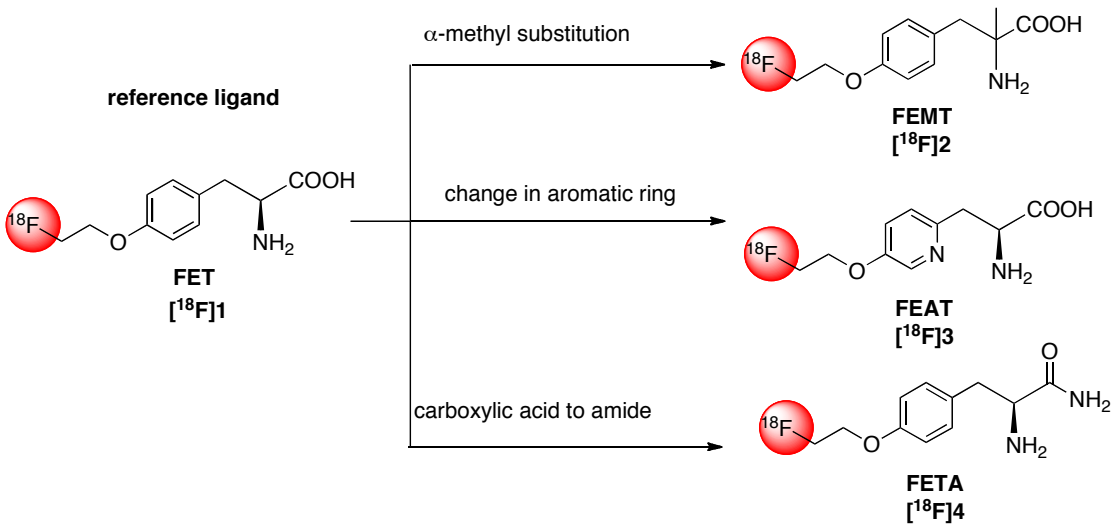

Figure 2.1. FET ([^{18}F]**1**) and its new analogs.

To pursue aromatic amino acid derivatives with better tumor-avid properties than FET ([^{18}F]**1**) and exploring the structure-activity relationships (SAR) of LATs, three new ^{18}F tyrosine derivatives were synthesized and evaluated (Figure 2.1): *O*-(2-[^{18}F]fluoroethyl)-α-methyl tyrosine (FEMT, [^{18}F]**2**), *O*-(2-[^{18}F]fluoroethyl)-2-L-

azatyrosine (FEAT, [^{18}F]**3**), and *O*-(2-[^{18}F]fluoroethyl)- L-tyrosineamide (FETA, [^{18}F]**4**). FEMT ([^{18}F]**2)** could be considered as fluoroalkyl derivative of well established SPECT tracer 3-[^{123}I]iodo-α-methyl-L-tyrosine (IMT).[27] We reasoned that FEAT ([^{18}F]**3)** might have specific uptake in cancer cells, because its analog 2-azatyrosine was reported to show antitumor activity and could reverse the *ras* transforming cancer cells to normal cell without significant effect on the growth of normal cells [28]. The amide derivative FETA ([^{18}F]**4**) was synthesized in hope that higher lipophilicity of [^{18}F]**4** may lead to improved pharmacokinetics compared to FET ([^{18}F]**1)**, such as reduced excretion through urinary tract.

2.2 Results and discussion

2.2.1 Synthesis of precursors and authentic standards for radiotracers

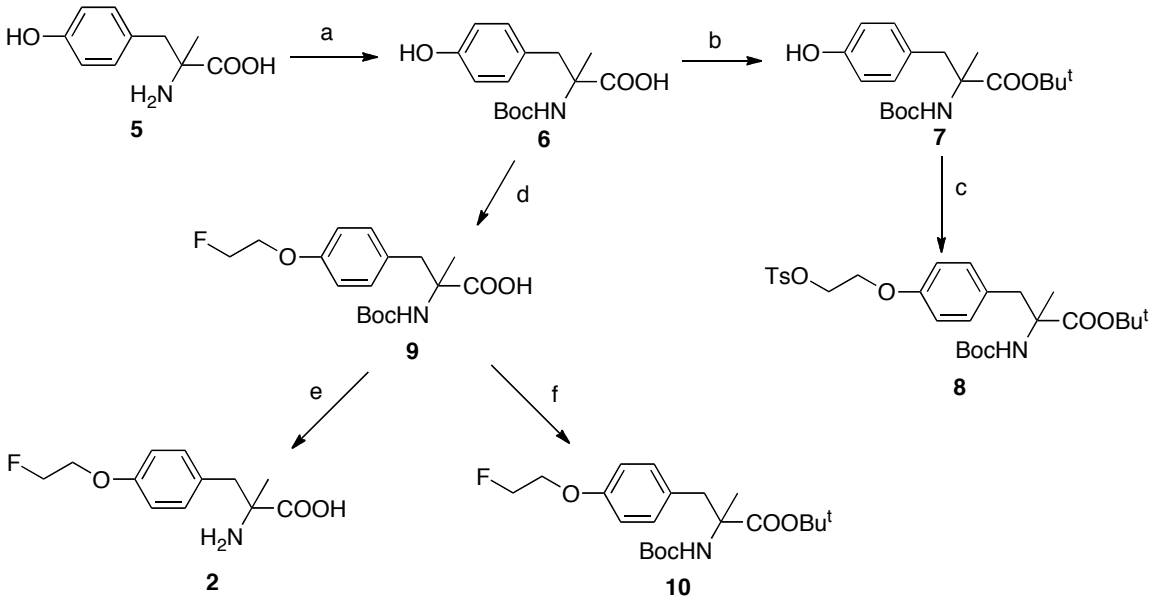

Scheme 2.1. Initial synthetic route of FEMT **2**. Reagents and conditions: a) $(Boc)_2O$, dioxane/H_2O, details as listed in Table 2.1; b) *tert*-butyl 2,2,2-trichloroacetimidate, $BF_3.Et_2O$, CH_2Cl_2/THF, 1 d, 45%; c) $TsO(CH_2)_2OTs$, K_2CO_3, DMF, 70 ^oC, 26 h, 70 ^oC, 13%; d) FCH_2CH_2Br, NaH, DMF,0 ^oC to 5 ^oC, 7 h, 88%; e) TFA, CH_2Cl_2, 30 min, 40%; f) *tert*-butyl trichlorloacetimidate, CH_2Cl_2/cyclohexane, $BF_3.Et_2O$, rt to 50 ^oC, 3 d, 21%.

Table 2.1: Boc protection result of **5** under various conditions:

Base	Temperature (^{o}C)	Reaction time	Yield (%)
$NaHCO_3$/NaOH	25	2 d	9
Me_4NOH	25	5 d	26
Et_3N	25	7 d	21
Et_3N	50	2 d	30

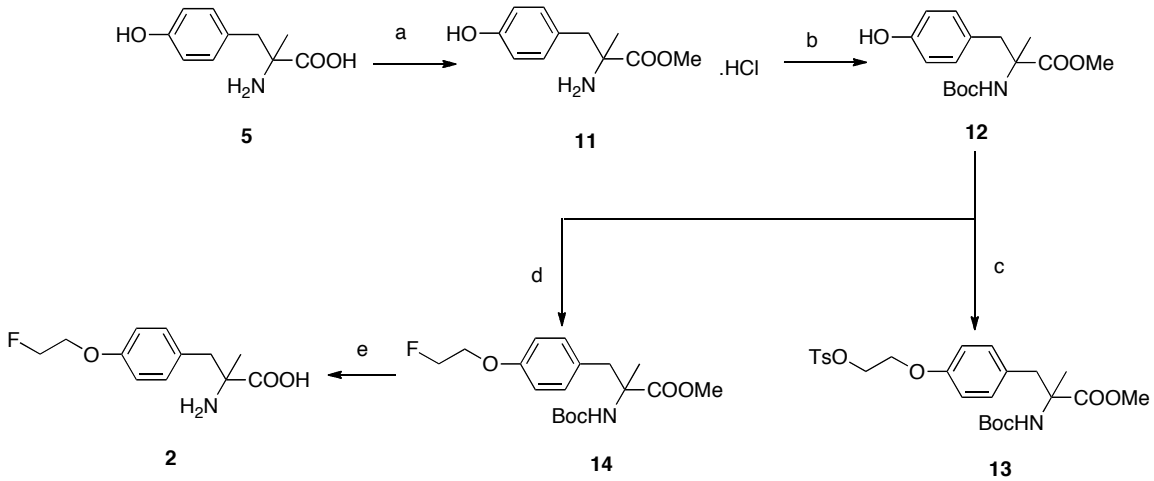

Scheme 2.2. Improved synthesis of FEMT **2**. Reagents and conditions: a) $SOCl_2$, MeOH, 0 ^{o}C to reflux, 16 h, 100% b): $(Boc)_2O$, Et_3N, MeOH, 50 ^{o}C, 3 d, 63%; c) NaH, DMF, $TsOCH_2CH_2OTs$, 0 ^{o}C to 5 ^{o}C, 6 h, 46%; d) NaH, DMF, FCH_2CH_2Br, 0 ^{o}C to rt, 6 h, 81%; e) 6N HCl, reflux, 2 h, 46%.

Cold standard for FEMT **2** was initially carried out as shown in Scheme 2.1 from commercially available α-methyl tyrosine **5**. The attempt of Boc protection of amino group of **5** had low yield (< 30%) and required long reaction time as shown in Table 2.1. This might be due to steric hindrance from the α-methyl group and limited solubility of **5** in water or organic solvents [29]. Since this synthetic route is flawed with low yield (i.e. yield of tosylate precursor and standard was no more than 2% and 10% respectively) and long reaction time, we then developed a new strategy as demonstrated in Scheme 2.2. Protecting the carboxylic acid group of **5** first could solve the solubility issue so subsequent Boc protection could be achieve with shorter reaction time and higher yield.

Methylation of the carboxylic group gave α-methyl tyrosine methyl ester **11** in quantitative yield. The subsequent Boc protection produced protected tyrosine **12** in good yield. Since direct nucleophilic radiofluorination is generally a better method than indirect labeling [30, 31], we prepared labeling precursors as protected *O*-tosylalkyl tyrosine derivatives. Tosylate precursor **13** was obtained in a yield of 46% after treating **12** with ethylene glycol ditosylate and NaH in DMF. Alkylation of **12** with 1-bromo-2-fluoroethane followed by deprotection in 6 N HCl, FEMT **2** was prepared with 23% overall yield.

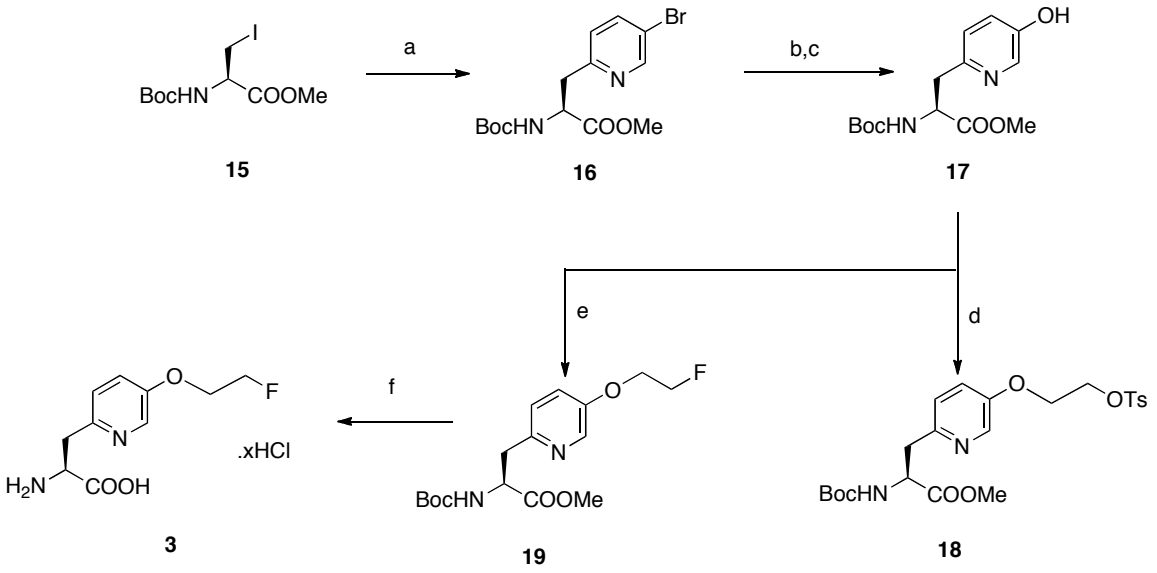

Scheme 2.3. Synthesis of FEAT **3**. Reagenet and conditions: a) (i) Zinc dust, I_2, DMF, rt, 1 h; (ii) 2,5-dibromopyridine, $Pd(PPh_3)Cl_2$, 68 ^oC, 2 h, 73%; b) bis(pinacolato) diboron, $Pd(dppf)Cl_2$, KOAc, 85 ^oC, 4 h; c) H_2O_2, CH_2Cl_2, 0 ^oC to rt, 16 h, 76%; d) $TsOCH_2CH_2OTs$, K_2CO_3, DMF, 70 ^oC, 47%; e) FCH_2CH_2Br, K_2CO_3, DMF, 70 ^oC, 2 h, 67%; f) 6 N HCl, reflux, 4 h, 75%.

For synthesis of FEAT **3**, the important intermediate is Boc-L-2-azatyrosine methyl ester **17,** which was prepared following the same procedure reported by Germain et al [32] via Negishi cross coupling using 2,5-dibromopyridine as precursor and subsequent hydroboration-oxidation reaction (Scheme 2.3). From this protected azatyrosine intermediate **17**, we could obtain labeling precursor **18** and FEAT **3** through

alkylation reactions as described in FEMT synthesis with 26 % and 28 % overall yield, respectively. We were interested in comparing the 2-azatyrosine and 3-azatyrosine derivatives to see how the position of N atom in aromatic ring affects ligands' activity. However, via Negishi coupling reaction, we could not obtain the intermediate with acceptable yield for synthesis of labeling precursor and standard of *O*-fluoroethyl 3-azatyrosine as shown in Scheme 2.4 and Table 2.2.

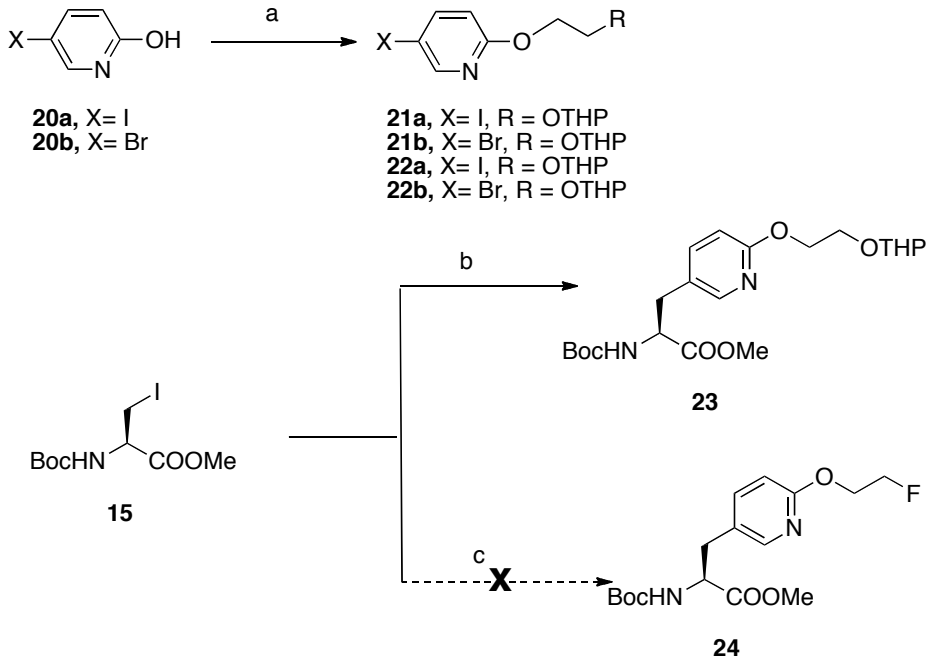

Scheme 2.4. Attempted synthesis of 3-azatyrosine derivative. Reagenet and conditions: a) PPh_3, DIAD, THF, $HO(CH_2)_2OTHP$ or $HO(CH_2)_2F$, -5°C-10°C, 2 h; b) **21a** or **21**b, Pd-catalyst, DMF, detailed condition and results as listed in **Table 2.2**; c) **22a** or **22b**, $Pd(PPh_3)_2Cl_2$, DMF, rt

Table 2.2: Conditions and results of synthesis of **23** via Negishi Coupling

X	Pd Catalyst (5 mol%)	Temperature	Reaction time (h)	Yield %
I	$Pd(PPh_3)_2Cl_2$	rt to 55°C	5	6%
I	$Pd(PPh_3)_2Cl_2$	rt	19	~1%
I	$Pd(dppf)Cl_2$	rt	28	~1%
Br	$Pd(PPh_3)_2Cl_2$	50°C to 65°C	21	No product
Br	$Pd(dppf)Cl_2$	50°C to 55°C	21	~1%
Br	$Pd(dppf)Cl_2$	70°C	30	5%
Br	PEPPSI	50°C	30	5%

Cold standard for FETA, **4** was prepared from Boc-L-tyrosine **25** in three steps (Scheme 2.5) – direct alkylation on phenol, coupling reaction with 2,4,6-trimethoxy benzylamide (Tmob-NH_2) and final deprotection reaction with trifluoroacetic acid. Tosylate precursor **30** was synthesized in a similar manner, except it required selectively protecting the ethoxyl group on phenol with TBDMS and removing the protecting group with TBAF after coupling reaction with Tmob-NH_2. Overall yield of FETA was 34% and of precursor **30** was 47%.

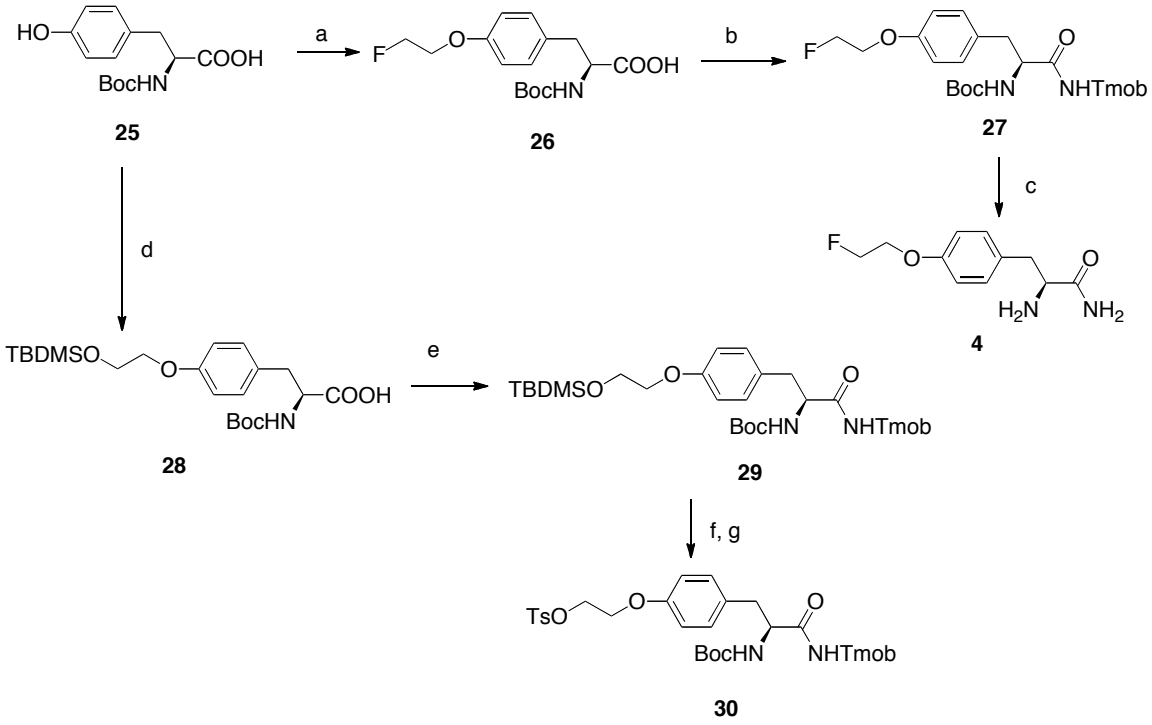

Scheme 2.5. Synthesis of FETA **4**. Reagents and conditions: a) NaH, FCH_2CH_2Br**,** DMF, 0 ^oC to rt,overnight, 84%; b): Tmob-NH_2.HCl, HOBt,DIPEA, HBTU, DMF, 0 ^oC to rt, 2 h, 80%; c) TFA, CH_2Cl_2, 4 h, 50%; d) NaH, $BrCH_2CH_2OTBDMS$, DMF, 0 ^oC to rt,overnight, 90%**;**e) Tmob-NH_2.HCl, HOBt,DIPEA, HBTU, DMF,0 ^oC to rt, 2 h, 77%;f) TBAF, THF, 1 h, 78%; g) TsCl, Et_3N, CH_2Cl_2, overnight, 87%.

2.2.2 Radiolabeling of tyrosine derivatives

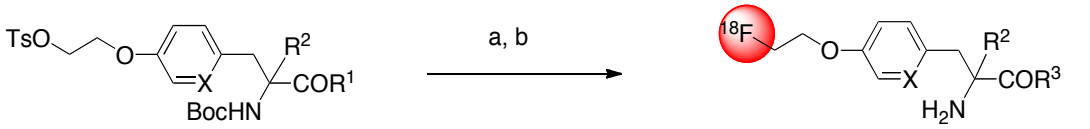

31, R^1= OBut, R^2 =H, X= CH
13, R^1 = OMe, R^2 = Me, X =CH
18, R^1 = OMe, R^2 = H, X= N
30, R^1 = NHTmob, R^2 = H, X = CH

[^{18}F]1, R^2 =H, R^3 = OH, X= CH
[^{18}F]2, R^2 = Me, R^3 = OH, X =CH
[^{18}F]3, R^2 = H, R^3 = OH, X= N
[^{18}F]4, R^2 = H, R^3 = NH_2, X= CH

Scheme 2.6. Radiolabeling reactions for tyrosine derivatives. Reagents and conditions: a) [^{18}F]KF, K[2.2.2], K_2CO_3, CH_3CN, 90 ^{o}C, 10 min; b) deprotection as listed in Table 2.3.

Table 2.3. Deprotection reaction conditions, average decay-corrected RCY and specific activities at end of synthesis (EOS).

Ligands	Deprotection reaction conditions	RCY (%)	Specific Activity (GBq/μmol)
[^{18}F]1	TFA, 60 ^{o}C, 10 min	44 ± 8	32 ± 12
[^{18}F]2	1) TFA, 60 ^{o}C, 5 min; 2) 2 N NaOH, 100 ^{o}C, 10 min	30 ± 8	13 ± 3
[^{18}F]3	6 M HCl, 120 ^{o}C, 10 min	37 ± 8	23 ± 12
[^{18}F]4	TFA, 60 ^{o}C, 10 min	5 ± 2	54 ± 12

*Values are means of three to six experiments; standard deviation is given in parentheses.

All of the ^{18}F labeled ligands, FET ([^{18}F]**1**), FEMT ([^{18}F]**2**), FEAT ([^{18}F]**3**), and FETA ([^{18}F]**4**), were prepared via nucleophilic substitution of tosylate with non-carrier-added [^{18}F]KF-K[2.2.2] complex in acetonitrile, followed by deprotection (Scheme 2.6). In general, fluorination reaction could reach completion within 10 min at 90 ^{o}C. Deprotection reaction conditions vary as shown in Table 2.3. All ligands were purified with semi-preparative HPLC and were prepared within 100 min in good radiochemical purity (RCP, > 95%) determined by both analytical HPLC and TLC. Results of labeling such as decay–corrected radiochemical yield (RCY) and specific activity were summarized in Table 2.3. It is noteworthy to point out that two-step deprotection was used for FEMT, first remove Boc using TFA and then cleave methyl group via reflux in NaOH solution. We have tried to use one-step deprotection by refluxing in 6 M HCl,

however, even after 20 min, fluorinated intermediate still could not be fully converted to final product FEMT. Another issue in preparation of these tyrosine derivatives is the low yield of FETA. We observed that using TFA at 60 ^{o}C for 10 min was not sufficient to fully remove the Tmob protecting group. But considering possible hydrolysis of FETA to FET, we did not increase reaction temperature or time to improve the deprotection rate.

2.2.3 In vitro cell uptake studies

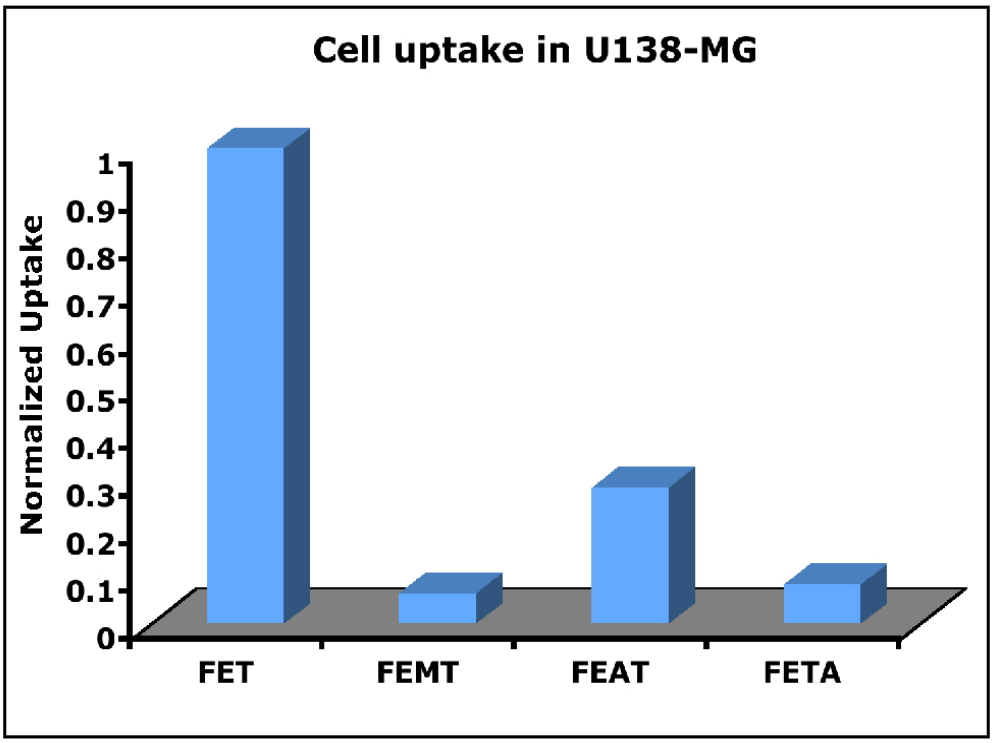

Figure 2.2[a] Uptake of new tyrosine derivatives in reference to FET ([^{18}F]**1**). Maximum uptake of ligands was normalized to FET's highest uptake in U138-MG.
[a]Experiment performed by Brain Lieberman [33].

After successfully synthesizing ^{18}F labeled tyrosine derivatives, we carried out cell uptake studies as initial biological evaluation in U-138 MG human glioblastoma cells. U-138 MG was used as positive control in uptake of FET and IMT [34, 35]. Since

FET ([^{18}F]**1)**, was used as reference compound, we chose U-138 MG to establish the standard for amino acid tracers' uptake. The cellular uptake of ^{18}F labeled tyrosine derivatives (Figure 2.2) followed the order of FET ([^{18}F]**1)** > FEAT ([^{18}F]**3)** > FEMT ([^{18}F]**2)** ≈ FETA ([^{18}F]**4)**.

The uptake of the tracers depends on the ligands' binding affinity to amino acid transporters and their transport rate. From the uptake results, we could make some inference about amino acid transporters substrate recognition. The low uptake of FEMT ([^{18}F]**2)**, the α-methyl substituted FET ([^{18}F]**1)**, indicates *O*-fluoroalkyl α-methyl tyrosine derivatives may not be good substrates for amino acid transporters. As we know, there are four subtypes of LATs discovered by now, designated as LAT1 to LAT4. Although they have significant overlap of substrate selectivity, it is suggested that some amino acid based tracers have preference towards specific subtypes of system L, in particular, FET ([^{18}F]**1)** probably prefer to be transported via LAT2 [16]. It is reported that α-methyl substitution is tolerated by LAT1 but no evidence suggest that LAT2 could accept α-methyl substitution as well,[26] this might be the reason that FEMT ([^{18}F]**2)** has significantly lower uptake than FET ([^{18}F]**1)**. FEAT ([^{18}F]**3)**, has a substituted pyridine side chain, which reduces its lipophilicity compared to FET ([^{18}F]**1)** and this potentially leads to its low uptake into cells. FETA ([^{18}F]**4)**, which substitutes carboxylic acid with amide, is a poor substrate. In agreement, tyramine, dopamine, as well as phenylalanine methyl ester, which lack the free carboxylic acid group, are not good substrates for amino acid transporters either.[26, 36] These results suggest that α-carboxylic acid might be essential amino acid transporters' substrate recognition.

2.3 Conclusion

In summary, three new potential PET imaging agents FEMT ([^{18}F]**2)**, FEAT ([^{18}F]**3)** and FETA ([^{18}F]**4)** were synthesized, radiolabeled and evaluated via cell uptake studies in U-138 MG. New tracers exhibited lower uptake compared to clinically utilized FET ([^{18}F]**1)**. Although these ligands might not be useful imaging agents, they provided insight for amino acid transporters' substrate recognition patterns.

2.4 Experimental Section

2.4.1 General information

All chemicals were purchased from Aldrich Chemical (St. Louis, MO) or TCI America (Portland, OR). The commercially available materials were used without further purification unless otherwise indicated. ^{1}H spectra and ^{13}C NMR was recorded by a Bruker DPX spectrometer at 200 MHz and 50 MHz respectively and referenced to NMR solvents as indicated. Chemical shifts are reported in ppm (δ), coupling constant *J* in Hz. High-resolution mass spectrometry (HRMS) data were obtained with an Agilent (Santa Clara, CA) G3250AA LC/MSD TOF system. Thin-layer chromatography (TLC) analyses were performed using silica gel 60 F_{254} plates (Merck, Germany). Crude compounds generally were purified by flash column chromatography (FC) packed with silica gel (Aldrich). [^{18}F]Fluoride was purchased from IBA Molecular (Somerset, NJ) as an [^{18}O]enriched aqueous solution of [^{18}F]fluoride. Solid-phase extraction (SPE) cartridges such as Sep-Pak QMA Light and Oasis HLB cartridges were purchased from Waters (Milford, MA). High performance liquid chromatography (HPLC) was performed on an

Agilent 1100 series system. [^{18}F]radioactivity was measured by gamma counter (Cobra II auto-gamma counter D5003 spectrometer, Canberra-Packard) in the 400-1600 keV energy range. Specific activity (SA) was calculated by comparing UV peak intensity of final products with calibration curves of corresponding non-radioactive standards of known concentrations. Cell lines were obtained from the American Tissue Culture Collection (ATCC) and cultured according to ATCC recommended conditions.

2.4.2 Synthesis of precursors and standards for radiolabeling

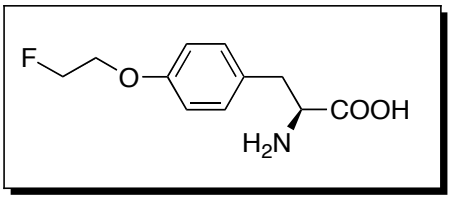

***O*-Fluoroethyl-L-tyrosine (1)**: ^{1}H-NMR (200MHz, Acetic acid-d4): δ = 7.24 (d, 2H, J = 8.6 Hz), 6.91 (d, 2H, J = 8.6 Hz), 4.73 (dt, 2H, J_1 = 47.4 Hz, J_2 = 4.0 Hz), 4.40 (dd, 1H, J_1 = 7.6 Hz, J_2 = 5.2 Hz), 4.22 (dt, 2H, J_1 = 29.2 Hz, J_2 = 4.0 Hz), 3.52-3.22 (m, 2H); ^{13}C NMR (50MHz, Acetic acid-d4) δ =173.1, 158.2, 130.8,126.9, 115.0, 81.9 (d, J = 167.5 Hz), 67.2 (d, J = 20.0 Hz), 55.8, 35.1; HRMS calcd for $C_{11}H_{14}FNO_3$ ($[M+H]^+$) 228.1036, found 228.1265. $[\alpha]^{23}_D$ -3.4^o (c 0.53, 6 N HCl).

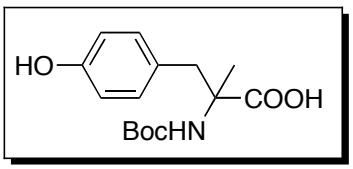

2-(*tert*-butoxycarbonylamino)-3-(4-hydroxyphenyl)-2-methylpropanoic acid (6): 2.0 to 5.0 equivalent base was added to a suspension of α-methyl tyrosine **5** in

dioxane/H_2O (1/1), the reaction mixture was cooled to 0°C and di-*tert*-butyl dicarbonate (1.5 equiv) was added and reaction mixture was kept under various temperature and time as shown in Table 1. Upon completion, 1N $KHSO_4$ was added to reaction mixture to adjust pH around 2 then extract with ethyl acetate three times. Combined organic layer was washed with brine and dried over Na_2SO_4. Solvent was removed under reduced pressure. Resulting crude product was purified by FC (Acetic acid/MeOH/CH_2Cl_2, 0.5/4/100). ^{1}H NMR (200MHz, MeOD-d4) δ =6.96 (d, 2H, *J* = 8.4 Hz), 6.67 (d, 2H, *J* =8.6 Hz), 3.17 (d, 1H, *J* = 13.6 Hz), 3.05 (d, 1H, *J* = 13.6 Hz), 1.47 (s, 9H), 1.39 (s, 3H). ^{13}C NMR (50MHz, $CDCl_3$) δ =177.8, 157.4, 156.7, 132.5, 128.8, 116.0, 80.5, 61.0, 41.9, 29.0, 23.8. HRMS calcd for $C_{15}H_{21}NO_5$ ($[M+Na]^+$) 318.1317, found 318.1314

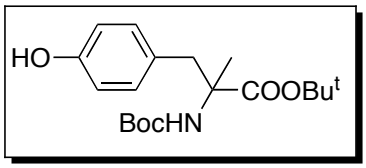

***tert*-butyl 2-(*tert*-butoxycarbonylamino)-3-(4-hydroxyphenyl)-2-methyl propanoate (7):** *tert*-butyl 2,2,2-trichloroacetimidate (473 mg, 2.16 mmol) was added to a solution of **6** (160 mg, 0.54 mmol) in metheylene chloride (2.0 mL) and THF (0.5 mL). Stirred at 40°C for 18 h. After reaction being quenched with $NaHCO_3$ (150 mg, 2.4 mmol), the resulting mixture was filtered and concentrated in vacuo and resulting residue was purified by FC (EtOAc/Hexanes, 15/85 to 25/75) to yield product as white foam. ^{1}H NMR (200 MHz, $CDCl_3$) δ =7.00 (d, 2H, *J* = 8.4 Hz), 6.73 (d, 2H, *J* =8.4 Hz), 5.20 (s, 1H), 3.31 (d, 1H, *J* = 13.6 Hz), 3.09 (d, 1H, *J* = 13.6 Hz), 1.53 (s, 3H), 1.47 (s, 18H). ^{13}C NMR (50 MHz, $CDCl_3$) δ = 173.2, 167.9, 155.1,154.6, 132.5, 128.2, 115.1, 82.1, 79.5,

60.5, 40.9, 28.9, 27.2, 24.9. HRMS calcd for $C_{19}H_{29}NO_5$ ([M+Na]$^+$) 374.1943, found 374.1942.

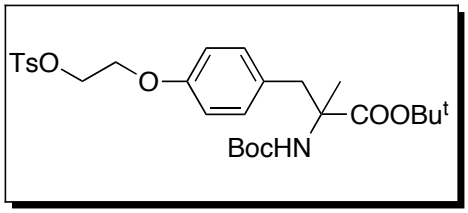

***tert*-butyl 2-(*tert*-butoxycarbonylamino)-2-methyl-3-(4-(2(tosyloxy)ethoxy) phenyl)propanoate (8): 7** (207 mg, 0.67mmol) was dissolved in 1mL dry DMF and added to NaH (60% in mineral oil, 40mg, 1.0mmol) in 4mL DMF at 0°C and reaction mixture was stirred at 0°C for 1h.1, 2-bis(tosyloxy)ethane (371 mg, 1.0 mmol) in 1mL DMF was added and reaction continued for 5h at 0 to 5°C. After reaction, reaction solution was diluted with 60mL EtOAc and washed with 5mL water twice and then 5mL brine. Organic layer dried over Na_2SO_4 and solvent was removed under reduced pressure. Crude mixture was purified by FC ($MeOH/CH_2Cl_2$, 0.5/100). ^{1}H-NMR (200MHz, $CDCl_3$): δ = 7.82 (d, 2H, *J* = 8.4 Hz), 7.35 (d, 2H, *J* = 8.4 Hz), 7.06 (d, 2H, *J* = 8.6 Hz), 6.68 (d, 2H, *J* = 8.6 Hz), 4.36 (dd, 2H, J_1 = 6.0 Hz, J_2=3.5 Hz), 4.13 (dd, 2H, J_1 = 5.8 Hz, J_2=3.8 Hz), 3.33 (d, 1H, *J* = 13.6 Hz), 3.09 (d, 1H, *J* = 13.6 Hz), 2.46 (s, 3H), 1.52 (s, 3H), 1.47 (s, 18H). ^{13}C NMR (50MHz, $CDCl_3$) δ =173.3, 157.2, 154.5,145.1, 133.4, 131.5, 130.1, 128.3, 114.4, 82.2, 79.4, 68.4, 65.8, 60.7, 40.7, 28.7, 28.2, 24.2, 21.8. HRMS calcd for $C_{28}H_{39}NO_8S$ ([M+Na]$^+$) 570.2294, found 570.2289.

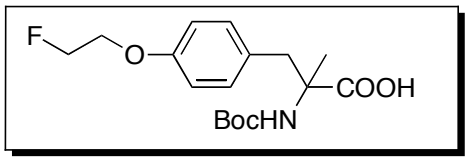

2-(*tert*-butoxycarbonylamino)-3-(4-(2-fluoroethoxy)phenyl)-2 methylpropanoic acid (9): *N*-Boc α-methyltyrosine (**6,** 127 mg, 0.43mmol) was dissolved in 1mL dry DMF and added to NaH (60% in mineral oil, 43mg, 1.1mmol) in 2 mL DMF at 0°C and reaction mixture was stirred at 0°C for 1 h.1-Bromo-2-fluoro ethane (108 mg, 0.86 mmol) in 0.5mL DMF was added and reaction continued for 6 h at 0 to 5°C. After reaction, reaction solution was diluted with 60mL EtOAc and washed with 5mL water twice and then 5mL brine. Organic layer dried over Na_2SO_4 and solvent was removed under reduced pressure. Crude mixture was purified by FC (Acetic acid/EtOAc/Hexanes, 0.5/25/75). ^{1}H-NMR (200MHz, $CDCl_3$): δ = 10.4 (s, 1H), 7.08 (d, 2H, *J* = 8.6 Hz), 6.84 (d, 2H, *J* = 8.6 Hz), 5.11 (s, 1H), 4.75 (dt, 2H, J_1 = 47.4 Hz, J_2 =4.0 Hz), 4.18 (dt, 2H, J_1 = 28.0 Hz, J_2 =4.0 Hz), 3.24 (s, 2H), 1.54 (s, 3H) 1.47 (s, 9H). ^{13}C NMR (50MHz, $CDCl_3$) δ =180.3, 162.1, 157.1, 155.2, 131.4, 130.1, 114.2, 82.0 (d, *J* = 169.5 Hz), 79.5 , 67.1 (d, *J* = 20.5 Hz), 60.4, 40.6, 28.4, 24.7.HRMS calcd for $C_{17}H_{24}FNO_5$ ($[M+Na]^+$) 364.1536, found 364.1539.

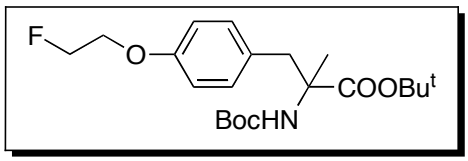

***tert*-butyl 2-(*tert*-butoxycarbonylamino)-3-(4-(2-fluoroethoxy)phenyl)-2-methylpropanoate (10):** To solution of **9** (60 mg, 0.19 mmol) in 2 mL CH_2Cl_2/cyclohexane (1:1) was added *tert*-butyl 2,2,2-trichloro acetimidate (166 mg, 0.78

mmol). Stirred at 50 °C for 1 d. After being quenched with $NaHCO_3$ (70 mg, 0.8 mmol), the reaction was filtered and concentrated in vacuo and resulting residue was purified by FC (EtOAc/Hexanes, 10/9) to yield product as white solid. ^{1}H NMR (200MHz, $CDCl_3$) δ =7.07 (d, 2H, J = 8.6 Hz), 6.83 (d, 2H, J =8.6 Hz), 5.19 (s, 1H), 4.75 (dt, 2H, J_1 = 47.2 Hz, J_2 =4.2 Hz), 4.20 (dt, 2H, J_1 = 27.8 Hz, J_2 =4.2 Hz), 3.34 (d, 1H, J = 13.6 Hz), 3.11 (d, 1H, J = 13.6 Hz), 1.53 (s, 3H), 1.48 (s, 18H). ^{13}C NMR (50MHz, $CDCl_3$) δ =173.3, 157.6, 154.6, 131.5, 129.9, 114.5, 82.2, 82.1 (d, J = 169.5 Hz), 79.4, 67.4 (d, J = 21.0 Hz), 60.7, 40.8, 28.7, 28.2, 24.2. HRMS calcd for $C_{21}H_{32}FNO_5$ ($[M+Na]^+$) 420.2162, found 420.2154.

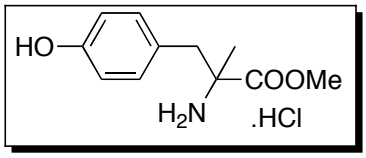

Methyl 2-amino-3-(4-hydroxyphenyl)-2-methylpropanoate (11): Thionyl chloride (3.7 mL, 51.2 mmol) was added to a suspension of α-methyltyrosine (**5**, 1.00 g, 5.12 mmol) in 25 mL methanol at 0°C. The reaction mixture was refluxed overnight. After concentrated *in vacuo*, 1.3 g transparent oil was obtained for use in the next step, as product without further purification. ^{1}H NMR (200 MHz, MeOD-d4) δ = 7.00 (d, 2H, J = 8.6 Hz), 6.77 (d, 2H, J = 8.4 Hz), 3.83 (s, 3H), 3.19 (d, 1H, J = 14.2 Hz), 3.00 (d, 1H, J = 14.2 Hz), 1.59 (s, 3H); ^{13}C NMR (50 MHz, MeOD-d4) δ = 172.4, 158.7, 132.4, 124.8, 117.0, 62.2, 54.0, 43.5, 22.5; HRMS calcd for $C_{11}H_{15}NO_3$ ($[M+H]^+$) 210.1130, found 210.1137.

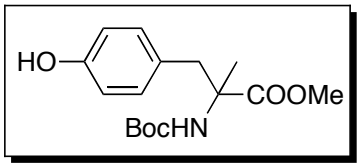

Methyl 2-(*tert*-butoxycarbonylamino)-3-(4-hydroxyphenyl)-2-methylpropane -ate or *N*-Boc α-methyltyrosine methyl ester (12): Triethylamine was added to a solution of α-methyltyrosine methyl ester (**11**, 2.37 g, 11 mmol) in 25 mL methanol. The reaction mixture was cooled to 0°C. Di-*tert*-butyl dicarbonate (2.23 g, 10.2 mmol) was added, and stirred at 50°C for 2d. Upon completion, the combined organic layer was washed with brine and then dried over Na_2SO_4. Solvent was removed under reduced pressure. Resulting crude product was purified by FC (EtOAc/Hexanes, 15/85 to 25/75). ^{1}H NMR (200 MHz, $CDCl_3$) δ =6.95 (d, 2H, *J* = 8.4 Hz), 6.73 (d, 2H, *J* = 8.6 Hz), 5.12 (s, 1H), 3.76 (s, 3H), 3.28 (d, 1H, *J* = 13.6 Hz), 3.11 (d, 1H, *J* = 13.6 Hz), 1.56 (s, 3H), 1.48 (s, 9H); ^{13}C NMR (50 MHz, $CDCl_3$) δ =174.9, 155.5, 154.9, 131.2, 115.4, 79.7, 60.6, 52.6, 41.6, 28.5, 23.6; HRMS calcd for $C_{16}H_{23}NO_5$ ($[M+Na]^+$) 332.1474, found 332.1464

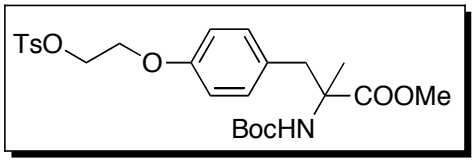

Methyl 2-(*tert*-butoxycarbonylamino)-2-methyl-3-(4-(2-(tosyloxy)ethoxy) phenyl) propanoate (13): *N*-Boc α-methyltyrosine methyl ester (**12,** 133 mg, 0.43 mmol) was dissolved in 1 mL dry DMF and added to NaH (16 mg, 0.65 mmol) in 2 mL DMF at 0°C. The reaction mixture was stirred at 0°C for 1h. 1, 2-bis(tosyloxy)ethane (240 mg, 0.65 mmol) in 0.5 mL DMF was added and the reaction continued for 5h at 0 to

5 °C. After the reaction, the solution was diluted with 60 mL EtOAc and washed twice with 5 mL water and then 5 mL brine. The organic layer was dried over Na_2SO_4 and solvent was removed under reduced pressure. Crude mixture was purified by FC (MeOH/ CH_2Cl_2, 0.5/100). ^{1}H-NMR (200 MHz, $CDCl_3$): δ = 7.83 (d, 2H, *J* = 8.2 Hz), 7.35 (d, 2H, *J* = 8.4 Hz), 6.97 (d, 2H, *J* = 8.4 Hz), 6.70 (d, 2H, *J* = 8.2 Hz), 5.11 (s, 1H), 4.36 (dd, 2H, J_1 = 6.0 Hz, J_2=3.6 Hz), 4.13 (dd, 2H, J_1 = 6.0 Hz, J_2=3.8 Hz), 3.31 (d, 1H, *J* = 13.8 Hz), 3.12 (d, 1H, *J* = 13.6 Hz), 2.46 (s, 3H), 1.56 (s, 3H), 1.47 (s, 9H); ^{13}C NMR (50 MHz, $CDCl_3$) δ =174.6, 157.3, 154.5, 145.1, 133.3, 131.2, 130.0, 129.4, 128.2, 114.6, 79.7, 68.3, 65.7, 60.6, 53.6, 52.6, 41.2, 28.6, 23.8, 21.8; HRMS calcd for $C_{28}H_{39}NO_8S$ ($[M+Na]^+$) 572.2294, found 572.2289.

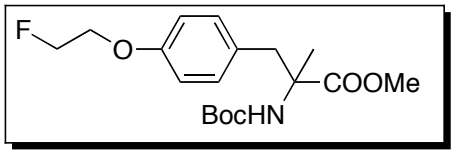

Methyl 2-(*tert*-butoxycarbonylamino)-3-(4-(2-fluoroethoxy)phenyl)-2-methyl propaneate (14): *N*-Boc α-methyltyrosine methyl ester (**12,** 274 mg, 0.89 mmol) was dissolved in 1 mL dry DMF and added to NaH (34 mg, 1.33 mmol) in 4 mL DMF at 0°C. The reaction mixture was stirred at 0°C for 1h. 1-Bromo-2- fluoroethane (223 mg, 1.77 mmol) in 1 mL DMF was added and reaction continued for 6h at 0 to 5°C. After the reaction, the solution was diluted with 60 mL EtOAc and washed with 5 mL water twice and then 5 mL brine. The organic layer was dried over Na_2SO_4 and solvent was removed under reduced pressure. Crude mixture was purified by FC (EtOAc/Hexanes, 15/85). ^{1}H NMR (200 MHz, $CDCl_3$) δ =7.01 (d, 2H, *J* = 8.6 Hz), 6.84 (d, 2H, *J* =8.6 Hz), 5.11 (s, 1H), 4.75 (dt, 2H, J_1 = 47.2 Hz, J_2 =4.2 Hz), 4.20 (dt, 2H, J_1 = 27.8 Hz, J_2 =4.2 Hz), 3.76

(s, 3H), 3.32 (d, 1H, J = 13.8 Hz), 3.14 (d, 1H, J = 13.6 Hz), 1.56 (s, 3H), 1.48 (s, 9H); ^{13}C NMR (50 MHz, $CDCl_3$) δ =174.6, 157.7, 154.6, 131.3, 129.3, 114.6, 82.1 (d, J =169.5 Hz), 79.7, 67.3 (d, J =20.5 Hz), 60.7, 52.6, 41.3, 28.6, 23.8; HRMS calcd for $C_{18}H_{26}FNO_5$ ([M+Na]$^+$) 378.1693, found 360.1693.

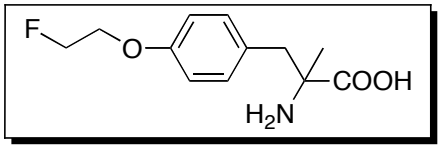

2-amino-3-(4-(2-fluoroethoxy)phenyl)-2-methylpropanoic acid or *O*-Fluoroethyl α-methyl tyrosine (2): Methyl 2-(*tert*-butoxycarbonylamino)-3-(4-(2-fluoroethoxy)phenyl) -2-methyl propanoate (**14**, 154 mg, 0.43 mmol) was dissolve in 7 mL 6 N HCl. The reaction mixture was stirred at reflux for 2.5 h. After evaporated to dryness, the resulting solid was dissolved in 2 mL MeOH. The solution was adjusted to pH ~7 with 5% NH_4OH resulting a white precipitate. The suspension was left in the refrigerator overnight and then filtered to produce *O*-fluoroethyl α-methyl tyrosine as a white solid. ^{1}H NMR (200 MHz, TFA-D+$CDCl_3$) δ =7.11 (d, 2H, J = 7.6 Hz), 6.93 (d, 2H, J =7.4 Hz), 4.77 (dt, 2H, J_1 = 47.2 Hz, J_2 =4.0 Hz), 4.21 (dt, 2H, J_1 = 28.0 Hz, J_2 =4.0 Hz), 3.41 (d, 1H, J = 14.2 Hz), 3.16 (d, 1H, J = 14.8 Hz), 1.78 (s, 3H); ^{13}C NMR (50 MHz, TFA-D+$CDCl_3$) δ =175.4, 159.2, 131.4, 124.0, 116.4, 82.3 (d, J = 168.5 Hz), 67.9 (d, J = 20.0 Hz), 62.8, 41.9, 21.9; HRMS calcd for $C_{12}H_{16}FNO_3$ ([M+Na]$^+$) 264.1012, found 264.0922.

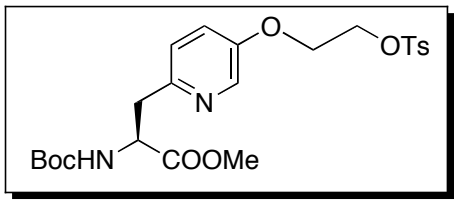

(*S*)-methyl 2-(*tert*-butoxycarbonylamino)-3-(5-(2-(tosyloxy)ethoxy)pyridin-2-yl) propaneate (18): Boc-L-azatyrosine methylester (**17,** 60 mg, 0.2 mmol) was dissolved in 2 mL DMF. K_2CO_3 (84 mg, 0.6 mmol) and 1,2-bis(tosyloxy)ethane (112 mg, 0.3 mmol) was added sequentially. The mixture was stirred at 70 ^oC for 3h. After the reaction, the mixture was diluted with 30 mL Et_2O and washed with 5 mL water twice and then 5 mL brine. The organic layer was dried over Na_2SO_4 and solvent was removed under reduced pressure. Crude mixture was purified by FC ($MeOH/CH_2Cl_2$, 2:100) to yield light yellow foam. ^{1}H-NMR (200 MHz, $CDCl_3$): δ = 8.10-8.08 (m, 1H), 7.82 (d, 2H, *J* = 7.8 Hz), 7.36 (d, 2H, *J* = 8.2 Hz), 7.05-7.03 (m, 2H), 5.76 (d, 1H, *J* = 8.0 Hz), 4.67-4.62 (m, 1H), 4.40-4.36 (m, 2H), 4.20-4.15 (m, 2H), 3.70 (s, 3H), 3.22-3.19 (m, 2H), 2.46 (s, 3H), 1.43 (s, 9H); ^{13}C NMR (50 MHz, $CDCl_3$) δ = 172.4, 155.4, 153.1, 149.9, 145.1, 137.2, 132.9, 129.9, 128.0, 123.8, 122.1, 79.7, 67.8, 66.0, 53.4, 52.2, 38.5, 28.3, 21.6; HRMS calcd for $C_{23}H_{30}N_2O_8S$ ($[M+H]^+$) 495.1801, found 495.1787; $[\alpha]^{24}_D$ +13.2^o (c 0.67, $CHCl_3$).

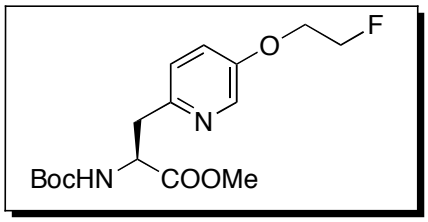

(*S*)-methyl 2-(*tert*-butoxycarbonylamino)-3-(5-(2-fluoroethoxy)pyridin-2-yl)propanoate (19): Boc-L-azatyrosine methylester (**17,** 45 mg, 0.15 mmol) was

dissolved in 1 mL DMF. K_2CO_3 (62 mg, 0.45 mmol) and 1-bromo-2-fluoroethane (38 mg, 0.3 mmol) were added sequentially. The mixture was stirred at 70°C for 2h. After the reaction, the mixture was diluted with 30 mL Et_2O and washed with 5 mL water twice and then 5 mL brine. The organic layer was dried over Na_2SO_4 and solvent was removed under reduced pressure. Crude mixture was purified by FC ($MeOH/CH_2Cl_2$, 2:100) to yield a light yellow viscous liquid. ^{1}H-NMR (200 MHz, $CDCl_3$): δ = 8.24 (d, 1H, *J* = 2.8 Hz), 7.17 (dd, 1H, J_1 = 8.4, J_2= 2.8 Hz), 7.06 (d, 1H, *J* = 8.6 Hz), 5.79 (d, *J* = 7.8 Hz), 4.90-4.85 (m, 1H), 4.65-4.52 (m, 2H), 4.33-4.28(m, 1H), 4.19-4.14 (m, 1H), 3.70 (s, 3H), 3.21-3.24 (m, 2H), 1.43 (s, 9H); ^{13}C NMR (50 MHz, $CDCl_3$) δ = 172.6, 155.6, 153.6, 150.0, 137.3, 124.1, 122.5, 81.8 (d, *J* =170.0 Hz), 79.8, 67.8 (d, *J* = 20.5 Hz), 53.5, 52.3, 38.7, 28.5; HRMS calcd for $C_{16}H_{23}FN_2O_5$ ($[M+H]^+$) 343.1669, found 343.1680. $[\alpha]^{24}_D$ +18.7° (c 0.93, $CHCl_3$).

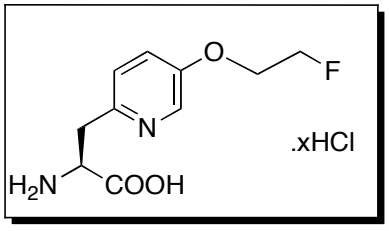

(*S*)-2-amino-3-(5-(2-fluoroethoxy)pyridin-2-yl)propanoic acid (3): 5mL 6M HCl was added to a 10 mL round bottom flask of (*S*)-methyl 2-(*tert*-butoxycarbonylamino)-3-(5-(2-fluoroethoxy)pyridin-2-yl)propanoate (**14**, 82 mg, 0.24 mmol) and refluxed for 4h. After the reaction, the mixture was diluted with 5 mL H_2O. The solution was washed with 2 mL CH_2Cl_2 three times. Aqueous phase was then concentrated under reduced pressure to yield light yellow foam. ^{1}H-NMR (200 MHz, MeOD-d4): δ = 8.62 (d, 1H, *J* = 2.6 Hz), 8.28 (dd, 1H, J_1 = 8.8, J_2= 2.2 Hz), 8.10 (d, 1H,

J = 9.0 Hz), 4.95-4.92 (m, 1H), 4.70-4.68 (m, 1H), 4.62-4.57 (m, 2H), 4.49-4.46 (m, 1H), 3.69 (d, 2H, *J* = 7.2 Hz); ^{13}C NMR (50 MHz, MeOD+D_2O) δ = 170.0, 158.2, 144.8, 133.6, 131.3, 130.3, 82.9 (d, *J* =168.5 Hz), 71.0 (d, *J* = 19.5 Hz), 53.2, 34.3; HRMS calcd for $C_{10}H_{13}FN_2O_3$ ([M+Na]$^+$) 229.0988, found 229.0987. $[\alpha]^{23}_D$ +36.6^o (c 0.30, 6 N HCl).

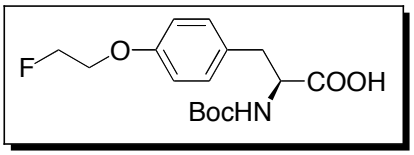

(*S*)-2-(*tert*-butoxycarbonylamino)-3-(4-(2-fluoroethoxy)phenyl)propanoic acid (26): *N*-Boc L-tyrosine (**25,** 563 mg, 2 mmol) was dissolved in 5 mL dry DMF and added to NaH (95%, 127mg, 5 mmol) in 15 mL DMF at 0°C. The reaction mixture was stirred at 0°C for 1h. 1-bromo-2-fluoroethane (504 mg, 4 mmol) was added and the reaction continued overnight from 0°C to room temperature. After the reaction, the solution was acidified to a pH of approximately 2 and extracted with ether (20 mL) three times. The combined organic layer was washed with brine (10 mL), dried over $MgSO_4$ and then concentrated *in vaccuo*. Crude mixture was purified by FC (AcOH/MeOH/ CH_2Cl_2, 0.5/3/100) to afford **26** as white foam. ^{1}H-NMR (200 MHz, $CDCl_3$): δ = 7.12 (d, 2H, *J* = 8.4 Hz), 6.86 (d, 2H, *J* = 8.6 Hz), 4.99 (d, 1H, *J* = 6.6 Hz), 4.86 (t, 1H, *J* = 4.2 Hz), 4.65-4.55 (m, 2H), 4.19 (dt, 2H, J_1 = 27.8 Hz, J_2 = 4.2 Hz), 3.19- 3.01(m, 2H), 1.42 (s, 9H); ^{13}C NMR (50 MHz, $CDCl_3$) δ =176.3, 157.8, 155.6, 130.7, 128.8, 115.0, 82.1 (d, *J* = 169.5 Hz), 67.4 (d, *J* = 20.5 Hz), 54.6, 37.1, 28.4; HRMS calcd for $C_{16}H_{22}FNO_5$ ([M+Na]$^+$) 350.1380, found 350.1378; $[\alpha]^{24}_D$ -13.1^o (c 1.1, MeOH).

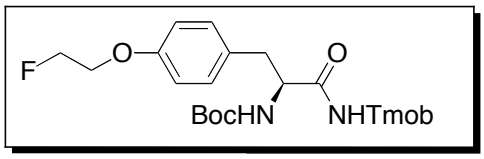

(*S*)-tert-butyl 3-(4-(2-fluoroethoxy)phenyl)-1-oxo-1-(2,4,6-trimethoxybenzyl amino)propan-2-ylcarbamate (27): Diisopropylethylamine (169 mg, 1.3 mmol) was added to a solution of propanoic acid **(26,** 130 mg, 0.4 mmol), 2,4,6-trimethoxybenzylamine hydrochloride (102 mg, 0.44 mmol) and 1-HOBt (70 mg, 0.52 mmol) in DMF (4 mL). The solution was cooled to 0^{o}C before HBTU (183 mg, 0.48 mmol) was added in one portion. Continue at 0^{o}C for 30 min and then room temperature for another 1.5 h. The reaction mixture was diluted with 15 mL EtOAc and 10 mL 10% citric acid. The aqueous layer was extracted twice with 15 mL EtOAc and the combined organic layer was washed with 5 mL saturated $NaHCO_3$ and 5 mL brine. The organic layer was dried over $MgSO_4$ and solvent was removed under reduced pressure. Crude mixture was purified by FC (EtOAc/Hexanes, 50/50), which produced **27** as a white solid. ^{1}H-NMR (200MHz, $CDCl_3$): δ = 7.06 (d, 2H, J = 8.6 Hz), 6.73 (d, 2H, J = 8.6 Hz), 6.09 (s, 2H), 5.84 (s, 1H), 5.19 (s, 1H), 4.74 (dt, 2H, J_1 = 47.4 Hz, J_2= 4.2 Hz), 4.50-4.27 (m, 2H), 4.24-4.11 (m, 2H), 4.08 (t, 1H, J = 4.2 Hz), 3.82 (s, 3H), 3.76 (s, 6H), 3.06-2.84 (m, 2H), 1.40 (s, 9H); ^{13}C NMR (50MHz, $CDCl_3$) δ =170.2, 161.1, 159.4, 157.4, 155.4, 130.6, 129.9, 114.8, 106.7, 90.8, 82.1 (d, J = 169.5 Hz), 80.0, 67.3 (d, J = 20.5 Hz), 56.4, 55.9, 55.6, 38.6, 32.4, 28.5; HRMS calcd for $C_{26}H_{35}FN_2O_7$ ([M+H]$^{+}$) 507.2507, found 507.2508; $[\alpha]^{24}_{D}$ -17.1^{o} (c 0.98, $CHCl_3$).

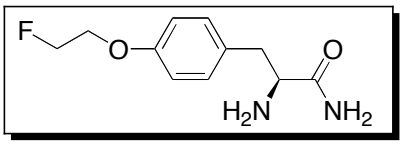

***O*-fluoroethyl tyrosine amide (4):** Propanylcarbamate (**27**, 127 mg, 0.25 mmol) was added to 1.5 mL trifluoroacetic acid and 50 μL dimethyl sulfide, a free radical scavenger. The reaction mixture was stirred in room temperature for 4 h. Upon completion, the mixture was concentrated under reduced pressure to remove TFA. The resulting mixture was dissolved in water (5 mL) and washed with ether (5 mL). The aqueous layer was neutralized to pH ~ 7 with 5% NH_4OH and extracted with ethyl acetate (15 mL) three times. Crude mixture was purified by preparative TLC (Et_3N/MeOH/CH_2Cl_2, 1/7/100), which afforded **4** as a yellowish liquid. ^{1}H-NMR (200MHz, MeOD-D_4): δ = 7.35 (d, 2H, *J* = 8.6 Hz), 7.03 (d, 2H, *J* = 8.6 Hz), 4.85 (dt, 2H, J_1 = 47.4 Hz, J_2 = 4.0 Hz), 4.62 (t, 1H, *J* = 7.0 Hz), 4.33 (dt, 2H, J_1 = 28.8 Hz, J_2 = 4.0 Hz), 3.43-3.18 (m, 2H); ^{13}C NMR (50MHz, MeOD-d4) δ =178.0, 159.3, 131.7, 130.7, 116.1, 83.3 (d, *J* = 167.5 Hz), 68.8 (d, *J* = 20.0 Hz), 57.2, 40.9; HRMS calcd for $C_{11}H_{15}FN_2O_2$ ($[M+H]^+$) 227.1196, found 227.1213. $[\alpha]^{24}_D$ -14.3^o (c 0.57, MeOH).

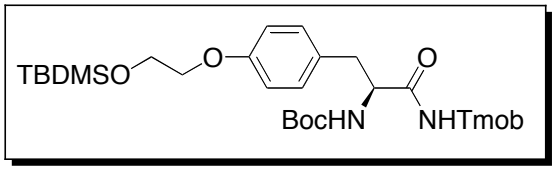

(*S*)-*tert*-butyl 3-(4-(2-(*tert*-butyldimethylsilyloxy)ethoxy)phenyl)-1-oxo-1-(2,4,6-trimethoxybenzyl amino)propan-2-ylcarbamate (29): Diisopropylethylamine (1.25 g, 9.7 mmol) was added to a solution of propanoic acid **(28,** 1.3 g, 3 mmol), 2,4,6-trimethoxybenzylamine hydrochloride (772 mg, 3.3 mmol) and 1-HOBt (527 mg, 3.9

mmol) in DMF (30 mL). The solution was cooled to 0°C before HBTU (1.35 g, 3.6 mmol) was added in one portion. Continue at 0 °C for 30 min and then room temperature for another 1.5 h. The reaction mixture was diluted with 30 mL EtOAc and 30 mL 10% citric acid. The aqueous layer was extracted twice with 30 mL EtOAc and the combined organic layer was washed with 10 mL saturated $NaHCO_3$ and 10 mL brine. The organic layer was dried over $MgSO_4$ and solvent was removed under reduced pressure. Crude mixture was purified by FC (EtOAc/Hexanes, 35/65) to produce **29** as white foam. ^1H NMR (200 MHz, $CDCl_3$) δ = 7.04 (d, 2H, *J* = 8.6 Hz), 6.73 (d, 2H, *J* =8.4 Hz), 6.09 (s, 2H), 5.88 (s, 1H), 5.19(s, 1H), 4.41-4.38 (m, 2H), 4.20-4.16(m, 1H), 3.96 (s, 4H), 3.82 (s, 3H), 3.76 (s, 6H), 3.06-2.83 (m, 2H), 1.40 (s, 9H), 0.92 (s, 9H), 0.11 (s, 6H); ^{13}C NMR (50 MHz, $CDCl_3$) δ =170.3, 161.1, 159.4, 158.0, 155.4, 130.5, 129.2, 114.7, 106.7, 90.8, 79.9, 69.5, 62.2, 56.5, 55.9, 55.5, 38.6, 32.4, 28.5, 26.1, 18.6; HRMS calcd for $C_{32}H_{50}N_2O_8Si$ ($[M+H]^+$) 619.3415, found 619.3416.

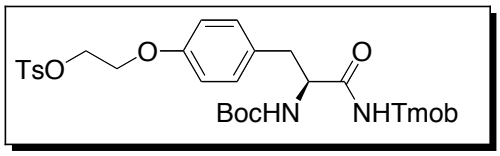

(*S*)-2-(4-(2-(*tert*-butoxycarbonylamino)-3-oxo-3-(2,4,6-trimethoxybenzyl amino)propyl)phenoxy) ethyl 4-methylbenzenesulfonate (30): A THF solution of TBAF (1 M in THF) was added to a solution of 2mL propanylcarbamate (**29**, 390 mg, 0.63 mmol). The reaction continued for 1 h before diluted with 10 mL water. The aqueous solution was extracted with ether (15 mL × 3). The combined organic layer was washed with brine and then dried over $MgSO_4$. Solvent was removed under reduced pressure. Resulting crude product was purified by FC (EtOAc/Hexanes, 75/25).

Deprotection product was then dissolved in 5 mL CH_2Cl_2, added Et_3N (200 mg, 2 mmol), TsCl (112 mg, 0.6 mmol) and DMAP (6 mg, 0.05 mmol), reaction continued overnight. Dilute reaction mixture with 40 mL CH_2Cl_2 and then washed with 5 mL saturated NaHCO3 and 5 mL brine. Organic layer dried over $MgSO_4$ and solvent was removed under reduced pressure. Crude mixture was purified by FC (EtOAc/Hexanes, 60/40) to produce 20 as yellow foam. ^{1}H NMR (200 MHz, $CDCl_3$) δ = 7.82 (d, 2H, *J* = 8.2 Hz), 7.35 (d, 2H, *J* = 8.0 Hz), 7.01 (d, 2H, *J* = 8.4 Hz), 6.60 (d, 2H, *J* = 8.4 Hz), 6.08 (s, 2H), 5.86 (s, 1H), 5.18 (s, 1H), 4.49-4.28 (m, 4H), 4.18-4.05 (m, 3H), 3.81 (s, 3H), 3.75 (s, 6H), 3.04-2.77 (m, 2H), 2.46 (s, 3H), 1.40 (s, 9H); ^{13}C NMR (50 MHz, $CDCl_3$) δ =170.2, 161.4, 159.4, 157.0, 155.4, 145.1, 133.3, 130.6, 128.2, 114.7, 106.6, 90.8, 80.0, 68.3, 65.7, 56.4, 55.9, 55.6, 38.6, 32.4, 28.5, 21.8; HRMS calcd for $C_{33}H_{42}N_2O_{10}S$ ($[M+Na]^+$) 681.2458, found 681.2463; $[\alpha]^{24}_D$ -13.4^o (c 1.05, $CHCl_3$).

2.4.3 Radiochemistry

In general, [^{18}F]Fluoride was passed through a Sep-Pak light QMA cartridge (Waters, preconditioned with 10 mL 1 N $NaHCO_3$, 10 mL water and dried with N_2). The ^{18}F activity was eluted with 1.1 mL Kryptofix 222 K[2.2.2] /K_2CO_3/CH_3CN/H_2O solution (11 mg/2 mg/ 0.93 mL/0.17 mL), azeotropically dried twice under N_2 at 110^{o}C. Then 5 mg precursor in 1 mL anhydrous CH_3CN was added into ^{18}F. Fluorination reaction continued for 10 min at 90^{o}C. Chemical, radiochemical purity and specific activity of radioligands were analyzed with analytical HPLC and TLC. TLC system: NH_4OH/MeOH/ CH_2Cl_2, 1/6/14, FET R_f is 0.3, FEMT R_f is 0.4, FETA is 0.6. TLC system: NH_4OH/ MeOH/ CH_2Cl_2, 1/10/10, FEAT R_f is 0.4. Semi-Preparative HPLC was

carried out on a column (Phenomenex Gemini C18 semi-preparative column, 10 × 250 mm, 5 μm). Radiochemical purity was determined by analytical HPLC (Phenomenex Gemini C18 analytical column, 4.6 ×250 mm, 5 μm, UV detector set at 275 nm) and TLC. Three solvent systems were used in analytical HPLC: A: ethanol/0.1 % formic acid, 10/90 (for FET and FEMT) or 2/98 (FEAT), flow rate 1mL/min; B: Gradient: 0-2 min: 100% 10mM ammonium formate buffer (AFB); 2-5min: ACN: AFB (70:30); 5-10 min: 100% ACN; 10-15% 100% AFB, flow rate 1mL/min; C: MeOH/0.1% NH_3, 40/60, 1mL/min. For analytic HPLC solvent system A (ethanol/ 0.1% formic acid, 10/98 for FET/ FEMT and 2/98 for FEAT), retention time was 5.8 min for FET, 7.2min for FEMT and 5.5 min for FEAT respectively. For solvent system B, retention time was 7.3 min for FET, 7.0 min for FEMT, 7.6 min for FEAT and 7.8 min for FETA respectively. With solvent system C, retention time was 5.2 min for FETA. Details regarding purification and deprotection reactions were described in the following paragraphs:

FET ([^{18}F]1): After fluorination, the reaction mixture was injected to semi-preparative HPLC, eluent MeOH/H_2O (80:20), flow rate 3 mL/min. Radioactive peak between 10.5 min to 12 min was collected and then diluted with 20 mL water, loaded on HLB oasis cartridge (preconditioned with 1 mL ethanol and 5 mL water) and then eluted with 1mL ethanol. Solvent was removed under N_2, and then 0.25 mL TFA was added, and heated at 60^{o}C for 10 min. TFA was removed with a N_2 flow, and then 1 mL water was added to produce the final product.

FEMT ([^{18}F]2): After fluorination, the reaction mixture was diluted with 10 mL water, loaded on an Oasis HLB cartridge (preconditioned with 1 mL ethanol and 5 mL water), washed twice with 2 mL water, eluted with 1mL CH_2Cl_2. Dry CH_2Cl_2 under a N_2

flow, and 0.5 mL TFA was added to the reaction mixture. The reaction continued at 60°C for 5 min. TFA was blow dried, and then 0.5 mL 2N NaOH was added, and refluxed at 100°C for 10 min. The reaction mixture was neutralized with 2N HCl and then ~0.5mL PBS buffer was added, and loaded on a semi-preparative HPLC (ethanol/H_2O, 10/90, flow rate 3.5 mL/min). Fraction containing FEMT (between 12 to 13 min) was collected.

FEAT ([^{18}F]3): After fluorination, the reaction mixture was injected into a semi-preparative HPLC (MeOH/H_2O, 65/35, flow rate 3mL/min), and a radioactive peak between 9.5 to 11 min was collected. Diluted with 20 mL water then loaded on an oasis HLB cartridge and eluted with 1mL ethanol. The solution was added to 0.5 mL 6M HCl, refluxed at 120°C for 10 min, neutralized with 2 N NaOH, and added to PBS buffer to adjust pH ~6.

FETA ([^{18}F]4): After fluorination, the reaction mixture was diluted with 10 mL water, loaded on an Oasis HLB cartridge (preconditioned with 1 mL ethanol and 5 mL water), washed twice with 2 mL water, and eluted with 1mL ethanol. Ethanol was dried under a N_2 flow, and 0.25 mL TFA was added to the reaction mixture. The reaction continued at 60°C for 10 min. TFA was blow dried and then 1 mL water was added and loaded on a semi-preparative HPLC (methanol/0.1% NH_3, 4/6, flow rate 3 mL/min). Fraction containing FEMT (between 11 to 13 min) was collected, diluted with 20 mL water, loaded on a HLB cartridge and eluted with 1mL ethanol. Ethanol was removed under N_2 and final product was dissolved in 1 mL water.

2.4.4 In vitro cell studies

Cell culture: U-138 MG in Eagle's Minimum Essen-tial Medium (EMEM), supplemented with 10% Fetal Bovine Serum (FBS) and 1% streptomycin. Cells were incubated at 37^{o}C under 5% CO_2 and were subcultured by trypsinization using 0.25% trypsin-EDTA. **Cell uptake studies**: cells were seeded at 2×10^5 cells/well in 12 well tissue culture plates. After 24 h of incubation at 37°C, cells formed monolayer and reached confluence. Cells were washed three times with warmed phosphate-buffered saline (PBS) solution and were incubated with 1 mL of PBS containing approximately 0.5 MBq (14 μCi) of ligands. Uptake experiments were run for 5, 30, 60 and 120 min at 37°C. After incubation, PBS was quickly removed, and the cells were washed three times with cold PBS (w/o Ca++ and Mg++) and then lysed with 350 μL 1 N NaOH. Transfer resulting solution to test tubes for radioactivity measurement. The uptake results were normalized to protein content and to the total activity administered. Results are expressed as the percentage of radioactivity accumulated per 100 μg protein.

2.5 References

[1] Buerkle A and Weber WA. Imaging of tumor glucose utilization with positron emission tomography. Cancer Metastasis Rev 2008;27:545-54.

[2] Cheson BD, Pfistner B, Juweid ME, Gascoyne RD, Specht L, Horning SJ, et al. Revised response criteria for malignant lymphoma. J Clin Oncol 2007;25:579-86.

[3] Kelloff GJ, Hoffman JM, Johnson B, Scher HI, Siegel BA, Cheng EY, et al. Progress and promise of FDG-PET imaging for cancer patient management and oncologic drug development. Clin Cancer Res 2005;11:2785-808.

[4] Paul AK and Abdel-Nabi H. Cancer imaging agents for positron emission tomography: Beyond FDG. Current Medical Imaging Reviews 2007;3:178-85.

[5] McConathy J and Goodman Mark M. Non-natural amino acids for tumor imaging using positron emission tomography and single photon emission computed tomography. Cancer metastasis reviews 2008;27:555-73.

[6] Inoue T, Kim EE, Wong FC, Yang DJ, Bassa P, Wong WH, et al. Comparison of fluorine-18-fluorodeoxyglucose and carbon-11-methionine PET in detection of malignant tumors. J Nucl Med 1996;37:1472-6.

[7] Singhal T, Narayanan TK, Jain V, Mukherjee J, and Mantil J. 11C-L-methionine positron emission tomography in the clinical management of cerebral gliomas. Mol Imaging Biol 2008;10:1-18.

[8] Hatazawa J, Ishiwata K, Itoh M, Kameyama M, Kubota K, Ido T, et al. Quantitative evaluation of L-[methyl-C-11] methionine uptake in tumor using positron emission tomography. J Nucl Med 1989;30:1809-13.

[9] Derlon JM, Bourdet C, Bustany P, Chatel M, Theron J, Darcel F, et al. [11C]L-methionine uptake in gliomas. Neurosurgery 1989;25:720-8.

[10] Wester HJ, Herz M, Weber W, Heiss P, Senekowitsch-Schmidtke R, Schwaiger M, et al. Synthesis and radiopharmacology of O-(2-[18F]fluoroethyl)-L-tyrosine for tumor imaging. J Nucl Med 1999;40:205-12.

[11] Inoue T, Tomiyoshi K, Higuichi T, Ahmed K, Sarwar M, Aoyagi K, et al. Biodistribution studies on L-3-[fluorine-18]fluoro-alpha-methyl tyrosine: a potential tumor-detecting agent. J Nucl Med 1998;39:663-7.

[12] Garnett ES, Firnau G, and Nahmias C. Dopamine visualized in the basal ganglia of living man. Nature 1983;305:137-8.

[13] Schuster DM, Votaw JR, Nieh PT, Yu W, Nye JA, Master V, et al. Initial experience with the radiotracer anti-1-amino-3-18F-fluorocyclobutane-1-carboxylic acid with PET/CT in prostate carcinoma. J Nucl Med 2007;48:56-63.

[14] Schuster DM, Nye JA, Nieh PT, Votaw JR, Halkar RK, Issa MM, et al. Initial experience with the radiotracer anti-1-amino-3-[18F]Fluorocyclobutane-1-carboxylic acid (anti-[18F]FACBC) with PET in renal carcinoma. Mol Imaging Biol 2009;11:434-8.

[15] Rau FC, Weber WA, Wester HJ, Herz M, Becker I, Kruger A, et al. O-(2-[(18)F]Fluoroethyl)- L-tyrosine (FET): a tracer for differentiation of tumour from inflammation in murine lymph nodes. Eur J Nucl Med Mol Imaging 2002;29:1039-46.

[16] Langen KJ, Hamacher K, Weckesser M, Floeth F, Stoffels G, Bauer D, et al. O-(2-[18F]fluoroethyl)-L-tyrosine: uptake mechanisms and clinical applications. Nucl Med Biol 2006;33:287-94.

[17] Ishiwata K, Kawamura K, Wang WF, Furumoto S, Kubota K, Pascali C, et al. Evaluation of O-[11C]methyl-L-tyrosine and O-[18F]fluoromethyl-L-tyrosine as tumor imaging tracers by PET. Nucl Med Biol 2004;31:191-8.

[18] Tang G, Wang M, Tang X, Luo L, and Gan M. Synthesis and evaluation of O-(3-[18F]fluoropropyl)-L-tyrosine as an oncologic PET tracer. Nucl Med Biol 2003;30:733-9.

[19] Arstad E and Robins EG. PET radiotracers.; 2007, p. 32.

[20] Laverman P, Boerman OC, Corstens FH, and Oyen WJ. Fluorinated amino acids for tumour imaging with positron emission tomography. Eur J Nucl Med Mol Imaging 2002;29:681-90.

[21] Plathow C and Weber WA. Tumor cell metabolism imaging. J Nucl Med 2008;49 Suppl 2:43S-63S.

[22] Mastroberardino L, Spindler B, Pfeiffer R, Skelly PJ, Loffing J, Shoemaker CB, et al. Amino-acid transport by heterodimers of 4F2hc/CD98 and members of a permease family. Nature 1998;395:288-91.

[23] Yanagida O, Kanai Y, Chairoungdua A, Kim DK, Segawa H, Nii T, et al. Human L-type amino acid transporter 1 (LAT1): characterization of function and expression in tumor cell lines. Biochim Biophys Acta 2001;1514:291-302.

[24] Sakata T, Ferdous G, Tsuruta T, Satoh T, Baba S, Muto T, et al. L-type amino-acid transporter 1 as a novel biomarker for high-grade malignancy in prostate cancer. Pathol Int 2009;59:7-18.

[25] Fuchs BC and Bode BP. Amino acid transporters ASCT2 and LAT1 in cancer: partners in crime? Semin Cancer Biol 2005;15:254-66.

[26] Uchino H, Kanai Y, Kim DK, Wempe MF, Chairoungdua A, Morimoto E, et al. Transport of amino acid-related compounds mediated by L-type amino acid transporter 1

(LAT1): insights into the mechanisms of substrate recognition. Mol Pharmacol 2002;61:729-37.

[27] Langen K-J, Pauleit D, and Coenen HH. 3-[123I]iodo-a-methyl-L-tyrosine: uptake mechanisms and clinical applications. Nucl Med Bio 2002;29:625-31.

[28] Monden Y, Hamano Takaku F, Shindo Okada N, and Nishimura S. Azatyrosine. Mechanism of action for conversion of transformed phenotype to normal. Ann N Y Acad Sci 1999;886:109-21.

[29] Liu WQ, Vidal M, Olszowy C, Million E, Lenoir C, Dhotel H, et al. Structure-activity relationships of small phosphopeptides, inhibitors of Grb2 SH2 domain, and their prodrugs. J Med Chem 2004;47:1223-33.

[30] Hamacher K and Coenen HH. Efficient routine production of the F-18-labelled amino acid O-(2-[F-18]fluoroethyl)-L-tyrosine. Appl. Radiat. Isot. 2002;57:853-6.

[31] Krasikova RN, Kuznetsova OF, Fedorova OS, Maleev VI, Saveleva TF, and Belokon YN. No carrier added synthesis of O-(2 '-[F-18]fluoroethyl)-L-tyrosine via a novel type of chiral enantiomerically pure precursor, Ni-II complex of a (S)-tyrosine Schiff base. Bioorg. Med. Chem. 2008;16:4994-5003.

[32] Germain H, Harris CS, Renaud F, and Warin N. Efficient Large-Scale Synthesis of Boc-L-azatyrosine. Syn. Commun. 2009;39:523-30.

[33] Wang L, Qu W, Lieberman B, Ploessl K, and Kung HF. Synthesis and in vitro evaluation of 18F labeled tyrosine derivatives as potential positron emission tomography (PET) imaging agents. Bioorg Med Chem Lett 2010;20:3482-5.

[34] Prante O, Blaser D, Maschauer S, and Kuwert T. In vitro characterization of the thyroidal uptake of O-(2-[(18)F]fluoroethyl)-L-tyrosine. Nucl Med Biol 2007;34:305-14.

[35] Prante O, Deichen JT, Hocke C, and Kuwert T. Characterization of uptake of 3-[(131)I]iodo-alpha-methyl-L-tyrosine in human monocyte-macrophages. Nucl Med Biol 2004;31:365-72.

[36] Morimoto E, Kanai Y, Kim do K, Chairoungdua A, Choi HW, Wempe MF, et al. Establishment and characterization of mammalian cell lines stably expressing human L-type amino acid transporters. J Pharmacol Sci 2008;108:505-16.

Chapter 3

Synthesis, uptake mechanism characterization and biological evaluation of ^{18}F labeled fluoroalkyl L-phenylalanine analogs as potential tumor imaging agents for PET

3.1 Introduction

Malignant tumors can be detected by imaging their increased metabolic rates for glucose, lipids and amino acids [1]. One interesting metabolic process as a target for metabolic tumor imaging is increased protein metabolism in proliferating cancer cells. Avid uptake of amino acids is a normal feature of rapidly proliferating cells [2]. A number of radiolabeled amino acids (Figure 3.1) were developed and have established role in clinical applications, especially in brain tumor imaging [3, 4]. Amino acid based tracers could overcome certain limitations of most commonly used 2-[^{18}F]fluoro-2-deoxy-D-glucose (FDG), namely high accumulation in inflammatory tissues and high uptake in normal brain tissues [4].

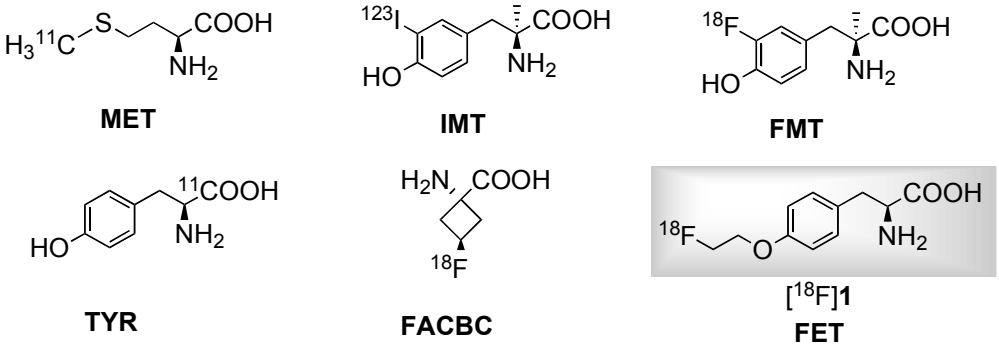

Figure 3.1. Some clinically utilized amino acid based tracers

Uncontrolled and accelerated growth of cancer cells lead to elevated rate of protein synthesis and increased uptake of amino acids as energy source as well as carbon and nitrogen source in the synthesis of nucleotides, amino sugars et al [5]. Some natural amino acid based tracers such as [^{11}C]methionine (MET) and [^{11}C]tyrosine (TYR), their uptake reflects transport, protein synthesis and non-protein metabolic pathways such as transamination and transmethylation, which makes imaging kinetic analysis difficult [6-

8]. While uptake of non-natural amino acids such as *O*-(2-[^{18}F]fluoroethyl)-L-tyrosine (FET, [^{18}F]**1**) [9], 3-[^{18}F]fluoro-α-methyl-L-tyrosine (FMT) [10], anti-1-amino-3-[^{18}F]fluoro-cyclobutyl-1-carboxylic acid (FACBC) [11], 3-[^{123}I]-α-methyl-L-tyrosine (IMT) [12] represents mainly transport activity but not protein synthesis. It appears that their differences in protein metabolism do not translate into difference in clinical applicability[3]. Moreover, ^{18}F ($t_{1/2}$ = 109.8 min) and ^{123}I ($t_{1/2}$ = 13.2 h) labeled non-natural amino acid derivatives have advantage of longer half-life than ^{11}C ($t_{1/2}$ = 20.2 min) and are generally more stable in vivo which simplifies image analysis [3, 4, 13]. For these reason, non-natural amino acids have been a main focus in current development of amino acid tracers [3, 14, 15].

Amino acids are taken up into cells mainly through specific membrane associated carrier proteins. Increased uptake of amino acids is mediated through increased expression and activity of amino acid transporters. Amino acid transporters identified so far are solute carrier transporters (SLC), which are classified into a number of transporter systems based on their sodium dependence, substrate specificity, kinetics, regulatory properties and sensitivity to pH and specific inhibitors [16]. Most commonly existing amino acid transporter systems in mammalian cells responsible for transporting neutral amino acids are system A (alanine preferring), ASC (alanine-serine-cystine preferring) and system L (leucine preferring) [17]. Sodium-independent amino acid transport system L (LATs), which is a major route for transporting large branched and aromatic amino acids has attracted special interest [18]. Studies demonstrated that system L is a promising target for developing PET tumor imaging agents [3, 4, 19]. The broad substrate selectivity of LATs enables it to transport amino acid-related compounds. A number of

substrates of LATs, such as MET, FET, FACBC, IMT, are clinically utilized for imaging brain cancer, head and neck cancer, lung cancer and prostate cancer et al [3, 4, 15]. System L is commonly upregulated in many tumors and correlated with tumor growth and prognosis [19-21]. There are four subtypes of LATs identified and characterized in molecular level, designated LAT1 to LAT4 [22]. In particular, LAT1 is most studied. LAT1 is primarily expressed in brain, placenta and tumors and closely correlated with angiogenesis [23], cell proliferation [23] and prognosis of patients with astrocytoma [24], non-small cell lung cancer (NSCLC) [25] and prostate cancer [26].

Phenylalanine and tyrosine derivatives, which are primarily LATs substrate, have proven to be useful tumor imaging agents [3, 4]. In particular, FET ([^{18}F]**1)** is one of the first ^{18}F labeled amino acid tracers that could be prepared in large quantity for clinical use and satellite distribution similar to FDG [27]. FET is useful for detecting brain tumors and head and neck squamous carcinoma, but its applications in peripheral tumors are somewhat limited [28, 29]. Another clinically utilized system L substrate *p*-[^{123}I]iodo-L-phenylalanine (IPA) demonstrated potential for imaging brain tumor as well [30]. This led us to develop its fluoroalkyl derivatives, which are also structural analogs of FET. Our goal is to develop new amino acid tracers with improved in vivo pharmacokinetics than FET, which could lead to a higher tumor uptake and/or lower urinary excretion that may be beneficial for imaging tumors in urinary tract such as prostate cancer, urinary bladder carcinomas and cervical cancer [31, 32]. Eliminating oxygen to form direct linkage of fluoroalkyl chain to phenyl ring provides a way to alter ligands' lipophilicity as well as to reduce length of side chain. In this study, we describe the synthesis, radiolabeling and biological evaluation of two new phenylalanine derivatives, *p*-(2-

[^{18}F]fluoroethyl)-L-phenylalanine (FEP, [^{18}F]**2**) and *p*-(3-[^{18}F]fluoropropyl)-L-phenylalanine (FPP, [^{18}F]**3**) (Figure 3.2). Clinically utilized FET ([^{18}F]**1**) was used as reference in biological evaluation of new ligands.

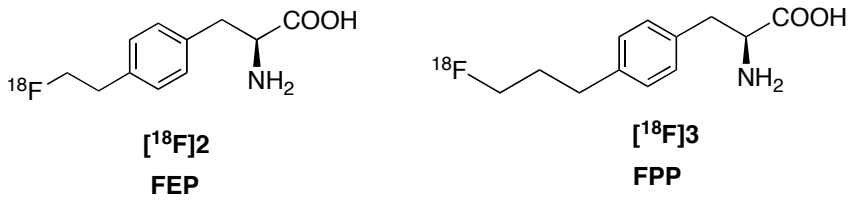

Figure 3.2. Chemical structures of new phenylalanine derivatives

3.2 Results and Discussion

3.2.1 Synthesis of precursors and authentic standards

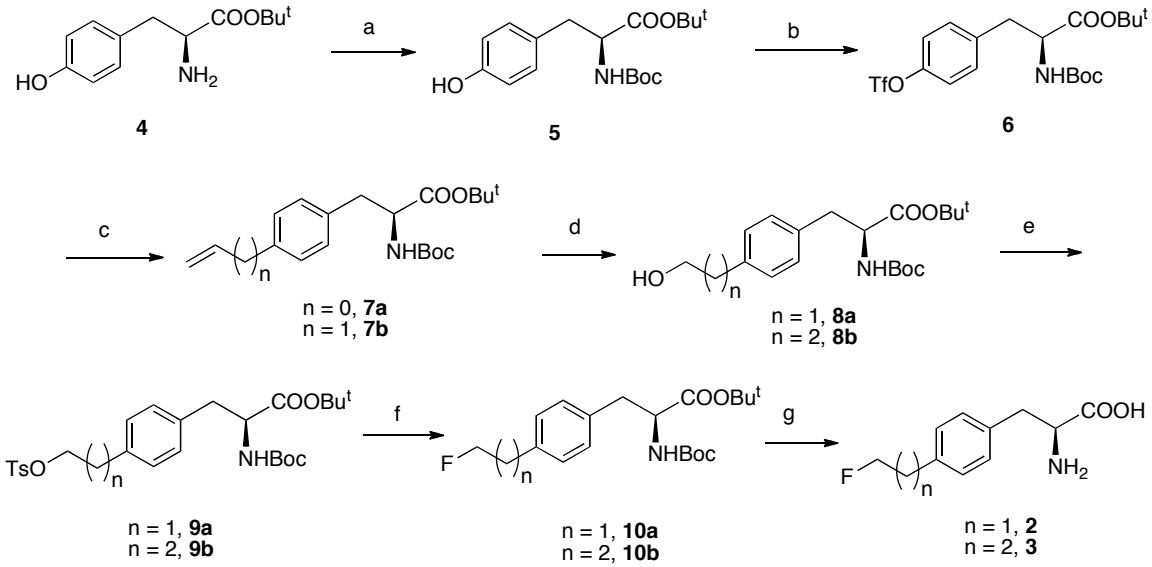

Scheme 3.1. Synthesis precursors and standards **2** and **3** for radiolabeling. Reagents and Conditions: a) $(Boc)_2O$, $NaHCO_3$, MeOH, H_2O, rt, 89%; b) 2. Tf_2O, pyridine, CH_2Cl_2, 0°C, 93%; c) Tributyl vinyltin or tributyl allyltin, LiCl, $Pd(PPh_3)_2Cl_2$, DMF, 70°C, 92% (n = 0) or 95% (n = 1); d) 9-BBN, THF, NaOH, H_2O_2, 86% (n = 1) or 88% (n = 2); e) TsCl, Et_3N, CH_2Cl_2, 92% (n = 1) or 75% (n = 2); f) i. NaI, acetone, reflux; ii. AgF, CH_3CN, 50% (n = 1) or 58% (n = 2); g) TFA, CH_2Cl_2, 81% (n = 1) or 64% (n = 2).

An efficient synthesis of fluoroalkyl phenylalanine derivatives **2** and **3** was carried out as shown in Scheme 3.1. The tosylate precursors **9a** and **9b** for labeling could be prepared in five steps in an overall yield of 60 and 52% respectively starting from commercially available L-tyrosine *tert*-butyl ester. Standard Boc protection of amine group and then triflation of phenol group on protected tyrosine **5** afforded triflate **6** in 83% yield. Triflate **6** then underwent Stille cross-coupling reaction with vinyl or allyl tributylstanne and Pd catalyst $Pd(PPh_3)_2Cl_2$ in anhydrous DMF at 70 ^oC for 1 h to yield corresponding alkenes. Hydroboration alkenes **7a** or **7b** with 9-BBN and subsequent oxidation with sodium peroxide afforded aliphatic alcohol **8a** and **8b** in 86 to 88% yield. We chose 9-BBN as hydroboration reagent because of its high regio-selectivity in comparison to BH_3 reagent, initial reaction with BH_3·THF had low yield (< 20%). Tosylation of the alcohol compounds afforded labeling precursors in 75 to 92% yield. Initially we tried to use diethylaminosulfur trifluoride **(**DAST) to covert aliphalic alcohol **8a** directly to fluoride **10a**, however under this reaction condition, it is difficult to obtain chemically pure product. In addition, commonly used fluorination reagent tetrabutylammonium fluoride (TBAF) might cause isomerization resulting fluorinated product in racemic form, so here we choose to adapt mild fluorination condition in the neutral solution. After a two-step fluorination – tosylate **9a** or **9b** was first convert to iodide by refluxing with sodium iodide in acetone and then fluorinated by reacting with silver fluoride, and deprotection with TFA, the standard **2** and **3** were obtained in an overall yield of 24% and 19% respectively. The enantiomeric purity of precursors and standards for radiolabeling is >95% analyzed by chiral HPLC.

3.2.2 Radiosynthesis of phenylalanine derivatives

Preparation of FEP ([^{18}F]**2**) and FPP ([^{18}F]**3**) was carried out via a two-step reaction as shown in Scheme 3.2. First step was no-carrier-added (NCA) nucleophilic fluorination with dried TBA^{18}F and $TBAHCO_3$ in acetonitrile. Intermediate [^{18}F]**10a** or [^{18}F]**10b** was then subjected to semi-preparative HPLC purification and HLB oasis solid phase extraction to eliminate unreacted ^{18}F fluoride and other by-products. Second step was to remove protecting groups using TFA at 60 °C. The results of labeling reactions were summarized in Table 3.1. Enantiomerically pure [^{18}F]**2** and [^{18}F]**3** could be prepared in 90 min with high radio purity (> 95% as measured by analytical HPLC and TLC), moderate to good radiochemical yield (11 to 37%) and high specific activity (21 to 69 GBq/μmol) at the end of synthesis.

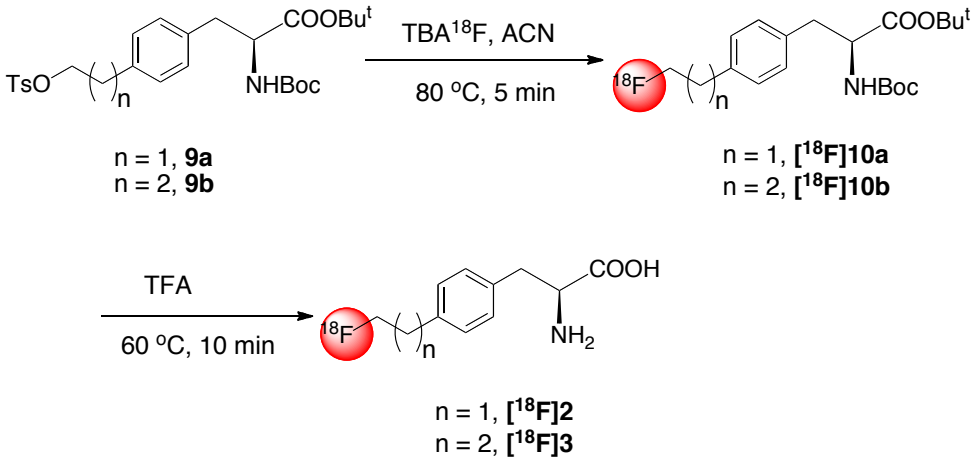

Scheme 3.2. Radiolabeling of FEP ([^{18}F]**2**) and FPP ([^{18}F]**3**)

Table 3.1. Overall synthesis time, decay-corrected RCY, radiochemical purity (RCP), enantiomeric purity and specific activity (EOS) *

Ligands	Synthesis time (min)	RCY (%)	RCP (%)	Enantiomeric Purity (%)	Specific activity (GBq/ μmol)
[^{18}F]**2**	75–82	27–37	> 95	> 95	31–69
[^{18}F]**3**	78–90	11–23	> 95	> 95	21–25

*Data obtained from two to six experiments

3.2.3 Cell uptake studies

At first, we compared the time dependent uptake of new ligands FEP ([^{18}F]**2**) and FPP ([^{18}F]**3**) to clinically utilized FET ([^{18}F]**1**) in 9L gliosarcoma cells (Figure 3.3). Uptake of tracers was measured at selected time points up to 2 h. Three ligands demonstrated very similar kinetics, reaching maximum uptake within 60 min and then washed out. The uptake follows order FEP ([^{18}F]**2**)> FET ([^{18}F]**1**) ≈ FPP ([^{18}F]**3**). The maximum uptake of FEP is about 1.4 fold of FET. In vitro uptake studies showed FEP had a high accumulation and good retention in 9L glioma cells. The uptake results indicate that shorter side chain length may be more desirable for aromatic amino acid tracers. This agrees with the results reported by Tsukada et al, they found the shorter ^{18}F-fluoroalkyl chain length L-tyrosine provided a better tumor-to-blood ratio [33].

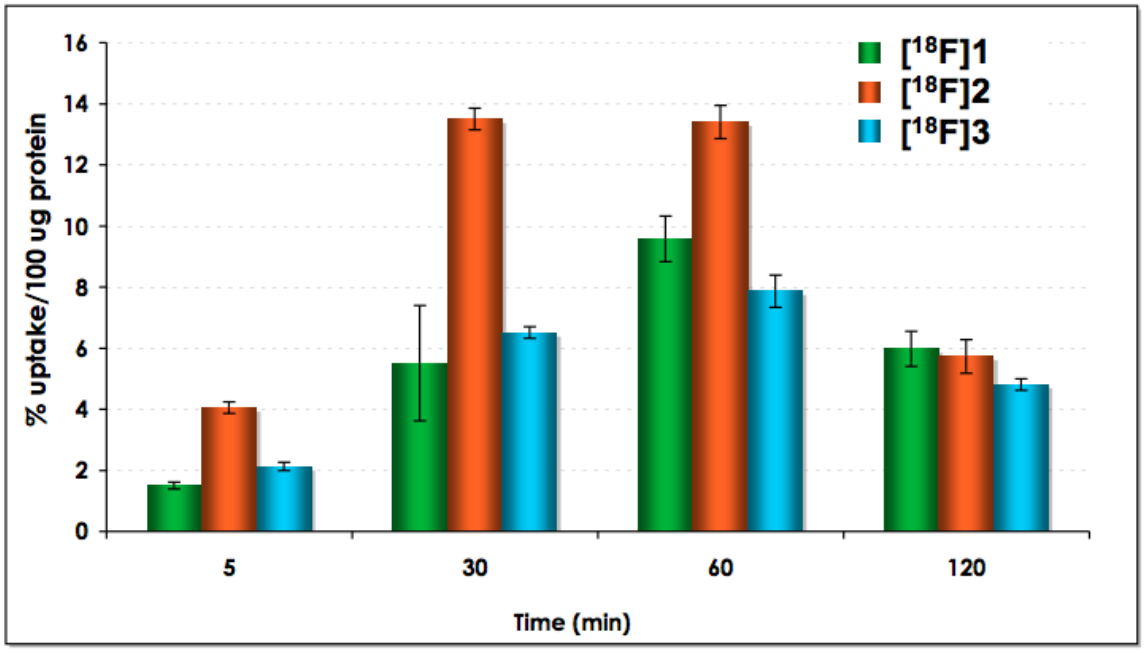

Figure 3.3. Time course of uptake of FET ([^{18}F]**1**), FEP ([^{18}F]**2**) and FPP ([^{18}F]**3**) in 9L glioma cells. The uptake value was represented as % uptake/100 ug protein, mean ± SD (n = 3).

3.2.4 Uptake mechanism studies of FEP

Uptake of amino acid based tracers depends on a group of amino acid transport systems, which often have substantial overlap in substrate selectivity and thus a single radiolabeled amino acid can be substrate for multiple amino acid transport systems. We are interested in characterizing the uptake mechanism of FEP ([^{18}F]**2**) into tumor cells. To achieve this goal, we conducted competitive uptake inhibition studies using inhibitors specific for system A, ASC and L, given that transport of neutral amino acids into mammalian cells is predominantly via these systems [21]. The uptake of FEP ([^{18}F]**2**) was measure in absence of inhibitors as well as in the presence of concentration from 0.5 to 5 mM of *N*-methyl-α-aminoisobutyric acid (MeAIB), L-alanine (L-Ala), L-serine(L-Ser), 2-amino-bicylo[2.2.1]heptane-2-carboxylic acid (BCH), D-methionine and *N*-Ethyl maleimide (NEM). The specificity and structure of the inhibitors are listed in Table 3.2.

Table 3.2 Inhibitors and their specificity towards amino acid transport systems

Inhibitors	Structure	Specificity
MeAIB	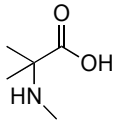	System A
L-Ser	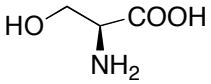	System ASC,
L-Ala	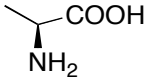	ASC, A, LAT2
BCH	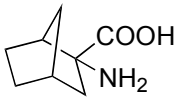	System L, B^0, $B^{0,+}$
D-Met	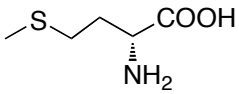	LAT1
NEM	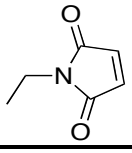	LAT2, LAT3, LAT4

MeAIB is selective inhibitor of system A while L-Ala and L-Ser are inhibitors of system ASC. BCH is primarily an inhibitor for sodium independent system L but it is also an inhibitor for sodium dependent system B^0 and $B^{0,+}$ [17]. To measure the contribution from sodium dependent transport systems, we carried out sodium dependence studies comparing uptake in sodium-free buffer to uptake in PBS. To further explore the preference of FEP towards the subtypes of LATs, we carried out competitive inhibition studies using D-Met, specific inhibitor for LAT1 and *N*-ethylmaleimide (NEM), inhibitor for other subtypes LAT2 to LAT4 [22, 34].

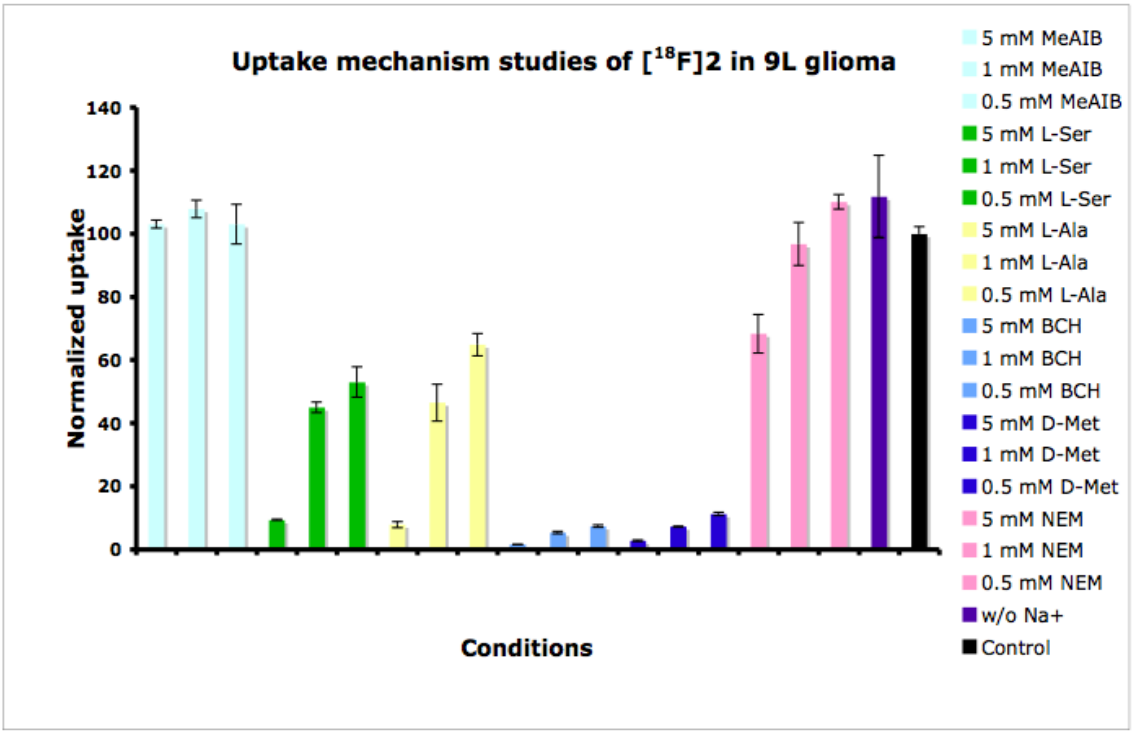

Figure 3.4. Summary of uptake characterization studies of FEP ([^{18}F]**2**) in 9L gliomas. Results were normalized to uptake of [^{18}F]**2** in PBS solution at 30 min. Data are expressed as mean ± SD (n = 3)

The studies were performed with a 30 min incubation time and the results were normalized to uptake of FEP in phosphate buffer solution (PBS) in absence of inhibitors as summarized in Figure 3.4. Uptake of FEP ([^{18}F]**2**) is sodium independent since

replacing Na^+ with choline showed no difference. The effect of inhibition is concentration dependent. Uptake of FEP is most sensitive to inhibitor of LATs. 5 mM BCH can inhibit more than 98% of uptake. On the contrast, no inhibition was observed using MeAIB, which indicates system A has no contribution in uptake of FEP. Inhibition of ASC via L-Ala or L-Ser has some effect but not as significant as system L, maximum inhibition at 5 mM is about 90%. The results demonstrated that FEP ([^{18}F]**2**) was selective substrate for sodium independent transporter system L. Futhermore, LAT1 specific inhibitor D-Met has very similar effect as BCH. The impact of NEM on the uptake is much less compared to D-Met, the maximum inhibition at 5 mM is ~30%, this suggests uptake of FEP may prefer LAT1 in comparison to other subtypes of LATs. It is an interesting difference in comparison to previously reported FET ([^{18}F]**1**), which is suggested to be selectively transported via LAT2. [27] There is some advantage targeting LAT1 because it plays a critical role in cell growth and proliferation and shows increased transport activity in many malignant tumors [19, 20]. LAT1 expression is rarely detected in nontumor areas, in contrast, LAT2 is more ubiquitously expressed and has a high level of expression in small intestine, kidney, placenta, as well as tissues rich in (re)absorbing epithelia [35]. Some cancer cells such as C6 rat glioma, HeLa cervix carcinoma cells and R1M rhabdomyosarcoma have high expression of LAT1 but showed no upregulation of LAT2. [36, 37] In such cancer cells lack of expression of LAT2, FEP ([^{18}F]**2**) might have advantage over FET ([^{18}F]**1**). Further investigations are needed to confirm the amino acid transport systems involved in the uptake process.

3.2.5 Biodistribution studies of FEP

From in vitro studies results, FEP seemed to be a potential tracer that worth further investigations, so in vivo evaluations were conducted. The in vivo biodistribution studies were carried out in fisher rats bearing 9L tumor model, which is a well-established animal model mimicking clinical glioblastoma multiform and a number of amino acid based tracers used this model for biological evaluations [11, 38]. The distribution of radioactivity in selective peripheral tissues and organs and the regional radioactivity distribution in rat brain at 30 min and 60 min after injection of FEP were shown in Table 3.3.

Table 3.3[a]. Biodistribution of FEP in Fisher rats with 9L xenograft. After single intravenous injection, results reprented as % ID/g, mean ± SD (six rats per time point)

Organs	30 min	60 min
Blood	0.73 ± 0.08	0.65 ± 0.05
Heart	0.70 ± 0.07	0.63 ± 0.05
Muscle	0.58 ± 0.05	0.62 ± 0.05
Lung	0.68 ± 0.08	0.61 ± 0.05
Kidney	0.72 ± 0.05	0.63 ± 0.05
Pancreas	2.66 ± 0.20	2.45 ± 0.27
Spleen	0.75 ± 0.06	0.69 ± 0.05
Liver	0.71 ± 0.07	0.63 ± 0.05
Skin	0.57 ± 0.07	0.60 ± 0.09
Brain	0.53 ± 0.03	0.52 ± 0.05
Bone	0.41 ± 0.03	0.41 ± 0.04
Tumor[b]	0.82 ± 0.06	0.90 ± 0.20
Tumor/Brain	1.55	1.73
Tumor/Muscle	1.41	1.45

[a]Experiment carried out by Brian Lieberman [39]

[b]Tumor n = 5 per time point.

The results showed FEP had higher accumulation in 9L tumor compared to surrounding organs and tissues. The tumor to brain and tumor to muscle ratio increased

slightly from 30 to 60 min (from 1.55 to 1.73). Tumor to blood ratio increases from 1.12 at 30 min to 1.38 at 60 min. The highest uptake was found in the pancreas, accumulation in other organs is lower than that in tumor. Bone uptake is not significant, which indicates that FEP ([^{18}F]**2**) is metabolically stable. Similar to FET ([^{18}F]**1)** [38], FEP ([^{18}F]**2)** had high uptake in pancreases. This is typical for labeled amino acid analog in rodents, which might due to high protein turnover in pancreas. Tumor uptake, bone uptake and tumor to muscle ratio is comparable to reported FET results in the same rat tumor model, but FEP seems to have slightly higher normal brain uptake compared with FET resulting lower tumor to brain ratio [38].

3.2.6 Small animal imaging studies

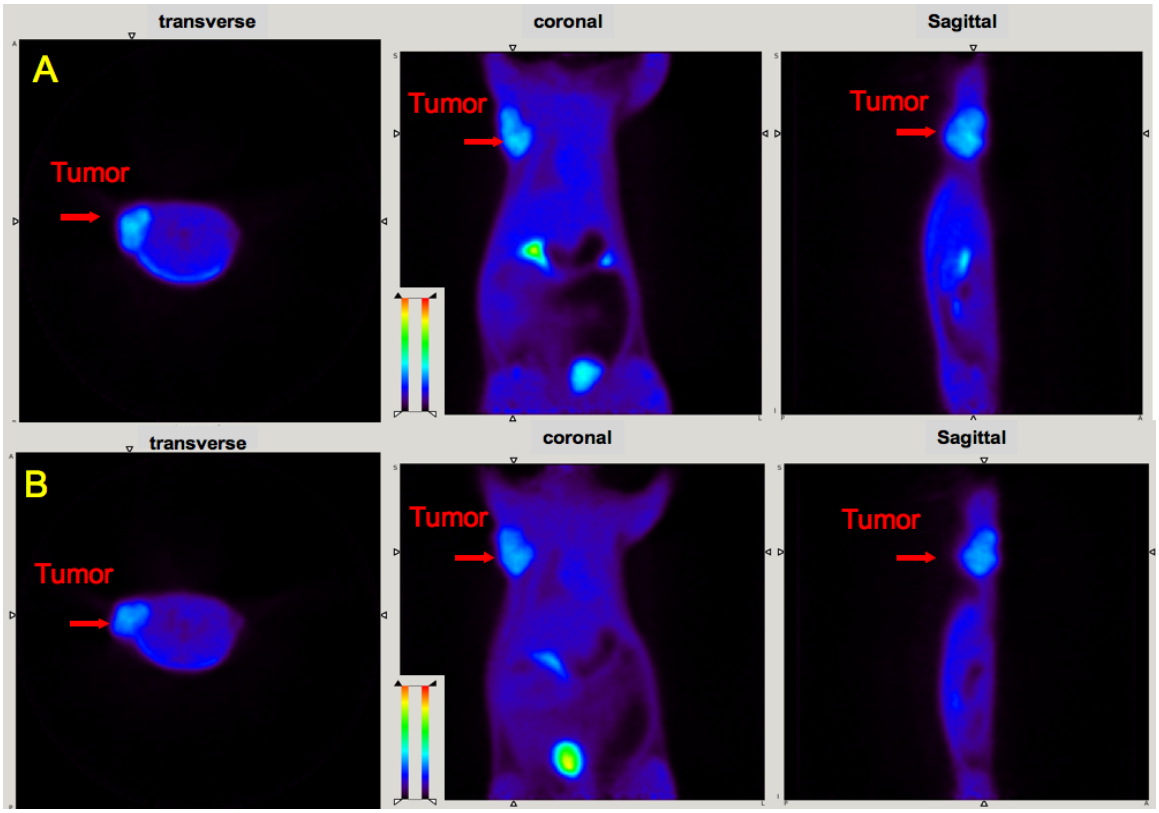

Figure 3.5[a]. Small animal PET images of FEP ([^{18}F]**2**, A) and FET ([^{18}F]**1**,B) in tumor bearing rats. Color-coded PET images from summed 2 h data in transverse, coronal and sagital view from left to right followed injection of FEP and FET are shown. The arrowhead points to the 9L tumor.
[a]Experiment carried out by Brian Lieberman [39]

Finally, the in vivo tumor imaging in the rats bearing 9L model was examined. Small animal PET imaging studies in living rats were performed and time-activity curves were generated by drawing region of interest to assess the kinetics of FEP ([^{18}F]**2**) in comparison to FET ([^{18}F]**1**). FET and FEP exhibited very similar results as shown in Figure 3.5, a summed 2 h image. Tracers kinetics were similar as demonstrated in Time activity curve in Figure 3.6. Both tracers have higher accumulations in tumors than surrounding background. After 20 min of intravenous injection of FEP, radioactivity in heart and muscle reached a plateau (Figure 3.6a). FEP had prolonged accumulation in 9L tumors with a slow steadily increase in 2 h imaging period. High urinary excretion was observed for both tracers, which is typical for tyrosine and phenylalanine analogs. Tumor to muscle ratio of these two ligands is comparable, which rapidly reached a plateau within 20 min (as shown in Figure 3.7). Imaging results indicate FEP ([^{18}F]**2**) is compared to FET ([^{18}F]**1**), both are suitable for brain tumor imaging.

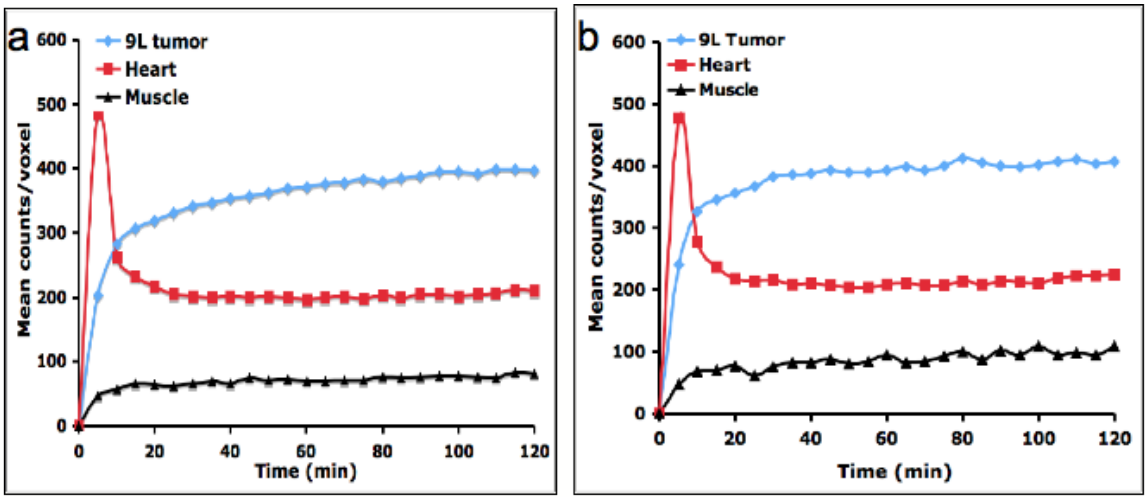

Figure 3.6[a]**:** Time-activity curve after injection of FEP ([^{18}F]**2**) (**a**) and FET ([^{18}F]**1**) in the rats (**b**)
[a]Experiment carried out by Brian Lieberman [39]

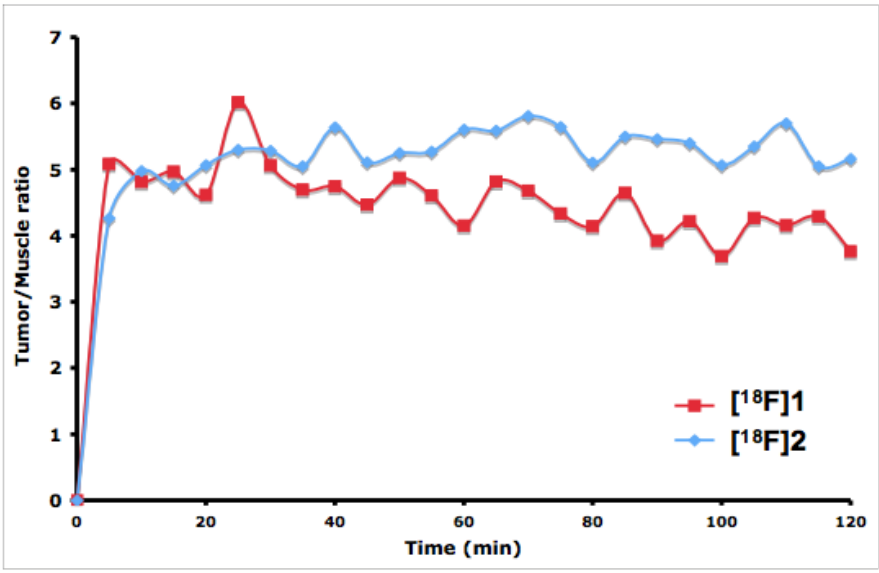

Figure 3.7 Comparison of FEP ([^{18}F]**2**) and FET ([^{18}F]**1**) tumor to muscle (T/M) ration.

3.3 Materials and methods

3.3.1. General

In additional to what described in Chapter two, section **2.4.1**, the animal experiments were carried out in compliance with ethics and animal welfare according to regulation requirements.

3.3.2. Synthesis of precursors and authentic standards for radiotracers

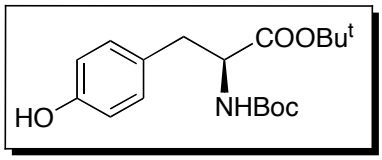

3.3.2.1 (S)-tert-butyl 2-(tert-butoxycarbonylamino)-3-(4-hydroxyphenyl)propanoate (5)

L-tyrosine *tert*-butyl ester (**4**, 949 mg, 4 mmol) was added to a round-bottom flask and dissolved in 40 mL MeOH/H_2O (2:1). To this mixture was added $NaHCO_3$ (1.008 g, 12 mmol) followed by Boc_2O (1.31 g, 6 mmol). The reaction mixture was allowed to stir

for 4 h until completion as determined by TLC analysis (MeOH/CH_2Cl_2, 5/100). Upon completion, the mixture was concentrated under reduced pressure to remove methanol and then resulting solution diluted with water and extracted with EtOAc. Combined organic layer washed with brine and dried over Na_2SO_4, then concentrated under reduced pressure and purified by FC (MeOH/CH_2Cl_2, 5/100) to afford the product as white foam. ^{1}H NMR (200 MHz, $CDCl_3$) δ = 7.04 (d, 2H, *J* = 8.6 Hz), 6.75 (d, 2H, *J* = 8.6 Hz), 4.98 (d, 1H, *J* = 8.0 Hz), 4.43-4.36 (m, 1H), 2.98 (d, 2H, *J* = 5.8 Hz), 1.43 (s, 18H). ^{13}C NMR (50 MHz, $CDCl_3$) δ = 171.5, 155.6, 155.4, 130.8, 128.0, 115.6, 82.4, 55.4, 37.9, 28.5, 28.2. HRMS calcd for $C_{18}H_{27}NO_5$ ($[M+Na]^+$) 360.1997, found 360.1986. $[\alpha]^{24}_D$ +39.3^o (c 0.29, $CHCl_3$).

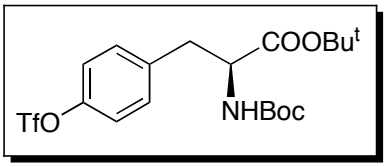

3.3.2.2. (S)-tert-butyl2-(tert-butoxycarbonylamino)-3-(4-(trifluoromethylsulfonyloxy) phenyl)propanoate (6)

5 (515 mg, 1.53 mmol) and pyridine (302 mg, 3.82 mmol) in CH_2Cl_2 at 0 ^{o}C was added Tf_2O (385 μL, 2.29 mmol) dropwise. Reaction stirred for 45 min at 0 ^{o}C. Then dilute with CH_2Cl_2 (50 mL), washed with 1 N NaOH (5 mL), 10% citric acid (5 mL) and brine (10 mL). The organic layer was dried over $MgSO_4$, filtered and concentrated in vacuo. The residue was purified by FC (EtOAC/Hexanes, 1/9) to give **5** as light yellow liquid. ^{1}H NMR (200 MHz, $CDCl_3$) δ = 7.28 (d, 2H, *J* = 8.8 Hz), 7.19 (d, 2H, *J* = 9.0 Hz), 5.07 (d, 1H, *J* = 7.2 Hz), 4.53-4.37 (m, 1H), 3.07 (d, 2H, *J* = 6.0 Hz), 1.42 (s, 9H), 1.38 (s, 9H). ^{13}C NMR (50 MHz, MeOD) δ = 172.7, 157.9, 150.1, 140.0, 132.7, 122.4, 83.1,

80.8, 57.02, 38.4, 28.8, 28.3. HRMS calcd for $C_{19}H_{26}F_3NO_7S$ ($[M+Na]^+$) 492.1280, found 492.1299. $[\alpha]^{24}_D$ +28.7° (c 1.0, $CHCl_3$).

3.3.2.3. Stille cross-coupling for synthesis of 7a and 7b

Triflate **6** (1.0 equiv) in DMF was added to flamed dried flask containing LiCl (3.0 eqiv), $Pd(PPh_3)_2Cl_2$ (0.05 equiv), tributyl(vinyl)tin or tributyl(allyl)tin (1.3 equiv) in DMF. Reaction mixture was degassed for 5 min and then heated at 70 °C for 90 min at which point TLC indicated completion of reaction. The mixture was cooled to room temperature, diluted with water and then extracted three times with ether, combined organic layer was washed with brine, dried over $MgSO_4$, filtered and concentrated. Crude products were purified by FC (EtOAc/Hexanes, 5/95) to afford products as white solids.

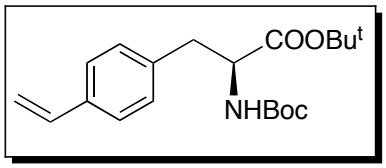

3.3.2.3.1 (S)-tert-butyl 2-(tert-butoxycarbonylamino)-3-(4-vinylphenyl)propanoate **(7a)**

Yield: 92%. ^{1}H NMR (200 MHz, $CDCl_3$) δ = 7.34 (d, 2H, *J* = 8.0 Hz), 7.14 (d, 2H, *J* = 8.2 Hz), 6.70 (dd, 1H, *J* = 17.6, 10.8 Hz), 5.73 (d, 1H, *J* = 17.6 Hz), 5.23 (d, 1H, *J* =10.8 Hz), 4.99 (d, 1H, *J* = 7.8 Hz), 4.54-4.37 (m, 1H), 3.05 (d, 2H, *J* = 6.0 Hz), 1.43 (s, 18H). ^{13}C NMR (50 MHz, $CDCl_3$) δ = 171.1, 155.3, 136.8, 136.5, 136.3, 129.9, 126.4, 113.7, 82.3, 79.9, 55.1, 38.5, 28.5, 28.2. HRMS calcd for $C_{20}H_{29}NO_4$ ($[M+Na]^+$) 370.1994, found 370.2001. $[\alpha]^{24}_D$ +42.7° (c 1.13, $CHCl_3$).

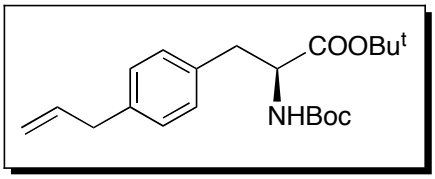

***3.3.2.3.2 (S)-tert-butyl 2-(tert-butoxycarbonylamino)-3-(4-allylphenyl)propanoate* (7b)**

Yield: 95%. ^{1}H NMR (200 MHz, $CDCl_3$) δ = 7.20-7.10 (m, 4H), 6.06-5.85 (m, 1H), 5.10 (d, 1H, *J* = 5.8 Hz), 5.05-4.96 (m, 2H), 4.54-4.37 (m, 1H), 3.36 (d, 2H, *J* = 6.8 Hz) 3.02 (d, 2H, *J* = 6.0 Hz), 1.43 (s, 18H). ^{13}C NMR (50 MHz, $CDCl_3$) δ =171.1, 155.2, 138.7, 137.6, 134.2, 129.7, 128.7, 115.8, 82.0, 79.7, 55.1, 40.0, 38.3, 28.5, 28.1. HRMS calcd for $C_{21}H_{31}NO_4$ ($[M+Na]^+$) 384.2151, found 384.2133. $[\alpha]^{24}_D$ +33.7^o (c 0.47, $CHCl_3$).

3.3.2.4. Hydroboration-oxidation reaction for synthesis of 8a and 8b

To solution of corresponding alkene **7a** or **7b** in THF, 0.5 M 9-BBN in THF (3.0 equiv) was added dropwise, stirred for 3 h at room temperature. The solution was then cooled to 0 ^{o}C , 3 N NaOH solution was added followed by H_2O_2 (30% in H_2O). Reaction continued at room temperature for additional 3 h, the biphasic mixture was treated with saturated $Na_2S_2O_3$ and extract three times with EtOAc, combined organic extracts were washed with brine, dried over $MgSO_4$, filtered and concentrated. The crude mixtures were purified with FC (EtOAc/Hexanes, 3/7) to give products as clear viscous liquids.

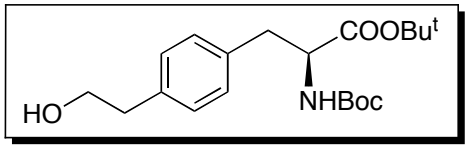

***3.3.2.4.1. (S)-tert-butyl 2-(tert-butoxycarbonylamino)-3-(4-(2-hydroxyethyl)phenyl) propanoate* (8a)**

Yield: 86%. ^{1}H NMR (200 MHz, $CDCl_3$) δ = 7.20-7.08 (m, 4H), 4.99 (d, 1H, *J* = 6.8 Hz), 4.52-4.37 (m, 1H), 3,85 (t, 2H, *J* = 6.6 Hz), 2.98 (d, 2H, *J* = 5.8 Hz), 2.85 (t, 2H, *J* = 6.6 Hz), 1.42 (s, 18H). ^{13}C NMR (50 MHz, $CDCl_3$) δ = 171.1, 155.2, 137.3, 134.4, 129.7, 129.0, 82.0, 79.7, 63.6, 55.0, 38.9, 38.2, 28.3, 28.0. HRMS calcd for $C_{20}H_{31}NO_5$ ($[M+H]^+$) 366.2280, found 366.2281. $[\alpha]^{21}_D$ +41.4^o (c 0.75, $CHCl_3$).

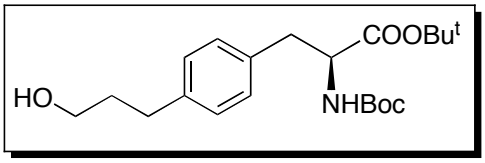

3.3.2.4.2. (S)-tert-butyl 2-(tert-butoxycarbonylamino)-3-(4-(2-hydroxypropyl)phenyl) propanoate **(8b)**

Yield: 88%. ^{1}H NMR (200 MHz, $CDCl_3$) δ = 7.15-7.06 (m, 4H), 5.00 (d, 1H, *J* = 7.8 Hz), 4.49-4.37 (m, 1H), 3.67 (t, 2H, *J* = 6.4 Hz), 3.01 (d, 2H, *J* = 5.8 Hz), 2.68 (t, 2H, *J* = 6.6 Hz), 1.94-1.83 (m, 2H), 1.42 (s, 18H). ^{13}C NMR (50 MHz, $CDCl_3$) δ = 171.2, 155.3, 140.6, 134.0, 129.7, 128.6, 82.1, 79.9, 63.3, 55.1, 38.4, 34.4, 31.9, 28.5, 28.2. HRMS calcd for $C_{21}H_{33}NO_5$ ($[M+Na]^+$) 402.2256, found 402.2410. $[\alpha]^{24}_D$ +30.7^o (c 0.93, $CHCl_3$).

3.3.2.5. Tosylation reaction for synthesis of precusors 9a and 9b

Corresponding hydroxyl compounds **8a or 8b** (1.0 equiv) in 5mL CH_2Cl_2 was added Et_3N (3.0 equiv) and TsCl (1.2 equiv). Reaction continued at room temperature for 20 h. The solution was diluted with CH_2Cl_2, washed with saturated $NaHCO_3$ and brine. Orangic layer was dried over $MgSO_4$, filtered and concentrated. Purify via FC (EtOAc/Hexanes, 2/8) to afford products as clear viscous liquid.

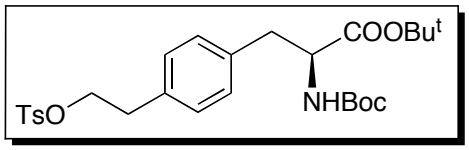

***3.3.2.5.1. (S)-tert-butyl 2-(tert-butoxycarbonylamino)-3-(4-(2-(tosyloxy)ethyl)phenyl) propanoate* (9a)**

Yield: 92%. ^{1}H NMR (200 MHz, $CDCl_3$) δ = 7.72 (d, 2H, *J* = 8.2 Hz), 7.31 (d, 2H, *J* = 8.0 Hz), 7.11-7.00 (m, 4H), 4.97 (d, 1H, *J* = 7.8 Hz), 4.48-4.36 (m, 1H), 4.19 (t, 2H, *J* = 7.2 Hz), 3.02 (d, 2H, *J* = 5.6 Hz), 2.93 (t, 2H, J = 7.2 Hz), 2.45 (s, 3H), 1.43 (s, 18H). ^{13}C NMR (50 MHz, $CDCl_3$) δ = 171.0, 155.2, 144.8, 135.3, 134.9, 133.4, 130.0, 129.0, 128.0, 82.2, 79.9, 70.6, 55.0, 38.3, 35.2, 28.5, 28.1, 21.8. HRMS calcd for $C_{27}H_{37}NO_7S$ ($[M+Na]^+$) 542.2188, found 542.2221. $[\alpha]^{23}_D$ +28.0^o (c 1.35, $CHCl_3$).

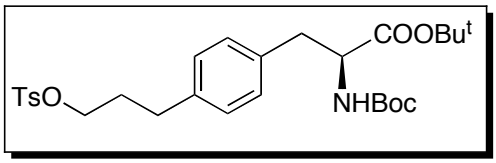

***3.3.2.5.2. (S)-tert-butyl 2-(tert-butoxycarbonylamino)-3-(4-(2-(tosyloxy)propyl)phenyl) propanoate* (9b)**

Yield: 75%. ^{1}H NMR (200 MHz, $CDCl_3$) δ = 7.79 (d, 2H, *J* = 8.2 Hz), 7.35 (d, 2H, *J* = 8.0 Hz), 7.08-6.97 (m, 4H), 4.98 (d, 1H, *J* = 7.6 Hz), 4.48-4.36 (m, 1H), 4.03 (t, 2H, *J* = 6.2 Hz), 3.00 (d, 2H, *J* = 5.6 Hz), 2.61 (t, 2H, *J* = 7.8 Hz), 2.46 (s, 3H), 2.02 -1.85 (m, 2H), 1.42 (s, 18H). ^{13}C NMR (50 MHz, $CDCl_3$) δ = 171.0, 155.2, 144.9, 139.1, 134.5, 133.5, 130.0, 129.8, 128.6, 128.1, 82.2, 79.9, 69.8, 55.1, 38.4, 31.3, 30.7, 28.5, 28.2, 21.8. HRMS calcd for $C_{28}H_{39}NO_7S$ ($[M+H]^+$) 534.2525, found 534.2518. $[\alpha]^{22}_D$ +29.5^o (c 0.40, $CHCl_3$).

3.3.2.6. Fluorination for synthesis of 10a and 10b

Corresponding tosylate **9a** and **9b** (1.0 equiv) in 5 mL acetone was added sodium iodide (5.0 equiv). The reaction mixture was refluxed for 1 h and then filtered and concentrated. Residue was dissolved in CH_2Cl_2, filtered and concentrated again to afford clear liquid. This intermediate product was redissolved in CH_3CN, silver fluoride (4.0 mmol) was added in the solution and reaction continued at room temperature for 1 d at dark. Reaction mixture was then filtered and concentrated, purified with FC to afford products as light yellow viscous liquids.

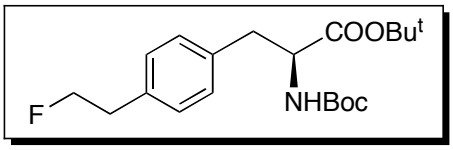

3.3.2.6.1. (S)-tert-butyl 2-(tert-butoxycarbonylamino)-3-(4-(2-fluoroethyl)phenyl) propanoate **(10a)**

Yield: 50%. ^{1}H NMR (200 MHz, $CDCl_3$) δ = 7.18-7.05 (m, 4H), 4.99 (d, 1H, *J* = 7.8 Hz), 4.73 (t, 1H, 6.6 Hz), 4.53-4.35 (m, 2H), 3.10-3.00 (m, 3H), 2.93 (t, 1H, *J* = 6.6 Hz), 1.42 (s, 18H). ^{13}C NMR (50 MHz, $CDCl_3$) δ = 171.2, 155.3, 135.9, 135.1, 130.0, 129.2, 84.2 (d, *J* = 168.5 Hz), 82.2, 55.1, 38.5, 36.8 (d, *J* = 20.0 Hz), 28.5, 28.2. HRMS calcd for $C_{20}H_{30}FNO_4$ ($[M+Na]^+$) 390.2057, found 390.2063. $[\alpha]^{23}_D$ +38.0^o (c 0.45, $CHCl_3$).

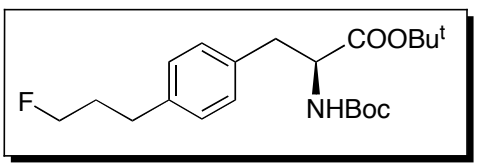

3.3.2.6.2. (S)-tert-butyl 2-(tert-butoxycarbonylamino)-3-(4-(2-fluoropropyl)phenyl) propanoate **(10b)**

Yield: 58%. ^{1}H NMR (200 MHz, $CDCl_3$) δ = 7.20-7.07 (m, 4H), 4.98 (d, 1H, *J* = 8.0 Hz), 4.57 (t, 1H, 6.0 Hz), 4.48-4.30 (m, 2H), 3.02 (d, 2H, *J* = 5.8 Hz), 2.72 (t, 1H, *J* = 7.6 Hz), 2.12-1.96 (m, 2H), 1.43 (s, 18H). ^{13}C NMR (50 MHz, $CDCl_3$) δ = 171.2, 155.3, 139.8, 134.3, 129.9, 128.7, 83.3 (d, *J* = 164.0 Hz), 82.2, 79.9, 55.1, 38.4, 32.2 (d, *J* = 20.0 Hz), 31.1, 28.5, 28.2. HRMS calcd for $C_{21}H_{32}FNO_4$ ($[M+Na]^+$) 404.2213, found 404.2242. $[\alpha]^{24}_D$ +36.2^o (c 1.4, $CHCl_3$).

3.3.2.7. Deprotection reaction for synthesis of 2 and 3

Corresponding protected compound **10a** and **10b** (1.0 equiv) in CH_2Cl_2 was added trifluoroacetic acid (TFA), stirred for 2 h to 4h at which point TLC indicated completion of reaction. Reaction mixture was concentrated in vacuo and residue was then dissolved in 2 mL methanol, adjust pH to 6-7 with 5% NH_4OH at which point white precipitate formed. The mixture was refrigerated overnight and then subjected to filtration, the solid was washed with methanol and dried in vacuo to afford products as white solids.

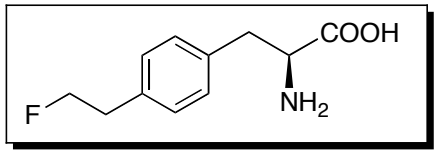

3.3.2.7.1. (S)-2-amino-3-(4-(2-fluoroethyl)phenyl)propanoic acid **(2)**

Yield: 81%. ^{1}H NMR (200 MHz, MeOD+TFA-D) δ = 7.17-7.05 (m, 4H), 4.58 (dt, 2H, *J* = 47.2, 6.2 Hz), 4.21 (dd, 1H, *J* = 7.6, 5.4 Hz), 3.35-3.08 (m, 2H), 2.97 (dt, 2H, *J* = 24.6, 6.2 Hz). ^{13}C NMR (50 MHz, D_2O+DCl) δ = 171.0, 137.6, 132.1, 129.6, 85.1 (d,

J = 156 Hz), 54.0, 35.6 (d, *J* = 19.5 Hz), 35.1. HRMS calcd for $C_{11}H_{14}FNO_2$ ($[M+H]^+$) 212.1087, found 212.1086. $[\alpha]^{23}_D$ -5.8° (c 0.75, 6N HCl).

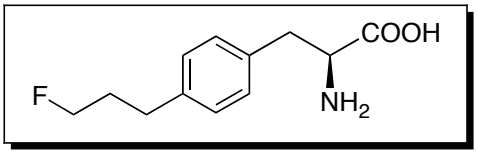

***3.3.2.7.2. (S)-2-amino-3-(4-(2-fluoropropyl)phenyl)propanoic acid* (3)**

Yield: 64%. ^{1}H NMR (200 MHz, D_2O+DCl) δ = 6.79-6.69 (m, 4H), 4.09 (t, 1H, *J* = 6.0 Hz), 3.90-3.80 (m, 2H), 2.73(ddd, 2H, *J* = 14.6, 5.8, 7.6 Hz), 2.19 (t, 2H, *J* = 7.6 Hz), 1.59-1.31 (m, 2H). ^{13}C NMR (50 MHz, D_2O+DCl+MeOD) δ = 172.0, 142.5, 132.3, 130.5,130.2, 85.7 (d, *J* = 156.5 Hz), 55.0, 36.1, 32.1 (d, *J* = 19.0 Hz), 31.2. HRMS calcd for $C_{12}H_{16}FNO_2$ ($[M+H]^+$) 226.1243, found 226.1256. $[\alpha]^{24}_D$ -5.7° (c 0.45, 6N HCl).

3.3.3.Radiosynthesis

[^{18}F]Fluoride trapped a Sep-Pak light QMA cartridge (pre-conditioned with 10 mL 1 N $NaHCO_3$, 10 mL water and dried with N_2) was eluted with 0.6 mL tetrabutylammonium bicarbonate ($TBAHCO_3$) solution (21.5 mg $TBAHCO_3$ in 0.3 mL CH_3CN and 0.3 mL H_2O). The ^{18}F activity was dried azeotropically under N_2 at 110 °C. Precursor **9a** or **9b** (5 mg) in 1 mL anhydrous CH_3CN was then added into dried ^{18}F, fluorination reaction continued for 5 min at 80 °C. After fluorination, reaction mixture was injected to semi-preparative HPLC on Phenomenex Gemini C-18 column (10 × 250 mm, 5 μm). Intermediates [^{18}F]**10a** and [^{18}F]**10b** were eluted with methanol/0.1% formic acid in water (80/20). Radioactive peak between 11 min to 13 min was collected and then

diluted with 20-25 mL water, loaded on HLB oasis cartridge (preconditioned with 10 mL ethanol and 10 mL water), washed with 2 mL water and then eluted with 1 mL ethanol. Removing ethanol under N_2 at 60 ^oC. TFA was then added, deprotection reaction continued at 60 ^oC for 10 min. After removing TFA with N_2 flow, 1 mL sterile water was added to formulate final product. Chemical and radiochemical purity (RCP) were determined by analytical HPLC performed on a Phenomenex Gemini C-18 column (4.6 × 250 mm, 5 μm) eluted by solvent system A: methanol/0.1% formic acid (20/80) at flow rate of 1 mL/min and TLC (NH_4OH/MeOH/ CH_2Cl_2, 1/6/14). Retention time was 6.9 min for [^{18}F]**2** and 7.6 min for [^{18}F]**3**. Enantiomeric purity was determined with a chirobiotic-T (Aldrich, St. Louis, MO) chiral column (5μ, 250 × 4.6 mm) using solvent system B: ethanol/ H_2O (50/50) at flow rate of 0.5 mL/min. Retention time was 9.7 min for [^{18}F]**2** and 10.6 min for [^{18}F]**3**.

3.3.4. In vitro cell uptake studies and transport characterization studies

Brain gliosarcoma cell line 9L was purchased from ATCC (Manassas, VA). The 9L cells were cultured in Dulbecco's Modified Eagle's Medium (DMEM, GIBCO BRL, Grand Island, NY) supplemented with 10% fetal bovine serum (Hycolne, Logan, UT) and 1% penicillin/ streptomycin. Cells were maintained in T-75 culture flask under humidified incubator conditions (37 ^oC, 5% CO_2) and were routinely passaged at confluence. Tumor cells were plated at a concentration of 2.0 × 10^5 cells/well 24 h in culturing media prior to cell uptake and inhibition studies. On the day of experiment, the media was aspirated and the cells were washed three times with 1 mL of warm phosphate

buffered saline (PBS, containing 0.90 mM of Ca^{2+} and 1.05 mM of Mg^{2+}). Each assay condition was performed in triplicates.

For cell uptake studies, ligand of choice was mixed within PBS solution and was then added to each well (~500,000 cpm/mL/well). The cells were incubated at 37 °C for 5, 30, 60, 120 min. At the end of the incubation period, the wells were aspirated free of ligand and then the residual cells were washed 3 times with 1 mL ice cold PBS without Ca^{2+} and Mg^{2+}. After washing with ice cold PBS, 350 μL 1 M NaOH was used to lyse the cells. The lysed cells were collected onto filter paper and counted using a gamma counter (Packard Cobra). Together with the sample of initial dose. 100 μL of the cell lysate was used for determination of protein concentration by Lowry method. The data was normalized as percentage uptake of initial dose relative to 100 μg protein content (% ID/100 μg protein).

In inhibition studies, [^{18}F]**2** was mixed with specific inhibitors in concentration of 0.5 mM, 1 mM and 5 mM in PBS solution. In sodium dependence studies, PBS buffer was replaced with Na^+ free solution (143 mM choline chloride, 2.68 mM KCl and 1.47 mM KH_2PO_4). The cells were incubated at 37 °C for 30 min. The procedure following incubation was the same as in cell uptake studies. The data was normalized in reference to uptake of [^{18}F]**2** without any inhibitor in PBS solution.

3.3.5. Biodistribution in Fisher rats with 9L glioma tumors

F344 rats were purchased from Charles Rivers Laboratory (Malvern, PA). Xenografts using 9L cells in F344 rats were accomplished by injecting 4-5 million

cells/xenograft. The cells suspended in PBS solution (0.2 mL) were injected subcutaneously into each of shoulder flanks of the F344 rat. The growth of the tumor was monitored daily for two weeks. When the volume of the tumors reached 1 cm, the rat tumor model was used for biodistribution or microPET imaging studies. Animals were fasted for 12-18 hours prior to the procedure. Saline solution containing the radioactive compounds in a small volume (0.2 mL) was injected into the lateral tail vein under isoflurane anesthesia (1-2%, 1 L/min oxygen). The animals were sacrificed at 30 and 60 min time points post-injection by cardiac excision under anesthesia. Six rats were sacrificed at each time point. The organs of interest and tumors were removed and weighed. The radioactivity in each tissue was measured using gamma counter together with sample of the initial dose. Results were expressed as the percentage of the injected dose per gram (%ID/g) of tissue. Each value represents the mean ± SD of six rats unless otherwise noted.

3.3.6. Small animal imaging with a microPET

PET imaging studies were performed on a Phillips Mosaic small animal PET scanner, which has an imaging field of view of 11.5 cm. Under isoflurane anesthesia (1-2%, 1L/min oxygen) the tumor bearing F344 rats as described before were injected with 30-37 MBq (0.8-1 mCi) of activity via an intravenous injection into the lateral tail vein. Data acquisition began immediately following the intravenous injection. Dynamic scans were conducted over a period of 2 h (5 min/frame; image voxel size 0.5 mm^3). Rats were visually monitored for breathing and a heating pad was used to maintain body temperature throughout the entire procedure. Images were reconstructed and region of

interest (ROI) analysis was performed using AMIDE software (http://amide.sourceforge.net/).

3.4. Conclusion

In summary, we prepared new optically pure phenylalanine derivatives FEP ([^{18}F]**2**) and FPP ([^{18}F]**3**) in high radiochemical purity, good radiochemical yield (11-37%) and high specific activity (21-69 GBq/μmol). Cellular uptake in 9L glioma demonstrated that FEP had a higher uptake than FPP and previously reported FET ([^{18}F]**1**). Uptake mechanism studies suggested that accumulation of FEP into 9L cells was predominantly via system L. In vivo biodistributon studies using rats bearing 9L glioma tumor model showed that FEP had higher uptake in 9L glioma than surrounding organs. Small animal PET imaging studies demonstrated that FEP was comparable to FET. These results indicate that FEP ([^{18}F]**2**) is a potential useful PET tumor imaging agent.

3.5 References

[1] Plathow C and Weber WA. Tumor cell metabolism imaging. J Nucl Med 2008;49 Suppl 2:43S-63S.

[2] van Waarde A and Elsinga PH. Proliferation markers for the differential diagnosis of tumor and inflammation. Curr Pharm Des 2008;14:3326-339.

[3] McConathy J and Goodman Mark M. Non-natural amino acids for tumor imaging using positron emission tomography and single photon emission computed tomography. Cancer metastasis reviews 2008;27:555-73.

[4] Jager PL, Vaalburg W, Pruim J, de Vries EG, Langen KJ, and Piers DA. Radiolabeled amino acids: basic aspects and clinical applications in oncology. J Nucl Med 2001;42:432-45.

[5] Ganapathy V, Thangaraju M, and Prasad PD. Nutrient transporters in cancer: Relevance to Warburg hypothesis and beyond. Pharmacol Ther 2008.

[6] Fujibayashi Y, Kawai K, Yonekura Y, Matsumoto K, Konishi J, and Yokoyama A. Problems of [S-methyl-11C]-L-methionine as a protein synthesis marker in the pancreas. Ann Nucl Med 1990;4:29-33.

[7] Ishiwata K, Enomoto K, Sasaki T, Elsinga PH, Senda M, Okazumi S, et al. A feasibility study on L-[1-carbon-11]tyrosine and L-[methyl-carbon-11]methionine to assess liver protein synthesis by PET. J Nucl Med 1996;37:279-85.

[8] Willemsen AT, van Waarde A, Paans AM, Pruim J, Luurtsema G, Go KG, et al. In vivo protein synthesis rate determination in primary or recurrent brain tumors using L-[1-11C]-tyrosine and PET. J Nucl Med 1995;36:411-9.

[9] Heiss P, Mayer S, Herz M, Wester HJ, Schwaiger M, and Senekowitsch-Schmidtke R. Investigation of transport mechanism and uptake kinetics of O-(2-[18F]fluoroethyl)-L-tyrosine in vitro and in vivo. J Nucl Med 1999;40:1367-73.

[10] Inoue T, Tomiyoshi K, Higuichi T, Ahmed K, Sarwar M, Aoyagi K, et al. Biodistribution studies on L-3-[fluorine-18]fluoro-alpha-methyl tyrosine: a potential tumor-detecting agent. J Nucl Med 1998;39:663-7.

[11] Yu W, Williams L, Camp VM, Olson JJ, and Goodman MM. Synthesis and biological evaluation of anti-1-amino-2-[18F]fluoro-cyclobutyl-1-carboxylic acid (anti-2-[18F]FACBC) in rat 9L gliosarcoma. Bioorg Med Chem Lett;20:2140-3.

[12] Prante O, Deichen JT, Hocke C, and Kuwert T. Characterization of uptake of 3-[(131)I]iodo-alpha-methyl-L-tyrosine in human monocyte-macrophages. Nucl Med Biol 2004;31:365-72.

[13] Couturier O, Luxen A, Chatal JF, Vuillez JP, Rigo P, and Hustinx R. Fluorinated tracers for imaging cancer with positron emission tomography. Eur J Nucl Med Mol Imaging 2004;31:1182-206.

[14] Fowler JS, Ding YS, and Volkow ND. Radiotracers for positron emission tomography imaging. Semin Nucl Med 2003;33:14-27.

[15] Laverman P, Boerman OC, Corstens FH, and Oyen WJ. Fluorinated amino acids for tumour imaging with positron emission tomography. Eur J Nucl Med Mol Imaging 2002;29:681-90.

[16] Hyde R, Taylor PM, and Hundal HS. Amino acid transporters: roles in amino acid sensing and signalling in animal cells. Biochem J 2003;373:1-18.

[17] Palacin M, Estevez R, Bertran J, and Zorzano A. Molecular biology of mammalian plasma membrane amino acid transporters. Physiol Rev 1998;78:969-1054.

[18] Christensen HN. Role of amino acid transport and countertransport in nutrition and metabolism. Physiol Rev 1990;70:43-77.

[19] Yanagida O, Kanai Y, Chairoungdua A, Kim DK, Segawa H, Nii T, et al. Human L-type amino acid transporter 1 (LAT1): characterization of function and expression in tumor cell lines. Biochim Biophys Acta 2001;1514:291-302.

[20] Fuchs BC and Bode BP. Amino acid transporters ASCT2 and LAT1 in cancer: partners in crime? Semin Cancer Biol 2005;15:254-66.

[21] Saier MH, Jr., Daniels GA, Boerner P, and Lin J. Neutral amino acid transport systems in animal cells: potential targets of oncogene action and regulators of cellular growth. J Membr Biol 1988;104:1-20.

[22] Bodoy S, Martin L, Zorzano A, Palacin M, Estevez R, and Bertran J. Identification of LAT4, a novel amino acid transporter with system L activity. J Biol Chem 2005;280:12002-11.

[23] Kaira K, Oriuchi N, Imai H, Shimizu K, Yanagitani N, Sunaga N, et al. l-type amino acid transporter 1 and CD98 expression in primary and metastatic sites of human neoplasms. Cancer Sci 2008;99:2380-6.

[24] Nawashiro H, Otani N, Shinomiya N, Fukui S, Ooigawa H, Shima K, et al. L-type amino acid transporter 1 as a potential molecular target in human astrocytic tumors. Int J Cancer 2006;119:484-92.

[25] Kaira K, Oriuchi N, Imai H, Shimizu K, Yanagitani N, Sunaga N, et al. Prognostic significance of L-type amino acid transporter 1 expression in resectable stage I-III nonsmall cell lung cancer. Br J Cancer 2008;98:742-8.

[26] Sakata T, Ferdous G, Tsuruta T, Satoh T, Baba S, Muto T, et al. L-type amino-acid transporter 1 as a novel biomarker for high-grade malignancy in prostate cancer. Pathol Int 2009;59:7-18.

[27] Langen KJ, Hamacher K, Weckesser M, Floeth F, Stoffels G, Bauer D, et al. O-(2-[18F]fluoroethyl)-L-tyrosine: uptake mechanisms and clinical applications. Nucl Med Biol 2006;33:287-94.

[28] Pauleit D, Stoffels G, Schaden W, Hamacher K, Bauer D, Tellmann L, et al. PET with O-(2-18F-Fluoroethyl)-L-Tyrosine in peripheral tumors: first clinical results. J Nucl Med 2005;46:411-6.

[29] Lau EW, Drummond KJ, Ware RE, Drummond E, Hogg A, Ryan G, et al. Comparative PET study using F-18 FET and F-18 FDG for the evaluation of patients with suspected brain tumour. J Clin Neurosci 2010;17:43-9.

[30] Hellwig D, Ketter R, Romeike BF, Sell N, Schaefer A, Moringlane JR, et al. Validation of brain tumour imaging with p-[123I]iodo-L-phenylalanine and SPECT. Eur J Nucl Med Mol Imaging 2005;32:1041-9.

[31] Shreve PD, Anzai Y, and Wahl RL. Pitfalls in oncologic diagnosis with FDG PET imaging: physiologic and benign variants. Radiographics 1999;19:61-77; quiz 150-1.

[32] Ahlstrom H, Malmstrom PU, Letocha H, Andersson J, Langstrom B, and Nilsson S. Positron emission tomography in the diagnosis and staging of urinary bladder cancer. Acta Radiol 1996;37:180-5.

[33] Tsukada H, Sato K, Fukumoto D, and Kakiuchi T. Evaluation of D-isomers of O-F-18-fluoromethyl, O-F-18-fluoroethyl and O-F-18-fluoropropyl tyrosine as tumour imaging agents in mice. European Journal of Nuclear Medicine and Molecular Imaging 2006;33:1017-24.

[34] Tomi M, Mori M, Tachikawa M, Katayama K, Terasaki T, and Hosoya K. L-type amino acid transporter 1-mediated L-leucine transport at the inner blood-retinal barrier. Invest Ophthalmol Vis Sci 2005;46:2522-30.

[35] Rossier G, Meier C, Bauch C, Summa V, Sordat B, Verrey F, et al. LAT2, a new basolateral 4F2hc/CD98-associated amino acid transporter of kidney and intestine. J Biol Chem 1999;274:34948-54.

[36] Kersemans V, Cornelissen B, Kersemans K, Bauwens M, Dierckx RA, De Spiegeleer B, et al. 123/125I-labelled 2-iodo-L: -phenylalanine and 2-iodo-D: -phenylalanine: comparative uptake in various tumour types and biodistribution in mice. Eur J Nucl Med Mol Imaging 2006;33:919-27.

[37] Urakami T, Sakai K, Asai T, Fukumoto D, Tsukada H, and Oku N. Evaluation of O-[(18)F]fluoromethyl-D-tyrosine as a radiotracer for tumor imaging with positron emission tomography. Nucl Med Biol 2009;36:295-303.

[38] Lee TS, Ahn SH, Moon BS, Chun KS, Kang JH, Cheon GJ, et al. Comparison of 18F-FDG, 18F-FET and 18F-FLT for differentiation between tumor and inflammation in rats. Nucl Med Biol 2009;36:681-6.

[39] Wang L, Qu W, Lieberman BP, Plössl K, and Kung HF. Synthesis, uptake mechanism characterization and biological evaluation of 18F labeled fluoroalkyl phenylalanine analogs as potential PET imaging agents. Nucl Med Bio 2010 (In press).

Chapter 4

Synthesis and comparative biological evaluation of L- and D-isomers of ^{18}F labeled fluoroalkyl phenylalanine derivatives as tumor imaging agents

4.1 Introduction

Amino acids are essential for growth of cancer cells as a source for energy and building blocks for protein synthesis [1]. Unregulated amino acid transport and increased protein synthesis rate are well-known characteristics of tumor cells. A number of amino acids based tracers demonstrated improved imaging characteristics relative to the most commonly used [^{18}F]fluoro-2-deoxy-D-glucose (FDG) for certain cancers, particularly for imaging of brain tumors because of their low uptake in cortical normal tissue and inflammatory tissues [2, 3].

Currently, most of clinically utilized amino acid tracers for PET and SPECT are L-isomers. A number of L-amino acids and their derivatives have demonstrated promising clinical results such as ^{11}C labeled natural amino acids [^{11}C]L-methionine (MET) [4] and ^{18}F or ^{123}I labeled non-natural amino acids, 3-[^{123}I]Iodo-α-methyl-L-tyrosine (L-[^{123}I]IMT) [5], cis-4-[^{18}F]fluoro-L-proline [6], L-6-[^{18}F]fluoro-DOPA [7], anti-1-amino-3-[^{18}F]fluoro-cyclobutyl-1-carboxylic acid (FACBC) [8], *O*-[^{18}F]fluoroethyl-L-tyrosine(L-FET, [^{18}F]**1**) [9, 10]. Non-natural amino acid tracers could overcome certain shortcomings of natural amino acids resulting from short half-life of ^{11}C and susceptibility to non-protein metabolic pathways. They generally exhibit increased uptake in tumor cells while show no incorporation into protein and remain metabolically stable in the cells [2, 11]. This suggests upregulation of amino acid transport is the dominating process for increased uptake of non-natural amino acid tracers and incorporation into protein is not necessary. Amino acid transport systems A (alanine preferring), ASC (alanine-serine-cysteine preferring) and L (leucine preferring) have been found to be

upregulated in tumor cells and they are targets of oncogene and protooncogene actions [12, 13]. In particular, systems L amino acid transporter system (LATs), which plays a critical role in angiogenesis, tumor growth and proliferation [14, 15], is a main focus for developing amino acid based tumor imaging agents [2, 3, 16].

D-amino acids have been suggested to be potentially useful tumor specific imaging agents since 1970s. This suggestion stemmed from the observation that some ^{14}C labeled D-amino acids had preferred uptake in tumor-bearing mice compared to their corresponding L-isomers [17]. Because D-amino acids are not commonly utilized in mammalian cells, they are considered to be non-natural, their increased uptake into tumor cells is mainly the result of over-expression of amino acid transporters [18]. It has been shown that LAT1 (one of four subtypes of LATs), transports certain D-amino acids such as D-phenylalanine (Phe), D-leucine (Leu) and D-methionine (Met) with high affinity [19-21]. But not all subtype of LATs could tolerate D-amino acids. LAT2 for example, is seterospecific for L-Phe, Leu, Met et al [22]. Of all subtypes of system L, LAT1 in particular, is closely correlated with angiogenesis, cell proliferation [15] and prognosis of patients with a variety of cancers such as astrocytoma, non-small cell lung cancer (NSCLC) and prostate cancer [23-25]. Due to the current knowledge of transport systems, especially about LAT1, there has been increased interest in developing D-amino acid based tracers. The reported results in comparative studies of L- and D-amino acid compounds are somewhat controversial. On one hand, there were studies demonstrated low uptakes of D-amino acid tracers in tumors. D-[^{11}C]MET was shown to have lower uptake in brain tumors than L-[^{11}C]MET [26]. D-FET had negligible accumulation in mice brain [10] as well as in SW707 colon carcinoma cells [27] compared to that of the

L-isomer. On the other hand, there are a number of reports showing that some D-amino acid derivatives have improved tumor-imaging properties than their corresponding L-isomers. Evaluations of *O*-[^{18}F]fluoromethyl-, fluoroethyl- and fluoropropyl-tyrosine in tumor bearing mice demonstrated D-isomers have higher tumor-to-blood or tumor-to-pancreas ratio [28]. Comparison of D- and L-isomer of 2-[$^{123/125}$I]Iodo-tyrosine showed D-isomer cleared faster from blood and had a lower overall body background [29]. 2-[^{123}I]iodo-D-phenylalanine demonstrated similar advantage over its L-isomer [30]. Moreover, several D-isomers showed preferential transport at the blood-brain barrier (BBB) compared with their L-isomers, such as cis-4-[^{18}F]fluoro-D-proline [31, 32] and D-FET (in porcine brain)[33].

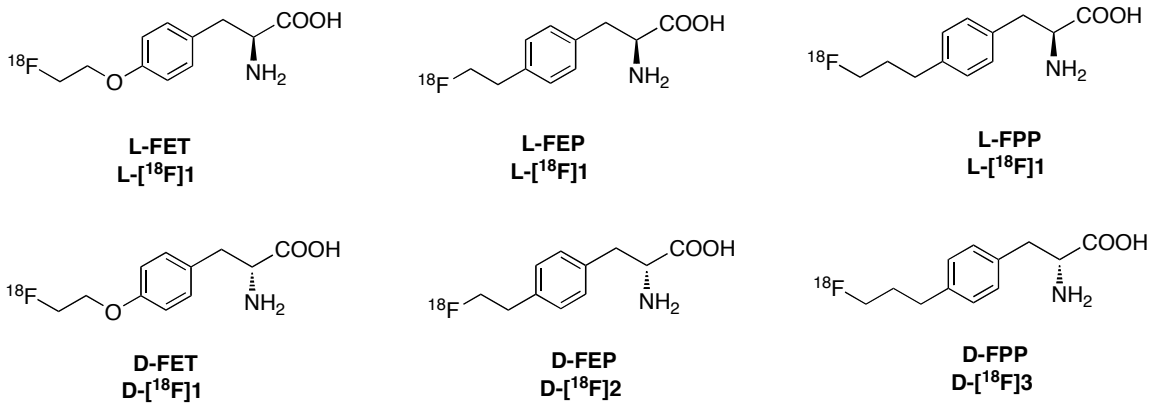

Figure 4.1. Chemical structures of L- and D- ^{18}F labeled tyrosine and new phenylalanine derivatives

We recently reported new ^{18}F labeled L-phenylalanine derivatives, *p*-(2-[^{18}F]fluoroethyl)-L-phenylalanine (L-FEP, L-[^{18}F]**2**) and *p*-(3-[^{18}F]fluoropropyl)-phenylalanine (L-FPP, L-[^{18}F]**3**) (as shown in Figure 4.1) [34]. L-FEP was shown to be comparable in imaging rat with 9L tumors as L-FET ([^{18}F]**1**), which is a clinically utilized PET tracer for imaging brain tumor and head and neck squamous cell carcinomas [9]. The goal of this study is to evaluate the potential of D-isomer of fluoroalkyl

phenylalanine derivatives as tumor imaging agents in comparison with their corresponding L-isomers in vitro in 9L rat glioma cells and in vivo in rats bearing 9L tumor models.

4.2 Results and Discussion

4.2.1 Synthesis of labeling precursors and standards

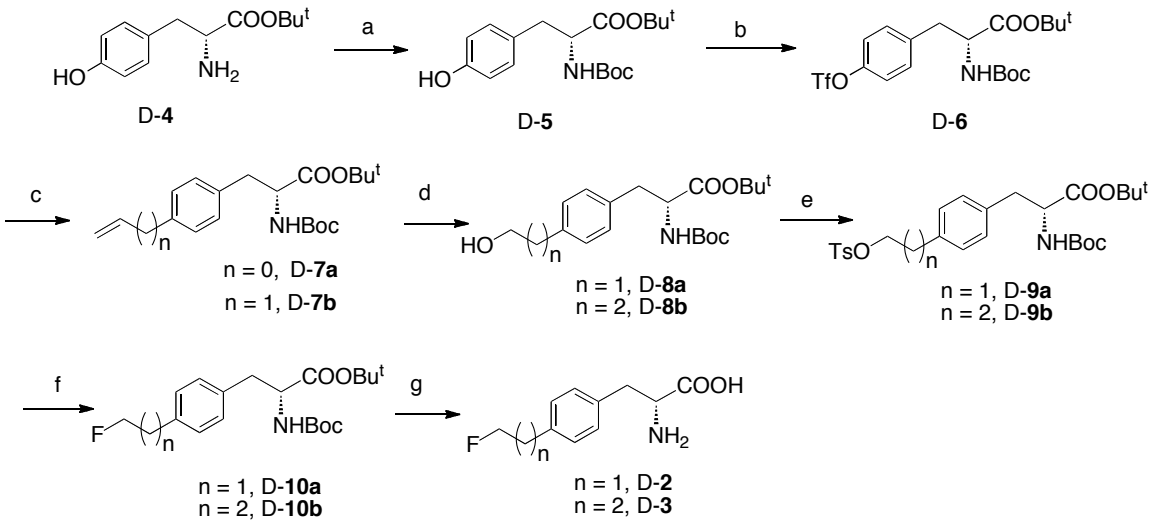

Scheme 4.1. Synthesis of labeling precursors and standards **2** and **3**. Reagents and conditions: a) $(Boc)_2O$, $NaHCO_3$, MeOH, H_2O, rt , 4h, 75%; b) Tf_2O, pyridine, CH_2Cl_2, 0°C, 81%; c) Tributyl vinyltin or tributyl allyltin, LiCl, $Pd(PPh_3)_2Cl_2$, DMF, 70°C, 90% (n = 0) or 94% (n = 1); d) 9-BBN, THF, NaOH, H_2O_2, 67% (n = 1) or 70% (n = 2); e) TsCl, Et_3N, CH_2Cl_2, 77% (n = 1) or 84% (n = 2); f) i. NaI, acetone, reflux; ii. AgF, CH_3CN, 45% (n = 1) or 79% (n = 2); g) TFA, CH_2Cl_2, 52% (n = 1) or 71% (n = 2).

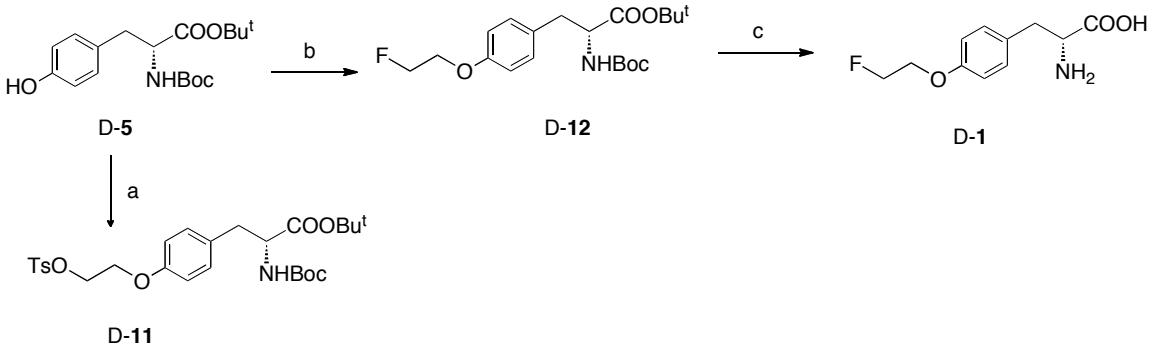

Scheme 4.2. Synthesis of precursor and standard **1**. Reagents and conditions: a) $TsO(CH_2)_2OTs$, K_2CO_3, DMF, 70°C, 4h, 61%; b) FCH_2CH_2Br, DMF, K_2CO_3, 70°C 2h, 76%; c) TFA, CH_2Cl_2, 56%.

Here we showed the synthesis of D-isomers, preparation of corresponding L-isomers was carried out in the same manner except the starting materials were in L-isomeric form. Preparation of D-isomer of tosylate precursor and standard for labeling FEP ([^{18}F]**2**) and FPP ([^{18}F]**3**) was shown in Scheme 4.1 which followed the synthesis of its corresponding L-isomer as described in details in Chapter 3 [34]. D-**2** and D-**3** was 7% and 19%. Although L-FET is well established, synthesis of cold standard for D-FET has rarely been reported. So here we briefly described as in Scheme 4.2. It is modified from reported procedure for L-FET by Hamacher, K. [35]. Precursor and standard for labeling D-FET were readily prepared via direct alkylation on phenol group of D-**5** with overall yields of 46% and 32% respectively. The optical rotation of all compounds was measured to monitor their enantiomeric purity. The enantiomeric purity of the tosylate precursors and standards for radiosynthesis was >95%, measured by chiral HPLC.

4.2.2 Radiolabeling of L- and D-FET, FEP and FPP

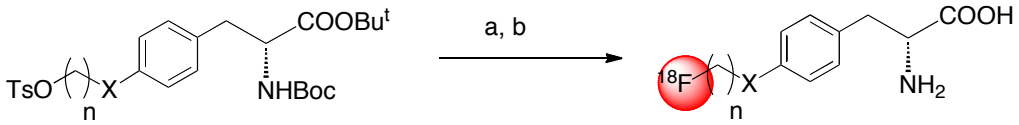

n = 2, X = O, D-**11**
n = 1, X = C, D-**9a**
n = 2, X = C, D-**9b**

n = 2, X = O, D-[^{18}F]**1**
n = 1, X = C, D-[^{18}F]**2**
n = 2, X = C, D-[^{18}F]**3**

Scheme 4.3. Radiolabeling of D-FET ([^{18}F]**1**), FEP ([^{18}F]**2**) and FPP ([^{18}F]**3**). Reagent and conditions: a) TBA^{18}F, $TBAHCO_3$, CH_3CN, 80 ^{o}C, 5 min; b) TFA, 60 ^{o}C, 10 min.

Table 4.1. Synthesis time, decay-corrected radiochemical yields (RCY), radiochemical purity (RCP), enantiomeric purity and specific activity (EOS). *

Ligands	Synthesis time (min)	RCY (%)	RCP (%)	Enantiomeric Purity (%)	Specific activity (GBq /μmol)
L- and D-[^{18}F]**1**	79-85	21-45	> 95	> 95	26-44
L- and D-[^{18}F]**2**	75-82	23-37	> 95	> 95	31-75
L- and D-[^{18}F]**3**	78-90	11-23	> 95	> 95	21-25

*Data were obtained from two to six experiments

Radiosynthesis of ^{18}F-fluoroalkyl tyrosine and phenylalanine derivatives was carried out via a two-step reaction as shown in Scheme 4.3 – non-carried-added (NCA) nucleophilic fluorination with TBA^{18}F and TBAHCO$_3$ in CH$_3$CN followed by acid hydrolysis in TFA. This is an efficient process suitable for potential clinical applications in the future. Intermediates were purified by semi-preparative HPLC to separate from non-reacted ^{18}F fluoride, remaining precursors and by-products. After removing TFA, final products were redissolved in water, in which pH was ~ 6. In order to achieve valid comparative evaluation of L- and D-isomers of amino acid analogues as tumor-detecting agents, the quality control of enantiomeric purity was a critical factor because the uptake and kinetics of D-isomers in organs was demonstrated to be significantly different from those of the corresponding L-isomers [28]. We determined the enantiomeric purity via HPLC on chiral column and the configuration of both isomers was confirmed by comparison with those standard "cold" compounds. In additional, radiochemical purity was analyzed via HPLC on C-18 column and TLC. The results of radiosythesis (summarized in Table 4.1) demonstrated optically and chemically pure tracers (purity was > 95%) were efficiently prepared with moderate to good radiochemical yield (11-45%) and high specific activity (21-75 GBq/μmol).

It is noteworthy to point out that our initial attempts to carry out nucleophilic fluorination reaction using Kryptofix K[2.2.2]^{18}F and K$_2$CO$_3$ in acetonitrile at 90 ^{o}C led to significant racemization. There were 28-35% of the final products in the epimerized form. To investigate the source of racemization, we examined the ratio of L- and D-isomer after fluorination reaction as well as in final products measured by chiral HPLC (Figure 4.2). The HPLC profiles showed that racemization occurred in the first step –

fluorination reaction, the intermediates were mixtures of L- and D- isomers. Moreover, the ratio of L- and D-isomer was the same for the fluorinated intermediates and the final products, which suggest no further racemization occurred during acid deprotection. In nucleophilic fluorination, the pH of K[2.2.2]^{18}F/K_2CO_3 solution is ~ 10, thus the racemization reaction is likely a base-catalyzed reaction. It was reported that factors such as pH and temperature of the reaction solution affect the rate of racemization [36]. Higher pH and temperature lead to faster racemization. In order to obtain the optically pure ligands, we then carried out fluorination reaction using TBA^{18}F/$TBAHCO_3$ in CH_3CN at 80 ^{o}C, pH of this reaction solution is ~ 8, much lower than that of K[2.2.2]^{18}F/K_2CO_3 solution. Under this condition, the enantiomerically purity of ligands was improved to >95%, which could be considered to be optically pure, as shown in Figure 4.3.

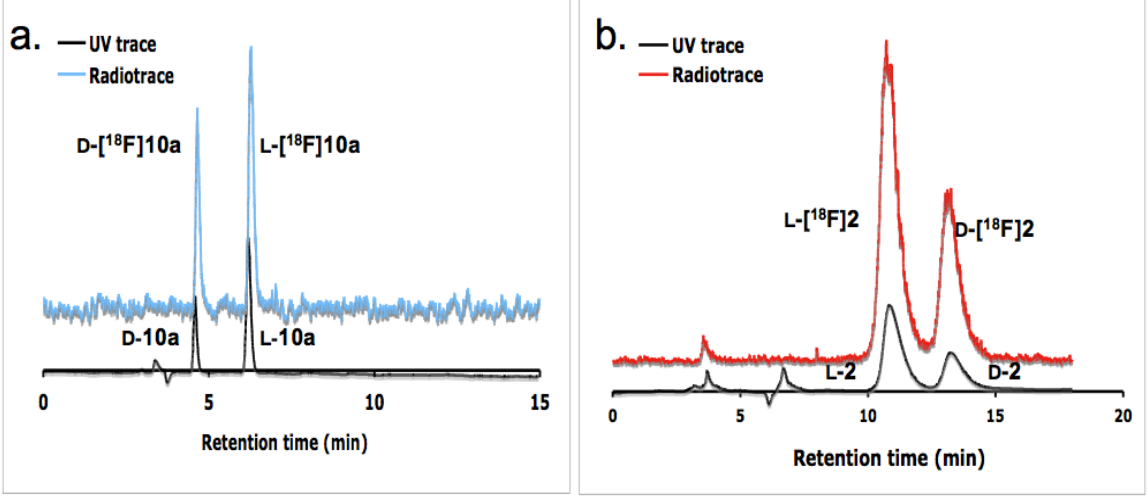

Figure 4.2. HPLC profile of fluorination intermediate [^{18}F]**10a** (**a**) and final products FEP ([^{18}F]**2**) (**b**) under condition using K[2.2.2]/K^{18}F at 90 ^{o}C for radiofluorination. Blue or red colored line is the result from radioactive detector and black line is the result from UV trace of coinjection with standard compounds.

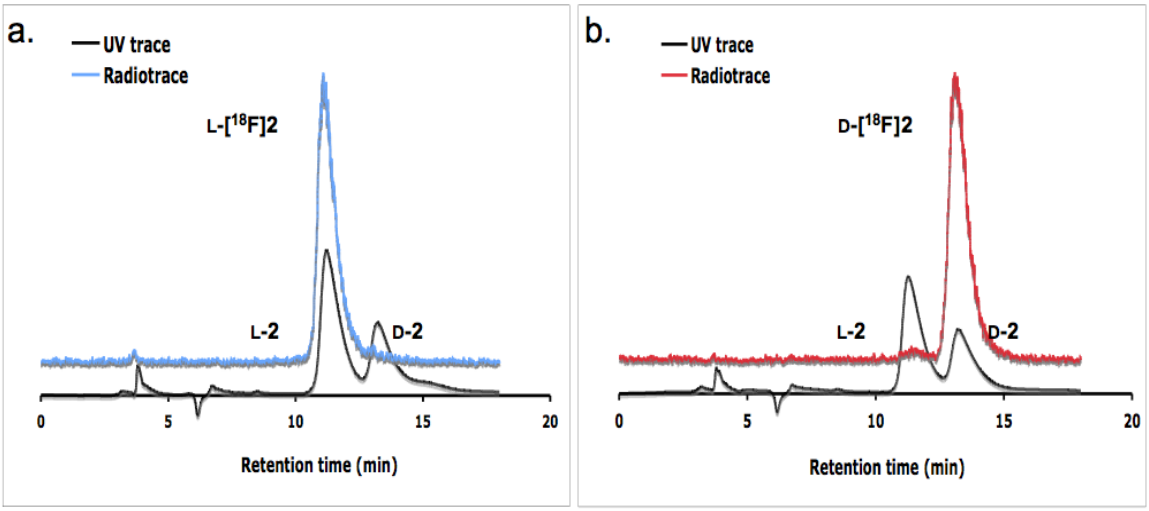

Figure 4.3. HPLC profile with L-isomer (**a**) and D-isomer (**b**) of FEP ([^{18}F]**2**). Blue or red colored line is the result from radioactive detector and black line is the result from UV trace of coinjection with "cold" standards.

4.2.3 Cell uptake studies

We evaluated L- and D- isomers of new phenylalanine derivatives FEP ([^{18}F]**2**) and FPP ([^{18}F]**3**) by examining their time dependent uptake of in 9L glioma cells. Their uptake was compared with L- and D-FET ([^{18}F]**1**), for which comparative uptake studies have been reported before [27, 33]. Uptake of tracers was measured at selective time points up to 2 h and the results were summarized in Figure 4.4. L-isomers showed a fast initial uptake, quickly reached maximum uptake within 60 min and then washed out. In contrast, D-isomers had slow linear uptake over 2 h period. Uptake of L-isomer was significantly higher (4.3 to 16.0 fold) than that of the corresponding D-isomers, which is consistent with other reported in vitro studies comparison L and D-isomers of tyrosine derivatives [27, 37]. These results suggested that the cellular uptake of amino acid tracers was mediated via highly stereo-specific amino acid transport systems.

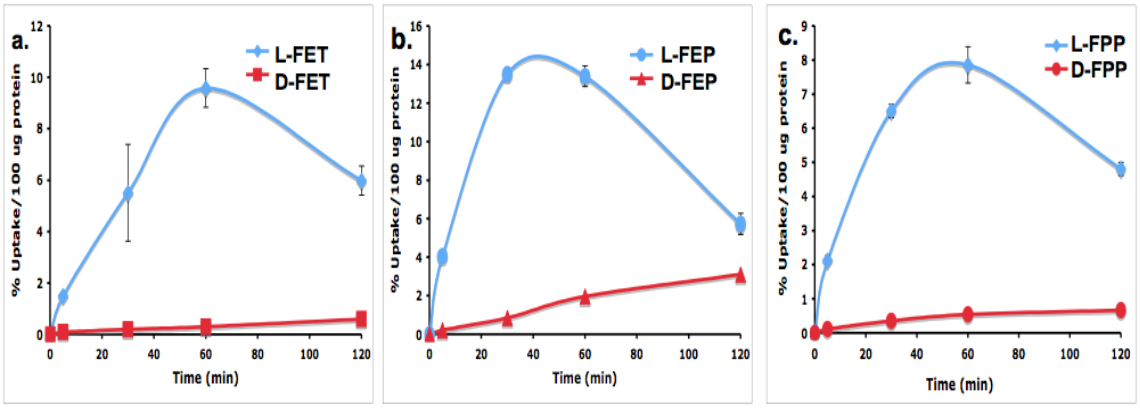

Figure 4.4. Comparative cellular uptake of L- and D-FET ([^{18}F]**1**) (**a**), L- and D-FEP ([^{18}F]**2**) (**b**) and L- and D-FPP ([^{18}F]**3**) (**c**) in 9L glioma cells. The uptake value was represented as %uptake/100 ug protein, mean ± SD.

Uptake of L and D-FPP ([^{18}F]**3**) was comparable to that of corresponding isomer of FET ([^{18}F]**1**), while uptake of [^{18}F]FEP ([^{18}F]**2**) was notably higher. Maximum uptake of L-FEP was 1.4 fold of L-FET and D-FEP was 5.2 fold of D-FET. The difference between L- and D- isomers is the smallest in FEP. The major differences among these tracers are lipophilicity and fluoroalkyl chain length. Tracers' lipophilicity follows the order of FPP (Log D = -0.73) > FEP (Log D = -1.00)>FET (Log D = -1.51) [10] while alkyl chain length follows the order of FEP <FET ≈ FPP. From the uptake result, it appears that a shorter fluoroalkyl chain length might be more desirable for aromatic amino acid tracers. These results suggested both isomers of FEP ([^{18}F]**2**) may worth further investigations.

4.2.4 Transport characterization studies

Amino acid transport systems play an essential role in uptake of amino acid ligands in tumor cells. An amino acid tracer could be substrate for a number of amino acid transport systems with overlapping substrate selectivity. To examine and compare

the amino acid transport systems involved in uptake of L- and D-FEP ([^{18}F]**2**), we conducted a series of inhibition studies and sodium dependence studies in 9L glioma. The uptake of FEP was measure in absence as well as in the presence of 0.5 to 5 mM of specific inhibitor (as shown in Figure 4.5.). We focus on system A, ASC and L because the transport of neutral amino acids in mammalian cells is predominantly through these systems and they are most commonly upregulated amino acid transport systems in cancer cells [12, 14].

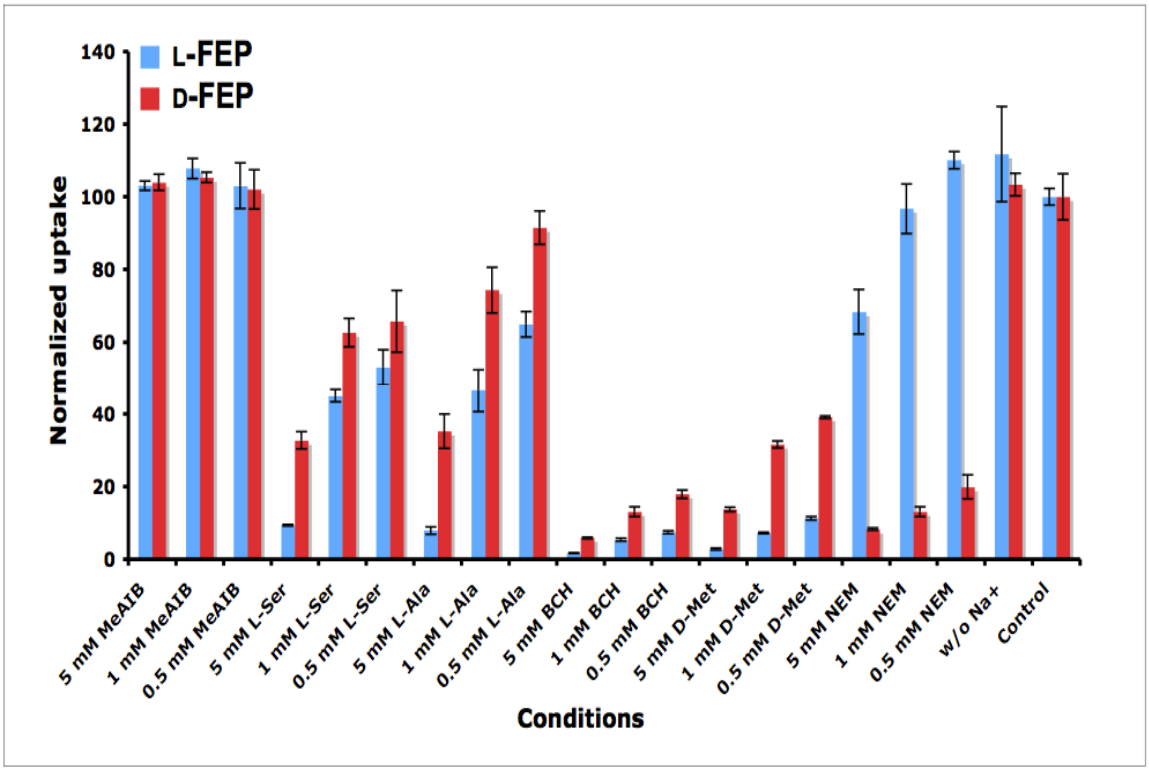

Figure 4.5. Transport characterization studies of L- and D-FEP ([^{18}F]**2**) in 9L glioma cells. Results were normalized to uptake of each isomer's uptake in PBS solution at 30 min. Data was expressed as mean ± SD (n = 3).

The uptake of L- and D-FEP ([^{18}F]**2**) was not affected by presence of *N*-methyl-α-aminoisobutyric acid (MeAIB), which is a specific inhibitor for system A. The uptake of both isomers exhibited similar concentration dependent inhibition by system ASC

inhibitors L-serine (Ser) and L-alanine (Ala). However, L-FEP was more affected by the presence of inhibitors in comparison with D-FEP, for example, 5 mM of L-Ser could inhibit 90% of uptake of L-FEP while it can only reduce 67% uptake of D-isomer. Both isomers uptake was strongly inhibited by 2-amino-bicylo[2.2.1]heptane-2-carboxylic acid (BCH), a selective inhibitor of LATs. 5 mM of BCH could inhibit 98% and 94% uptake of L- and D-FEP respectively. Since BCH is not only an inhibitor for sodium independent system L but also an inhibitor for sodium dependent system B^0 and $B^{0,+}$ [38], we then conducted sodium dependence studies to examine the contribution from sodium dependent transport systems. Uptake of both isomers remained unchanged when replacing PBS solution with Na^+-free buffer (NaCl was replaced with choline chloride as reported [22]. These results suggest that L- and D-FEP are selective substrates for LATs.

There are four subtypes of system L amino acid transport systems isolated and characterized, with differences in topology, substrate selectivity and tissue distribution, designated LAT1 to LAT4 [39]. LAT1 has attracted special interests because its expression is rarely detected in non-tumor areas and is closely correlated with angiogenesis, cell proliferating and prognosis of certain cancers [24, 25]. We were especially interested in LAT1 since it is known that LAT1 could transport D-isomers of phenylalanine, in contrast, the other subtype LAT2 could not. D-Met [40], a specific inhibitor for LAT1, had very similar impact on uptake of L-FEP as BCH. It was not as potent as BCH towards D-isomer, 5 mM of D-Met could inhibit 86% of the uptake. Inhibition using *N*-ethylmaleimide (NEM), an inhibitor for LAT2 to LAT4 but not LAT1 [39], had dramatically different effect on uptake of L- and D-FEP. While uptake of D-isomer was strongly inhibited by NEM with maximum inhibition of 92% at 5 mM

concentration, uptake of L-isomer could only reduced up to 30%. These results indicated that L-FEP preferred system L subtype LAT1 but D-FEP did not exhibit the same preference. D-FEP appears to have different transport characteristics from D-Phe since it has been reported that LAT2, LAT3 and LAT4 could not transport D-Phe [39, 41]. Of four subtypes, LAT3 is the most sensitive to NEM inhibition (80% inhibition in comparison to 40% for LAT2 and LAT4 or 20% for LAT1 at 5 mM concentration) [39]. This might indicate LAT3 is involved in the transport of D-FEP in addition to LAT1.

4.2.5. Small animal PET imaging studies

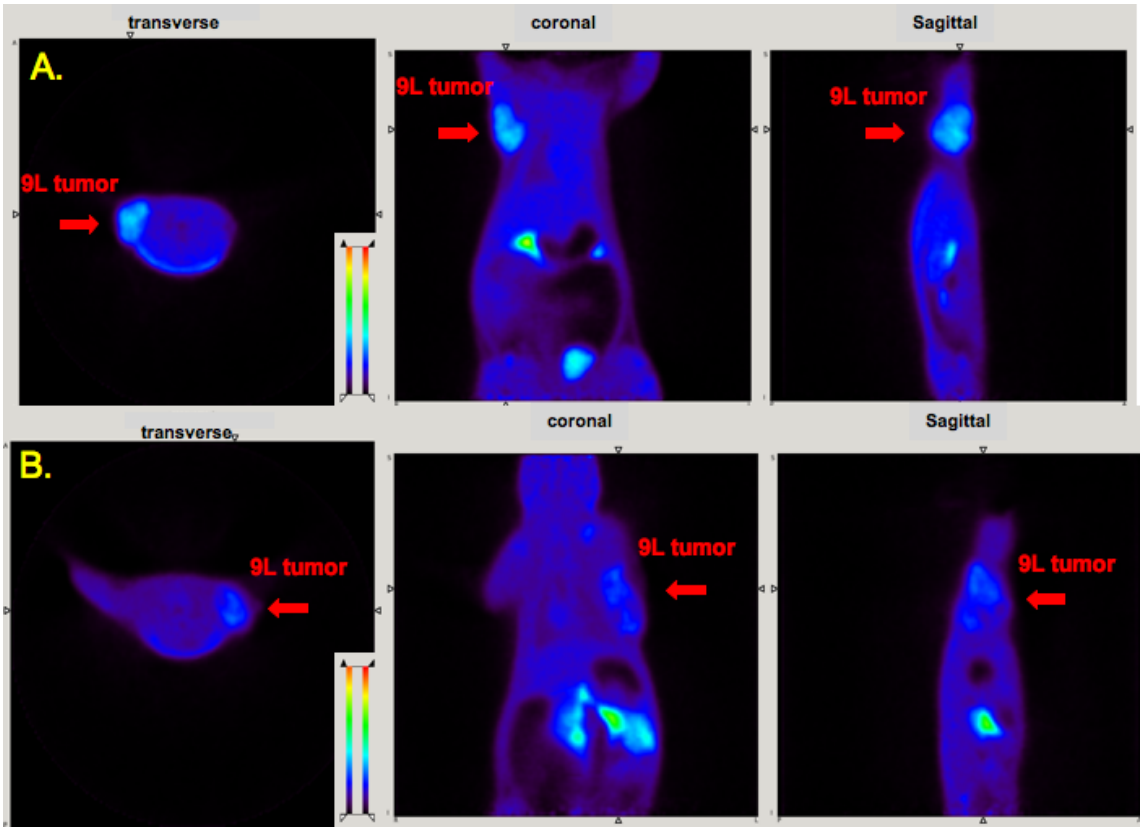

Figure 4.6[a]. Small animal PET images of L-FEP (A) and D-FEP (B) in tumor bearing rats. Color-coded PET images from summed 2 hour data in transverse, coronal and sagittal view from left to right followed injection of L- and D-FEP ([^{18}F]**2**) are shown. The arrowhead points to the 9L xerographs.
[a]Experiment carried out by Brian Lieberman [42]

From in vitro studies results, L- and D-FEP ([^{18}F]**2**) seemed to have potential as promising tumor-imaging agents, so we continued to carried out in vivo small animal PET imaging studies to compare these isomers' imaging properties. Fisher rats bearing 9L tumor model was used because it is a well-established animal model mimicking clinical glioblastoma multiform. Imaging studies could provide in vivo distribution data consistent with tissue dissection method. From this PET imaging study, we could assess and compare the accumulation of L- and D-FEP in 9L tumor and their in vivo kinetics.

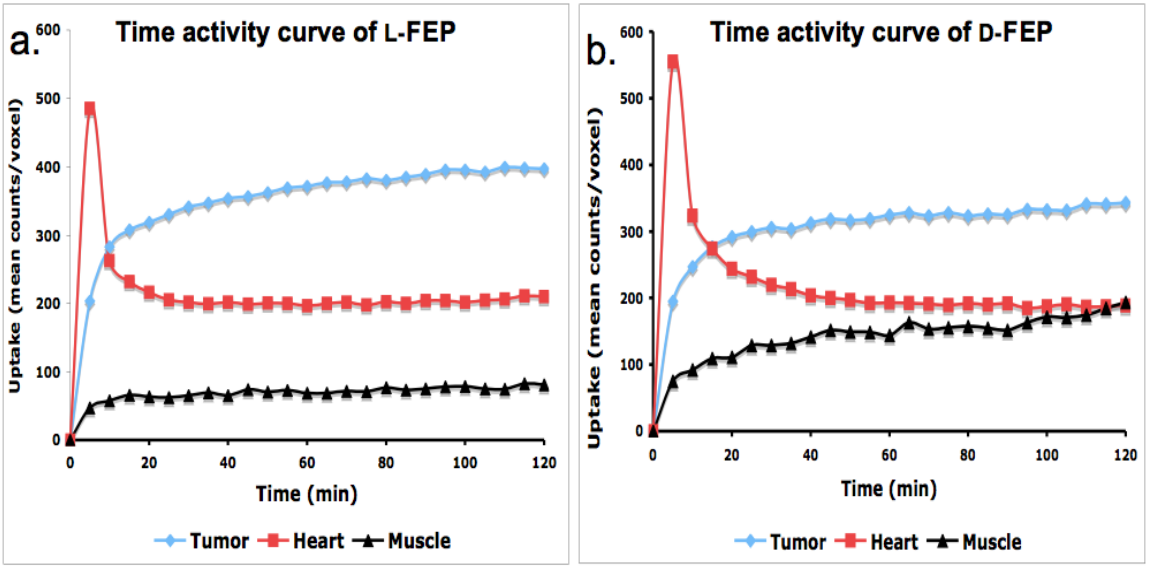

Figure 4.7. Time activity curves of L-FEP (**a**) and D-FEP (**b**) in the rat bearing 9L tumors.
[a]Experiment carried out by Brian Lieberman [42].

Data were acquired from rats administered ~37MBq (1 mCi) of L- or D-FEP ([^{18}F]**2**) via tail vein injection (Figure 4.6). Time-activity curves were generated by region of interest analysis to assess the kinetics (Figure 4.7). Results demonstrated 9L tumor could be imaged using either L- or D-FEP. Kinetics of L- and D-isomers were similar in that both tracers quickly reached the stable distributions within 20 min in tumor, heart and muscle. L-isomer showed slow increase in tumor uptake after 20 min while D-isomer exhibited slow increase in muscle uptake. L-FEP had higher uptake in tumor but the

difference was not very significant. However, D-FEP had higher uptake in muscle than the L-isomer, which results tumor-to-muscle ratio of D-FEP is lower in comparison to its L-isomer (Figure 4.8). This result is different from a number of other reports on tyrosine and phenylalanine derivatives that D-isomers had lower uptake in normal tissue, which leads to better contrast in imaging [28, 37, 43, 44].

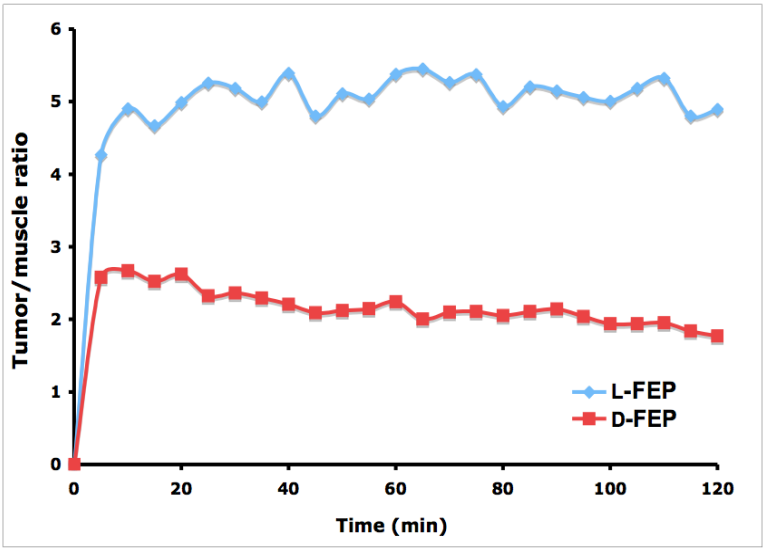

Figure 4.8. Comparison of tumor to muscle ratio of L- and D-FEP and in the rat bearing 9L tumors.

4.3. Conclusions

In conclusion, we prepared new enantiomerically and radiochemically pure L- and D-isomers of fluoroalkyl tyrosine and phenylalanine derivatives with good radiochemical yield and high specific activity. Cell uptake studies in 9L glioma demonstrated L-isomers had much faster and higher uptake in comparison with the gradual linear uptake of D-isomers over 2 h period. FEP ([^{18}F]**2**) had significantly higher uptake than FET ([^{18}F]**1**) in corresponding isomeric forms. Transport characterization studies suggested that accumulation of L- and D-FEP into 9L cells was predominantly via system L; L-FEP showed preferential uptake via LATs' subtype LAT1 but its D-isomer

did not exhibit the same preference. Small animal PET imaging studies using rats bearing 9L glioma tumor model demonstrated that both L- and D-FEP had higher uptake in 9L tumor than surrounding tissues, but D-FEP did not exhibit improved imaging characteristics than its corresponding L-isomer.

4.4. Materials and Methods

Details regarding General, Radiosynthesis procedure, In vitro cell uptake and transport characterization studies in 9L cells and Small animal PET imaging was the same as what described in Chapter **3**, Section **3.3**.

4.4.1. Synthesis of precursors and standards for labeling

The synthesis of L-isomers of **2** and **3** was described in Chapter 3, section 3.2.2. The corresponding D-isomers followed the same procedure and here we would present the NMR data on D-isomers.

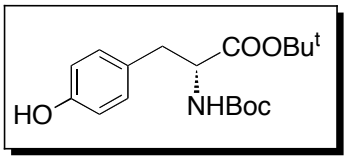

4.4.1.1 (R)-tert-butyl 2-(tert-butoxycarbonylamino)-3-(4-hydroxyphenyl)propanoate (5)

^{1}H NMR (200 MHz, $CDCl_3$) δ = 7.04 (d, 2H, *J* = 8.6 Hz), 6.75 (d, 2H, *J* = 8.6 Hz), 4.98 (d, 1H, *J* = 8.0 Hz), 4.43-4.36 (m, 1H), 2.98 (d, 2H, *J* = 5.8 Hz), 1.43 (s, 18H). $[\alpha]^{23}_D$ -39.7^o (c 0.39, $CHCl_3$).

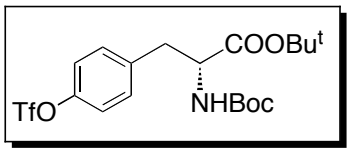

4.4.1.2 (R)-tert-butyl2-(tert-butoxycarbonylamino)-3-(4-(trifluoromethylsulfonyloxy) phenyl)propanoate **(6)**

^{1}H NMR (200 MHz, $CDCl_3$) δ = 7.28 (d, 2H, *J* = 8.8 Hz), 7.19 (d, 2H, *J* = 9.0 Hz), 5.07 (d, 1H, *J* = 7.2 Hz), 4.53-4.37 (m, 1H), 3.07 (d, 2H, *J* = 6.0 Hz), 1.42 (s, 9H), 1.38 (s, 9H). $[\alpha]^{24}_D$ -29.0^o (c 1.0, $CHCl_3$).

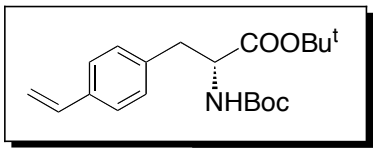

4.4.1.3.1 (R)-tert-butyl 2-(tert-butoxycarbonylamino)-3-(4-vinylphenyl)propanoate **(7a)**

^{1}H NMR (200 MHz, $CDCl_3$) δ = 7.34 (d, 2H, *J* = 8.0 Hz), 7.14 (d, 2H, *J* = 8.2 Hz), 6.70 (dd, 1H, *J* = 17.6, 10.8 Hz), 5.73 (d, 1H, *J* = 17.6 Hz), 5.23 (d, 1H, *J* =10.8 Hz), 4.99 (d, 1H, *J* = 7.8 Hz), 4.54-4.37 (m, 1H), 3.05 (d, 2H, *J* = 6.0 Hz), 1.43 (s, 18H). $[\alpha]^{24}_D$ -40.0^o (c 1.0, $CHCl_3$).

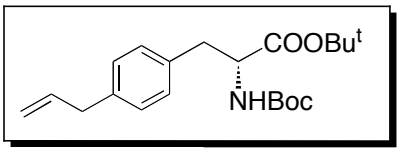

4.4.1.3.2 (R)-tert-butyl 2-(tert-butoxycarbonylamino)-3-(4-allylphenyl)propanoate **(7b)**

^{1}H NMR (200 MHz, $CDCl_3$) δ =7.26-7.10 (m, 4H), 6.06-5.85 (m, 1H), 5.10 (d, 1H, *J* = 5.8 Hz), 5.08-4.96 (m, 2H), 4.54-4.37 (m, 1H), 3.36 (d, 2H, *J* = 6.8 Hz) 3.03 (d, 2H, *J* = 6.0 Hz), 1.43 (s, 18H). $[\alpha]^{24}_D$ -34.8^o (c 0.50, $CHCl_3$).

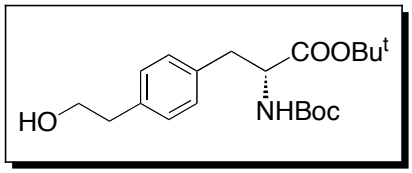

4.4.1.4.1 (R)-tert-butyl 2-(tert-butoxycarbonylamino)-3-(4-(2-hydroxyethyl)phenyl) propanoate **(8a)**

^{1}H NMR (200 MHz, $CDCl_3$) δ =7.20-7.08 (m, 4H), 4.99 (d, 1H, *J* = 6.8 Hz), 4.52-4.37 (m, 1H), 3.85 (t, 2H, *J* = 6.6 Hz), 2.98 (d, 2H, *J* = 5.8 Hz), 2.85 (t, 2H, *J* = 6.6 Hz), 1.42 (s, 18H). $[\alpha]^{21}_D$ -41.7^o (c 0.75, $CHCl_3$).

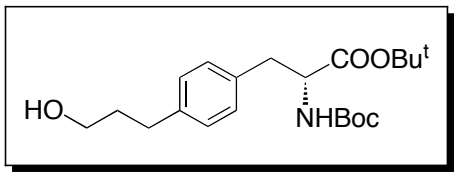

4.4.1.4.2 (R)-tert-butyl 2-(tert-butoxycarbonylamino)-3-(4-(2-hydroxypropyl)phenyl) propanoate **(8b)**

^{1}H NMR (200 MHz, $CDCl_3$) δ =7.15-7.06 (m, 4H), 5.00 (d, 1H, *J* = 7.8 Hz), 4.49-4.37 (m, 1H), 3.67 (t, 2H, *J* = 6.4 Hz), 3.02 (d, 2H, *J* = 6.0 Hz), 2.68 (t, 2H, *J* = 6.6 Hz), 1.94-1.83 (m, 2H), 1.42 (s, 18H). $[\alpha]^{24}_D$ -30.4^o (c 0.95, $CHCl_3$).

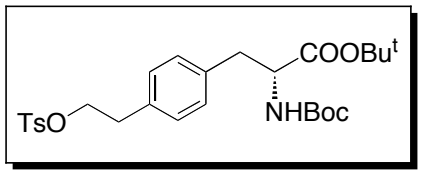

4.4.1.5.1 (R)-tert-butyl 2-(tert-butoxycarbonylamino)-3-(4-(2-(tosyloxy)ethyl)phenyl) propanoate **(9a)**

^{1}H NMR (200 MHz, $CDCl_3$) δ =7.72 (d, 2H, *J* = 8.2 Hz), 7.31 (d, 2H, *J* = 8.0 Hz), 7.11-7.00 (m, 4H), 4.97 (d, 1H, *J* = 7.8 Hz), 4.48-4.36 (m, 1H), 4.19 (t, 2H, *J* = 7.2 Hz), 3.02

(d, 2H, *J* = 5.6 Hz), 2.93 (t, 2H, *J* = 7.2 Hz), 2.45 (s, 3H), 1.43 (s, 18H). $[\alpha]^{23}_{D}$ -29.0° (c 0.87, $CHCl_3$).

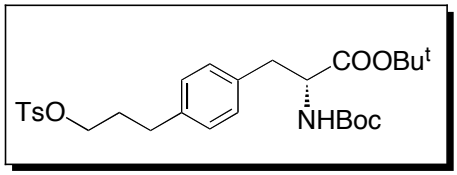

***4.4.1.5.2 (R)-tert-butyl 2-(tert-butoxycarbonylamino)-3-(4-(2-(tosyloxy)propyl)phenyl) propanoate* (9b)**

^{1}H NMR (200 MHz, $CDCl_3$) δ =7.79 (d, 2H, *J* = 8.2 Hz), 7.35 (d, 2H, *J* = 8.0 Hz), 7.08-6.97 (m, 4H), 4.97 (d, 1H, *J* = 7.6 Hz), 4.48-4.36 (m, 1H), 4.03 (t, 2H, *J* = 6.2 Hz), 3.00 (d, 2H, *J* = 5.8 Hz), 2.62 (t, 2H, *J* = 7.6 Hz), 2.46 (s, 3H), 2.04 -1.86 (m, 2H), 1.43 (s, 18H). $[\alpha]^{23}_{D}$ -27.7° (c 0.35, $CHCl_3$).

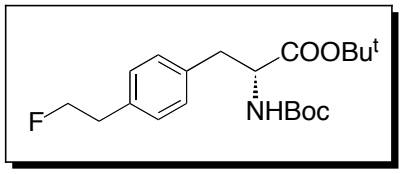

***4.4.1.6.1 (R)-tert-butyl 2-(tert-butoxycarbonylamino)-3-(4-(2-fluoroethyl)phenyl) propanoate* (10a)**

^{1}H NMR (200 MHz, $CDCl_3$) δ = 7.18-7.05 (m, 4H), 4.99 (d, 1H, *J* = 7.8 Hz), 4.73 (t, 1H, 6.6 Hz), 4.53-4.35 (m, 2H), 3.10-3.00 (m, 3H), 2.93 (t, 1H, *J* = 6.6 Hz), 1.42 (s, 18H). $[\alpha]^{23}_{D}$ -38.7° (c 0.47, $CHCl_3$).

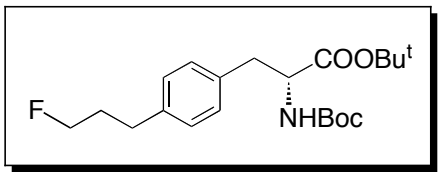

4.4.1.6.2 (R)-tert-butyl 2-(tert-butoxycarbonylamino)-3-(4-(2-fluoropropyl)phenyl) propanoate **(10b)**

^{1}H NMR (200 MHz, $CDCl_3$) δ =7.20-7.07 (m, 4H), 4.99 (d, 1H, *J* = 7.2 Hz), 4.57 (t, 1H, 6.0 Hz), 4.48-4.30 (m, 2H), 3.02 (d, 2H, *J* = 5.8 Hz), 2.72 (t, 1H, *J* = 7.6 Hz), 2.12-1.96 (m, 2H), 1.42 (s, 18H). $[\alpha]^{24}_D$ -37.0^o (c 0.90, $CHCl_3$).

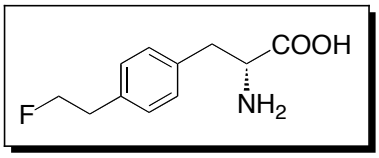

4.4.1.7 (R)-2-amino-3-(4-(2-fluoroethyl)phenyl)propanoic acid **(2)**

^{1}H NMR (200 MHz, D_2O+DCl) δ = 6.89-6.77 (m, 4H), 4.23 (dt, 2H, *J* = 47.0, 6.2 Hz), 3.90 (t, 1H, *J* = 6.6 Hz), 2.81 (ddd, 2H, *J*= 14.6, 5.4, 7.6 Hz), 2.54 (dt, 2H, *J* = 27.4, 6.0 Hz). $[\alpha]^{23}_D$ +5.8^o (c 0.5, 6N HCl).

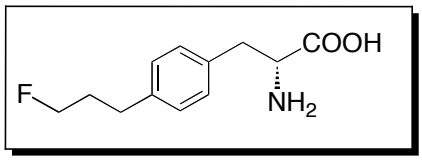

4.4.1.8 (R)-2-amino-3-(4-(2-fluoropropyl)phenyl)propanoic acid **(3)**

^{1}H NMR (200 MHz, D_2O+DCl) δ = 7.04-6.94 (m, 4H), 4.34 (t, 1H, *J* = 6.0 Hz), 4.13-4.04 (m, 2H), 2.98 (ddd, 2H, *J*= 14.6, 5.8, 7.6 Hz), 2.44 (t, 2H, *J*= 7.6 Hz), 1.84-1.57 (m, 2H). $[\alpha]^{24}_D$ +6.0^o (c 0.45, 6N HCl).

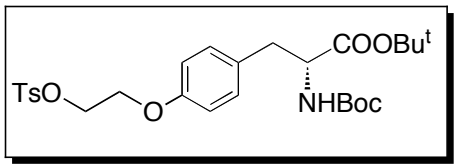

4.4.1.9 (R)-tert-butyl 2-(tert-butoxycarbonylamino)-3-(4-(2-(tosyloxy)ethoxy)phenyl) propanoate **(11)**

D-Boc-tyrosine-*tert*-butyl ester (**5,** 1.0 equiv) was dissolved in 5mL dry DMF. K_2CO_3 (3.0 equiv) and 1,2-bis(tosyloxy)ethane (2.0 equiv) was added sequentially. The mixture was stirred at 70 ^oC for 4h. After reaction, reaction solution was diluted with 60 mL ether, washed with 10 mL water and 10 mL brine. Organic layer dried over $MgSO_4$ and solvent was removed under reduced pressure. Crude mixture was purified by FC ($MeOH/CH_2Cl_2$, 1:200) to give final product D-**11** as white foam. D-**11**, ^{1}H-NMR (200 MHz, $CDCl_3$): δ = 7.83 (d, 2H, *J* = 8.4 Hz), 7.35 (d, 2H, *J* = 8.0 Hz), 7.06 (d, 2H, *J* = 8.6 Hz), 6.70 (d, 2H, *J* = 8.6 Hz), 4.98 (d, 1H, *J* = 8.2 Hz), 4.42-4.34 (m, 3H), 4.13 (t, 2H, *J* = 4.8 Hz), 2.98 (d, 2H, *J* = 5.8 Hz), 2.46 (s, 3H), 1.43 (s, 18H). $[\alpha]^{21}_D$ -24.2^o (c 1.05, $CHCl_3$). In comparison, *(S)-tert*-butyl 2-(tert-butoxycarbonylamino)-3-(4-(2-(tosyloxy)ethoxy)phenyl)propanoate (L-**11**), ^{1}H-NMR (200 MHz, $CDCl_3$): δ = 7.83 (d, 2H, *J* = 8.4 Hz), 7.35 (d, 2H, *J* = 8.0 Hz), 7.06 (d, 2H, *J* = 8.6 Hz), 6.70 (d, 2H, *J* = 8.6 Hz), 4.98 (d, 1H, *J* = 8.2 Hz), 4.42-4.34 (m, 3H), 4.13 (t, 2H, *J* = 4.8 Hz), 2.98 (d, 2H, *J* = 5.8 Hz), 2.46 (s, 3H), 1.43 (s, 18H). ^{13}C NMR (50 MHz, $CDCl_3$) δ = 171.1, 157.2, 155.3, 145.1, 133.2, 130.7, 130.0, 129.5, 128.2, 114.7, 82.2, 79.8, 68.3, 65.7, 55.2, 37.8, 28.5, 28.2, 21.8. HRMS calcd for $C_{27}H_{37}NO_8S$ ([M+Na]$^+$) 558.2138, found 558.2130. $[\alpha]^{21}_D$ +21.6^o (c 0.75, $CHCl_3$).

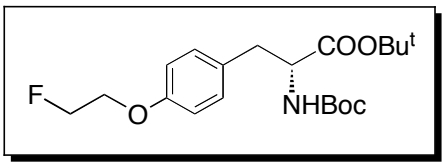

4.4.1.10 (R)-tert-butyl 2-(tert-butoxycarbonylamino)-3-(4-(2-fluoroethoxy)phenyl) propanoate **(12)**

D-Boc-tyrosine-*tert*-butyl ester (**5**, 1.0 equiv) was dissolved in 8 mL DMF. K_2CO_3 (325 mg, 3.0 equiv) and 1-bromo-2-fluoroethane (2.0 equiv) were added sequentially. The mixture was stirred at 70 ^oC for 4 h. After reaction, reaction mixture was diluted with 60 mL ether and washed with 10 mL water and 10 mL brine. Organic layer dried over $MgSO_4$ and solvent was removed under reduced pressure. Resulting product D-**12** was a clear viscous liquid. D-**12**, ^{1}H-NMR (200 MHz, $CDCl_3$): δ = 7.10 (d, 2H, *J* = 8.6 Hz), 6.86 (d, 2H, *J* = 8.6 Hz), 4.97 (d, 1H, *J* = 8.0 Hz), 4.75 (dt, 2H, J_1 = 47.2 Hz, J_2 =4.2 Hz), 4.42-4.28 (m, 1H), 4.20 (dt, 2H, J_1 = 27.6 Hz, J_2 =4.2 Hz), 2.98 (d, 2H, *J* = 5.8 Hz), 1.43 (s, 18H). $[\alpha]^{23}_D$ -35.0^o (c 0.42, $CHCl_3$). In comparison, *(S)-tert*-butyl 2-(tert-butoxycarbonylamino)-3-(4-(2-fluoroethoxy)phenyl)propanoate (L-**12**), ^{1}H-NMR (200 MHz, $CDCl_3$): δ = 7.10 (d, 2H, *J* = 8.6 Hz), 6.86 (d, 2H, *J* = 8.6 Hz), 4.97 (d, 1H, *J* = 8.0 Hz), 4.75 (dt, 2H, J_1 = 47.2 Hz, J_2 =4.2 Hz), 4.42-4.28 (m, 1H), 4.20 (dt, 2H, J_1 = 27.6 Hz, J_2 =4.2 Hz), 2.98 (d, 2H, *J* = 5.8 Hz), 1.43 (s, 18H). ^{13}C NMR (50 MHz, $CDCl_3$) δ = 171.2, 157.7, 155.3, 130.8, 129.4, 114.8, 82.2, 82.1 (d, *J* = 169.5 Hz), 79.9, 67.4 (d, *J* = 20.5 Hz), 55.2, 37.9, 28.5, 28.2. HRMS calcd for $C_{20}H_{30}FNO_5$ ($[M+Na]^+$) 406.2006, found 406.2042. $[\alpha]^{23}_D$ +32.1^o (c 0.40, $CHCl_3$).

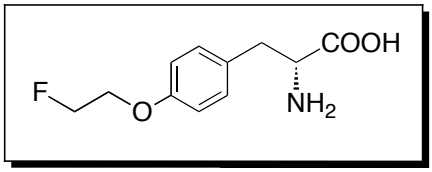

***4.4.1.11 (R)-2-amino-3-(4-(2-fluoroethoxy)phenyl)propanoic acid* (1)**

D-**12** (1.0 equiv) was dissolved in CH_2Cl_2 and equal volume of trifluoroacetic acid was added and reaction mixture was stirred in room temperature for 4 h. Upon completion, reaction mixture was concentrated under reduced pressure. Resulting solid

was dissolved in methanol and pH of the solution was adjusted to ~7 with 5% NH_4OH to form a white precipitate was formed. The suspension was kept overnight at 0 ^oC and filtered to afford D-**1** as whit solid. D-**1**, ^1H-NMR (D_2O+DCl): δ = 6.92 (d, 2H, *J* = 8.8 Hz), 6.66 (d, 2H, *J* = 8.8 Hz), 4.44 (dt, 2H, J_1 = 47.4 Hz, J_2 = 4.0 Hz), 4.05-3.98 (m, 2H), 3.87 (t, 1H, *J* = 4.0 Hz), 2.89 (ddd, 2H, *J*= 14.6, 5.6, 7.4 Hz). $[\alpha]^{23}_D$ +3.2^o (c 0.5, 6 N HCl). In comparison, *(S)-2*-amino-3-(4-(2-fluoroethoxy)phenyl)propanoic acid (L-**1**), ^1H-NMR (Acetic acid-d4): δ = 7.24 (d, 2H, *J* = 8.6 Hz), 6.91 (d, 2H, *J* = 8.6 Hz), 4.73 (dt, 2H, J_1 = 47.4 Hz, J_2 =4.0 Hz), 4.40 (dd, 1H, J_1 = 7.6 Hz, J_2 = 5.2 Hz), 4.22 (dt, 2H, J_1 = 29.2 Hz, J_2 = 4.0 Hz), 3.52-3.22 (m, 2H). ^{13}C NMR (50MHz, Acetic acid-d4): δ = 173.1, 158.2, 130.8, 126.9, 115.0, 81.9 (d, *J* = 167.5 Hz), 67.2 (d, *J* = 20.0 Hz), 55.8, 35.1. HRMS calcd for $C_{11}H_{14}FNO_3$ ($[M+H]^+$) 228.1036, found 228.1265. $[\alpha]^{23}_D$ -3.4^o (c 0.53, 6 N HCl).

4.4.2. Log D measurement

Partition coefficient was measured by mixing ligand with 3 g each of 1-octanol and sodium phosphate buffer (0.1 M, pH 7.4) in a test tube. The test tube was vortexed for 3 min at room temperature, followed by centrifuge for 5 min. Two weighted samples from 1-octanol and buffer layers were counted in a gamma counter. The partition coefficient was determined by calculating the ratio of cpm/g of 1-octanol to that of buffer. The measurement was done in duplicates.

4.5 References

[1] Ganapathy V, Thangaraju M, and Prasad PD. Nutrient transporters in cancer: relevance to Warburg hypothesis and beyond. Pharmacol Ther 2009;121:29-40.

[2] McConathy J and Goodman Mark M. Non-natural amino acids for tumor imaging using positron emission tomography and single photon emission computed tomography. Cancer Metastasis Rev 2008;27:555-73.

[3] Jager PL, Vaalburg W, Pruim J, de Vries EG, Langen KJ, and Piers DA. Radiolabeled amino acids: basic aspects and clinical applications in oncology. J Nucl Med 2001;42:432-45.

[4] Singhal T, Narayanan TK, Jain V, Mukherjee J, and Mantil J. 11C-L-methionine positron emission tomography in the clinical management of cerebral gliomas. Mol Imaging Biol 2008;10:1-18.

[5] Langen K-J, Pauleit D, and Coenen HH. 3-[123I]iodo-a-methyl-L-tyrosine: uptake mechanisms and clinical applications. Nuclear Medicine and Biology 2002;29:625-31.

[6] Langen KJ, Jarosch M, Hamacher K, Muhlensiepen H, Weber F, Floeth F, et al. Imaging of gliomas with Cis-4-[18F]fluoro-L-proline. Nucl Med Biol 2004;31:67-75.

[7] Koerts J, Leenders KL, Koning M, Portman AT, and van Beilen M. Striatal dopaminergic activity (FDOPA-PET) associated with cognitive items of a depression scale (MADRS) in Parkinson's disease. Eur J Neurosci 2007;25:3132-6.

[8] Schuster DM, Votaw JR, Nieh PT, Yu W, Nye JA, Master V, et al. Initial experience with the radiotracer anti-1-amino-3-18F-fluorocyclobutane-1-carboxylic acid with PET/CT in prostate carcinoma. J Nucl Med 2007;48:56-63.

[9] Langen KJ, Hamacher K, Weckesser M, Floeth F, Stoffels G, Bauer D, et al. O-(2-[18F]fluoroethyl)-L-tyrosine: uptake mechanisms and clinical applications. Nucl Med Biol 2006;33:287-94.

[10] Wester HJ, Herz M, Weber W, Heiss P, Senekowitsch-Schmidtke R, Schwaiger M, et al. Synthesis and radiopharmacology of O-(2-[18F]fluoroethyl)-L-tyrosine for tumor imaging. J Nucl Med 1999;40:205-12.

[11] Laverman P, Boerman OC, Corstens FH, and Oyen WJ. Fluorinated amino acids for tumour imaging with positron emission tomography. Eur J Nucl Med Mol Imaging 2002;29:681-90.

[12] McGivan JD and Pastor-Anglada M. Regulatory and molecular aspects of mammalian amino acid transport. Biochem J 1994;299 (Pt 2):321-34.

[13] Fuchs BC and Bode BP. Amino acid transporters ASCT2 and LAT1 in cancer: partners in crime? Semin Cancer Biol 2005;15:254-66.

[14] Saier MH, Jr., Daniels GA, Boerner P, and Lin J. Neutral amino acid transport systems in animal cells: potential targets of oncogene action and regulators of cellular growth. J Membr Biol 1988;104:1-20.

[15] Kaira K, Oriuchi N, Imai H, Shimizu K, Yanagitani N, Sunaga N, et al. l-type amino acid transporter 1 and CD98 expression in primary and metastatic sites of human neoplasms. Cancer Sci 2008;99:2380-6.

[16] Christensen HN. Role of amino acid transport and countertransport in nutrition and metabolism. Physiol Rev 1990;70:43-77.

[17] Tamemasa O, Goto R, and Suzuki T. Preferential incorporation of some 14C-labeled D-amino acids into tumor-bearing animals. Gann 1978;69:517-23.

[18] Friedman M. Chemistry, nutrition, and microbiology of D-amino acids. J Agric Food Chem 1999;47:3457-79.

[19] Kanai Y, Segawa H, Miyamoto K, Uchino H, Takeda E, and Endou H. Expression cloning and characterization of a transporter for large neutral amino acids activated by the heavy chain of 4F2 antigen (CD98). J Bio Chem 1998;273:23629-32.

[20] Uchino H, Kanai Y, Kim DK, Wempe MF, Chairoungdua A, Morimoto E, et al. Transport of amino acid-related compounds mediated by L-type amino acid transporter 1 (LAT1): insights into the mechanisms of substrate recognition. Mol Pharma 2002;61:729-37.

[21] Yanagida O, Kanai Y, Chairoungdua A, Kim DK, Segawa H, Nii T, et al. Human L-type amino acid transporter 1 (LAT1): characterization of function and expression in tumor cell lines. Biochim Biophys Acta 2001;1514:291-302.

[22] Segawa H, Fukasawa Y, Miyamoto K, Takeda E, Endou H, and Kanai Y. Identification and functional characterization of a Na+-independent neutral amino acid transporter with broad substrate selectivity. J Bio Chem 1999;274:19745-51.

[23] Nawashiro H, Otani N, Shinomiya N, Fukui S, Ooigawa H, Shima K, et al. L-type amino acid transporter 1 as a potential molecular target in human astrocytic tumors. Intern J Cancer 2006;119:484-92.

[24] Sakata T, Ferdous G, Tsuruta T, Satoh T, Baba S, Muto T, et al. L-type amino-acid transporter 1 as a novel biomarker for high-grade malignancy in prostate cancer. Pathol Int 2009;59:7-18.

[25] Kaira K, Oriuchi N, Imai H, Shimizu K, Yanagitani N, Sunaga N, et al. Prognostic significance of L-type amino acid transporter 1 expression in resectable stage I-III nonsmall cell lung cancer. Br J Cancer 2008;98:742-8.

[26] Bergstrom M, Lundqvist H, Ericson K, Lilja A, Johnstrom P, Langstrom B, et al. Comparison of the accumulation kinetics of L-(methyl-11C)-methionine and D-(methyl-11C)-methionine in brain tumors studied with positron emission tomography. Acta Radiol 1987;28:225-9.

[27] Heiss P, Mayer S, Herz M, Wester HJ, Schwaiger M, and Senekowitsch-Schmidtke R. Investigation of transport mechanism and uptake kinetics of O-(2-[18F]fluoroethyl)-L-tyrosine in vitro and in vivo. J Nucl Med 1999;40:1367-73.

[28] Tsukada H, Sato K, Fukumoto D, and Kakiuchi T. Evaluation of D-isomers of O-F-18-fluoromethyl, O-F-18-fluoroethyl and O-F-18-fluoropropyl tyrosine as tumour imaging agents in mice. Eur J Nucl Med Mol Imaging 2006;33:1017-24.

[29] Bauwens M, Lahoutte T, Kersemans K, Gallez C, Bossuyt A, and Mertens J. Comparison of the uptake of [123/125I]-2-iodo-D-tyrosine and [123/125I]-2-iodo-L-tyrosine in R1M rhabdomyosarcoma cells in vitro and in R1M tumor-bearing Wag/Rij rats in vivo. Nucl Med Biol 2006;33:735-41.

[30] Kersemans V, Cornelissen B, Bacher K, Kersemans K, Thierens H, Dierckx RA, et al. In vivo evaluation and dosimetry of 123I-2-iodo-D-phenylalanine, a new potential tumor-specific tracer for SPECT, in an R1M rhabdomyosarcoma athymic mouse model. J Nucl Med 2005;46:2104-11.

[31] Langen KJ, Hamacher K, Bauer D, Broer S, Pauleit D, Herzog H, et al. Preferred stereoselective transport of the D-isomer of cis-4-[18F]fluoro-proline at the blood-brain barrier. J Cereb Blood Flow Metab 2005;25:607-16.

[32] Langen KJ, Salber D, Hamacher K, Stoffels G, Reifenberger G, Pauleit D, et al. Detection of secondary thalamic degeneration after cortical infarction using cis-4-18F-fluoro-D-proline. J Nucl Med 2007;48:1482-91.

[33] Makrides V, Bauer R, Weber W, Wester HJ, Fischer S, Hinz R, et al. Preferred transport of O-(2-[18F]fluoroethyl)-D-tyrosine (D-FET) into the porcine brain. Brain Res 2007;1147:25-33.

[34] Wang L, Qu W, Lieberman BP, Plössl K, and Kung HF. Synthesis, uptake mechanism characterization and biological evaluation of 18F labeled fluoroalkyl phenylalanine analogs as potential PET imaging agents. Nucl Med Bio 2010 (In press).

[35] Hamacher K and Coenen HH. Efficient routine production of the 18F-labelled amino acid O-2-18F fluoroethyl-L-tyrosine. Applied Rad Isotopes 2002;57:853-6.

[36] Smith G and Sivakua T. Mechanism of the racemization of amino acids. Kinetics of racemization of arylglycines. J Org Chem 1983;48:627-34.

[37] Urakami T, Sakai K, Asai T, Fukumoto D, Tsukada H, and Oku N. Evaluation of O-[(18)F]fluoromethyl-D-tyrosine as a radiotracer for tumor imaging with positron emission tomography. Nucl Med Biol 2009;36:295-303.

[38] Palacin M, Estevez R, Bertran J, and Zorzano A. Molecular biology of mammalian plasma membrane amino acid transporters. Physiol Rev 1998;78:969-1054.

[39] Bodoy S, Martin L, Zorzano A, Palacin M, Estevez R, and Bertran J. Identification of LAT4, a novel amino acid transporter with system L activity. J Bio Chem 2005;280:12002-11.

[40] Tomi M, Mori M, Tachikawa M, Katayama K, Terasaki T, and Hosoya K. L-type amino acid transporter 1-mediated L-leucine transport at the inner blood-retinal barrier. Invest Ophthalmol Vis Sci 2005;46:2522-30.

[41] Babu E, Kanai Y, Chairoungdua A, Kim DK, Iribe Y, Tangtrongsup S, et al. Identification of a novel system L amino acid transporter structurally distinct from heterodimeric amino acid transporters. J Bio Chem 2003; 278:43838-45.

[42] Wang L, Lieberman B, Qu W, Ploessl K, and Kung HF. Synthesis and comparative biological evaluation of L- and D-isomers of 18F labeled fluoroalkyl phenylalanine derivatives as tumor imaging agents. Nucl Med Biol 2010 (Accepted).

[43] Tsukada H, Sato K, Fukumoto D, Nishiyama S, Harada N, and Kakiuchi T. Evaluation of D-isomers of O-11C-methyl tyrosine and O-18F-fluoromethyl tyrosine as tumor-imaging agents in tumor-bearing mice: comparison with L- and D-11C-methionine. J Nucl Med 2006;47:679-88.

[44] Kersemans V, Cornelissen B, Kersemans K, Bauwens M, Dierckx RA, De Spiegeleer B, et al. 123/125I-labelled 2-iodo-L: -phenylalanine and 2-iodo-D: -phenylalanine: comparative uptake in various tumour types and biodistribution in mice. Eur J Nucl Med Mol Imaging 2006;33:919-27.

Chapter 5

Radiosynthesis and in vitro evaluation of ^{11}C labeled ethanolamine derivatives as potential tumor imaging agents for PET

5.1 Introduction

Cancer cells exhibit significantly altered phospholipids metabolism compared with normal counterparts [1, 2]. Proliferating tumor cells have increased demand for phosphoglycerides that are essential in formation of cellular membranes. The most abundant phosphoglycerides in higher plants and animals are phosphatidylethanolamine (PtdEt) and phosphatidylcholine (PtdCho), which contain ethanolamine and choline as polar head group respectively [3].

Numerous ^{31}P-Magnetic resonance spectroscopic (MRS) studies have detected high levels of phoshphomonoester (PME) including phosphocholine (PCho) and phosphoethanolamine (PEt) in cancer cells [1, 2]. PCho, the product of choline kinase, is the first intermediate in the incorporation of choline into PtdCho through Kennedy pathway [4]. The increased concentration of PCho in cancer cells is largely due to upregulation and increased enzyme activity of choline kinase [5-7] and choline transporters [8]. Based on this aberrant tumor phospholipid metabolism, radiolabeled [^{11}C]choline (CH) [9] and its ^{18}F labeled derivatives fluoromethyl choline (FCho) and fluoroethyl choline (FEC) [10] (Figure 5.1) have been developed and successfully used for detection and staging various tumors including brain tumors and prostate cancers, which could improve on tumor detectability of most widely used FDG-PET [11, 12].

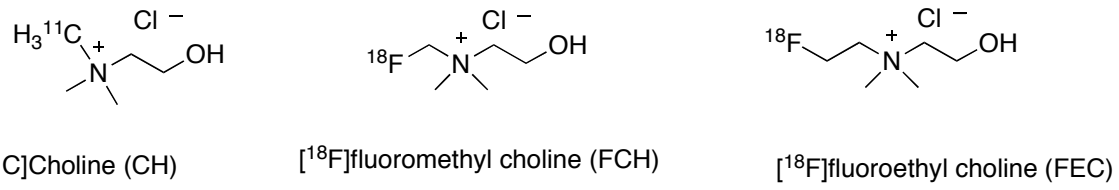

[^{11}C]Choline (CH) [^{18}F]fluoromethyl choline (FCH) [^{18}F]fluoroethyl choline (FEC)

Figure 5.1. Radiolabeled choline and its derivatives

Recent development of proton-decoupled ^{31}P-MRS method enabled the resolution of PEt and PCho peaks in vivo that were previously overlapped under the broad PME peak [13, 14]. This advance led to the discovery that PEt level in a number of cancers is significantly higher than PCho. For example, in human non-Hodgkin's lymphoma (NHL) the PEt/PCho ratio of 2.9 has been reported (Figure 5.2) [15]. Prevailing contribution from PEt in elevated PME signal has also been observed in various breast cancers [16, 17] and pediatric brain tumors [18]. This observation of higher concentration of PEt in tumor cells might indicate that ethanolamine, the precursor for PEt, could potentially more sensitive than choline as a probe for phospholipids metabolism.

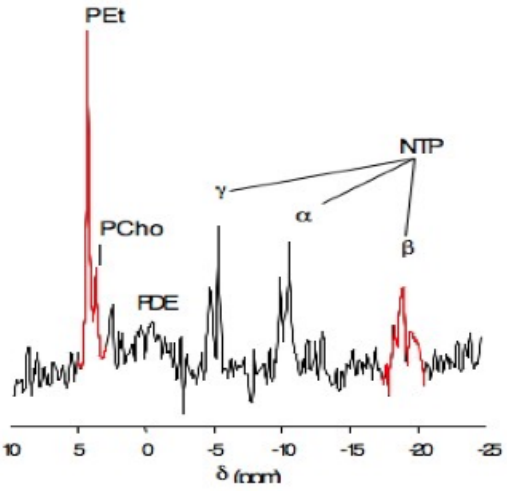

Figure 5.2. ^{31}P MR spectrum in a NHL patient. NTP, nucleotide triphosphate. PDE, phosphodiesters

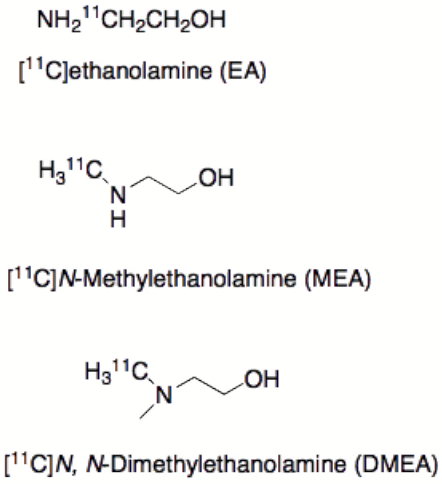

Figure 5.3. Radiolabeled ethanolamine and its methyl derivatives

In order to validate the potential of radiolabeled ethanolamine for cancer detection, we initially carried out in vitro studies using ^{14}C label compound. We compared uptake of [^{14}C]ethanolamine (EA), [^{14}C] N, N'-dimethyl ethanolamine (DMEA) and [^{14}C]choline (CH) in a wide variety of cancer cell lines including colorectal

cancer (HCT116), prostate (PC-3), melanoma (A375 and 1618), glioblastoma (SF767, A172), and lymphoma (DLCL2). Our results showed that [^{14}C]EA and [^{14}C]DMEA had significantly higher uptake than choline and their uptake depends on the proliferating status of the cells [19]. These preliminary results encouraged us to develop the corresponding ^{11}C labeled PET imaging agents (Figure 5.3). As consideration for ease of radiosynthesis, in this work we prepared [^{11}C]*N*-methylethanolamine (MEA) and [^{11}C]DMEA and carried out biological studies in vitro. In vivo biodistribution studies and imaging studies are in progress.

5.2 Results and Discussion

5.2.1 Comparison of ^{14}C labeled choline and ethanolamine as probe for cancer detection

Table 5.1. Cell type and their origins

Cell lines	Cell Type	Cell Origin
SF767	Glioblastoma Multiforme	Human Brain
A172	Glioblastoma Multiforme	Human Brain
1618	Melanoma	Human Skin
A375	Melanoma	Human Skin
PC3	Androgen Independent Prostate Carcinoma	Human Prostate
LnCap	Androgen Dependent Prostate Carcinoma	Human Prostate
DLCL2	Diffuse Large B-cell Lymphoma	Human Lymph Node
HCT116	Colorectal Adenocarcinoma	Human Colon

In vitro uptake studies were carried out with [^{14}C]EA, [^{14}C]DMEA and [^{14}C]CH in a diversity of human tumor cell lines, including two glioblastoma lines, an androgen dependent and an androgen independent prostate adenocarcinoma, two melanoma cell lines, a colorectal cancer cell line and a diffuse large B-cell lymphoma cell line (as shown in Table 5.1). Uptake of [^{14}C]MEA was compared to that of [^{14}C]CH in two prostate

cancer cell lines as well. Results showed that in all tumor cell lines tested, [^{14}C]EA and its derivatives had significant higher uptake (1.4 to 7.4) than [^{14}C]CH (Figure 5.4).

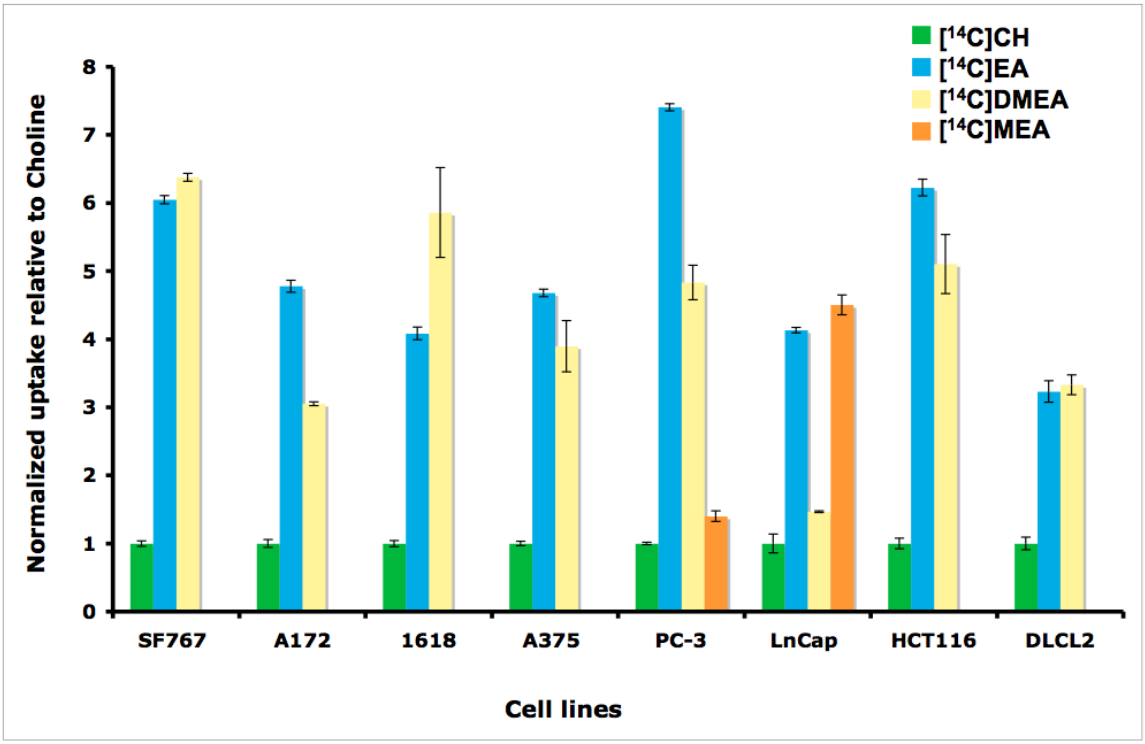

Figure 5.4[a]. Normalized uptake of [^{14}C]EA, [^{14}C]DMEA and [^{14}C]MEA relative to [^{14}C]CH in tumor cell lines.
[a]Uptake studies of [^{14}C]EA, [^{14}C]DMEA and [^{14}C]CH were carried out by Akiva Mintz [19].

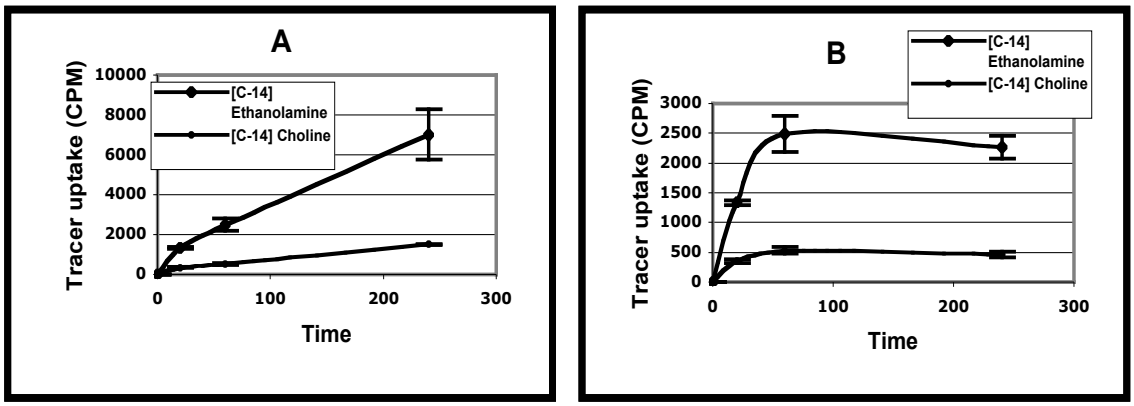

Figure 5.5[a]. Cellular uptake studies of [^{14}C]CH and [^{14}C]EA in A172 cells. Time course studies (A) and after 60 min, replacing tracer-containing media with regular media (B).
[a]Experiment carried out by Akiva Mintz [19].

We performed time course studies of [^{14}C]EA and [^{14}C]CH in A172 cells, which demonstrated continuous linear uptake of [^{14}C]EA after 4 hours of tracer exposure (Figure 5.5A). However, if the radiotracer was removed after 60 minutes, and replaced with non-tracer containing media, the radioactive counts in the cells were not significantly different after 180 minutes compared to immediately after 60 minutes of tracer incubation (Figure 5.5B). These results suggested the irreversible trapping of ethanolamine in tumor cells.

The preliminary results using ^{14}C labeled ligands demonstrate for the first time that ethanolamine and its derivatives could be potential useful oncologic imaging tracers for a number of cancers including brain and prostate cancer. Based on these findings, we then continued with preparation of ^{11}C labeled ethanolamine tracers that could potentially be utilized as PET imaging agents.

5.2.2 Radiolabeling of [^{11}C]EA, [^{11}C]MEA and [^{11}C]DMEA

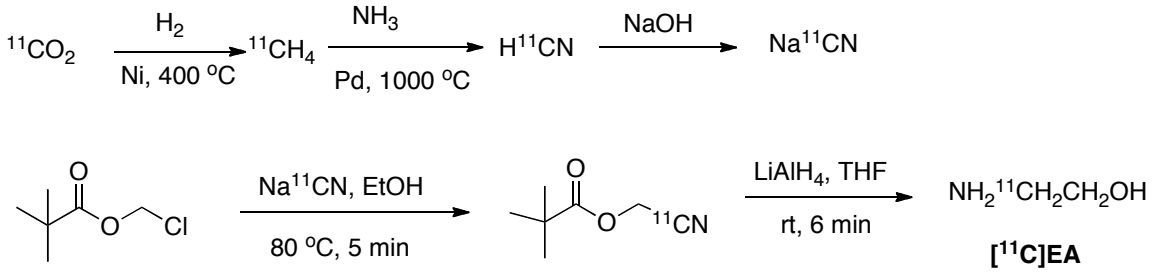

Scheme 5.1[a]. Radiolabeling of [^{11}C]EA.
[a]Synthesis carried out by Datta Ponde

Radiosynthesis of [^{11}C] EA, [^{11}C]MEA and [^{11}C]DMEA was carried out as shown in Scheme 5.1 and Scheme 5.2. [^{11}C]EA was recently synthesized by Dr. Datta Ponde employing procedure reported by Thorell et al with modifications [20].

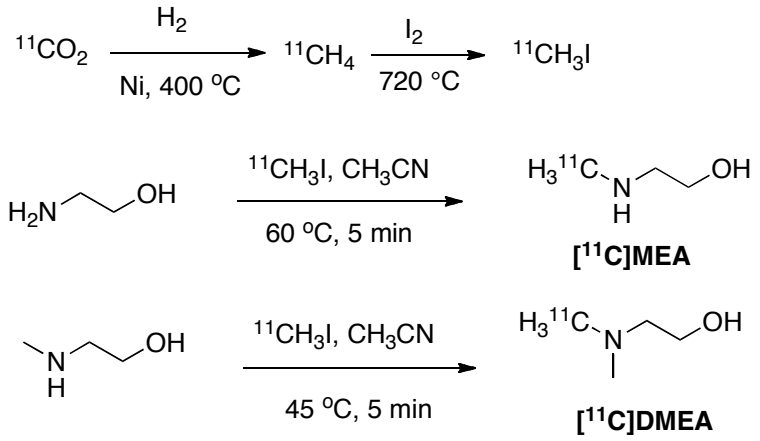

Scheme 5.2. Radiolabeling of [^{11}C]MEA and [^{11}C]DMEA

[^{11}C]MEA and [^{11}C]DMEA were labeled through methylation of ethanolamine and *N*-methylethanolamine respectively with [^{11}C]CH_3I prepared from [^{11}C]CO_2 using GE MeI box. Although these molecules have simple structure, the short half-life of ^{11}C posts strict limit on reaction time – within 20 min (one half-life period) is preferable. In additional, [^{11}C]CO_2 produced in a cyclotron target is not suitable labeling precursor for the synthesis of these ligands and need to be converted into [^{11}C]NaCN or [^{11}C]CH_3I for radiosynthesis. We were able to prepare radiochemically pure (>95%) [^{11}C]MEA and [^{11}C]DMEA within 20 min from end of bombardment (EOB) with good specific activity (~52 GBq/μmol or 1300 Ci/mmol) and high radiochemical yield (average 45 to 52%, decay corrected). Radiolabeled ligands were purified with silica cartridge. Radiochemical purity was analyzed by HPLC and TLC. The labeling procedure was carried out in automated synthetic module and is suitable for potential clinical applications. Several problems associated with purification and detection of these compounds made this seemly straightforward radiosynthesis an interesting challenge. We conducted a series of experiment to optimize their reaction condition, purification process and quality control.

5.2.2.1 Reaction condition studies

Table 5.2: Effect of temperature on radiolabeling of [^{11}C]MEA and [^{11}C]DMEA

Product	Temp (°C)	Radiochemical purity (%)	Experiments
[^{11}C] MEA	25	No reaction	1
[^{11}C] MEA	60	>95	>3
[^{11}C] DMEA	25	No reaction	1
[^{11}C] DMEA	45	>95	2
[^{11}C] DMEA	50	>95	>3
[^{11}C] DMEA	55	93±3	2
[^{11}C] DMEA	60	60±5	2
[^{11}C] DMEA	65	19±3	2

Temperature was a key factor in this labeling reaction (Table 5.2). No reaction was observed at room temperature in presence of base (NaOH or KOH) or without base. After careful increase of temperature it was observed that for the synthesis of [^{11}C] MEA, reaction can be carried out at 60°C. However, in the case of [^{11}C]DMEA, reaction should best be set between 45 to 55°C. At higher temperature (> 60°C), we have detected the formation of [^{11}C]CH (HPLC result Figure 5.6 as example) (50% to 80% in the final product as seen from analytical HPLC).

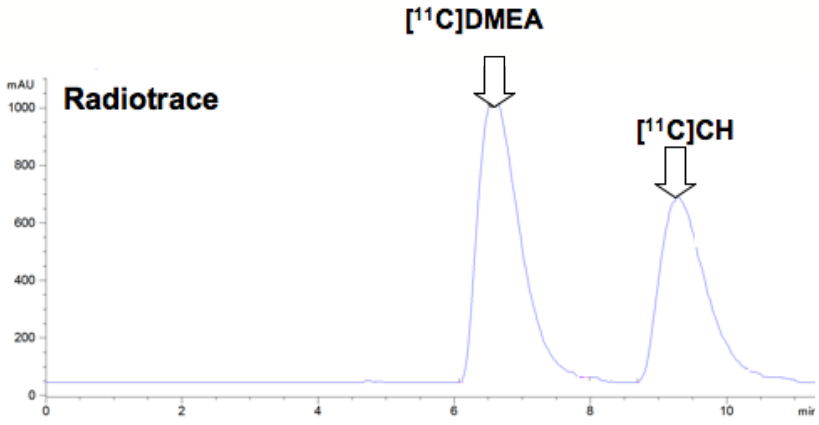

Figure 5.6. Formation of [^{11}C]CH in radiosynthesis of [^{11}C]DMEA at high temperature.

No base is required for this methylation reaction. A number of bases such as sodium hydroxide, potassium hydroxide and sodium hydride were tried initially, but no advantage was found, moreover, sodium hydride can produce the *O*-methylation side products. We also tried different solvents such as DMF, DMSO and CH_3CN, reaction time and yields were similar in these solvents. Since it is often more difficult to remove DMF and DMSO, we choose CH_3CN as reaction solvent.

5.2.2.2 Purification of [^{11}C]MEA and [^{11}C]DMEA

Table 5.3. Experimented purification methods and results

Purification methods	Results and comments
Sep-Pak C_{18} (light or plus) cartridges	could not appropriately trap products
Weak cation exchange cartridges	could not appropriately trap products
Strong cation exchange cartridge	could not be eluted with appropriate solvent
Semi-prep HPLC with cyano column	could not elute the products using water
Silica cartridges	retained products and then eluted with saline

For the purification of [^{11}C]MEA and [^{11}C]DMEA, we tried a number of cartridges such as Sep-Pak C_{18} (light or plus) and cation exchange cartridges (weak or strong) without success. In the case of the Sep-Pak C_{18} or weak cation exchange cartridge, most of the radioactivity could not be trapped on the cartridges and went into the waste. For strong cation exchange cartridge, although activity was retained in the cartridge, the products could only be eluted only with strong basic buffer solution such as 3 N ammonia hydroxide, which is not a pharmaceutically appropriate formula for further biological evaluations. Semi-prep HPLC with reverse phase cyano column [21] failed to elute the products using water at 1 mL/min. Finally silica cartridges were successfully implemented. The reaction mixture, which was diluted with water, was passed through

the silica cartridge followed by washing with ethanol, to remove excess of precursor, and then with 10 mL of water, to remove the residual ethanol. Final products were eluted with saline. 5 mL of saline was required to elute 925 to 1110 Mbq (25 to 30 mCi) of product. We measured the distribution of radioactivity after purification and found that ~70% of activity was eluted to final product while 20% of activity went to waste, 5% stayed on cartridge and 5% remained in the reaction vessel. The purification results were summarized in Table 5.3.

5.2.2.3 Quality control of [^{11}C]MEA and [^{11}C]DMEA

It is difficult to detect N-methyl ethanolamine and N, N-dimethyl ethanolamine using standard UV detector in HPLC system since they are not UV active. We choose to use refractometer, which has adequate sensitivity for detection of cold standard. To achieve the best separation between ethanolamine, N-methyl ethanolamine and N, N-dimethyl ethanolamine, we tried various HPLC conditions, such as 5 mM HCl solution, 0.25 M NaH_2PO_4/CH_3CN mixture in different ratios and found that isocratic 0.25 M NaH_2PO_4 was able to achieve best separation. The column used was strong cation exchange column (SCX). In each case, retention time difference between the precursor and product was more than 1 min, which made them easy to identify.

5.2.2.4 Automated synthetic module

Radiosynthesis of [^{11}C]MEA and [^{11}C]DMEA was carried out in an automated synthetic module as depicted in Figure 5.7. The components in this synthetic module

include a helium supply, ten three-way solenoid controlled flow valves, a T-shaped reaction vessel, two collection vials (one for the waste and one for the product) and a charcoal trap for volatile radioactivity. This automatic synthetic module requires little manual control and could potentially be used in clinical settings.

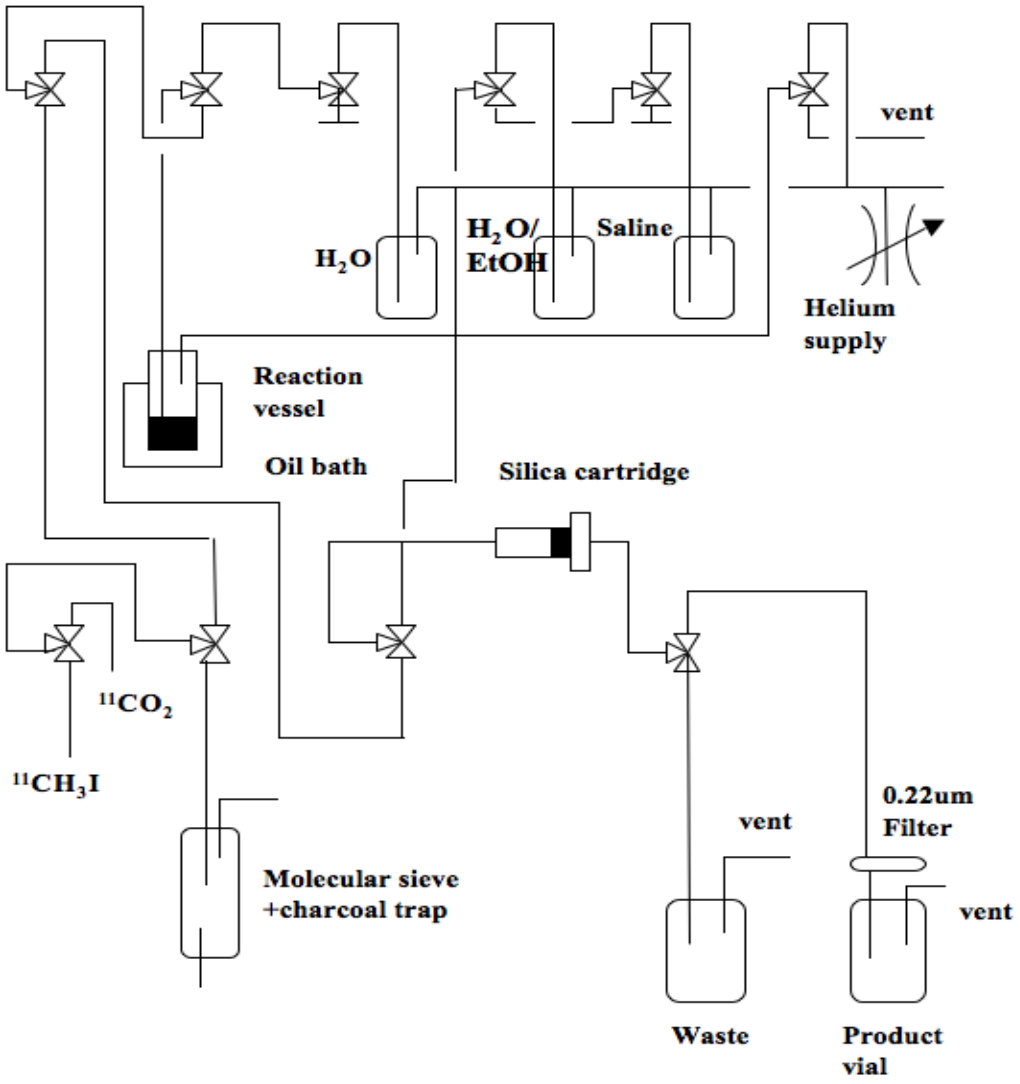

Figure 5.7. Schematic diagram of the automated system for the production of [^{11}C]MEA and [^{11}C]DMEA.

5.2.3 In vitro cell uptake studies

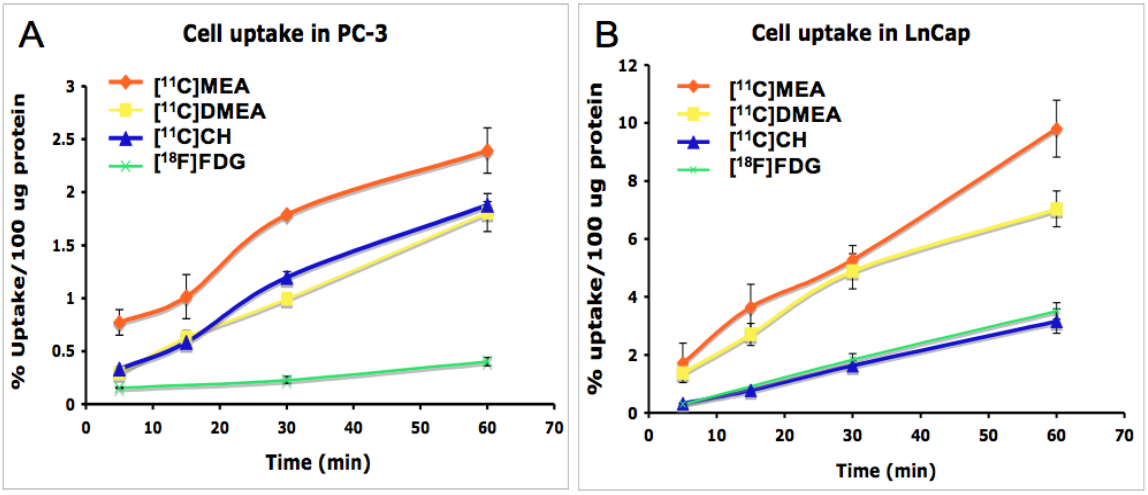

Figure 5.8. Cell uptake studies in PC-3 (A) and LnCap (B) prostate cancer cell lines.

After successful labeling [^{11}C]MEA and [^{11}C]DMEA, we first conducted the time-dependent cell uptake studies comparing these two ^{11}C labeled ethanolamine derivatives with clinically utilized [^{11}C]CH in androgen independent PC-3 and androgen dependent LnCap prostate cancer cell lines (Figure 5.8). The reason we chose PC-3 and LnCap for in vitro studies is that [^{11}C]CH is most established for imaging prostate cancers and androgen dependence of prostate cancer cells has clinical significance for cancer therapeutic plan and monitoring [22, 23]. Because cell uptake studies of these tracers were done in different days on different batch of cells, most widely used PET tracer [^{18}F]FDG was used as a reference ligand as well. All ligands demonstrated similar linear incremental cellular uptake in 1h time period. [^{11}C]MEA had 1.3 (in PC-3) to 3.1 (in LnCap) fold higher uptake in comparison to [^{11}C]CH at 60 min time point. Uptake of [^{11}C]DMEA in PC-3 was comparable to that of [^{11}C]CH and 2.2 fold higher in LnCap. All tracers had higher uptake in LnCap than in PC-3, the difference in uptake of [^{11}C]MEA and [^{11}C]DMEA was much larger than [^{11}C]CH. The uptake results suggested

that ethanolamine derivatives [^{11}C]MEA and [^{11}C]DMEA could be more sensitive tracers than [^{11}C]CH and thus worth further investigation. Uptake studies of [^{11}C]EA will be conducted in the near future.

5.2.4 Inhibition studies

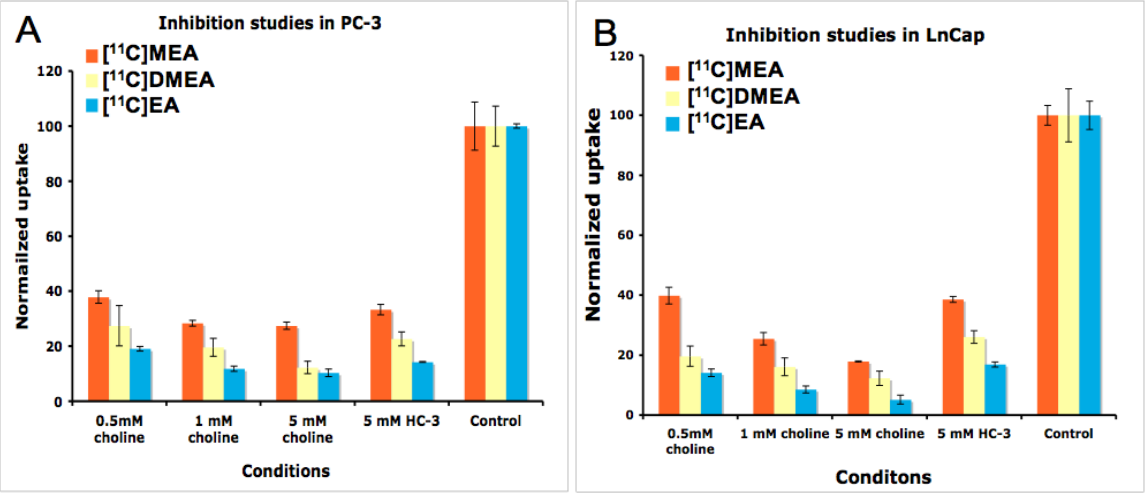

Figure 5.9. Inhibition studies result in PC-3 and LnCap.

We hypothesize that increased uptake of ethanolamine derivatives in cancer cells was result of upregulated ethanolamine/choline kinase and transport activity. We then carried out inhibition studies to characterize the uptake of tracer (Figure 5.9). It was of interest to measure the sensitivity of tracers' uptake to Hemicholinium 3 (HC-3) and choline. There were studies suggesting both choline and ethanolamine were transportable substrates of the same carrier-mediated mechanism [24]. HC-3 blocks membrane transport of ethanolamine and choline and inhibits choline kinase (Ki = 0.5 mM) but not ethanolamine kinase [25, 26]. Choline was a potent competitive inhibitor of ethanolamine kinase (Ki = 0.33–0.50 mM) [27]. PC-3 or LnCap cells were subjective to the inhibitors during preinhibition period of 10 min followed by incubation period for 60 min. The

effect of inhibition was similar in PC-3 and LnCap cell lines. Uptake of tracers showed concentration dependent inhibition by choline. The sensitivity to inhibitors followed the order [^{11}C]EA>[^{11}C]DMEA>[^{11}C]MEA. From this inhibition studies we could not conclude uptake of ethanolamine and its derivatives depends on ethanolamine kinase activity. The inhibitory effect of HC-3 was less pronounced than choline (5mM of HC-3 had similar effect as 0.5 mM choline), indicating contribution from ethanolamine kinase.

5.3 Conclusions

Based on preliminary studies with ^{14}C labeled ethanolamine tracers showing that ethanolamine could be a potential oncologic imaging tracer for altered phospholipids metabolism, we prepared positron emitting isotope labeled [^{11}C]EA, [^{11}C]MEA and [^{11}C]DMEA. Labeling of [^{11}C]MEA and [^{11}C]DMEA were carried out in the automatic synthetic module that was suitable for potential clinically applications. Radiochemically pure tracers could be obtained with good yields. In vitro cell uptake studies demonstrated that [^{11}C]MEA and [^{11}C]DMEA had higher uptake than clinically utilized [^{11}C]CH in prostate cancer cell lines. Further development such as metabolites analysis, biodistribution and small animal imaging studies of these ^{11}C labeled ethanolamine tracers is warranted.

5.4 Experimental Section

5.4.1 General

All reagents were purchased from Sigma-Aldrich and Fisher Scientific in ACS grade. All solvents were of HPLC analytical grade. Cartridges (C18, Silica, cation exchange) were purchased from Waters. Cancer cell lines were purchased from American type culture collection (ATCC; Manassas, VA). All cell lines were cultured and maintained under a 5%CO_2-humidified incubator at 37ºC according to standard cell culture protocol and in standard culture medium (GIBCO BRL, NY) recommended by the supplier. ^{14}C labeled tracers were purchased from American Radiolabeled Chemicals, Inc. (ARC, St. Louis, MO). HPLC was performed on a system (Agilent Technologies 1200 series) with quaternary pump, refractometer (HP HEWLETT PACKARD series 1100), variable wavelength-detector operating at 205 nm and NaI(Tl) radiation detector (EG&G ORTEC). The purity of all radioactive products was monitored with a strong cation exchange column (Agilent ZORBAX 300-SCX, 5uM, 4.6x250mm) using 100% 0.25M NaH_2PO_4 as eluent with flow rate at 1 mL/min. Radiochemical purity was also monitored by radio-Thin-Layer Chromatography (TLC) performed on aluminum sheets coated with silica gel 60 F_{254} (0.25 mm thickness, E. Merck, Darmstadt, Germany) and developed with MeOH/29% Ammonia hydroxide (3:1).

5.4.2 Radiochemistry

[^{11}C] CO_2 was produced by the $^{14}N(p,\alpha)^{11}C$ nuclear reaction using a nitrogen gas (N_2/0.5%O_2) target pressurized to 300 psi and bombarded with 22 MeV protons (20 min,

10 μA) produced by the Japanese Steel Corporation (JSW) cyclotron at the Hospital of University of Pennsylvania. [^{11}C] MeI was then prepared from [^{11}C] CO_2 using General Electric MeI microlab. When ready, [^{11}C] MeI was transferred with a stream of helium (80 mL/min) into a reaction vessel containing 1 mg of ethanolamine or N-methyl ethanolamine in 250 μL of acetonitrile (Figure 5.6). The reaction mixture was heated at 60^{0}C for [^{11}C]MEA or 45^{0}C for [^{11}C]MEA for 5 mins. At the end of 5 mins of reaction, the crude product was diluted with 3 mL of water and then passed through a silica cartridge (preconditioned with 3 mL of 5% of ethanol in water). The cartridge was washed with 8 mL of ethanol, 10 mL of water and then eluted with 5 mL of saline. The radiochemical purity of products was measured by analytical HPLC (0.25 M NaH_2PO_4, 1 mL/min) and raido-TLC (NH_4OH/MeOH, 1:4). The average decay-corrected radiochemical yield of this synthesis was 45 % (n = 4, EOB) for [^{11}C]MEA and 52% (n = 10, EOB) for [^{11}C]DMEA.

5.4.3 In vitro studies

Cellular uptake studies were performed using standard protocol. Briefly, ~200,000 cells were plated in 12-well tissue culture plates in triplicate and incubate for 48 hrs in growth media at which time >90% confluency was reached. On the day of study the media was refreshed using a volume of 1 mL of media or media containing selected inhibitors in each well. Then 1μCi of ^{14}C or 4μCi of ^{11}C labeled tracer of choice was added to each well and incubated for specific time period (from 5 min to 1h) at 37°C and 5% CO_2. Following incubation, cells were washed three times with cold PBS and lysed with NaOH. In case of ^{14}C labeled tracers, Sample (100 μL) of each radiotracer flask was

mixed with liquid scintillator and the radioactivity was counted by liquid scintillation. Experiments were performed in triplicates and the mean counts per minutes (CPM), were calculated together with standard deviation (SD). For ^{11}C labeled tracers, lysed cells were collected into filter paper and counted using a gamma counter (Cobra II auto-gamma counter D5003 spectrometer, Canberra-Packard). Protein concentration was determined using the Lowry protein assay and uptake values was normalized by the dose administered to each well.

5.5 References

[1] Podo F. Tumour phospholipid metabolism. NMR in biomedicine 1999;12:413-39.

[2] Ackerstaff E, Glunde K, and Bhujwalla ZM. Choline phospholipid metabolism: a target in cancer cells? Journal of cellular biochemistry 2003;90:525-33.

[3] Vance DE and Vance JE. Biochemistry of lipids, lipoproteins and membranes. 5th ed., Amsterdam ; Boston: Elsevier,2008.

[4] Kennedy EP. The biosynthesis of phospholipids. The American journal of clinical nutrition 1958;6:216-20.

[5] Ramirez de Molina A, Penalva V, Lucas L, and Lacal JC. Regulation of choline kinase activity by Ras proteins involves Ral-GDS and PI3K. Oncogene 2002;21:937-46.

[6] Ramirez de Molina A, Rodriguez-Gonzalez A, Gutierrez R, Martinez-Pineiro L, Sanchez J, Bonilla F, et al. Overexpression of choline kinase is a frequent feature in human tumor-derived cell lines and in lung, prostate, and colorectal human cancers. Biochemical and biophysical research communications 2002;296:580-3.

[7] Nakagami K, Uchida T, Ohwada S, Koibuchi Y, Suda Y, Sekine T, et al. Increased choline kinase activity and elevated phosphocholine levels in human colon cancer. Jpn J Cancer Res 1999;90:419-24.

[8] Katz-Brull R and Degani H. Kinetics of choline transport and phosphorylation in human breast cancer cells; NMR application of the zero trans method. Anticancer research 1996;16:1375-80.

[9] Hara T, Kosaka N, Shinoura N, and Kondo T. PET imaging of brain tumor with [methyl-11C]choline. J Nucl Med 1997;38:842-7.

[10] DeGrado TR, Baldwin SW, Wang S, Orr MD, Liao RP, Friedman HS, et al. Synthesis and evaluation of (18)F-labeled choline analogs as oncologic PET tracers. J Nucl Med 2001;42:1805-14.

[11] Hara T. 11C-choline and 2-deoxy-2-[18F]fluoro-D-glucose in tumor imaging with positron emission tomography. Mol Imaging Biol 2002;4:267-73.

[12] Mertens K, Slaets D, Lambert B, Acou M, De Vos F, and Goethals I. PET with (18)F-labelled choline-based tracers for tumour imaging: a review of the literature. European journal of nuclear medicine and molecular imaging 2010.

[13] Negendank W, Li CW, Padavic-Shaller K, Murphy-Boesch J, and Brown TR. Phospholipid metabolites in 1H-decoupled 31P MRS in vivo in human cancer: implications for experimental models and clinical studies. Anticancer research 1996;16:1539-44.

[14] Luyten PR, Bruntink G, Sloff FM, Vermeulen JW, van der Heijden JI, den Hollander JA, et al. Broadband proton decoupling in human 31P NMR spectroscopy. NMR in biomedicine 1989;1:177-83.

[15] Negendank WG, Padavic-Shaller KA, Li CW, Murphy-Boesch J, Stoyanova R, Krigel RL, et al. Metabolic characterization of human non-Hodgkin's lymphomas in vivo with the use of proton-decoupled phosphorus magnetic resonance spectroscopy. Cancer research 1995;55:3286-94.

[16] Lowry M, Porter DA, Twelves CJ, Heasley PE, Smith MA, and Richards MA. Visibility of phospholipids in 31P NMR spectra of human breast tumours in vivo. NMR in biomedicine 1992;5:37-42.

[17] Kalra R, Wade KE, Hands L, Styles P, Camplejohn R, Greenall M, et al. Phosphomonoester is associated with proliferation in human breast cancer: a 31P MRS study. British journal of cancer 1993;67:1145-53.

[18] Albers MJ, Krieger MD, Gonzalez-Gomez I, Gilles FH, McComb JG, Nelson MD, Jr., et al. Proton-decoupled 31P MRS in untreated pediatric brain tumors. Magn Reson Med 2005;53:22-9.

[19] Mintz A, Wang L, and Ponde DE. Comparison of radiolabeled choline and ethanolamine as probe for cancer detection. Cancer biology & therapy 2008;7:742-7.

[20] Thorell JO, Stoneelander S, and Elander N. DIFUNCTIONAL 2-CARBON MOLECULES DERIVED FROM [C-11] CYANIDE. J. Label. Compd. Radiopharm. 1994;34:383-90.

[21] Rosen MA, Jones RM, Yano Y, and Budinger TF. Carbon-11 choline: synthesis, purification, and brain uptake inhibition by 2-dimethylaminoethanol. J Nucl Med 1985;26:1424-8.

[22] Murillo H, Huang H, Schmidt LJ, Smith DI, and Tindall DJ. Role of PI3K signaling in survival and progression of LNCaP prostate cancer cells to the androgen refractory state. Endocrinology 2001;142:4795-805.

[23] Tavassoli P, Snoek R, Ray M, Rao LG, and Rennie PS. Rapid, non-destructive, cell-based screening assays for agents that modulate growth, death, and androgen receptor activation in prostate cancer cells. The Prostate 2007;67:416-26.

[24] Grassl SM. Choline transport in human placental brush-border membrane vesicles. Biochimica et biophysica acta 1994;1194:203-13.

[25] Hamza M, Lloveras J, Ribbes G, Soula G, and Douste-Blazy L. An in vitro study of hemicholinium-3 on phospholipid metabolism of Krebs II ascites cells. Biochemical pharmacology 1983;32:1893-7.

[26] Lloveras J, Hamza M, Chap H, and Douste-Blazy L. Action of hemicholinium-3 on phospholipid metabolism in Krebs II ascites cells. Biochemical pharmacology 1985;34:3987-93.

[27] Infante JP and Kinsella JE. Phospholipid synthesis in mammary tissue. Choline and ethanolamine kinases: kinetic evidence for two discrete active sites. Lipids 1976;11:727-35.

Chapter 6

Concluding Remarks and Future Directions

6.1 Concluding Remarks

Imaging of tumor cell metabolism continues to be a cornerstone of clinical and preclinical molecular imaging. It is not only used in tumor detection but also have significant impact on patient management via staging and monitoring response to therapy. Most widely used FDG-PET, which utilizes aberrant glucose metabolism in tumor cells, had several drawbacks that make it suboptimal for imaging certain cancers such as brain tumors and prostate cancer. A number of amino acid and choline derivatives have been developed based on altered tumor metabolism for amino acids and phospholipids respectively and demonstrated potential improvement over FDG in imaging brain tumors and prostate cancer. In this thesis we prepared a series of new ^{18}F label tyrosine and phenylalanine derivatives (chapter **2** to chapter **4**) targeting upregulated amino acid transport activity in cancer cells. These tracers were evaluated in comparison with clinically established tyrosine analog L-FET. Towards the end of this thesis work, we found a potentially useful imaging agent L-FEP. It could be efficiently labeled with good radiochemical yield and high purity. In vivo studies using rats bearing 9L tumor model demonstrated that L-FEP is comparable to clinically used L-FET. Transport characterization of L-FEP studies suggested that its uptake might reflect increased activity of LAT1 in tumor cells. We have also labeled a series of ^{11}C labeled ethanolamine derivatives (Chapter **5**) as potential PET imaging agents utilizing altered tumor phospholipids metabolism. Initial in vitro studies indicated ethanolamine derivatives might have improve sensitivity over reported [^{11}C]CH.

6.2 Future Directions

It is still not clear that whether L-FEP would have any advantage over L-FET as an imaging agent. To further validate the potential of L-FEP as brain imaging agents, orthotropic brain model in rats could be used. Uptake studies of L-FEP in peripheral tumor cell lines with high expression of LATs (R1M, HeLa et al) could be carried out to examine its potential for imaging peripheral tumors in comparison to L-FET. Additional studies with L-FEP can be done to confirm its selectivity for LAT1.

In vivo studies including biodistribution and small animal PET imaging studies on PC-3 and/or LnCap xenagraft model is in progress for evaluating ^{11}C labeled ethanolamine tracers. Metabolites analysis and phosphorylation studies could be conducted to examine whether uptake of these tracers correlates with upregulation of ethanolamine kinase and/or transport activity in Kennedy pathway.

Appendix A

^{1}H and ^{13}C NMR Spectra of compounds

A.1 ^{1}H and ^{13}C NMR spectra of key compounds in Chapter 2

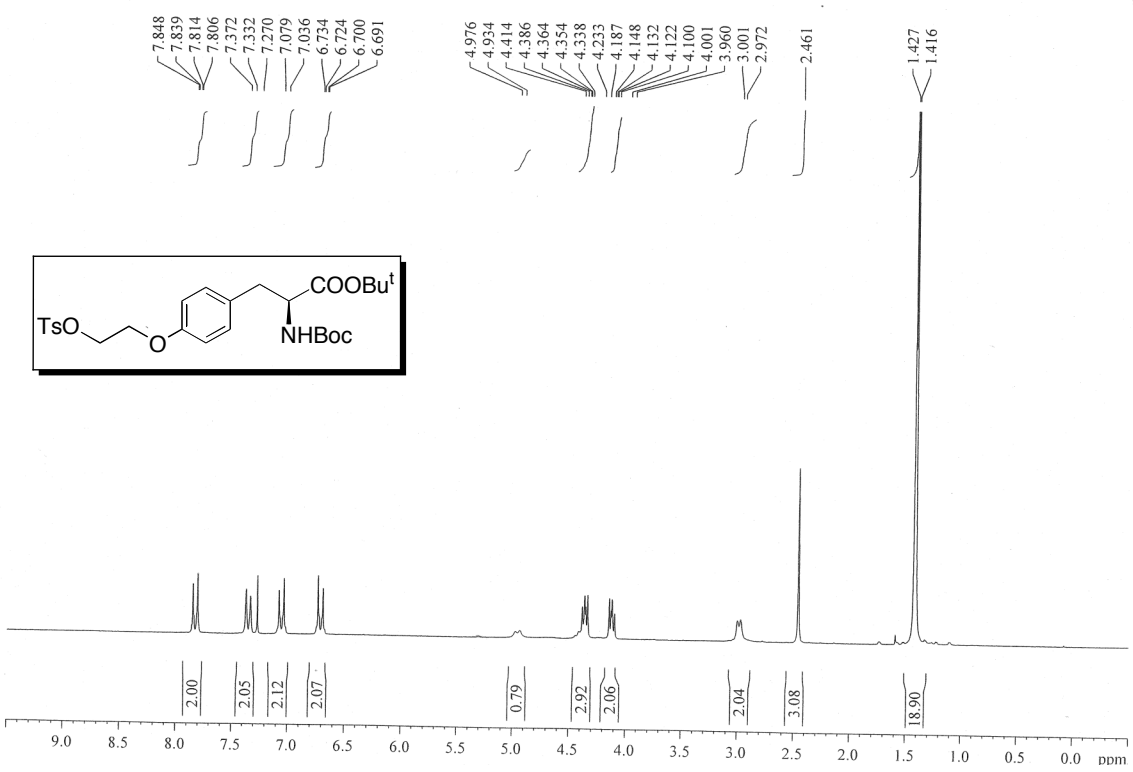

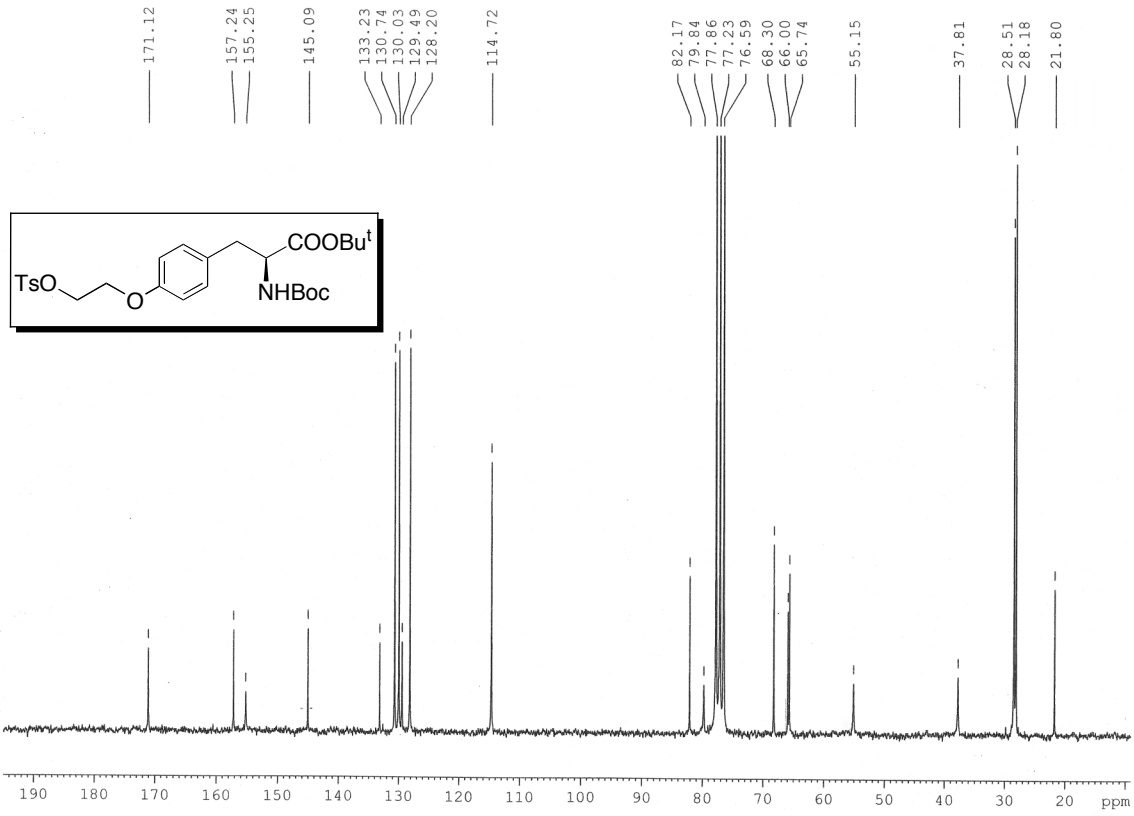

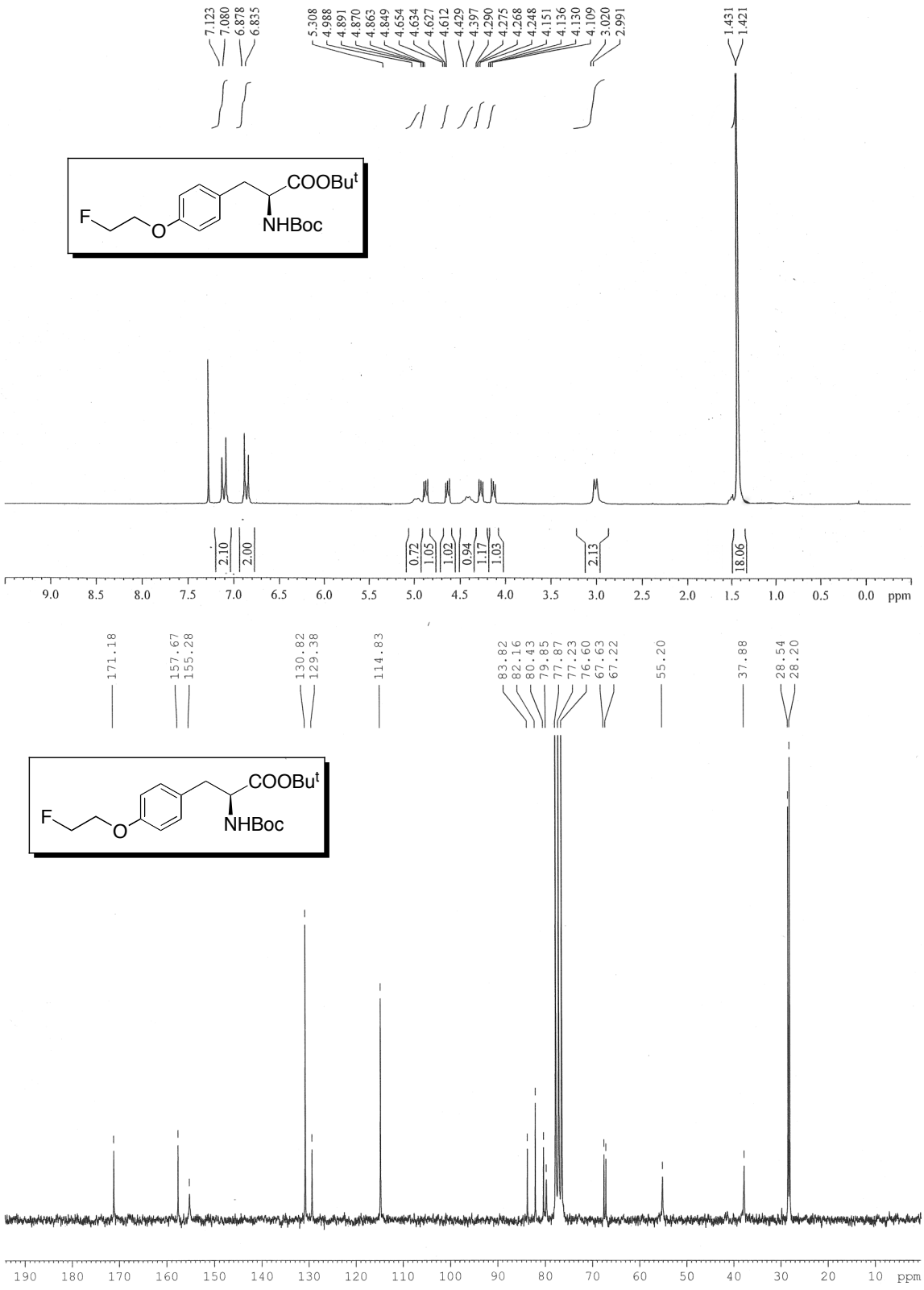
7.123
7.080
6.878
6.835
5.308
4.988
4.891
4.870
4.863
4.849
4.654
4.634
4.627
4.612
4.429
4.397
4.290
4.275
4.268
4.248
4.151
4.136
4.130
4.109
3.020
2.991
1.431
1.421
COOBu^t
NHBoc
F
O
2.10
2.00
0.72
1.05
1.02
0.94
1.17
1.03
2.13
18.06
ppm
171.18
157.67
155.28
130.82
129.38
114.83
83.82
82.16
80.43
79.85
77.87
77.23
76.60
67.63
67.22
55.20
37.88
28.54
28.20
ppm

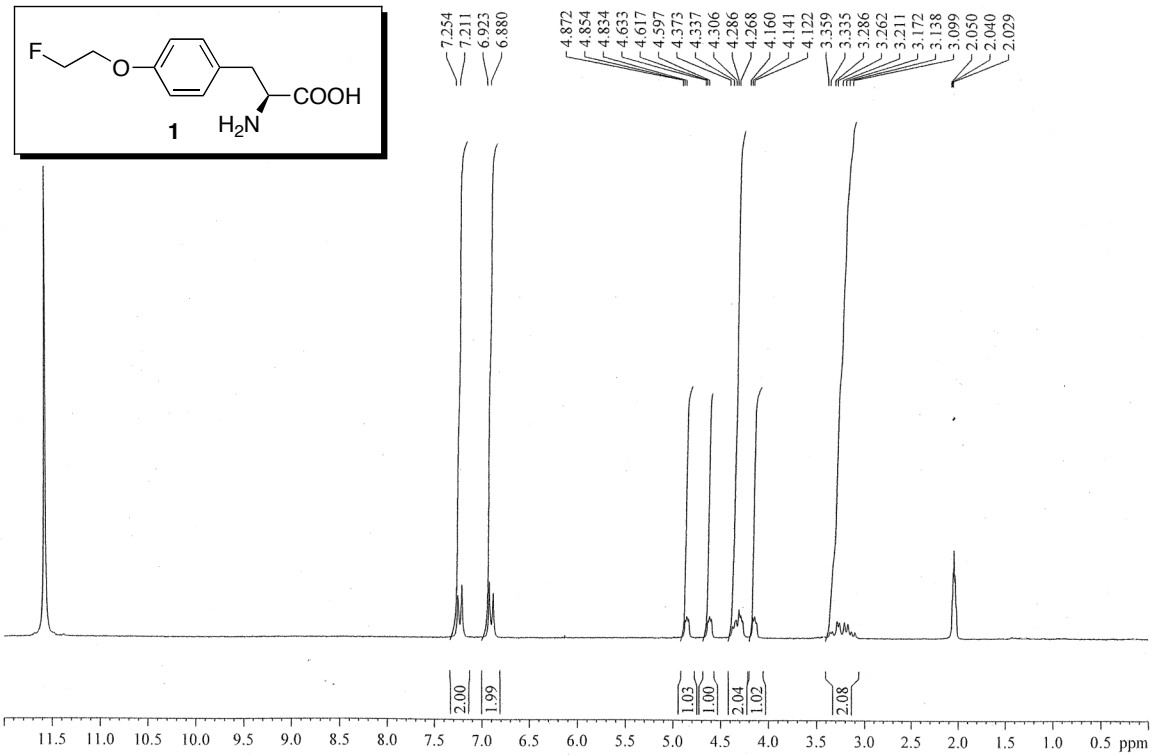
F
O
COOH
H_2N
1
7.254
7.211
6.923
6.880
4.872
4.854
4.834
4.633
4.617
4.597
4.373
4.337
4.306
4.286
4.268
4.160
4.141
4.122
3.359
3.335
3.286
3.262
3.211
3.172
3.138
3.099
2.050
2.040
2.029
2.00
1.99
1.03
1.00
2.04
1.02
2.08
11.5 11.0 10.5 10.0 9.5 9.0 8.5 8.0 7.5 7.0 6.5 6.0 5.5 5.0 4.5 4.0 3.5 3.0 2.5 2.0 1.5 1.0 0.5 ppm

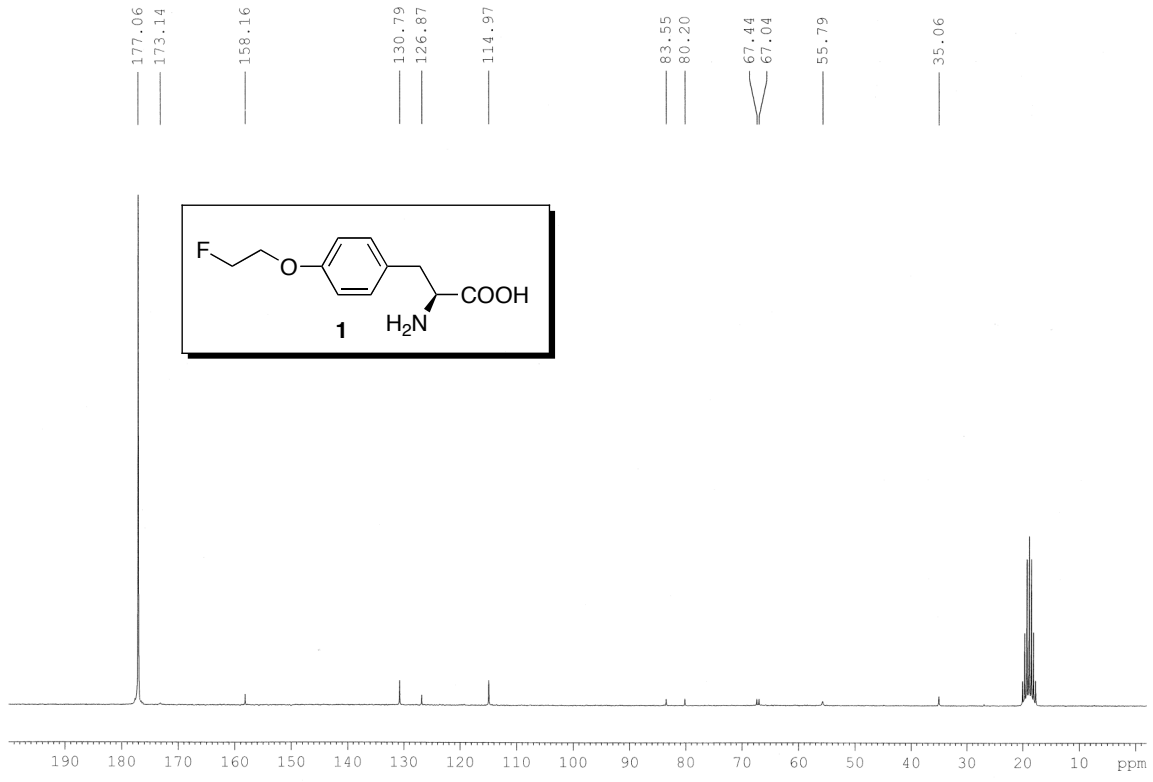
177.06
173.14
158.16
130.79
126.87
114.97
83.55
80.20
67.44
67.04
55.79
35.06
F
O
COOH
H_2N
1
190 180 170 160 150 140 130 120 110 100 90 80 70 60 50 40 30 20 10 ppm

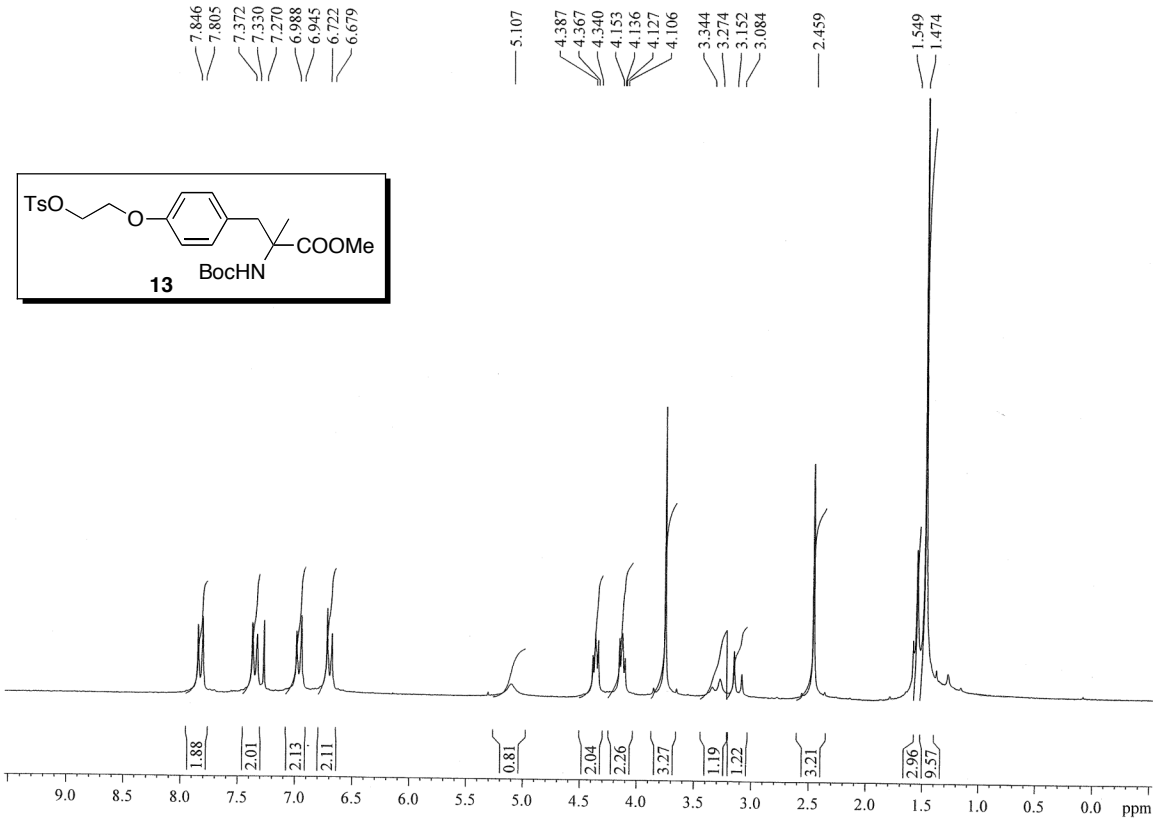
7.846
7.805
7.372
7.330
7.270
6.988
6.945
6.722
6.679
5.107
4.387
4.367
4.340
4.153
4.136
4.127
4.106
3.344
3.274
3.152
3.084
2.459
1.549
1.474
TsO
O
COOMe
BocHN
13
1.88
2.01
2.13
2.11
0.81
2.04
2.26
3.27
1.19
1.22
3.21
2.96
9.57
ppm

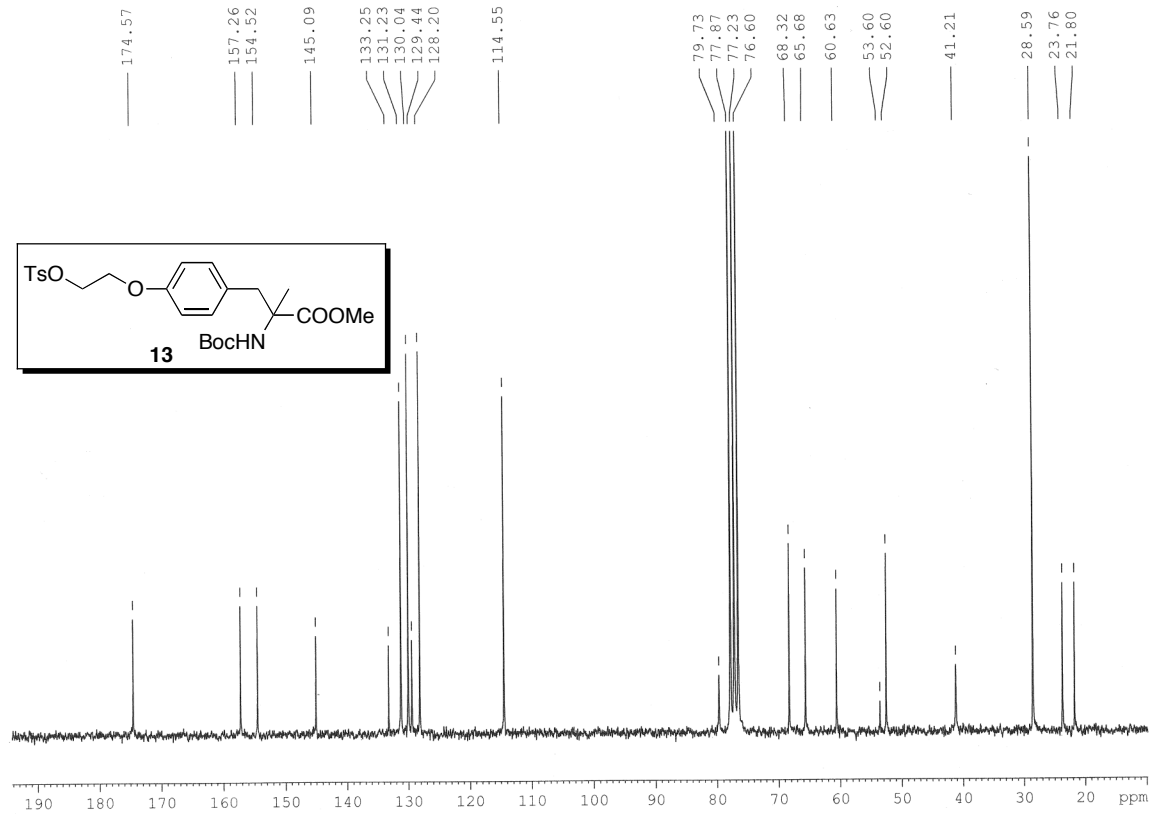
174.57
157.26
154.52
145.09
133.25
131.23
130.04
129.44
128.20
114.55
79.73
77.87
77.23
76.60
68.32
65.68
60.63
53.60
52.60
41.21
28.59
23.76
21.80
TsO
O
COOMe
BocHN
13
ppm

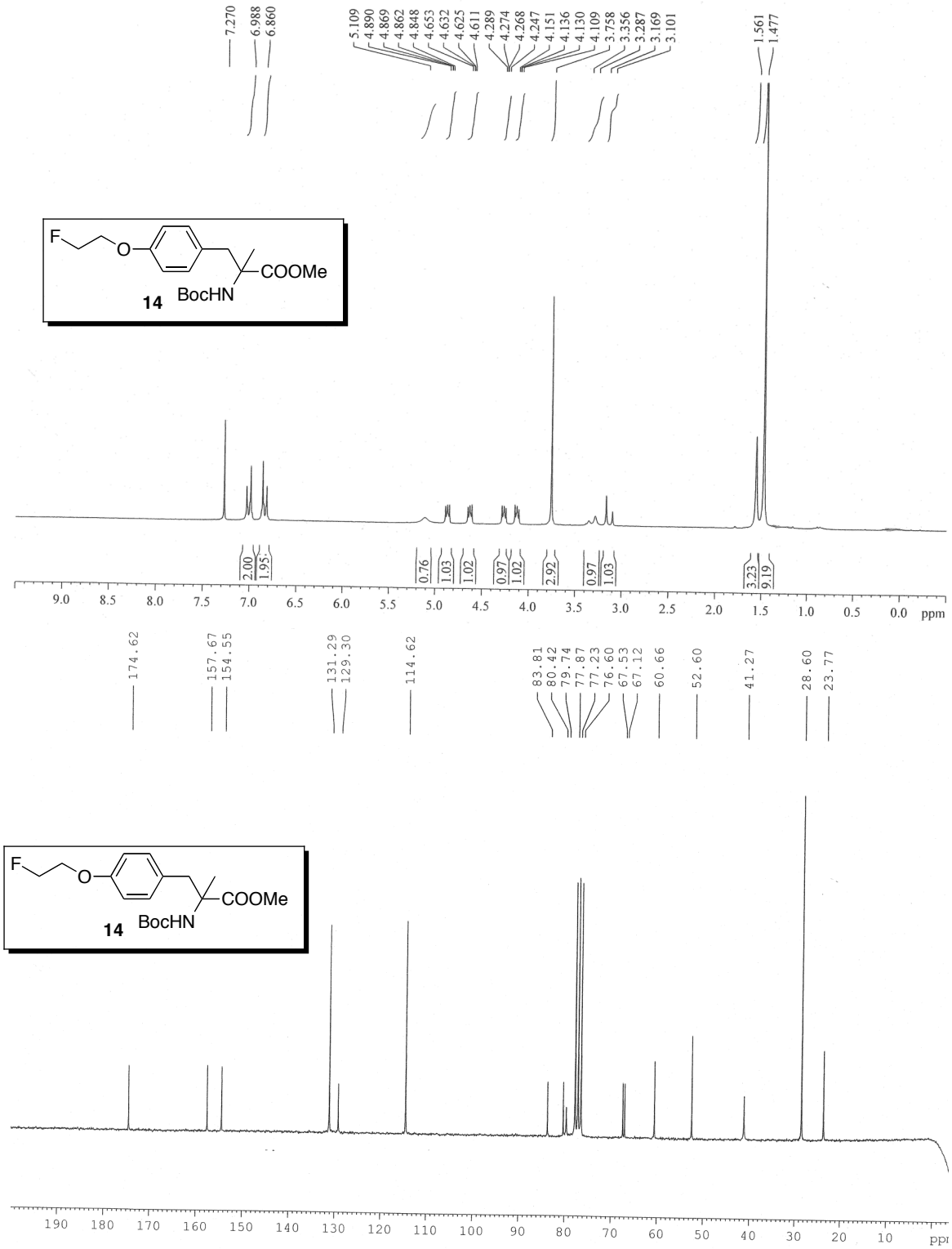
7.270
6.988
6.860
5.109
4.890
4.869
4.862
4.848
4.653
4.632
4.625
4.611
4.289
4.274
4.268
4.247
4.151
4.136
4.130
4.109
3.758
3.356
3.287
3.169
3.101
1.561
1.477
F
O
COOMe
BocHN
14
2.00
1.95
0.76
1.03
1.02
0.97
1.02
2.92
0.97
1.03
3.23
9.19
ppm
174.62
157.67
154.55
131.29
129.30
114.62
83.81
80.42
79.74
77.87
77.23
76.60
67.53
67.12
60.66
52.60
41.27
28.60
23.77

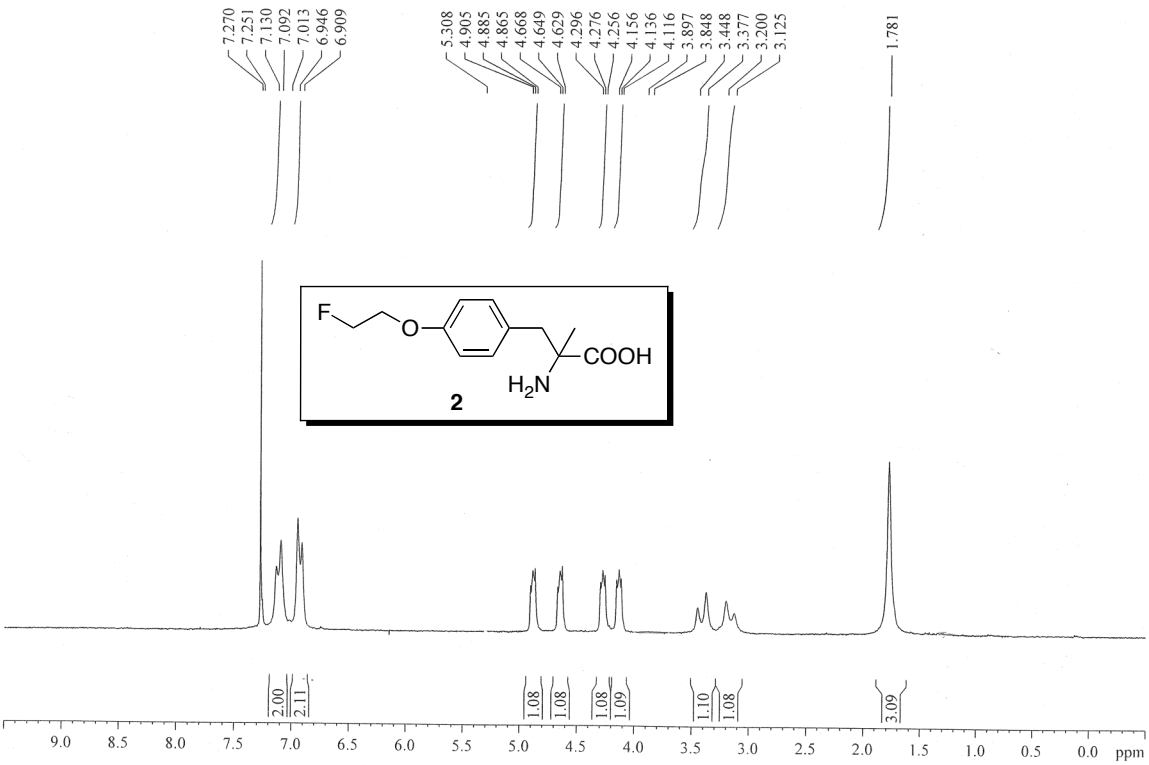
7.270
7.251
7.130
7.092
7.013
6.946
6.909
5.308
4.905
4.885
4.865
4.668
4.649
4.629
4.296
4.276
4.256
4.156
4.136
4.116
3.897
3.848
3.448
3.377
3.200
3.125
1.781
F
O
COOH
H2N
2
2.00
2.11
1.08
1.08
1.08
1.09
1.10
1.08
3.09
9.0 8.5 8.0 7.5 7.0 6.5 6.0 5.5 5.0 4.5 4.0 3.5 3.0 2.5 2.0 1.5 1.0 0.5 0.0 ppm

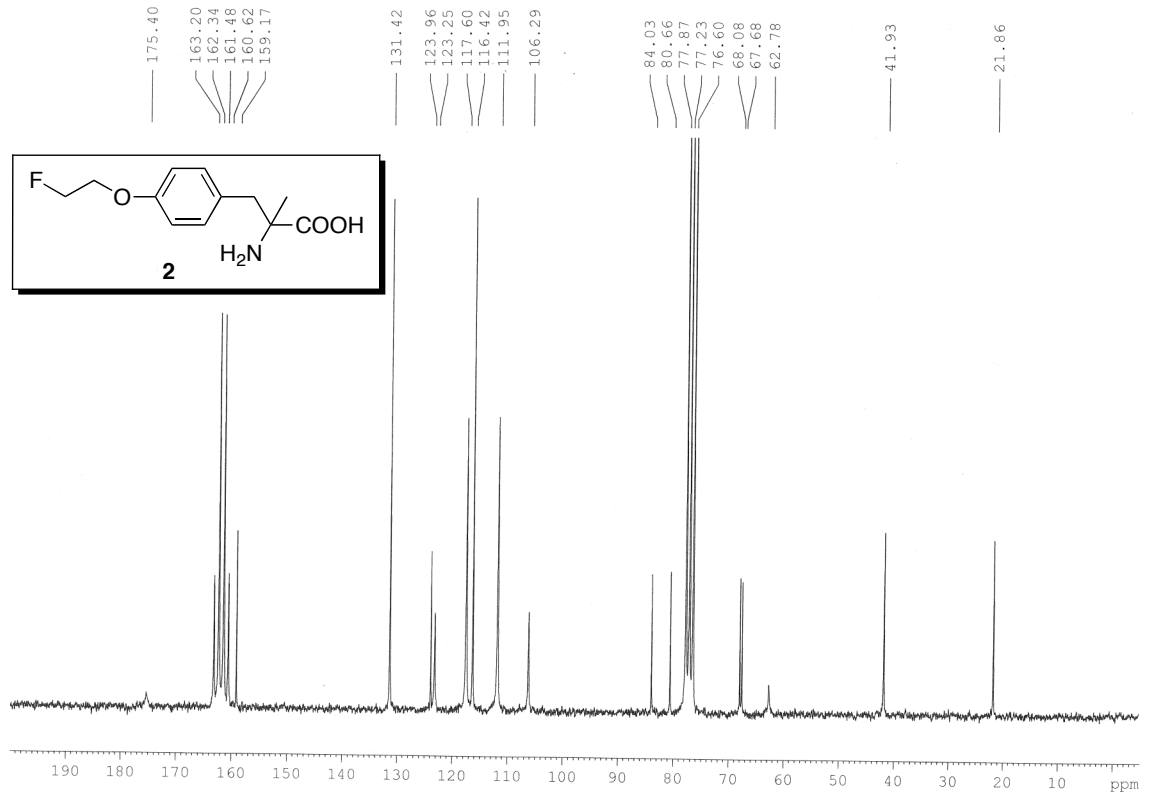
175.40
163.20
162.34
161.48
160.62
159.17
131.42
123.96
123.25
117.60
116.42
111.95
106.29
84.03
80.66
77.87
77.23
76.60
68.08
67.68
62.78
41.93
21.86
F
O
COOH
H2N
2
190 180 170 160 150 140 130 120 110 100 90 80 70 60 50 40 30 20 10 ppm

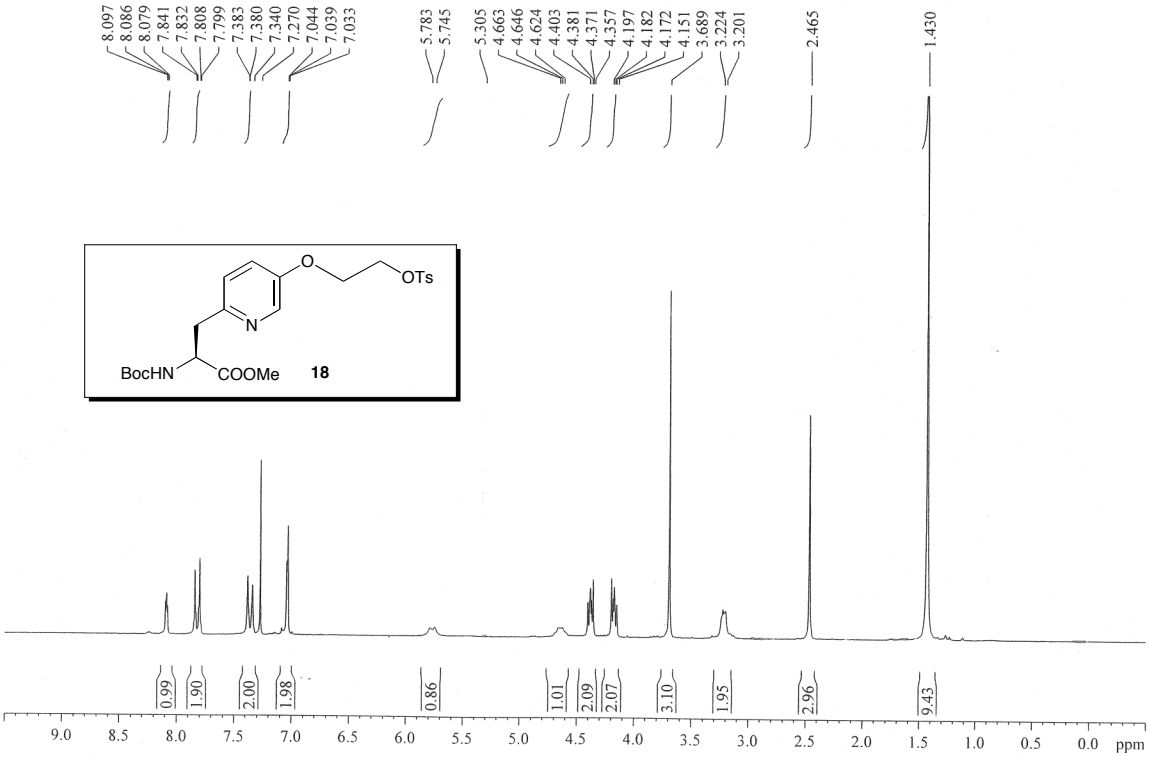
8.097
8.086
8.079
7.841
7.832
7.808
7.799
7.383
7.380
7.340
7.270
7.044
7.039
7.033
5.783
5.745
5.305
4.663
4.646
4.624
4.403
4.381
4.371
4.357
4.197
4.182
4.172
4.151
3.689
3.224
3.201
2.465
1.430
O
OTs
N
BocHN
COOMe
18
0.99
1.90
2.00
1.98
0.86
1.01
2.09
2.07
3.10
1.95
2.96
9.43
9.0 8.5 8.0 7.5 7.0 6.5 6.0 5.5 5.0 4.5 4.0 3.5 3.0 2.5 2.0 1.5 1.0 0.5 0.0 ppm

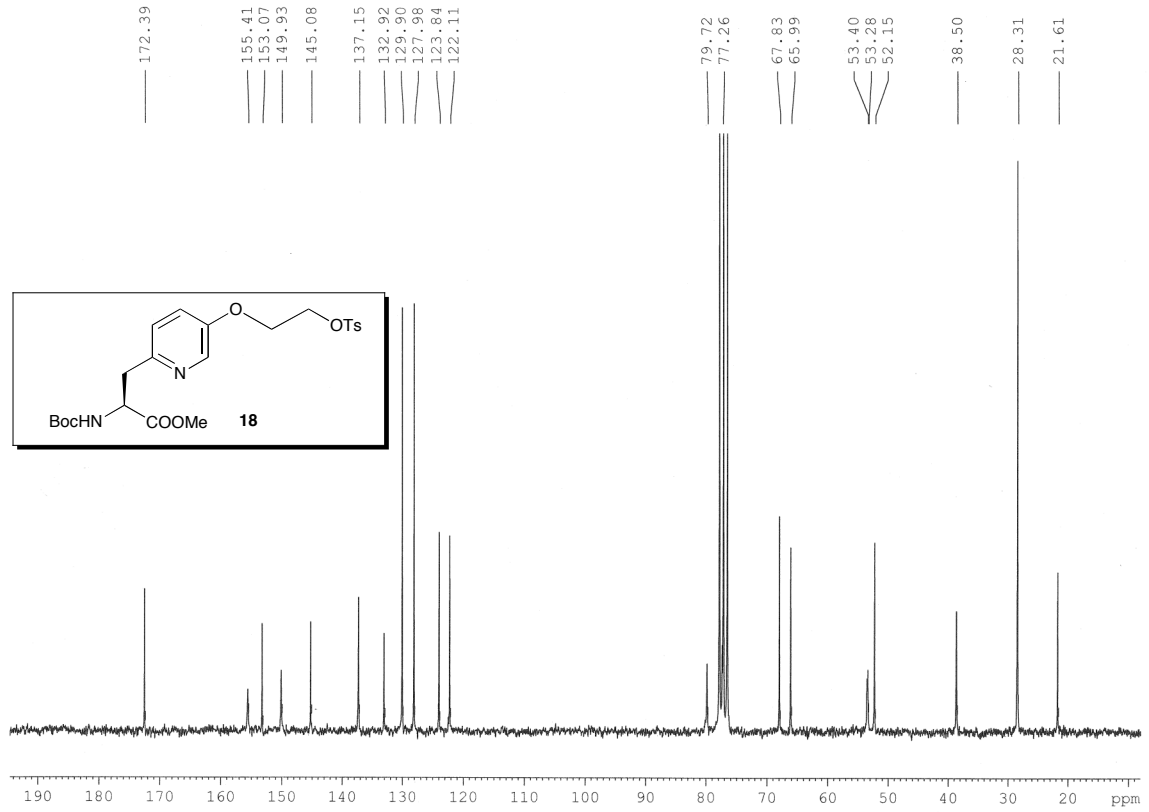
172.39
155.41
153.07
149.93
145.08
137.15
132.92
129.90
127.98
123.84
122.11
79.72
77.26
67.83
65.99
53.40
53.28
52.15
38.50
28.31
21.61
O
OTs
N
BocHN
COOMe
18
190 180 170 160 150 140 130 120 110 100 90 80 70 60 50 40 30 20 ppm

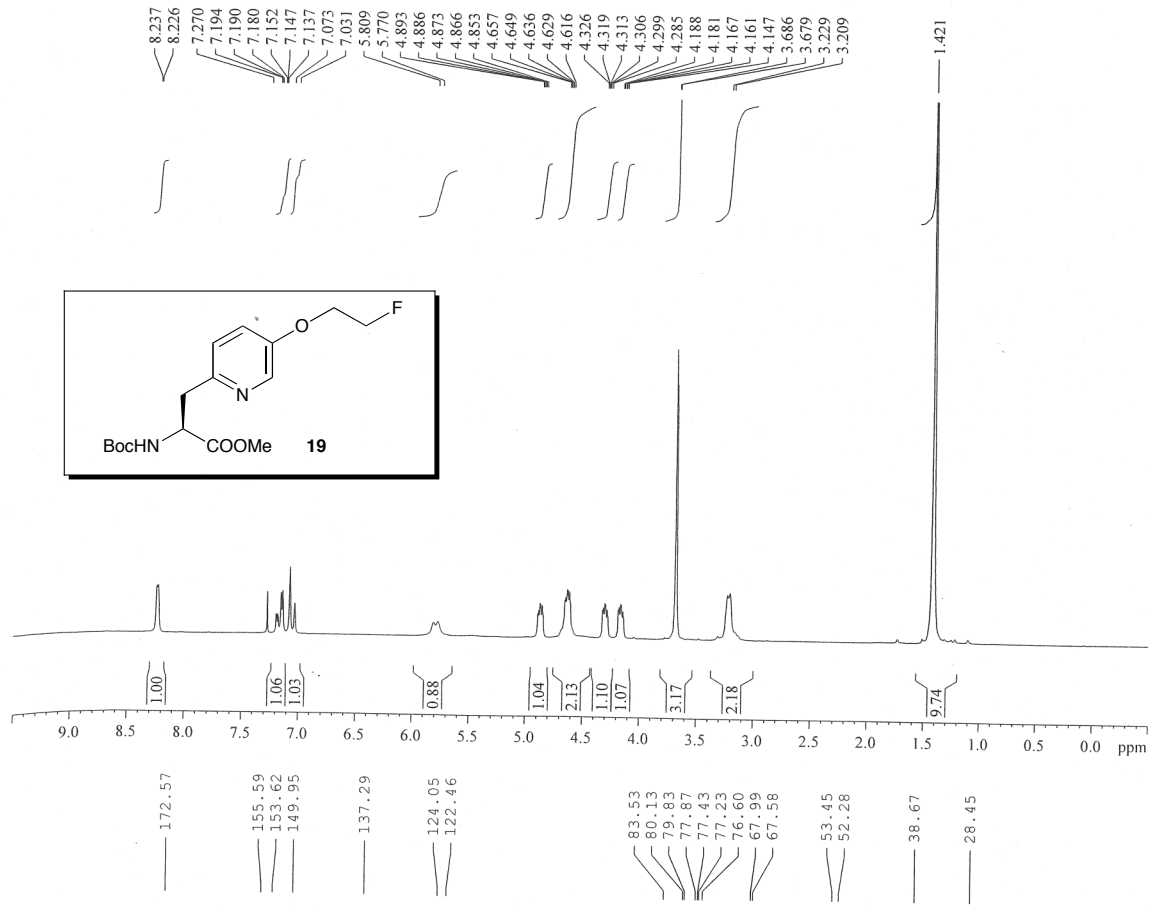
8.237
8.226
7.270
7.194
7.190
7.180
7.152
7.147
7.137
7.073
7.031
5.809
5.770
4.893
4.886
4.873
4.866
4.853
4.657
4.649
4.636
4.629
4.616
4.326
4.319
4.313
4.306
4.299
4.285
4.188
4.181
4.167
4.161
4.147
3.686
3.679
3.229
3.209
1.421
F
O
N
BocHN
COOMe
19
1.00
1.06
1.03
0.88
1.04
2.13
1.10
1.07
3.17
2.18
9.74
9.0
8.5
8.0
7.5
7.0
6.5
6.0
5.5
5.0
4.5
4.0
3.5
3.0
2.5
2.0
1.5
1.0
0.5
0.0
ppm

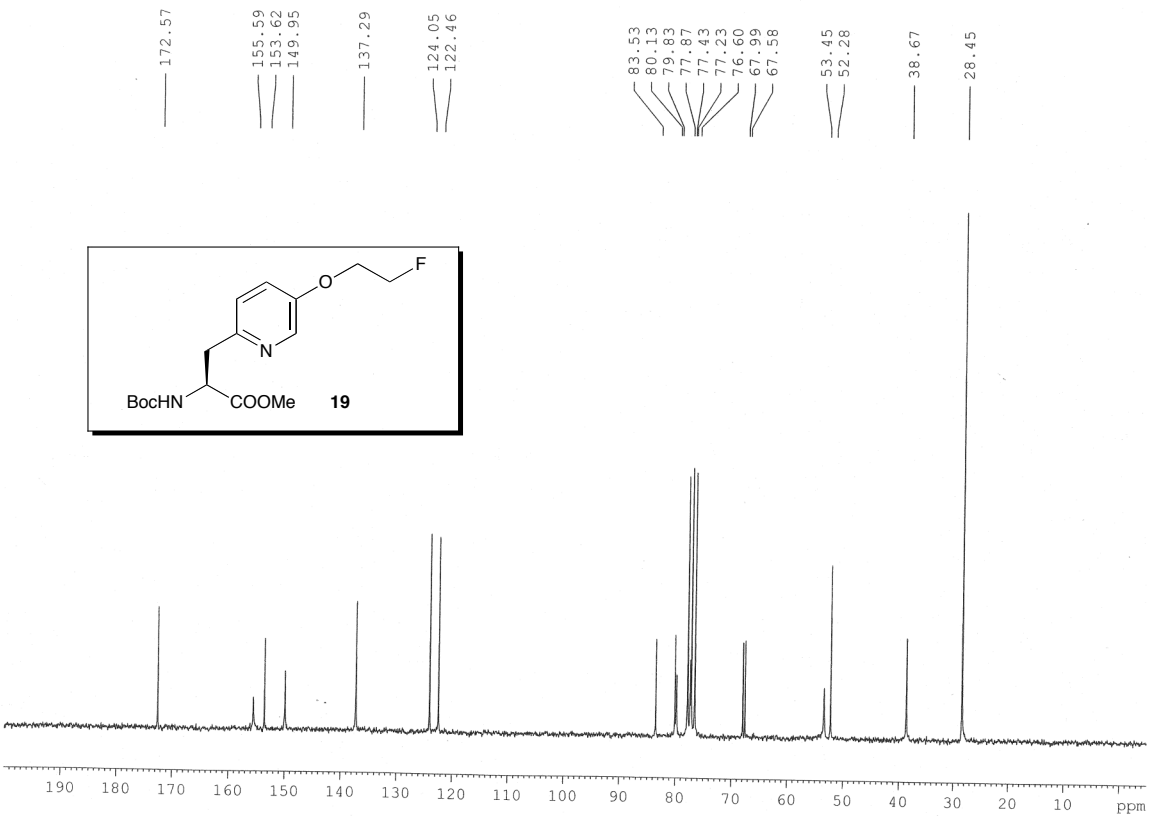
172.57
155.59
153.62
149.95
137.29
124.05
122.46
83.53
80.13
79.83
77.87
77.43
77.23
76.60
67.99
67.58
53.45
52.28
38.67
28.45
F
O
N
BocHN
COOMe
19
190
180
170
160
150
140
130
120
110
100
90
80
70
60
50
40
30
20
10
ppm

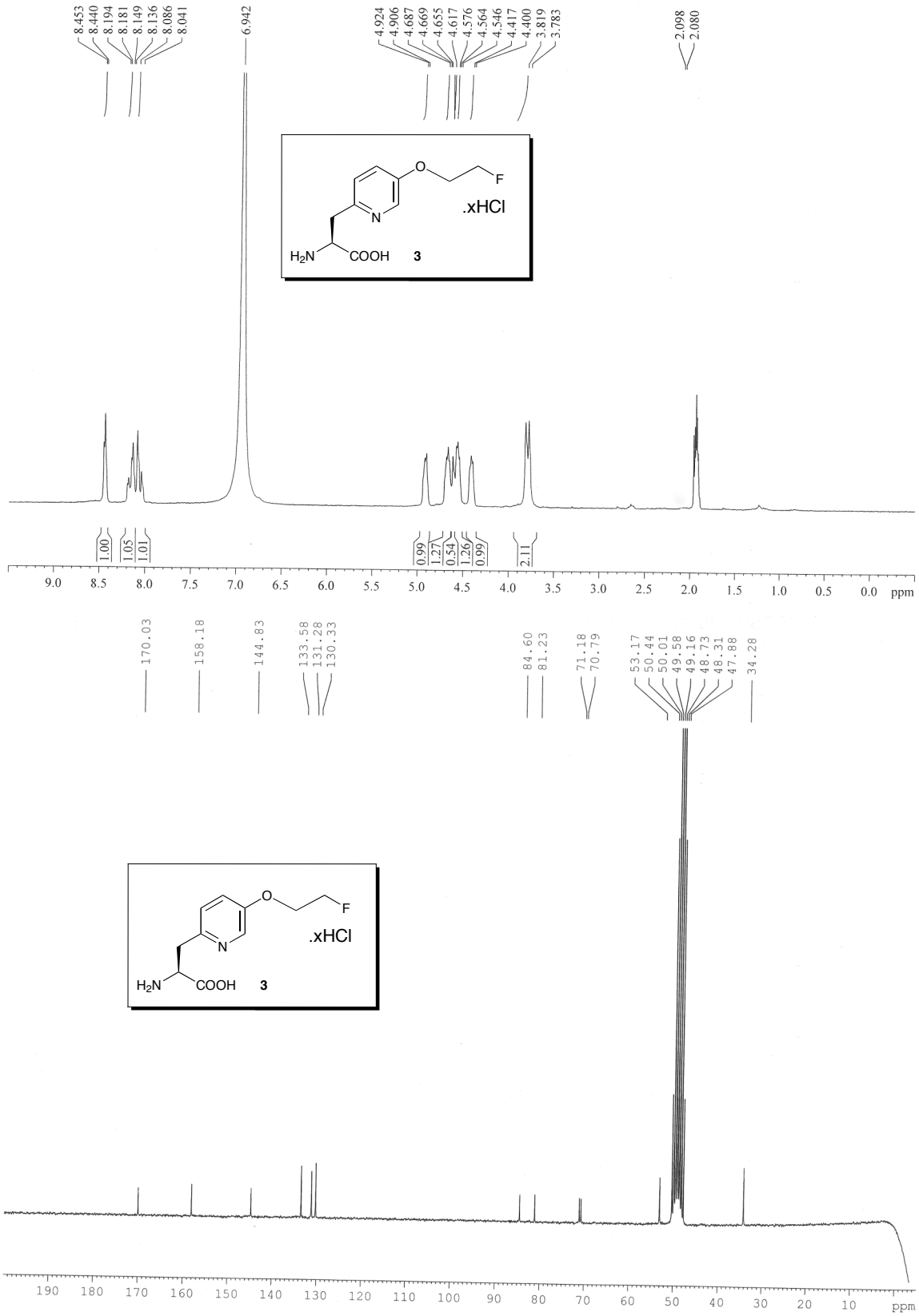
8.453
8.440
8.194
8.181
8.149
8.136
8.086
8.041
6.942
4.924
4.906
4.687
4.669
4.655
4.617
4.576
4.564
4.546
4.417
4.400
3.819
3.783
2.098
2.080
O
F
.xHCl
N
H2N
COOH
3
1.00
1.05
1.01
0.99
1.27
0.54
1.26
0.99
2.11
9.0 8.5 8.0 7.5 7.0 6.5 6.0 5.5 5.0 4.5 4.0 3.5 3.0 2.5 2.0 1.5 1.0 0.5 0.0 ppm
170.03
158.18
144.83
133.58
131.28
130.33
84.60
81.23
71.18
70.79
53.17
50.44
50.01
49.58
49.16
48.73
48.31
47.88
34.28
O
F
.xHCl
N
H2N
COOH
3
190 180 170 160 150 140 130 120 110 100 90 80 70 60 50 40 30 20 10 ppm

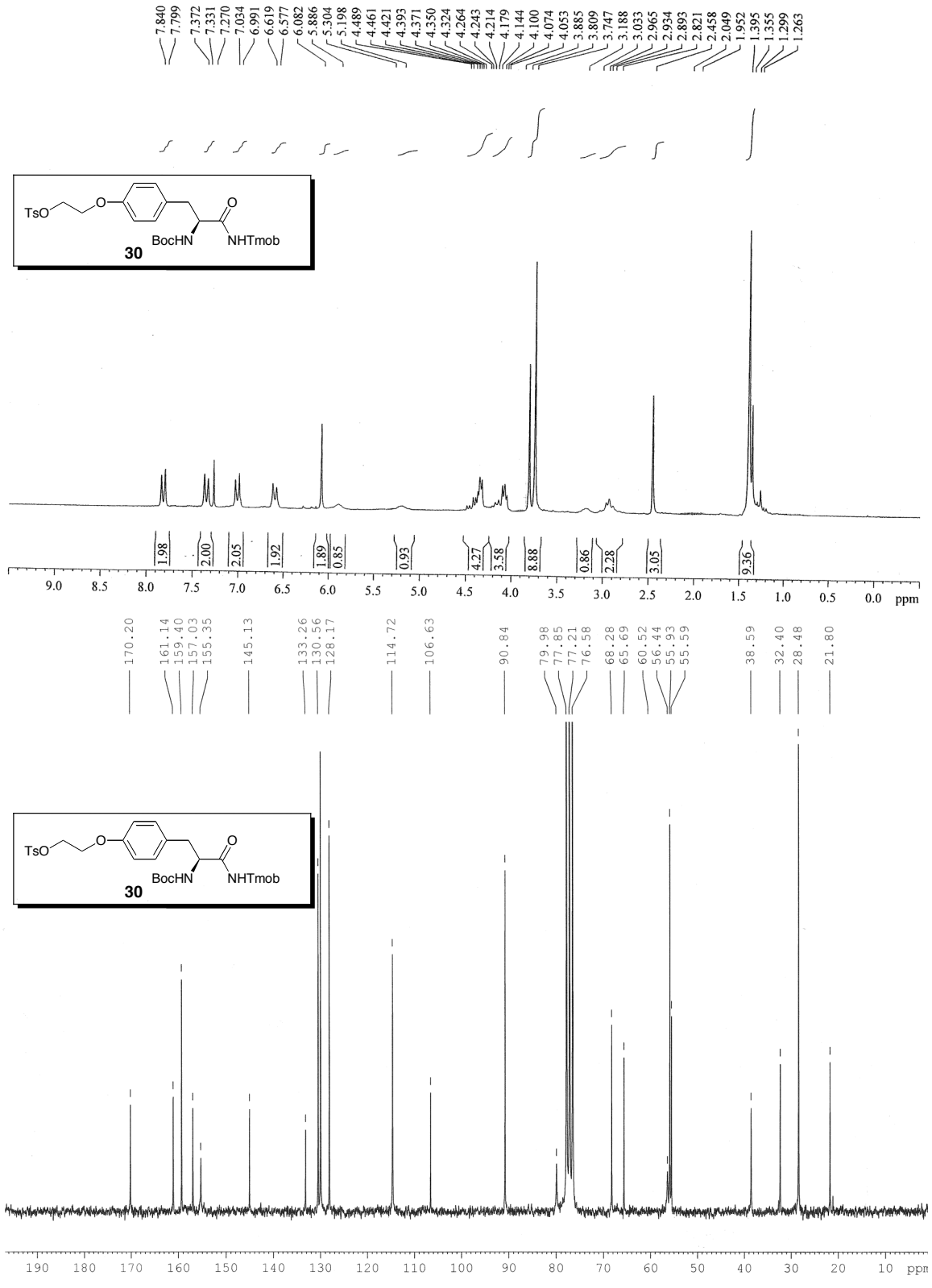
7.840
7.799
7.372
7.331
7.270
7.034
6.991
6.619
6.577
6.082
5.886
5.304
5.198
4.489
4.461
4.421
4.393
4.371
4.350
4.324
4.264
4.243
4.214
4.179
4.144
4.100
4.074
4.053
3.885
3.809
3.747
3.188
3.033
2.965
2.934
2.893
2.821
2.458
2.049
1.952
1.395
1.355
1.299
1.263
TsO
O
O
BocHN
NHTmob
30
1.98
2.00
2.05
1.92
1.89
0.85
0.93
4.27
3.58
8.88
0.86
2.28
3.05
9.36
9.0
8.5
8.0
7.5
7.0
6.5
6.0
5.5
5.0
4.5
4.0
3.5
3.0
2.5
2.0
1.5
1.0
0.5
0.0
ppm
170.20
161.14
159.40
157.03
155.35
145.13
133.26
130.56
128.17
114.72
106.63
90.84
79.98
77.85
77.21
76.58
68.28
65.69
60.52
56.44
55.93
55.59
38.59
32.40
28.48
21.80
TsO
O
O
BocHN
NHTmob
30
190
180
170
160
150
140
130
120
110
100
90
80
70
60
50
40
30
20
10
ppm

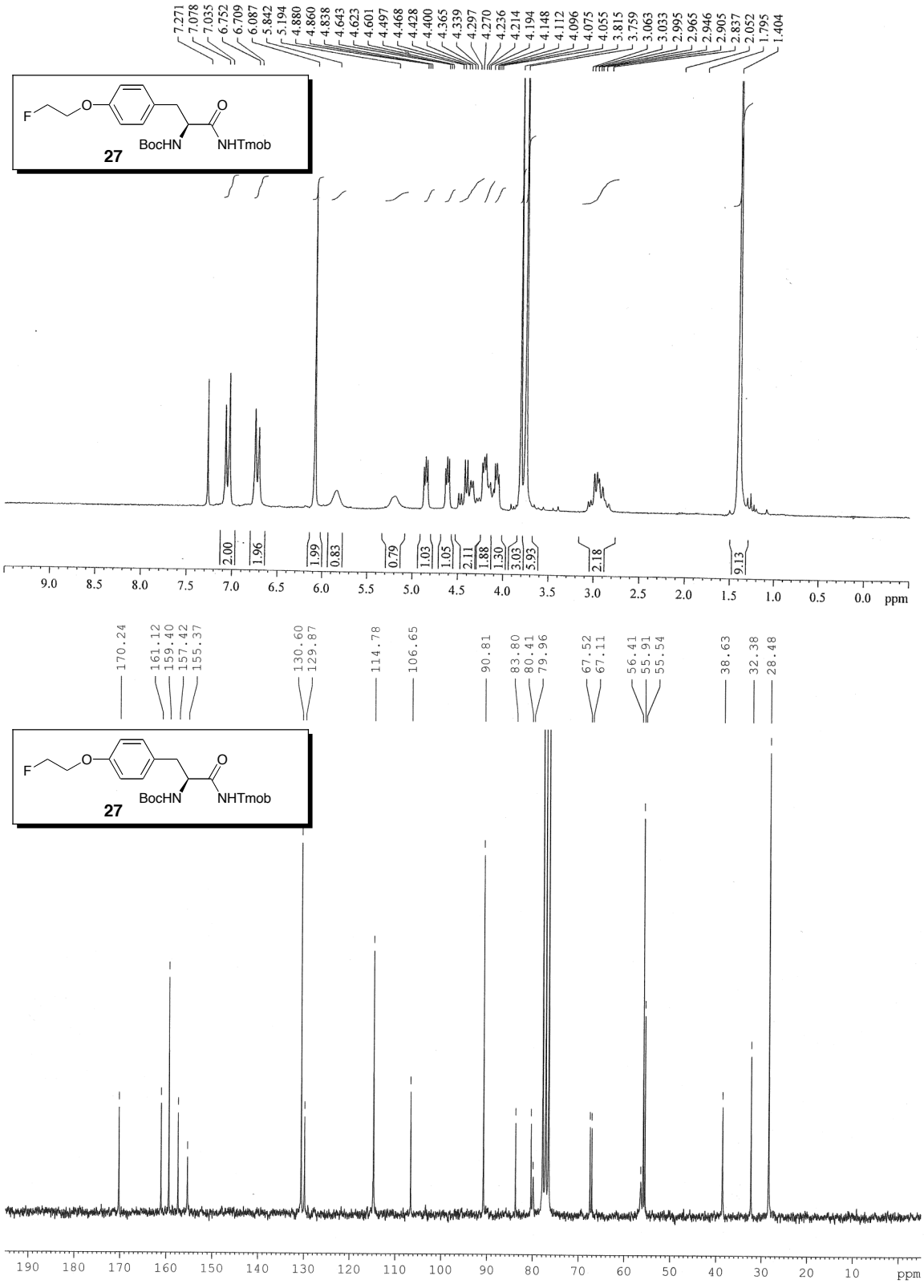
7.271
7.078
7.035
6.752
6.709
6.087
5.842
5.194
4.880
4.860
4.838
4.643
4.623
4.601
4.497
4.468
4.428
4.400
4.365
4.339
4.297
4.270
4.236
4.214
4.194
4.148
4.112
4.096
4.075
4.055
3.815
3.759
3.063
3.033
2.995
2.965
2.946
2.905
2.837
2.052
1.795
1.404
F
O
O
BocHN
NHTmob
27
2.00
1.96
1.99
0.83
0.79
1.03
1.05
2.11
1.88
1.30
3.03
5.93
2.18
9.13
ppm
170.24
161.12
159.40
157.42
155.37
130.60
129.87
114.78
106.65
90.81
83.80
80.41
79.96
67.52
67.11
56.41
55.91
55.54
38.63
32.38
28.48
ppm

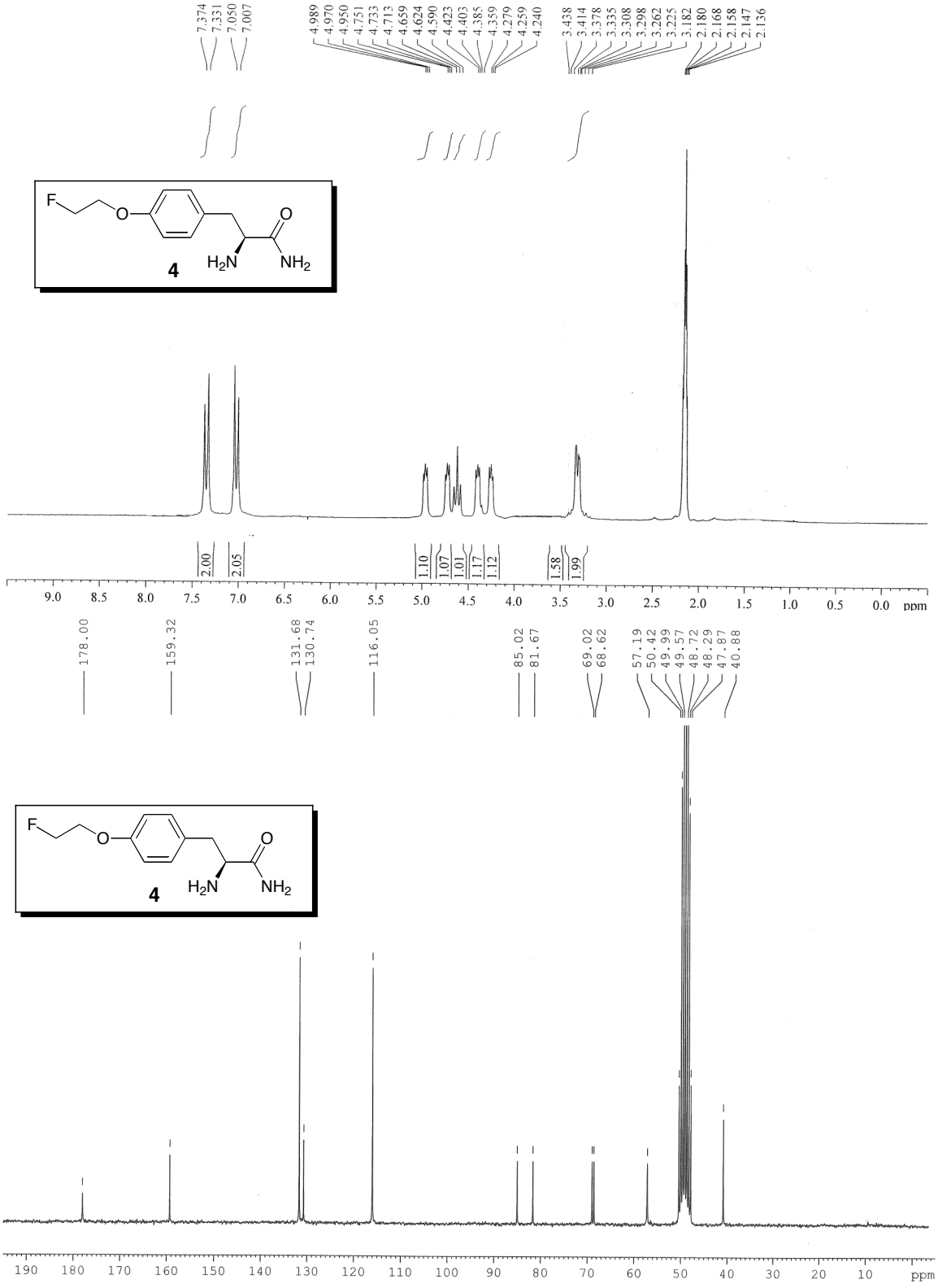
7.374
7.331
7.050
7.007
4.989
4.970
4.950
4.751
4.733
4.713
4.659
4.624
4.590
4.423
4.403
4.385
4.359
4.279
4.259
4.240
3.438
3.414
3.378
3.335
3.308
3.298
3.262
3.225
3.182
2.180
2.168
2.158
2.147
2.136
F
O
O
H2N
NH2
4
2.00
2.05
1.10
1.07
1.01
1.17
1.12
1.58
1.99
9.0 8.5 8.0 7.5 7.0 6.5 6.0 5.5 5.0 4.5 4.0 3.5 3.0 2.5 2.0 1.5 1.0 0.5 0.0 ppm
178.00
159.32
131.68
130.74
116.05
85.02
81.67
69.02
68.62
57.19
50.42
49.99
49.57
48.72
48.29
47.87
40.88
190 180 170 160 150 140 130 120 110 100 90 80 70 60 50 40 30 20 10 ppm

A.2 ^{1}H and ^{13}C NMR spectra of key compounds in Chapter 3

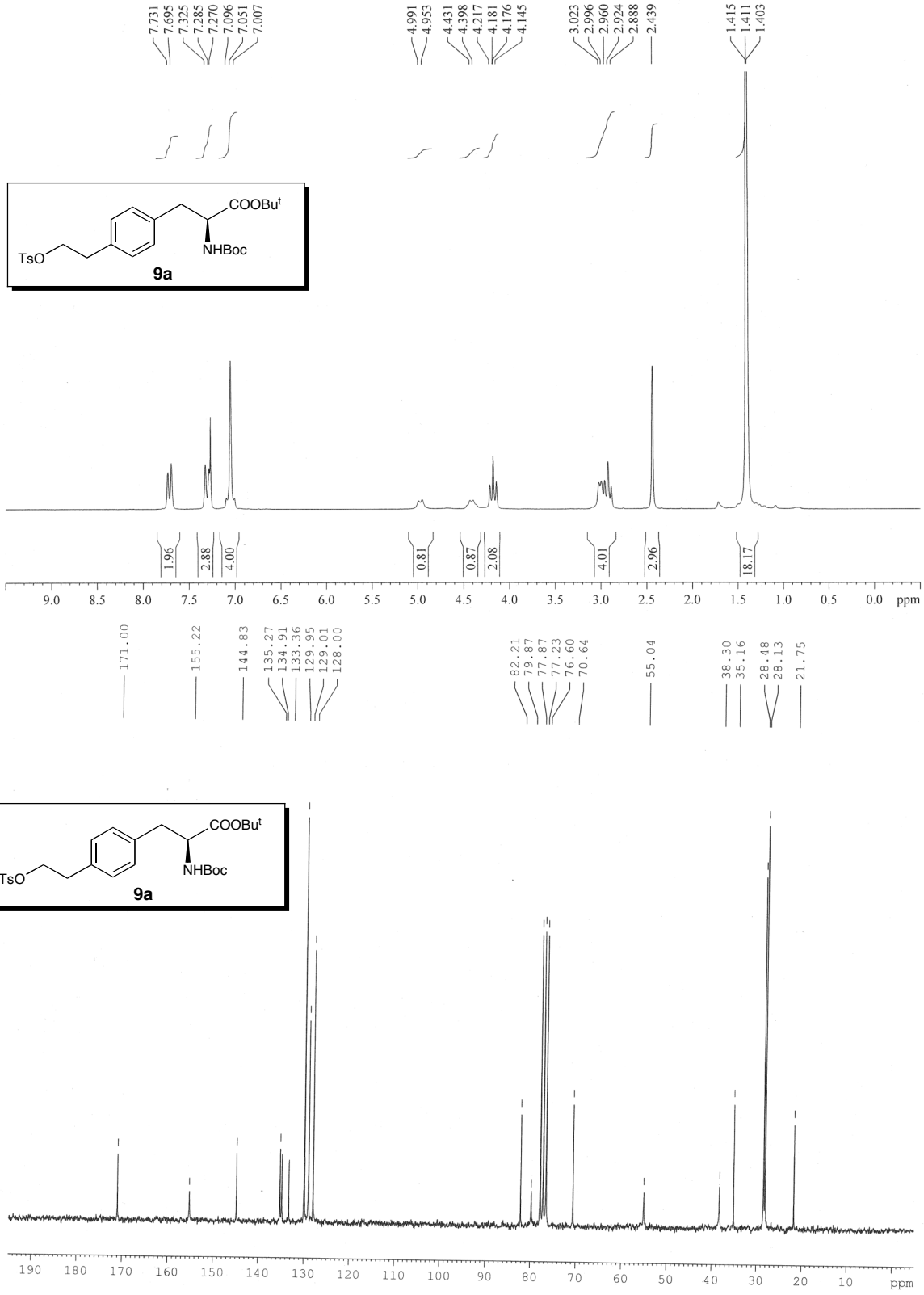

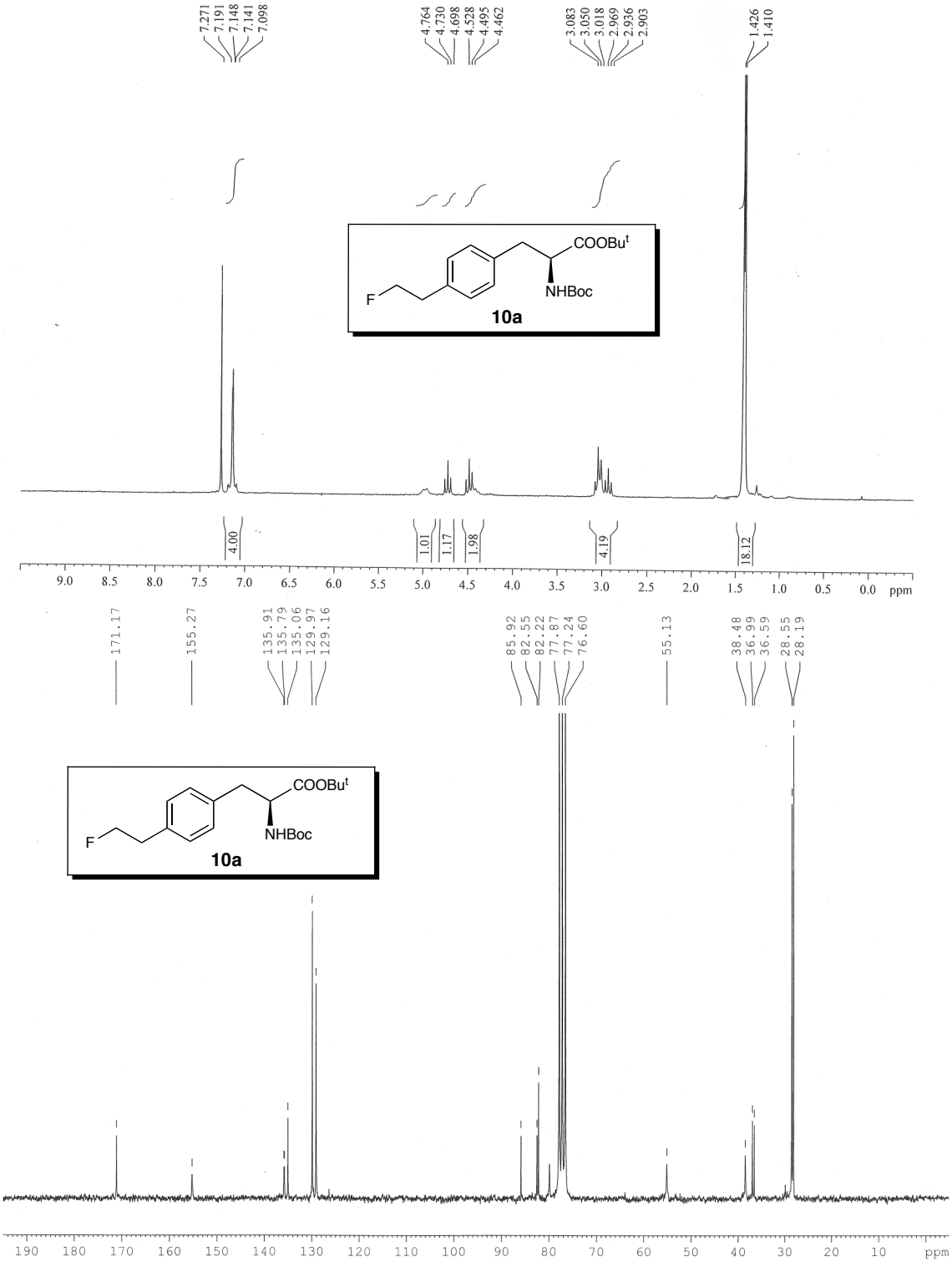
7.271
7.191
7.148
7.141
7.098
4.764
4.730
4.698
4.528
4.495
4.462
3.083
3.050
3.018
2.969
2.936
2.903
1.426
1.410
COOBu^t
NHBoc
F
10a
4.00
1.01
1.17
1.98
4.19
18.12
9.0 8.5 8.0 7.5 7.0 6.5 6.0 5.5 5.0 4.5 4.0 3.5 3.0 2.5 2.0 1.5 1.0 0.5 0.0 ppm
171.17
155.27
135.91
135.79
135.06
129.97
129.16
85.92
82.55
82.22
77.87
77.24
76.60
55.13
38.48
36.99
36.59
28.55
28.19
COOBu^t
NHBoc
F
10a
190 180 170 160 150 140 130 120 110 100 90 80 70 60 50 40 30 20 10 ppm

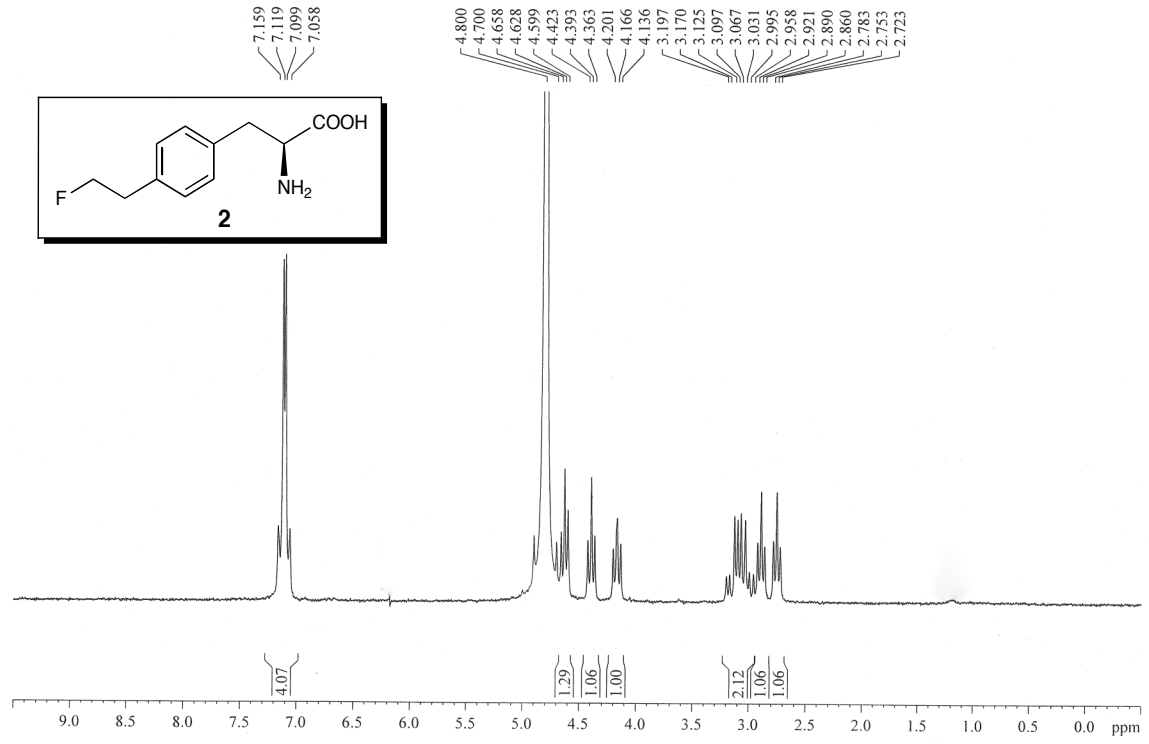
7.159
7.119
7.099
7.058
4.800
4.700
4.658
4.628
4.599
4.423
4.393
4.363
4.201
4.166
4.136
3.197
3.170
3.125
3.097
3.067
3.031
2.995
2.958
2.921
2.890
2.860
2.783
2.753
2.723
COOH
NH2
F
2
4.07
1.29
1.06
1.00
2.12
1.06
1.06
9.0 8.5 8.0 7.5 7.0 6.5 6.0 5.5 5.0 4.5 4.0 3.5 3.0 2.5 2.0 1.5 1.0 0.5 0.0 ppm

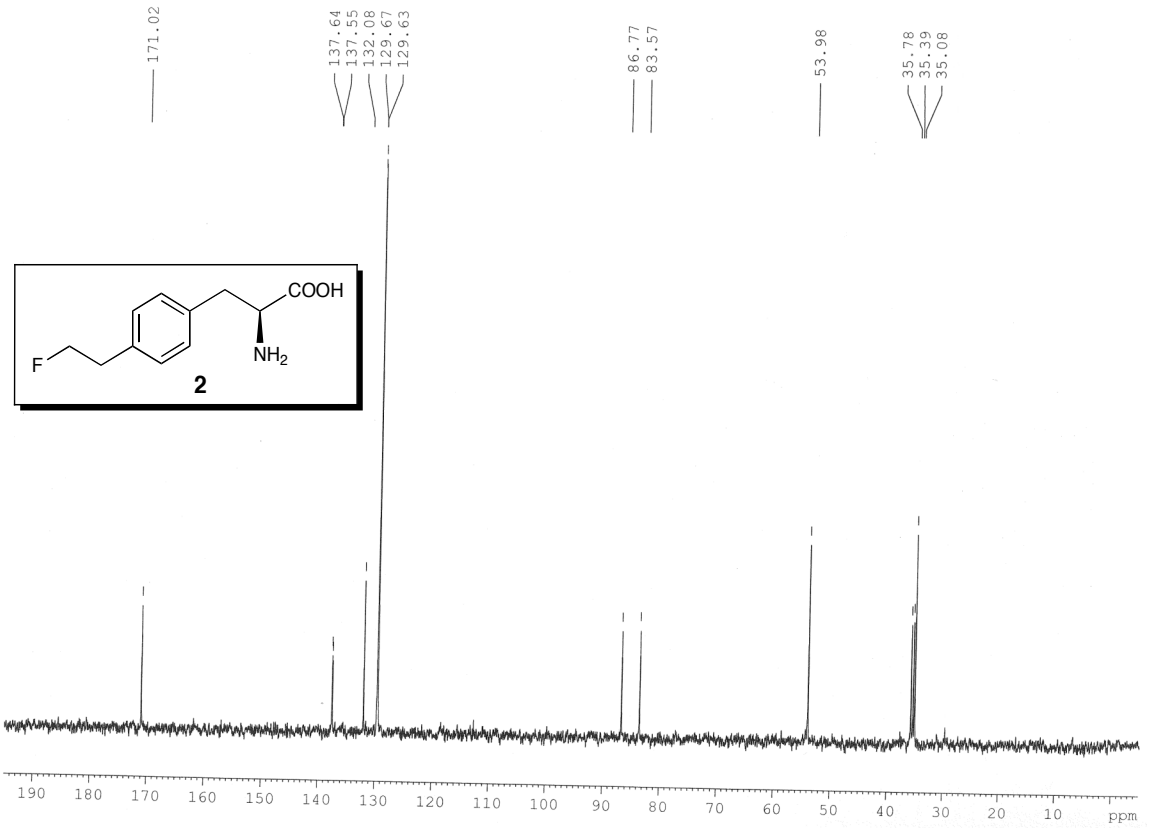
171.02
137.64
137.55
132.08
129.67
129.63
86.77
83.57
53.98
35.78
35.39
35.08
COOH
NH2
F
2
190 180 170 160 150 140 130 120 110 100 90 80 70 60 50 40 30 20 10 ppm

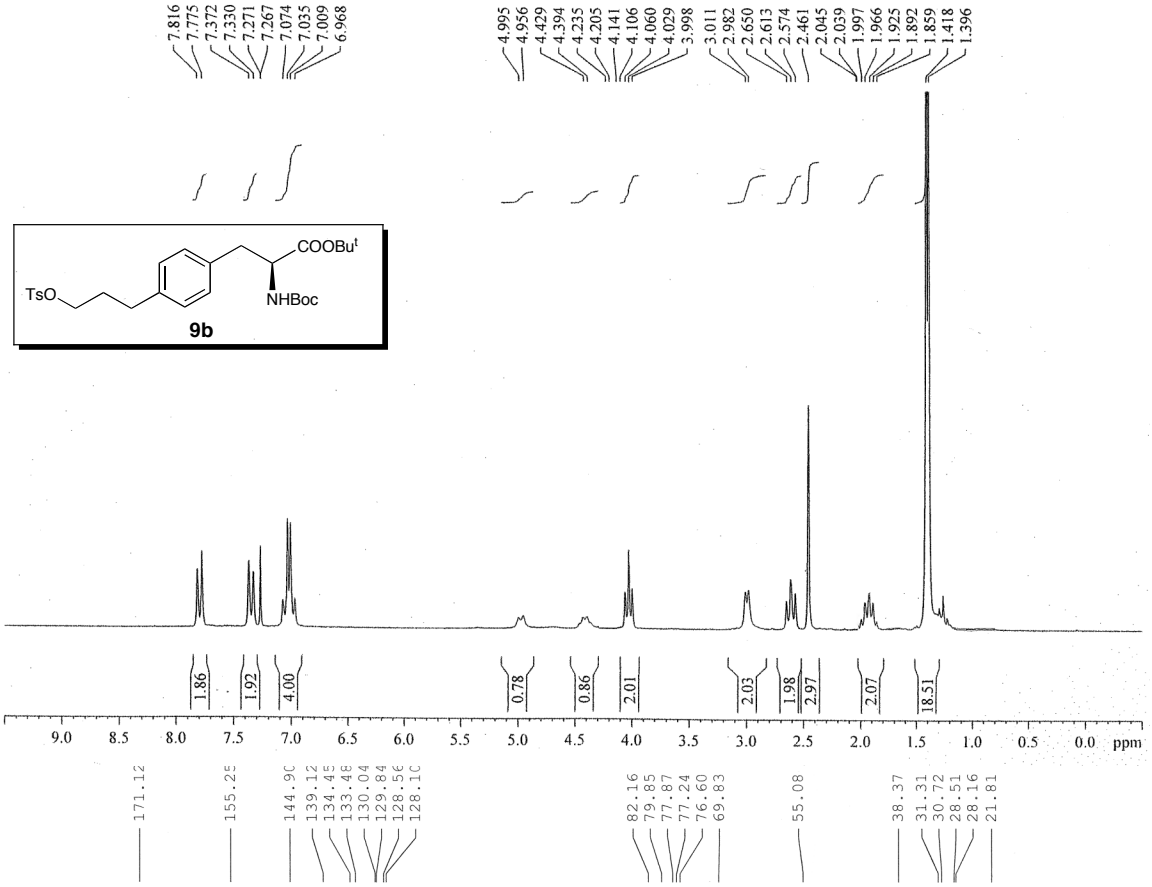
7.816
7.775
7.372
7.330
7.271
7.267
7.074
7.035
7.009
6.968
4.995
4.956
4.429
4.394
4.235
4.205
4.141
4.106
4.060
4.029
3.998
3.011
2.982
2.650
2.613
2.574
2.461
2.045
2.039
1.997
1.966
1.925
1.892
1.859
1.418
1.396
COOBu^t
TsO
NHBoc
9b
1.86
1.92
4.00
0.78
0.86
2.01
2.03
1.98
2.97
2.07
18.51
9.0
8.5
8.0
7.5
7.0
6.5
6.0
5.5
5.0
4.5
4.0
3.5
3.0
2.5
2.0
1.5
1.0
0.5
0.0
ppm

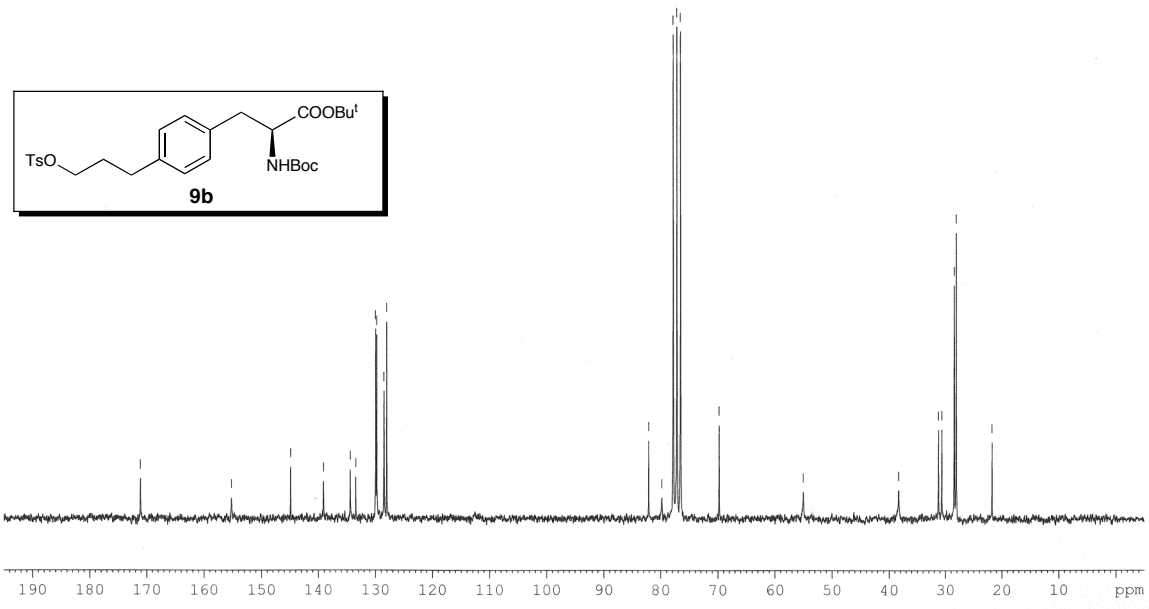
171.12
155.25
144.90
139.12
134.45
133.48
130.04
129.84
128.56
128.10
82.16
79.85
77.87
77.24
76.60
69.83
55.08
38.37
31.31
30.72
28.51
28.16
21.81
COOBu^t
TsO
NHBoc
9b
190
180
170
160
150
140
130
120
110
100
90
80
70
60
50
40
30
20
10
ppm

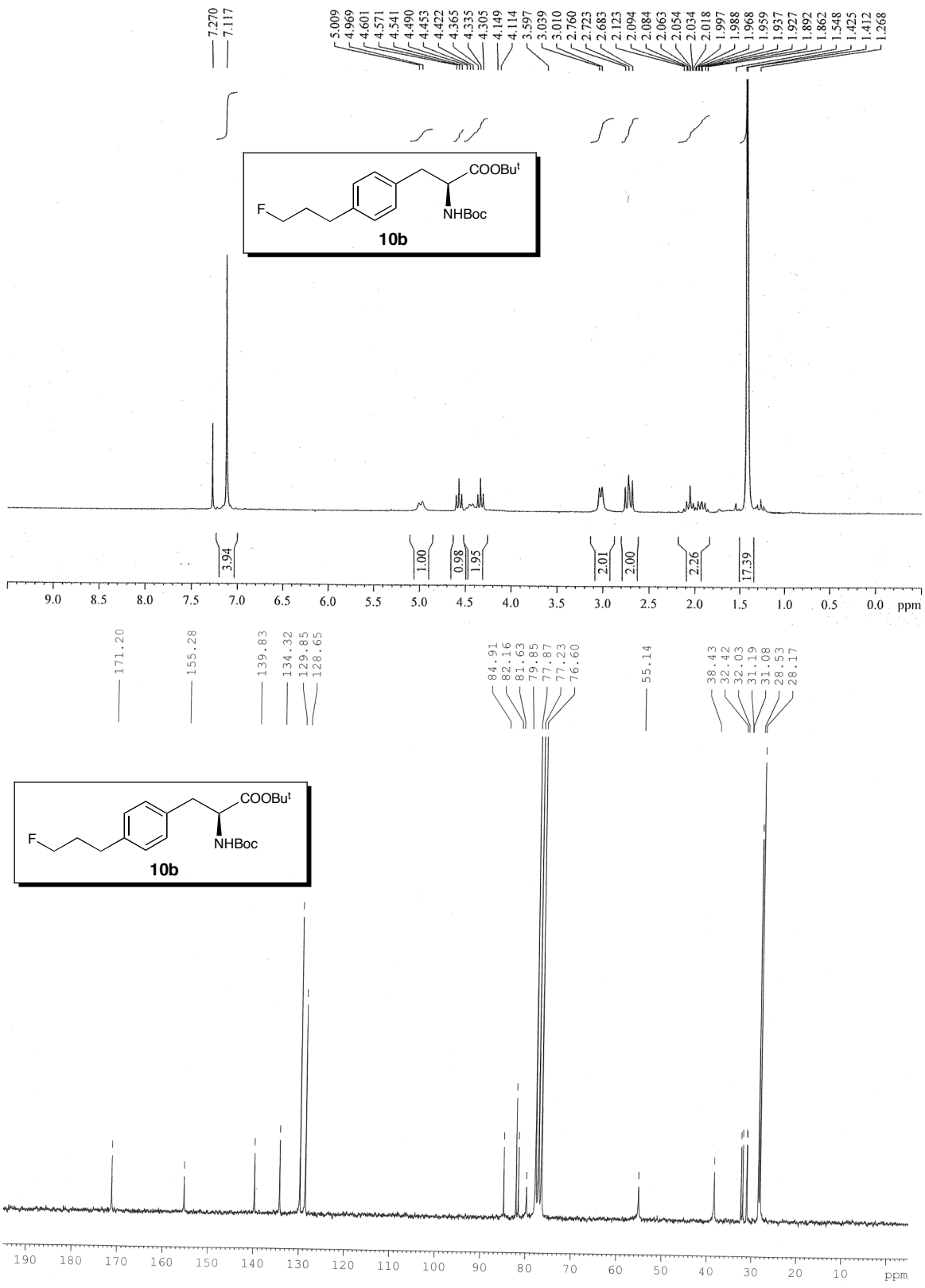
7.270
7.117
5.009
4.969
4.601
4.571
4.541
4.490
4.453
4.422
4.365
4.335
4.305
4.149
4.114
3.597
3.039
3.010
2.760
2.723
2.683
2.123
2.094
2.084
2.063
2.054
2.034
2.018
1.997
1.988
1.968
1.959
1.937
1.927
1.892
1.862
1.548
1.425
1.412
1.268
COOBu^t
NHBoc
F
10b
3.94
1.00
0.98
1.95
2.01
2.00
2.26
17.39
9.0 8.5 8.0 7.5 7.0 6.5 6.0 5.5 5.0 4.5 4.0 3.5 3.0 2.5 2.0 1.5 1.0 0.5 0.0 ppm
171.20
155.28
139.83
134.32
129.85
128.65
84.91
82.16
81.63
79.85
77.87
77.23
76.60
55.14
38.43
32.42
32.03
31.19
31.08
28.53
28.17
COOBu^t
NHBoc
F
10b
190 180 170 160 150 140 130 120 110 100 90 80 70 60 50 40 30 20 10 ppm

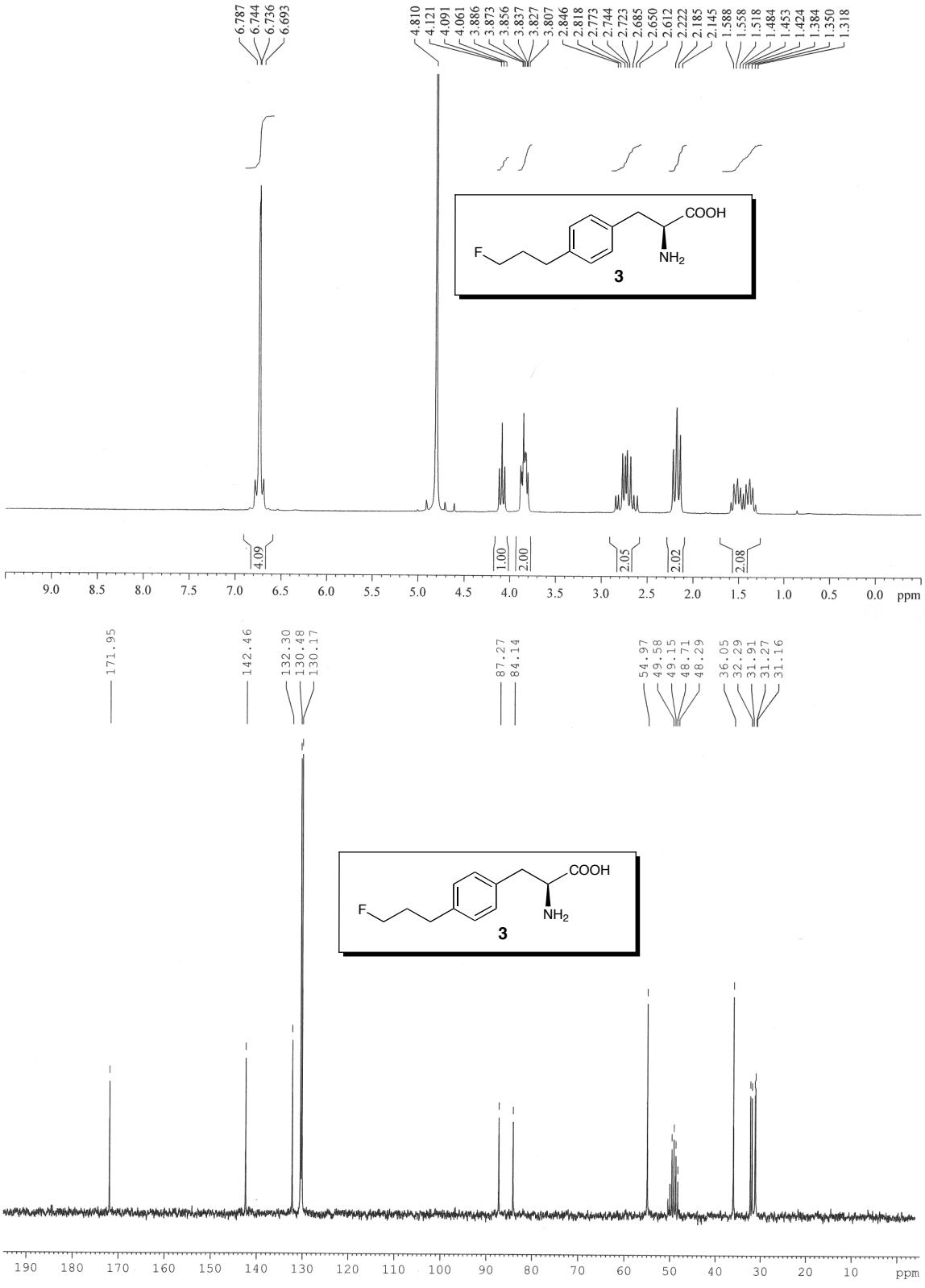
6.787
6.744
6.736
6.693
4.810
4.121
4.091
4.061
3.886
3.873
3.856
3.837
3.827
3.807
2.846
2.818
2.773
2.744
2.723
2.685
2.650
2.612
2.222
2.185
2.145
1.588
1.558
1.518
1.484
1.453
1.424
1.384
1.350
1.318
COOH
NH2
F
3
4.09
1.00
2.00
2.05
2.02
2.08
ppm
171.95
142.46
132.30
130.48
130.17
87.27
84.14
54.97
49.58
49.15
48.71
48.29
36.05
32.29
31.91
31.27
31.16
COOH
NH2
F
3
ppm

A.3 ^{1}H NMR spectra of D-isomers in Chapter 4

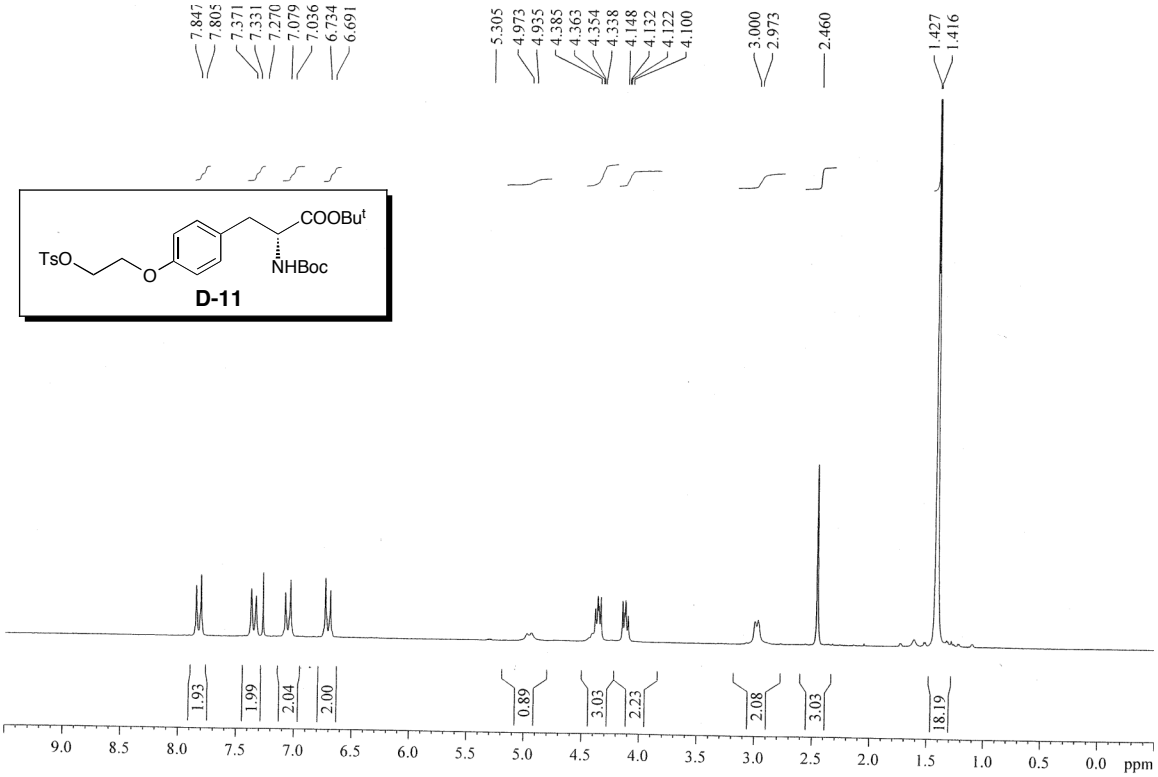

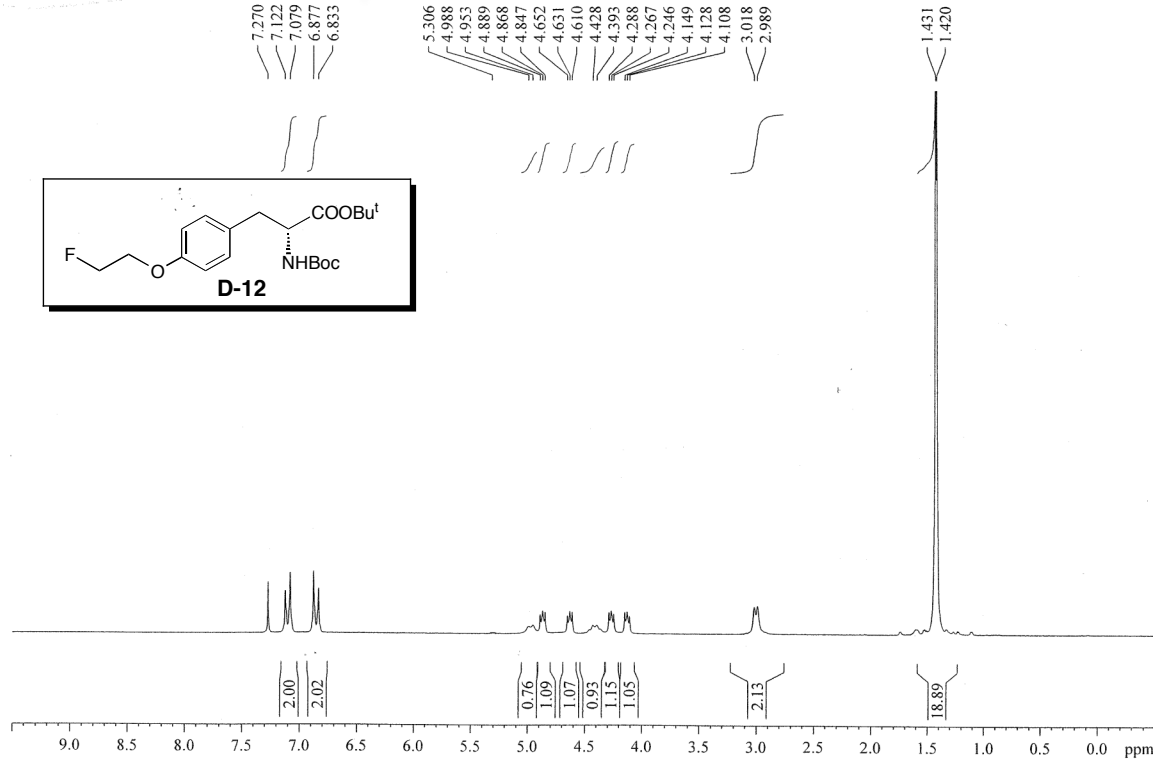

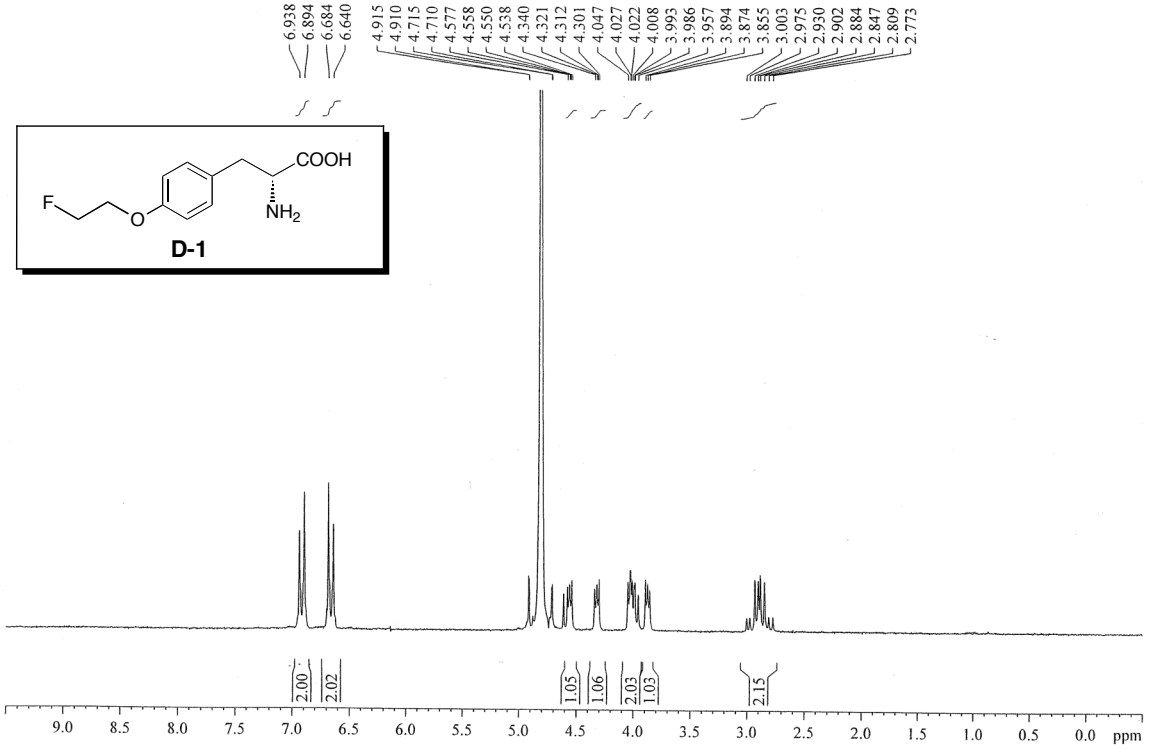
6.938
6.894
6.684
6.640
4.915
4.910
4.715
4.710
4.577
4.558
4.550
4.538
4.340
4.321
4.312
4.301
4.047
4.027
4.022
4.008
3.993
3.986
3.957
3.894
3.874
3.855
3.003
2.975
2.930
2.902
2.884
2.847
2.809
2.773
COOH
F
O
NH2
D-1
2.00
2.02
1.05
1.06
2.03
1.03
2.15
9.0 8.5 8.0 7.5 7.0 6.5 6.0 5.5 5.0 4.5 4.0 3.5 3.0 2.5 2.0 1.5 1.0 0.5 0.0 ppm

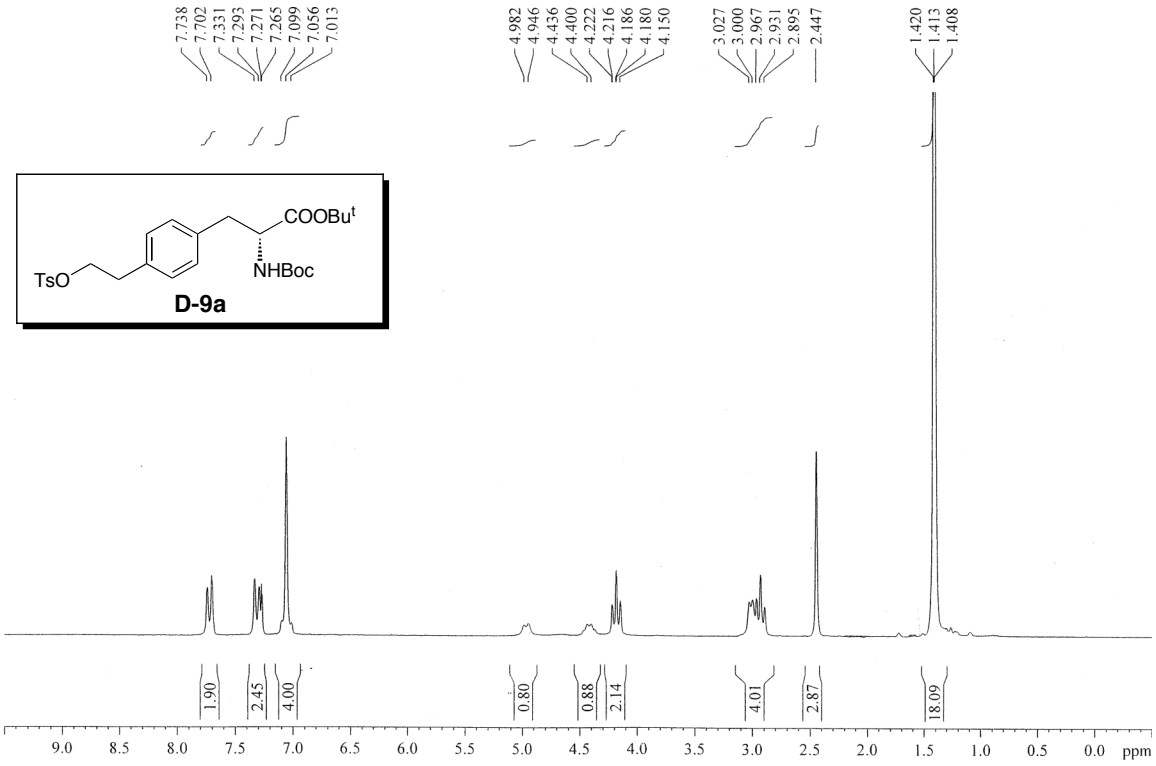
7.738
7.702
7.331
7.293
7.271
7.265
7.099
7.056
7.013
4.982
4.946
4.436
4.400
4.222
4.216
4.186
4.180
4.150
3.027
3.000
2.967
2.931
2.895
2.447
1.420
1.413
1.408
COOBu^t
TsO
NHBoc
D-9a
1.90
2.45
4.00
0.80
0.88
2.14
4.01
2.87
18.09
9.0 8.5 8.0 7.5 7.0 6.5 6.0 5.5 5.0 4.5 4.0 3.5 3.0 2.5 2.0 1.5 1.0 0.5 0.0 ppm

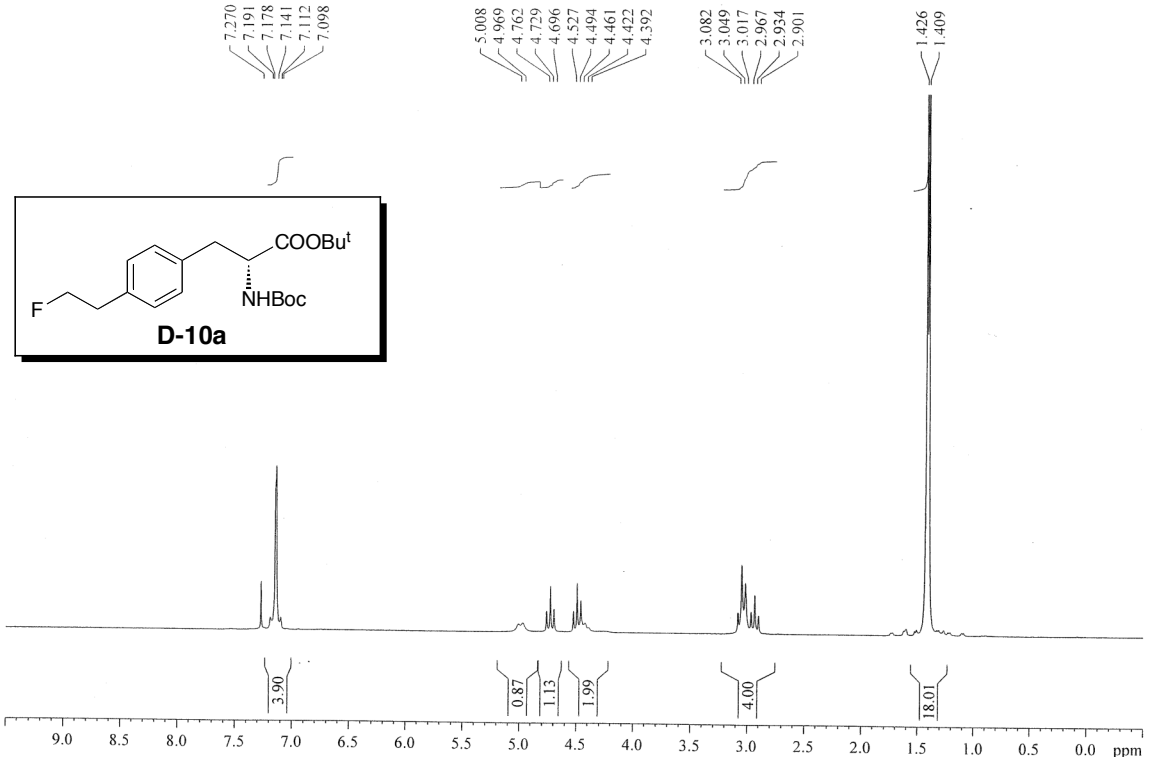
7.270
7.191
7.178
7.141
7.112
7.098
5.008
4.969
4.762
4.729
4.696
4.527
4.494
4.461
4.422
4.392
3.082
3.049
3.017
2.967
2.934
2.901
1.426
1.409
COOBu^t
NHBoc
F
D-10a
3.90
0.87
1.13
1.99
4.00
18.01
9.0 8.5 8.0 7.5 7.0 6.5 6.0 5.5 5.0 4.5 4.0 3.5 3.0 2.5 2.0 1.5 1.0 0.5 0.0 ppm

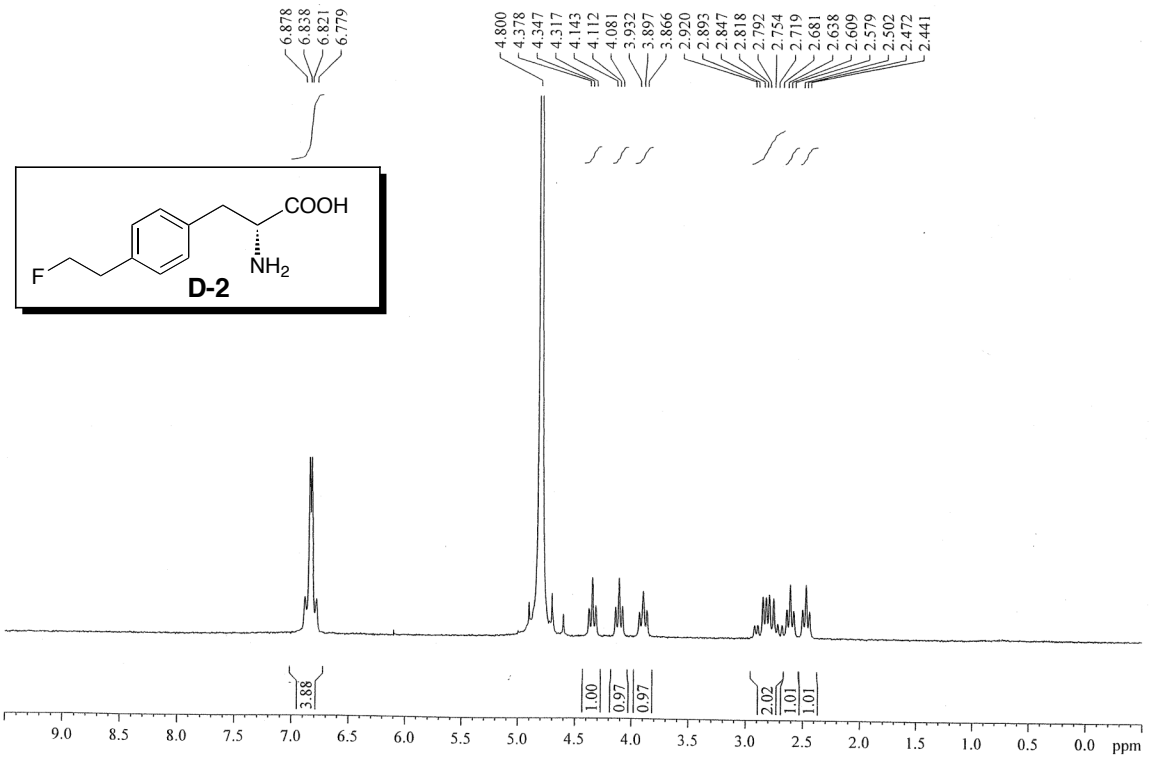
6.878
6.838
6.821
6.779
4.800
4.378
4.347
4.317
4.143
4.112
4.081
3.932
3.897
3.866
2.920
2.893
2.847
2.818
2.792
2.754
2.719
2.681
2.638
2.609
2.579
2.502
2.472
2.441
COOH
NH$_2$
F
D-2
3.88
1.00
0.97
0.97
2.02
1.01
1.01
9.0 8.5 8.0 7.5 7.0 6.5 6.0 5.5 5.0 4.5 4.0 3.5 3.0 2.5 2.0 1.5 1.0 0.5 0.0 ppm

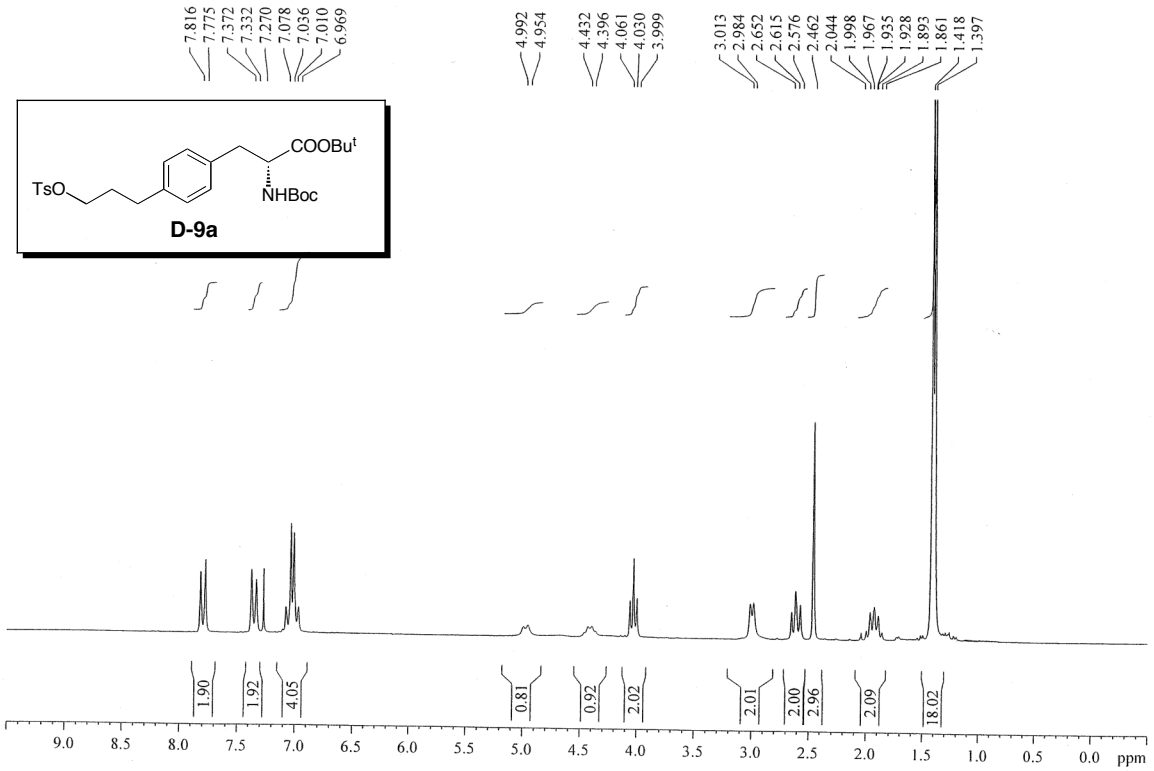
7.816
7.775
7.372
7.332
7.270
7.078
7.036
7.010
6.969
4.992
4.954
4.432
4.396
4.061
4.030
3.999
3.013
2.984
2.652
2.615
2.576
2.462
2.044
1.998
1.967
1.935
1.928
1.893
1.861
1.418
1.397
COOBu^t
TsO
NHBoc
D-9a
1.90
1.92
4.05
0.81
0.92
2.02
2.01
2.00
2.96
2.09
18.02
9.0 8.5 8.0 7.5 7.0 6.5 6.0 5.5 5.0 4.5 4.0 3.5 3.0 2.5 2.0 1.5 1.0 0.5 0.0 ppm

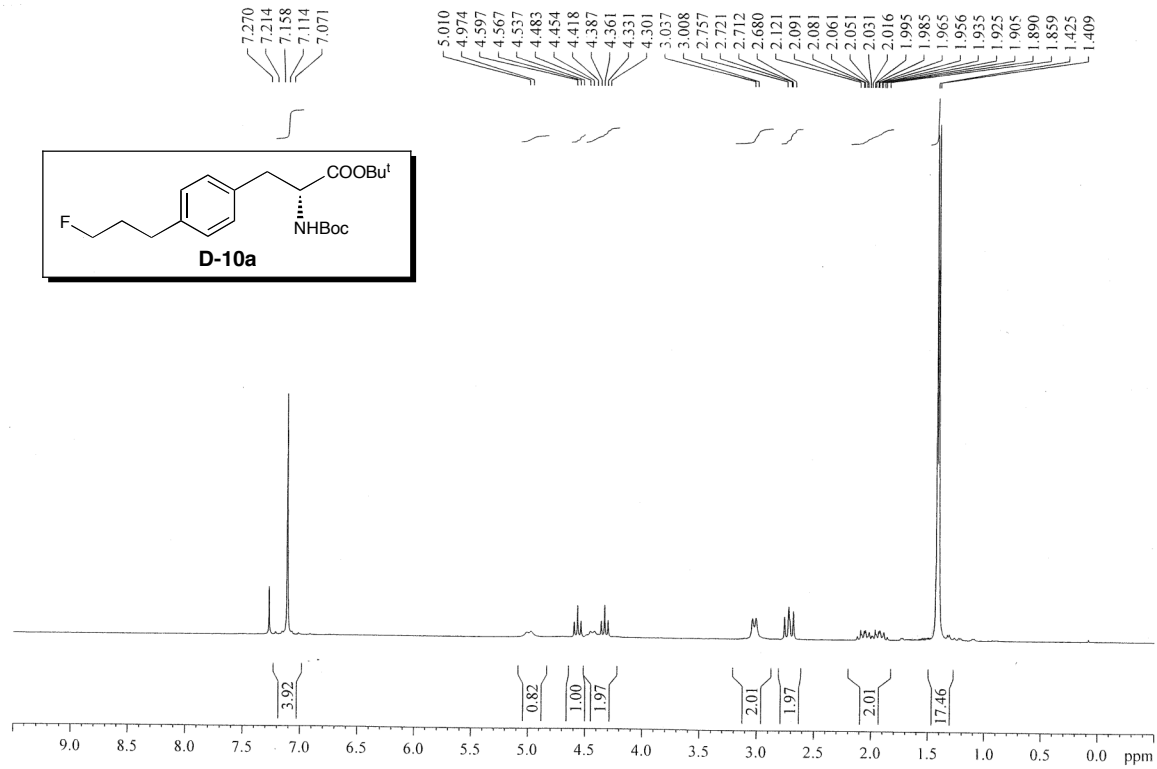
7.270
7.214
7.158
7.114
7.071
5.010
4.974
4.597
4.567
4.537
4.483
4.454
4.418
4.387
4.361
4.331
4.301
3.037
3.008
2.757
2.721
2.712
2.680
2.121
2.091
2.081
2.061
2.051
2.031
2.016
1.995
1.985
1.965
1.956
1.935
1.925
1.905
1.890
1.859
1.425
1.409
COOBu^t
F
NHBoc
D-10a
3.92
0.82
1.00
1.97
2.01
1.97
2.01
17.46
9.0 8.5 8.0 7.5 7.0 6.5 6.0 5.5 5.0 4.5 4.0 3.5 3.0 2.5 2.0 1.5 1.0 0.5 0.0 ppm

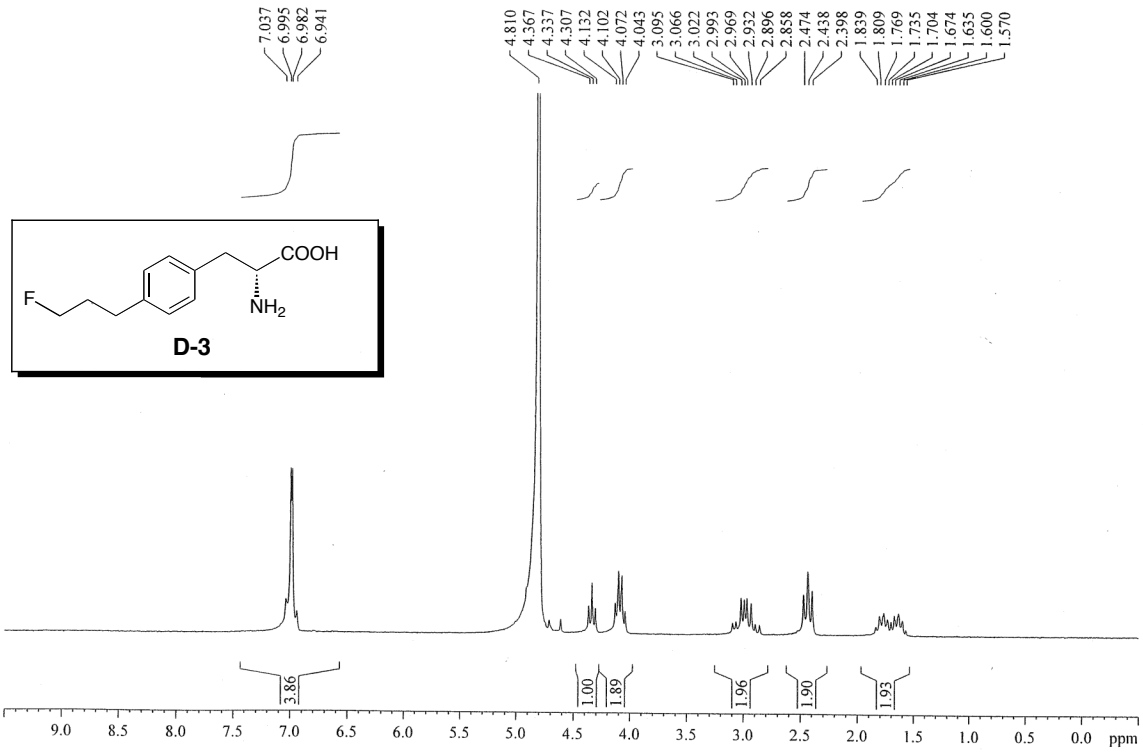
7.037
6.995
6.982
6.941
4.810
4.367
4.337
4.307
4.132
4.102
4.072
4.043
3.095
3.066
3.022
2.993
2.969
2.932
2.896
2.858
2.474
2.438
2.398
1.839
1.809
1.769
1.735
1.704
1.674
1.635
1.600
1.570
COOH
F
NH2
D-3
3.86
1.00
1.89
1.96
1.90
1.93
9.0
8.5
8.0
7.5
7.0
6.5
6.0
5.5
5.0
4.5
4.0
3.5
3.0
2.5
2.0
1.5
1.0
0.5
0.0
ppm